

THE MICRONISATION OF SYNTHETIC WAXES

by

Louis Koen

Thesis presented in partial fulfilment
of the requirements for the Degree

of

**MASTER OF SCIENCE IN ENGINEERING
(CHEMICAL ENGINEERING)**

in the Department of Chemical Engineering
at the University of Stellenbosch

Supervised by

Prof. Izak Nieuwoudt

Stellenbosch

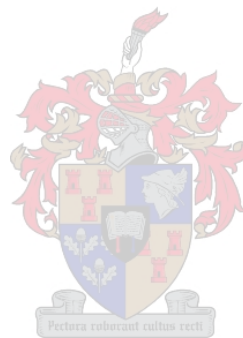
April 2003

DECLARATION

I, the undersigned, hereby declare that the work contained in this thesis is my own original work and that I have not previously in its entirety or in part submitted it at any university for a degree.

Signature: _____

Date: _____



ABSTRACT

Spherical wax particles with diameters of 5 μm and less are known to enhance the properties of powder and solvent-based coatings. Conventional methods, including spray freezing and jet milling, yield only 15 – 20 % of particles within this desired size range.

Recently, supercritical fluids have been used in the micronisation of a variety of polymers, pharmaceuticals and other inorganic solids. Of these processes, the Rapid Expansion of Supercritical Solutions (RESS) involves the expansion of a solid dissolved in a supercritical fluid over a nozzle. In the process the solubility of the solid is drastically decreased to yield high supersaturated conditions, resulting in a multitude of small and stable wax nuclei. The technique is known to produce small, solvent free particles with a narrow size distribution.

In this project, the RESS technique was applied to two commercial Fischer-Tropsch waxes: Paraflint C80 and Paraflint C105. Propane was selected as supercritical solvent due to its increased solvent power for paraffin wax compared to other conventional supercritical solvents such as carbon dioxide and ethane.

From theoretical studies, nozzle geometry, as well as nozzle inlet temperature, pressure and concentration was identified as the parameters most likely to influence the size and shape of the wax particles. Porous plate nozzles were chosen as expansion device due to lower pressure drop and higher flow rate of the expanding solution compared to conventional capillary nozzles.

Pre-expansion conditions of 125 to 160 $^{\circ}\text{C}$ and 125 – 180 bar were investigated. Wax concentrations up to 5 weight % were expanded through porous plate nozzles with pore sizes of 15, 25 and 60 μm .

It was found that small particles, less than 5 μm in size could readily be produced for the whole range of parameters investigated. Average particle sizes of less than 2 μm were found in virtually all cases. The C80 particles tended to be less smooth and of more angular shape than C105 particles. It is argued that the higher fraction of low

weight compounds softens the C80 wax particle surface, making them more susceptible to deformation and coagulation.

Experimental studies confirmed that a combination of lower temperature and higher pressure (175 bar and 130 °C) increases the chances for the formation of spherical particles. This combination corresponded to conditions furthest away from the dew point of the solution.

The 25 µm porous plate nozzle gave better results than the other nozzles, indicating that the characteristics of the nozzle could play a more important role than the pore size. SEM images indicated that this nozzle has a larger porosity, which could have resulted in lower pressure drops compared to the other nozzles.

Higher wax concentration did seem to give smaller individual particles, but particle shape visibly deteriorated as the concentration increased. From experiments with C105 wax, at these optimal conditions, it seems as if a maximum concentration between 4 and 5 % is achievable, above which the particle shape became flak-like with rough edges.

Due to limitations of the batch experimental set-up, especially regarding the reaching of steady state, it is strongly recommended that the obtained results be verified on pilot plant scale, where longer spray times can be achieved.

The RESS process for wax micronisation on industrial scale needs to be critically examined and higher pressure and solvent recycling costs would need to be weighed up against the lower wax recycling required to obtain the desired particles.

OPSOMMING

Sferiese was partikels met 'n deursnee van 5 μm en minder is bekend daarvoor dat dit die eienskappe van 'n verskeidenheid van poeier en oplosmiddel-gebaseerde deklae verbeter. Alledaagse metodes, waaronder sproeivries- en maalprosesse soos straalmaling, lewer slegs sowat 15 – 20 % van die partikels binne die gewenste partikelgrootte.

In die afgelope tyd is superkritiese vloeistof mikroniseringsprosesse gebruik om 'n verskeidenheid van polimere, farmaseutiese en ander anorganiese stowwe te mikroniseer. Die sogenaamde “Rapid Expansion of Supercritical Solutions (RESS)”-proses behels die ontspanning van 'n oplossing van die vaste stof en 'n superkritiese oplosmiddel oor 'n spuitstuk. In die proses verlaag die oplosbaarheid van die vaste stof drasties, sodat hoë superversadigde vlakke in 'n baie kort tydperk bereik word om 'n menigte klein en stabiele was kerne te vorm. Die tegniek is bekend daarvoor om fyn, oplosmiddelvrye partikels met 'n nou partikelgrootteverspreiding te lewer.

In hierdie projek is die RESS-prosesse ondersoek om twee Fischer-Tropsch wasse, C80 en C105, te mikroniseer. Propaan is as oplosmiddel gekies weens die verhoogde oplosbaarheid van paraffienwasse daarin vergeleke met ander konvensionele superkritiese oplosmiddels soos koolsuurgas en etaan. Poreuse skywe is as spuitstukke verkies weens die feit dat hoër vloeitempos en laer drukvalle oor hierdie spuitstukke verkry kan word.

Na 'n teoretiese ondersoek is spuitstukgeometrie, asook die temperatuur, druk en konsentrasie by die spuitstuginlaat geïdentifiseer as die prosesparameters wat die partikelgrootte en -verspreiding die waarskynlikste sal beïnvloed.

Daar is besluit om die spuitstuginlaatkondisies van 125 tot 160 $^{\circ}\text{C}$ en 125 tot 180 bar te ondersoek. Waskonsentrasie tot en met 5 massa % is deur poreuse skywe met gemiddelde poriegroottes van 15, 25 en 60 μm ontspan.

Klein waspartikels, met gemiddelde partikelgroottes van minder as 2 μm is in feitlik al die gevalle verkry. Die C80 waspartikels het geneig om minder glad en meer hoekig as die C105 partikels te wees. Hier word vermoed dat die hoër hoeveelheid lae

massa komponente die C80 waspartikeloppervlak versag en dit meer vatbaar maak vir vervorming en koagulasie.

Eksperimentele studies het getoon dat 'n kombinasie van laer temperature en hoër drukke (175 bar en 130 °C) by die spuitstukinlaat die kanse vir sferiese partikels vergroot. Hierdie temperatuur/druk kombinasie val saam met toestande verder weg van die doupunt van die oplossing.

Sover dit die spuitstukke aanbetref, het die 25 µm poreuse skywe beter resultate as die ander spuitstukke gelewer. Hier word vermoed dat die fisiese eienskappe van die spuitstuk 'n meer prominente rol as die poriegrootte speel. SEM foto's het getoon dat hierdie spuitstuk 'n groter porositeit, wat 'n laer druikeval tot gevolg kon gehad het, in vergelyking met die ander spuitstukke.

Dit blyk asof hoër waskonsentrasies lei tot kleiner individuele partikels, maar die vorm en oppervlak daarvan het sigbaar verswak by hoër konsentrasie. Vanuit eksperimente met C105 was, by die bovermelde optimale kondisies, wil dit voorkom asof 'n maksimum konsentrasie tussen 4 en 5 % haalbaar is, voordat die partikels 'n vlokkierige vorm met ruwe oppervlak aangeneem het.

Weens die beperkinge van die eksperimentele opstelling, word dit ten sterkste aanbeveel dat die resultate op loodsaanlegsskaal, waar langer sproeitye moontlik is, bevestig word.

Die RESS-proses behoort krities ondersoek te word en die hoër druk en oplosmiddel hersirkuleringskoste moet opgeweeg word teenoor die voordele van die laer was hersirkulering benodig om die gewenste partikels te lewer.

ACKNOWLEDGEMENTS

Firstly, I would like to thank SASOL (Pty) Ltd. and the National Research Foundation for the financial support offered to me during the course of this study.

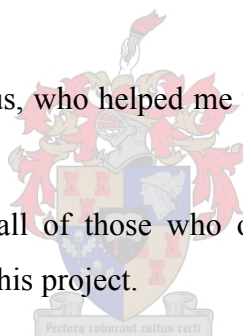
A special word of thanks goes to my study leader, prof. Izak Nieuwoudt, whose expertise and encouragement served as motivation during the turbulent times of this project.

Further, I would like to thank all the technical staff at the Department of Chemical Engineering for the processing of orders and construction of my experimental set-up.

Much gratitude is owed to Miranda Waldron and Niel Steenkamp at the Electron Microscope Units the University of Cape Town and University of Stellenbosch respectively.

I also wish to thank Karen Gous, who helped me verify the accuracy of the particle analysis method.

Lastly I would like to thank all of those who offered moral support during the difficult and emotional times of this project.



TER NAGEDAGTENIS AAN

François de Bruin

* 05/01/1979

† 25/05/2002

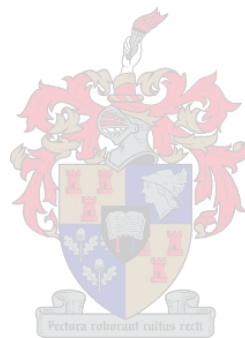


TABLE OF CONTENTS

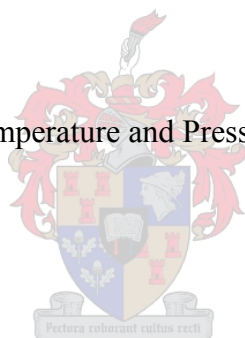
Declaration	i
Abstract	ii
Opsomming	iv
Acknowledgements	vi
Table of Contents	viii
List of Figures	xiii
List of Tables	xvi
List of Tables	xvi
1 An Introduction to Waxes	1
1.1 <i>Definition and Classification</i>	1
1.2 <i>Synthetic Waxes</i>	1
1.2.1 Fischer-Tropsch (FT) Waxes	2
1.2.2 Polyolefin Waxes	3
1.2.3 Properties of Synthetic Wax	4
1.3 <i>The Need for Wax Powders</i>	5
1.3.1 Application for Coatings	6
1.3.2 Particle Size and Shape Influence on Coating Characteristics	7
1.3.3 Current Micronisation Techniques	7
1.4 <i>An Alternative: Supercritical Fluid Processing</i>	9
1.5 <i>Project Definition and Goals</i>	10
2 Supercritical fluids	12
2.1 <i>Background</i>	12



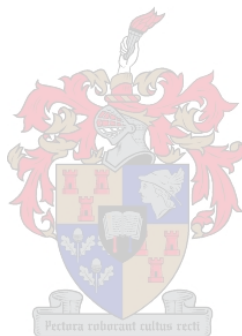
2.1.1	Properties	12
2.1.2	Early Developments and Studies	13
2.1.3	Industrial Applications	14
2.1.4	Recent Developments	17
2.1.5	Solvents	19
2.2	<i>Particles from Supercritical Fluid Processing</i>	20
2.3	<i>Rapid Expansion of Supercritical Solutions (RESS)</i>	21
2.3.1	Process Description	21
2.3.2	History	22
2.3.3	Applications	23
2.3.4	RESS Process Variables	28
2.4	<i>Anti-solvent Processes (GAS/SAS/ASES/SEDS)</i>	29
2.4.1	Process Description	29
2.4.2	History	32
2.4.3	Applications	33
2.4.4	Anti-solvent Process Variables	39
2.5	<i>Particles from Gas Saturated Solutions (PGSS)</i>	41
2.5.1	Principle	41
2.5.2	History	42
2.5.3	Applications	42
2.5.4	PGSS Process Variables	44
2.6	<i>Comparison of SCF Micronisation Processes</i>	45
2.7	<i>RESS of Paraffin Wax</i>	47
2.7.1	Finding a Suitable Solvent	47
2.7.2	Literature Overview of Wax Micronisation by RESS	49
2.8	<i>Conclusions</i>	50
3	RESS: A Theoretical Approach	51
3.1	<i>Supercritical Propane as a Solvent for Waxes</i>	51
3.2	<i>Nozzles and Pressure Profile</i>	52
3.2.1	Capillary Nozzles	53

3.2.2	Frit or Porous Plate Nozzles	54
3.2.3	Subsonic Flow Profile	54
3.2.4	Supersonic Flow Profile	57
3.3	<i>Homogeneous Nucleation</i>	58
3.4	<i>Condensation and Coagulation</i>	63
3.4.1	Collisions in Ideal Gases: Free Molecular	64
3.4.2	Collisions in Liquids: Continuum	66
3.4.3	Remarks	67
3.5	<i>Concluding Remarks</i>	68
3.5.1	Choice of Temperature and Pressure	68
3.5.2	Choice of Nozzle	69
3.5.3	Concentration Effects	69
4	Experimental Design and Procedure	71
4.1	<i>Experimental Set-up: Literature Overview</i>	71
4.1.1	Preparation of Pre-expansion Solution	71
4.1.2	Expansion of Solution	74
4.1.3	Precipitation and Particle Harvesting	74
4.1.4	Comparison of RESS Methods	75
4.2	<i>Design Considerations</i>	76
4.3	<i>Experimental Design</i>	77
4.3.1	Principle	77
4.3.2	Equilibrium Cell	78
4.3.3	Shut-off Valve and Spray Device	79
4.3.4	Expansion Vessel	81
4.4	<i>Experimental Procedure</i>	82
4.4.1	Loading of Equilibrium Cell	82
4.4.2	Phase Equilibrium	83
4.4.3	Spraying	84
4.4.4	Sample Preparation	85
4.5	<i>Product Analysis</i>	85

5	Results	86
5.1	<i>Dew Points for Propane/Wax Mixtures</i>	86
5.2	<i>Micronisation of C80 Wax</i>	87
5.2.1	The Influence of Concentration and Porous Plate Nozzles	87
5.2.2	The Influence of Temperature and Pressure	94
5.3	<i>Micronisation of C105 Wax</i>	98
5.3.1	The Influence of Concentration and Porous Plate Nozzles	98
5.3.2	The Influence of Temperature and Pressure	104
5.3.3	Upper Concentration Limit	108
5.4	<i>Repeatability of Experimental Data</i>	111
5.4.1	Repeatability Experiments	111
5.4.2	Repeatability of Particle Size Analysis	113
5.5	<i>The Effect of Wax Type</i>	114
5.6	<i>Discussion</i>	115
5.6.1	Pre-expansion Temperature and Pressure	115
5.6.2	Concentration	116
5.6.3	Expansion Nozzle	116
5.6.4	Production Rate	117
5.7	<i>Limitations of Experimental Set-up</i>	118
5.7.1	Steady State Temperature	118
5.7.2	Steady State Pressure	118
5.7.3	Further Testing	118
5.8	<i>Other Experimental Work</i>	119
5.9	<i>Concluding Remarks</i>	121
6	Conclusions and Recommendations	123
7	References	125
A	Experimental Data	136
B	Dew Points of Paraffin Wax	164



C	Calibration Data	166
D	Additional Experimental Procedures	168
	<i>Unloading and Cleaning of Equilibrium Cell</i>	<i>168</i>
	<i>Safety Considerations</i>	<i>169</i>
E	Properties of Chemicals Used	170
F	Mechanical Drawings	171
	<i>Equilibrium Cell</i>	<i>171</i>
	<i>Pressure Piston Unit</i>	<i>172</i>
	<i>Porous Plate Nozzle</i>	<i>173</i>
	<i>Precipitation Vessel</i>	<i>174</i>
G	Nomenclature	175
	<i>Symbols</i>	<i>175</i>
	<i>Greek Symbols</i>	<i>176</i>
	<i>Subscripts</i>	<i>176</i>
	<i>Superscripts</i>	<i>176</i>



LIST OF FIGURES

Figure 1-1: Fischer-Tropsch wax Process	2
Figure 1-2: The Ziegler-Natta polyethylene process (adapted from (Marcus 2002))	3
Figure 1-3: Distribution of a PE wax powder (adapted from (www.marcusoil.com July 2002))	6
Figure 1-4: SEM of wax produced by spray freezing	8
Figure 2-1 The Supercritical Fluid (SCF) Region of a Substance	12
Figure 2-2: The ROSE Process (McHugh and Krukoniš 1994)	16
Figure 2-3: Semi-batch RESS process	22
Figure 2-4: A Capillary Nozzle as used in RESS Set-up with Typical Pressure Profile	28
Figure 2-5: Batch GAS process	30
Figure 2-6: The SEDS process	31
Figure 2-7: Coaxial nozzle set-up for SEDS	32
Figure 2-8: Low dead volume mixing tee (Sievers 1999)	42
Figure 2-9: Comparison of Solvent Strength ((Du Rand 2000), (Schwarz 2001))	428
Figure 3-1: Phase Equilibria for Paraffin Waxes and Supercritical Propane (Schwarz 2001)	52
Figure 3-2: The Capillary Nozzle (left) and Porous Plate Nozzle	53
Figure 3-3: Different Sections of a Capillary Nozzle (Helfgen et al. 2002)	55
Figure 3-4: Flow profiles for capillary and porous plate nozzles (Adapted from (Berends 1994))	58
Figure 3-5: Schematical representation of Nucleation	59
Figure 3-6: : Variation of ΔG with embryo radius.	62
Figure 3-7: The processes of Condensation (left) and Coagulation (Adapted from (Weber and Thies 2000))	64
Figure 3-8: The Collision between solute particles	65
Figure 4-1: The Batch RESS Process	72
Figure 4-2: The RESS Semi-continuous Process	73
Figure 4-3: Experimental Equipment to be used	77

Figure 4-4: The Equilibrium Cell	78
Figure 4-5: Expansion of Supercritical Solution	80
Figure 4-6: Expansion vessel	81
Figure 4-7: Loading of the Equilibrium Cell	82
Figure 4-8: Phase Equilibrium Stage	83
Figure 4-9: Spraying Process	84
Figure 5-1: Particle Size Distribution at Various Concentrations at Pre-expansion Conditions of T = 160 °C, P = 150 bar, Pore Size = 15 µm.	89
Figure 5-2: C80 Particle Size Distribution at Various Concentrations at Pre-expansion Conditions of T = 160 °C, P = 150 bar, Pore Size = 60 µm.	90
Figure 5-3: C80 Particle Size Distribution at Various Concentrations at Pre-expansion Conditions of T = 160 °C, P = 150 bar, Pore Size = 25 µm.	91
Figure 5-4: Particle Shape Dependence on Concentration at Pre-expansion Conditions of T = 160 °C, P = 150 bar, Pore Size = 15 µm.	92
Figure 5-5: Particle Shape Dependence on Concentration at Pre-expansion Conditions of T = 160 °C, P = 150 bar, Pore Size = 60 µm.	93
Figure 5-6: Particle Shape Dependence on Concentration at Pre-expansion Conditions of T = 160 °C, P = 150 bar, Pore Size = 25 µm	93
Figure 5-7: C80 Particle Size Distribution at Various Pre-expansion Conditions of a 3 % solution expanded via a 15 µm Nozzle	95
Figure 5-8: C80 Particle Size Distribution at Various Pre-expansion Conditions of a 2 % solution expanded via a 60 µm Nozzle	96
Figure 5-9: Particle Shape Dependence on Pre-expansion Conditions of a 3 % solution expanded via a 15 µm Nozzle	97
Figure 5-10: Particle Shape Dependence on Pre-expansion Conditions of a 2 % solution expanded via a 60 µm Nozzle	97
Figure 5-11: C105 Particle Size Distribution at Various Concentrations at Pre-expansion Conditions of T = 130 °C, P = 175 bar, Pore Size = 60 µm	99
Figure 5-12: C105 Particle Size Distribution at Various Concentrations at Pre-expansion Conditions of T = 160 °C, P = 150 bar, Pore Size = 60 µm	100
Figure 5-13: C105 Particle Size Distribution at Various Concentrations at Pre-expansion Conditions of T = 160 °C, P = 150 bar, Pore Size = 25 µm	101
Figure 5-14: C105 Particle Shape Dependence on Concentration at Pre-expansion Conditions of T = 160 °C, P = 150 bar, Pore Size = 60 µm	102

Figure 5-15: C105 Particle Shape Dependence on Concentration at Pre-expansion Conditions of T = 160 °C, P = 150 bar, Pore Size = 25 μm	102
Figure 5-16: Particle Shape Dependence on Concentration at Pre-expansion Conditions of T = 130 °C, P = 175 bar, Pore Size = 60 μm	103
Figure 5-17: C105 Particle Size Distribution for Various Pre-expansion Conditions of a 2 % solution expanded via a 60 μm Nozzle	105
Figure 5-18: C105 Particle Size Distribution for Various on Pre-expansion Conditions of a 5 % solution expanded via a 60 μm Nozzle	106
Figure 5-19: C105 Particle Shape Dependence on Pre-expansion Conditions of a 2 % solution expanded via a 60 μm Nozzle	107
Figure 5-20: C105 Particle Shape Dependence on Pre-expansion Conditions of a 5 % solution expanded via a 60 μm Nozzle	107
Figure 5-21: Particle Shape Dependence on Concentration at Pre-expansion Conditions of T = 130 °C, P = 175 bar, Pore Size = 25 μm	109
Figure 5-22: Particle Shape Dependence on Concentration at Pre-expansion Conditions of T = 130 °C, P = 175 bar, Pore Size = 25 μm	111
Figure 5-23: Comparison of original run (left) and repeated run for C80 wax at pre-expansion conditions: T = 160 °C, P = 150 bar, x = 3.0 wt %, Pore size = 60 μm	112
Figure 5-24: Comparison of Particle Size Distribution of Original and Repeated Run	112
Figure 5-25: Sample on which Particle Size Repeatability Analysis were Performed	113
Figure 5-26: Comparison of n-C36 (left) and C80 wax at pre-expansion conditions: T = 160 °C, P = 150 bar, x = 2.0 wt %, Pore size = 15 μm	115
Figure 5-27: SEM Image of Inlet Flow Area of Porous Plate Nozzles	117
Figure 5-28: Proposed Continuous Pilot Plant	119
Figure 5-29: Comparison of n-C₃₆H₇₄ Particles obtained from expansion from 150 bar, 160 °C through 15 μm nozzle and different concentrations	120
Figure 5-30: Porous Mass of Particles found at 15 % C80 Concentration for a variety of conditions	121
Figure B-1: Equilibrium Cell used for C80 Dew Point Measurements (Schwarz 2001)	164
Figure C-1: Pressure Fluctuations with Temperature	166

LIST OF TABLES

Table 2-1: Critical constants of common gases (Perry and Green 1997)	20
Table 2-2: Comparison of the Supercritical Fluid Micronisation Processes	46
Table 4-1: Comparing Batch and Continuous Processes	75
Table 5-1: Dew Points of 3 % and 5.5 % C80 Wax Solution	86
Table 5-2: C80 Particle Sizes obtained from Various Nozzles and Concentrations at 150 bar and 160 °C	87
Table 5-3: C80 Particle Sizes obtained at Various Process Conditions	94
Table 5-4: C105 Particle Sizes obtained from Various Nozzles and Concentrations	98
Table 5-5: C105 Particle Sizes obtained at Various Process Conditions	104
Table 5-6: C105 Particle Sizes obtained from Various Concentrations at 175 bar and 130 °C via Expansion through a 25 µm Nozzle	108
Table 5-7: Results of Repeated Particle Size Determination	114
Table A-1: Summary of Experimental Conditions for C80 and C105 Experimental Runs	136
Table C-1: Pressure Calibration Data	166
Table E-1: Properties of Wax used in Experimental Investigations (www.mooremunger.com)	170
Table E-2: Composition of Propane Solvent used in Experimental Runs (www.afrox.co.za)	170

1 AN INTRODUCTION TO WAXES

1.1 Definition and Classification

Wax is a generic term that refers to a range of natural or synthetic products. Typically waxes do not consist of a single chemical compound, but are often very complex mixtures. Being oligomers, or polymers in many cases, the components differ in their molar mass, molar mass distribution, or in the degree of side-chain branching. Waxes may also contain several different functional groups (ie. carboxyl, alcohol, ester, keto, or amide groups).

Waxes are most conveniently subdivided into the following categories (www.wax.org July 2002):

- **Natural waxes** are of animal or plant origin. Examples include beeswax, carnauba wax and candelilla wax.
- **Mineral hydrocarbon waxes** are derived from mineral origin. Montan wax, for example, is derived from solvent extraction of lignite.
- **Petroleum waxes** are derived from crude petroleum. Paraffin and microcrystalline waxes are the main types of petroleum wax. They are the largest group of waxes, making up in excess of 95 % of the total world wax production.
- **Synthetic waxes** are products of polymerisation reactions. Fischer-Tropsch and polyethylene waxes are predominant.

In this project, the focus will be on the processing of synthetic waxes. The interested reader can gather detailed discussions on the other waxes from websites (www.wax.org July 2002) or from review articles (e.g. (Wolfmeier et al. 1996), (Letcher 1992)).

1.2 Synthetic Waxes

Synthetic waxes are products of polymerization reactions. As mentioned above, the two predominant products are Fischer-Tropsch and polyethylene waxes.

In 1935 the Fischer-Tropsch process yielded the first fully synthetic waxes. Polyethylene wax has been synthesized by the high-pressure process since 1939, and became available by the low-pressure Ziegler process after 1953 (Wolfmeier et al. 1996).

1.2.1 Fischer-Tropsch (FT) Waxes

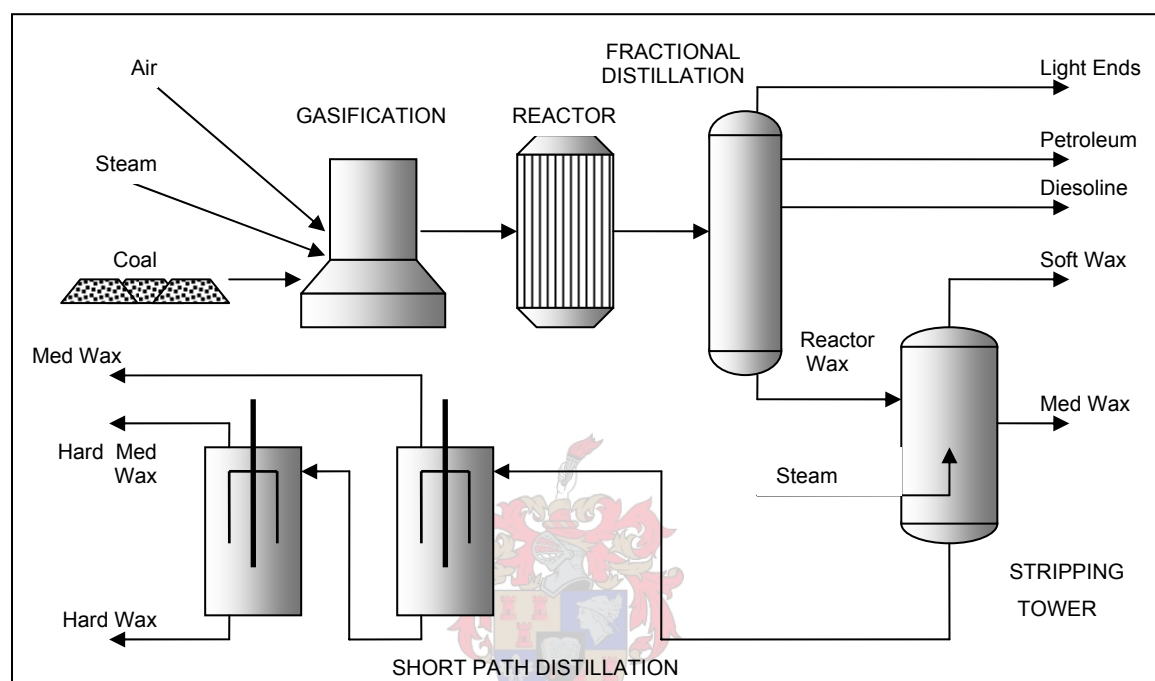


Figure 1-1: Fischer-Tropsch wax Process

Fischer-Tropsch waxes, also called polymethylene waxes, are products of the Fischer-Tropsch process. In the FT process, low-grade coal, water and air are used to produce synthesis gas. Synthesis gas consists mainly of carbon monoxide and hydrogen. The synthesis gas is fed to a reactor system where polymerization reactions at high pressure and temperature preferentially yield n-alkanes and n-alkenes.

The different alkane fractions are separated by fractional distillation. The reactor wax fraction is subjected to vacuum distillation and steam stripping, where first the soft waxes (C16 – C24) are separated from the medium (C22 – C38) and hard (C36 +) waxes.

The hard waxes may contain some hydroxyl groups, carbonyl groups and coloured components. These components are removed by hydrofining to obtain a white, hard wax practically free of alkenes, aromatics and sulphur compounds.

The hard wax is fractionated to obtain a number of fractions of hard wax. Currently, short path distillation techniques are used for fractionation of hard waxes.

1.2.2 Polyolefin Waxes

Polyolefin waxes are products from classical polymerisation reactions. The polymerisation reaction is initiated when the catalyst decomposes to generate radicals. This radical adds to an alkene molecule to create a new alkyl radical. A new ethene molecule adds to the alkyl radical and this process is repeated until a chain molecule forms. The reaction is terminated when the radical is consumed by addition of a regulator molecule (McMurry 1996). Two processes are mainly used to produce polyolefin waxes.

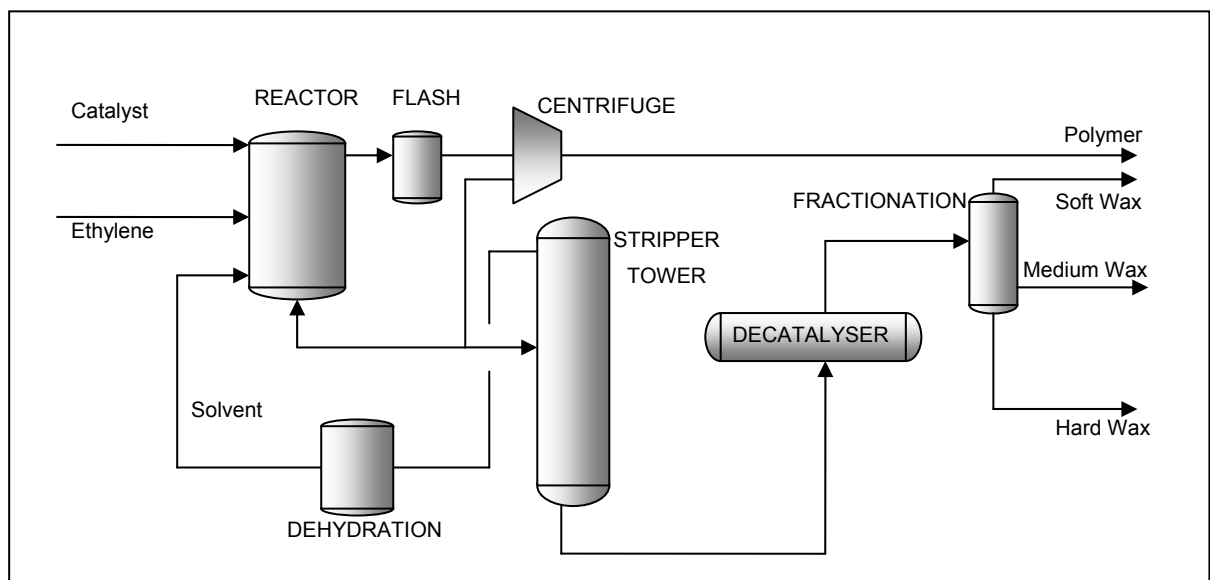


Figure 1-2: The Ziegler-Natta polyethylene process (adapted from (Marcus 2002))

The older of the two, the high-pressure process, is based on the high-pressure polymerisation of ethene (ethylene). Organic peroxides, such as benzoyl peroxide, are used as catalysts at high pressures of up to 3200 bar. The process is characterised by the formation of short ethyl and butyl side chains due to intramolecular transfer of the radical during the polymerisation process.

The Ziegler process is a more recent development and operates at much milder pressure. In this process any 1-alkene (α -olefin) can be polymerised over Ziegler catalysts, which are organometallic in nature. Classical Ziegler catalysts consisted of titanium tetrachloride and alkylaluminium compounds, but they had a low selectivity. The operating temperature here is in the region of 100 to 200 °C. Recently

metallocene catalysts have come to the fore as a replacement for these classical catalysts. These catalysts consist of a single metal atom held between two carbon rings. Metallocene catalysts are more active, yielding a product with a narrower molecular weight distribution. In addition, these catalysts allow for polymerisation at much lower temperatures than conventional catalysts. The great advantage of metallocene catalysts is that their structure can be varied to obtain waxes with different property profiles. (Kaminsky 2000) In one such variation, Boron is added to the standard metallocene structure. (www.cheresources.com November 2002) This catalyst works at atmospheric pressure and requires very little heat. These conditions are much more acceptable than those for the high pressure process, or those required with classical Ziegler catalysts. Research in this field is still continuing, and to date it has not been implemented on large industrial scale. (Kaminsky 2000)

To obtain straight chain waxes, ethylene is used as monomer. In Figure 1-2, a schematic diagram of a Ziegler process is given. The product consists of a mixture of high-density polyethylene and long-chained waxes. The reactor product is subsequently flashed to separate the polymer and wax fractions from the ethylene that did not react in the reactor system. The wax/polymer mixture from the flash vessel is separated in a centrifuge, the heavier polymer fraction being in the solid state. Some of the wax/solvent mixture is returned to the reactor system, and the remaining wax fraction is subjected to a number of purification steps, including steam stripping to remove the lighter wax fractions and solvent. The lighter fractions are dehydrated and returned to the reactor system. The wax is decatalysed, fractionated in a series of flashes and processed further to a desired form, such as blocks, pellets or powder.

1.2.3 Properties of Synthetic Wax

By variation in chain length and degree of branching, important factors such as melting point, hardness, crystallinity and melt viscosity can be tailored. For a paraffin wax, these properties increase with an increase in chain length. In contrast, these properties decrease with an increase in branching of waxes with the same molar mass. (EWF 2002)

Synthetic waxes are solid at ambient conditions, but can vary in consistency from soft and plastic to brittle and hard. The melting point ranges from about 40 °C to 120 °C.

Synthetic waxes are insoluble in water, but do dissolve in a range of non-polar solvents. This solubility is highly temperature and pressure dependant.

As with other waxes, synthetic waxes exhibit other desirable properties, including

- Low thermal and electrical conductivity
- Buffable under slight pressure
- Forms pastes or gels when dispersed in solvents.

1.3 The Need for Wax Powders

Waxes are sold in various forms, including prills, scales, blocks and powders. Powdered wax is especially useful in specialised coatings.

Wax powder consists of predominantly spherical particles, although broken (irregular) particles can also be produced. Typical powders on the market have average particle sizes of somewhere between 5 and 13 microns ((www.mooremunger.com July 2002), (www.marcusoil.com July 2002), (www.schuemann-sasol.com July 2002)), although some special powders have larger sizes (up to 200 μm) to impart a different texture to the coating.

However, these powders frequently also contain particles that are two to three times the average particle size. In Figure 1-3 a typical size distribution of a synthetic paraffin wax powder is given. The specific wax is polyethylene wax from the Marcus Oil and Chemical Company. It has a congealing point of approximately 115 °C and average molecular weight of 1100 g/mol. (www.marcusoil.com July 2002) The powder is sold as having a number average particle size of 5 μm .

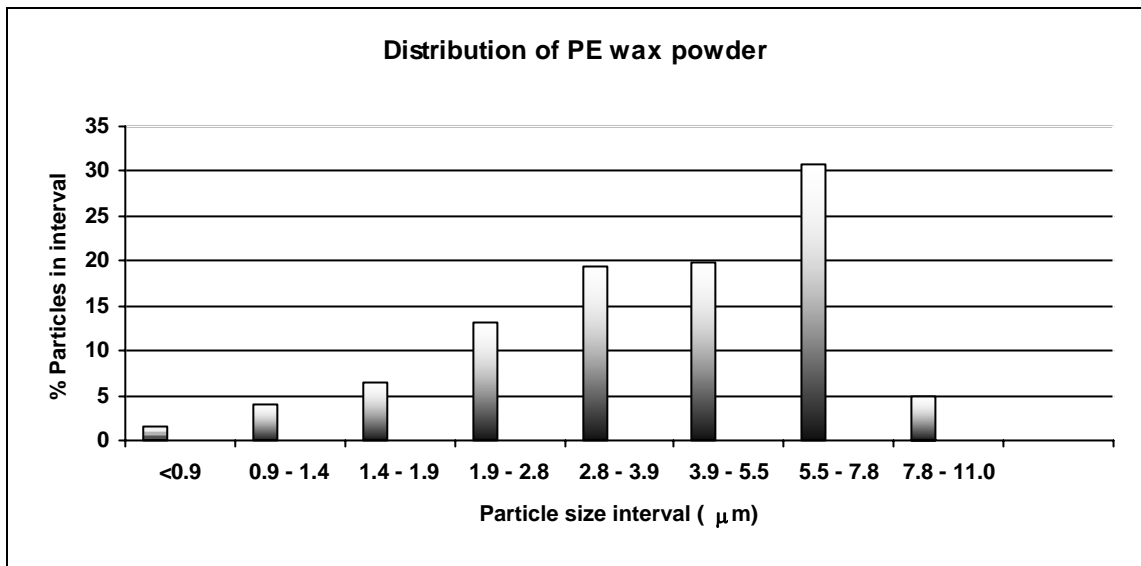


Figure 1-3: Distribution of a PE wax powder (adapted from (www.marcusoil.com July 2002))

1.3.1 Application for Coatings

Hard waxes are of particular interest in coating applications. There are certain desired features of coatings that wax can add or improve on. The following list touches on the most prominent ones. (BYK-Cera 1998), (BYK-Cera 1996)

- **Scratch Resistance:** Micronized hard waxes, will significantly improve the resistance to surface scratching.
- **Gloss Control:** Linear-structured waxes rapidly migrate to the coating surface, in the process reducing gloss of the surface.
- **Pigment Wetting:** Amide waxes enhance pigment wetting in powder coatings.
- **Degassing:** When coating absorbent surfaces, the wax supports the release of air bubbles, resulting in surfaces free of bubbles and blisters.
- **Texture Control:** Depending on the average size, size distribution and shape of the wax particles, the texture of the coating can be varied from rough to fine.
- **Abrasion Resistance:** The addition of wax is the most significant contributor to prevent printing inks from wearing away because of rubbing or grazing of the surface.
- **Soft Feel Affect:** When micronized waxes consist of small spherical particles, it will enhance the smooth feel of topcoats.

- **Water Repellence:** Synthetic waxes are hydrophobic, thus helping to protect surfaces susceptible to water damage.
- **Improved Sandability:** When added to wood paints and varnishes, the wax improves the sandability and hardness of the surface coating.

1.3.2 Particle Size and Shape Influence on Coating Characteristics

Spherical particles include particles that are more or less ball-shaped, some of which may be ellipsoidal or short bars having rounded contours. Broken particles are particles of any other irregular or rough shape.

Spherical particles are the more sought after product. They are far superior to broken particles when it comes to adding the properties of “slip”, abrasion resistance and scratch resistance in coatings. Furthermore their shape makes for a smoother texture of the coating. In contrast to broken particles, spherical particles do not cause dissipation of impinging light, leading to coatings with much more lustre.

The major advantage of broken particles is that they are more dispersible in solutions than spherical particles. Spherical particles have a lower surface area and are thus more difficult to wet. When stirred into inks and varnishes, spherical particles are subject to lower shear and are more difficult to distribute in these systems. For this reason spherical particles often need to be predispersed before being added to the system. (Kuehnle 1989)

A smaller particle imparts smoother texture. For every gram of wax, more particles are formed if the particle size is smaller. Thus a more uniform distribution in coatings is obtained with smaller wax particles than with larger ones.

1.3.3 Current Micronisation Techniques

Spray freezing is a process where a hot wax melt is forced through a binary spray nozzle and atomized into very fine droplets. Air or nitrogen is supplied to the nozzle as atomizing agent. The process temperature has to be above the wax melting point to prevent any form of nozzle blocking. In the subsequent cooling, the wax droplets solidify and forms spherical particles. Figure 1-4 shows an SEM photograph taken of a commercial spray frozen wax particles. The image shows the presence of a fairly wide distribution of particle sizes, as well as some fibre-like particles. The congealing

point of this wax, Spray 105, is approximately 105 °C. (www.schuemann-sasol.com July 2002)

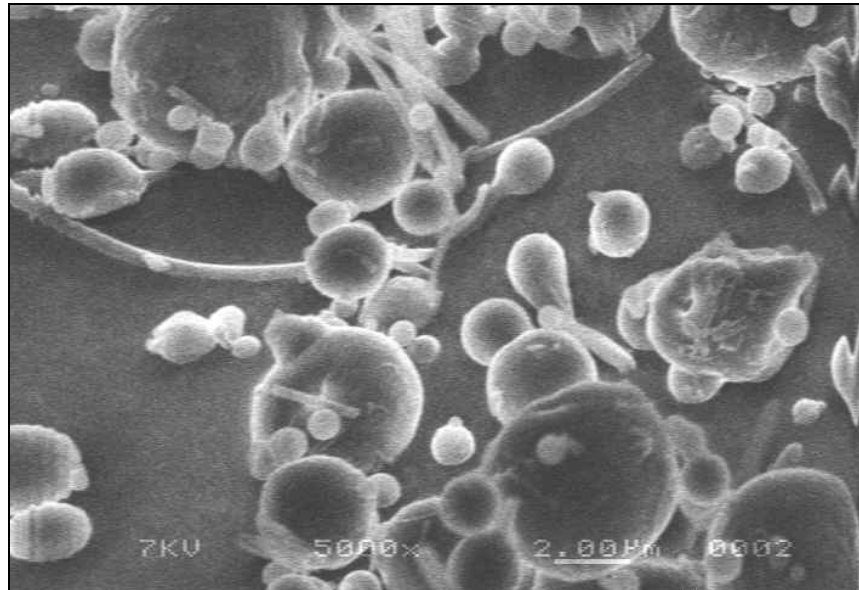


Figure 1-4: SEM of wax produced by spray freezing

The main problem of the current techniques is the low yield of particles within the desired size range. Only about 15 to 20 percent of the wax entering the process, exits within the desired size range. This causes excessive recycling of wax and an alternative process to reduce the recycling is favoured.

Jet milling is the most frequently used wax grinding technique. In the jet milling process, the particles are accelerated to supersonic speeds in a propellant such as air or another inert gas. The particles are then micronised when particles collide with each other or a surface. This application is very energy intensive and it is virtually impossible to obtain particles smaller than 20 μm . (Wolfmeier et al. 1996) To prevent melting of wax during the grinding process, liquid nitrogen or dried ice cooling is often applied to the grinding chamber.

A third, less frequently used process involves the spraying of a molten wax stream onto a surface of liquid nitrogen. Upon impact with the cold surface, the wax solidifies into perfectly spherical particles and falls to the bottom of the nitrogen bath where it is collected. The particle sizes obtainable from this process are typically in the order of 30 – 40 μm .

The two processes yield particles that are different in shape. The particles yielded in spray drying are spherical in shape, while particles obtained from jet milling are broken, irregular with a large surface area.

1.4 An Alternative: Supercritical Fluid Processing

The use of supercritical fluids to fractionate long chain paraffin waxes has been investigated. (Nieuwoudt 1994), (Crause 2001) It was concluded that supercritical wax fractionation could be economically competitive compared to current wax fractionation processes. If supercritical fluids can be successfully incorporated to fulfil other functions, such as wax micronization, its use on industrial scale will be much more viable. This project aims to investigate this possibility.

Supercritical fluids micronisation techniques have been investigated for a number of compounds. (e.g. (Chang and Randolph 1989), (Alessi et al. 1996), (Benedetti et al. 1997), (Chattopadhyay and Gupta 2001), (Debenedetti 1993), (Dixon et al. 1993), (Domingo et al. 1997), (Gallagher et al. 1991), (Griscik et al. 1995), (Jung and Perrut 2001), (Weidner et al. 2000), (Sievers et al. 1999), (Reverchon 1999)) Although knowledge of the topic existed for some time, it only came to prominence by the 1980's. Since then, extensive research has gone into the micronisation of a variety of pharmaceuticals, polymers and other compounds, both organic and inorganic. (Jung and Perrut 2001) The most prominent processes are based on the following principles:

- The solid is dissolved into a supercritical fluid. The solution is expanded over an orifice, such as a capillary nozzle. At some stage in or outside of the nozzle the solution becomes supersaturated and nucleation occurs, giving rise to a multitude of small particles. This process is called Rapid Expansion of Supercritical Solutions (RESS).
- The solid is dissolved into an organic liquid solvent. A supercritical fluid is added to the solution, reducing the solvent power of the liquid solvent. This gives rise to highly supersaturated solution and solid compound crystallises from solution as very small particles. This process is called Gas Anti-solvent (GAS).
- A supercritical fluid is dissolved into a molten substrate. As in the first process, the solution is expanded over a nozzle to conditions where the gas is

not soluble in the substrate. The expanding gas pulverizes the solid into small particles. This process is called Particles from Gas Saturated Solutions (PGSS).

A more detailed discussion on the use of supercritical fluids in micronisation processes follows in Chapter 2.

1.5 Project Definition and Goals

The ultimate goal of this project is to develop a method to micronise synthetic waxes produced in the industry. The characteristics of the final product must be comparable to that obtained through current methods, which are:

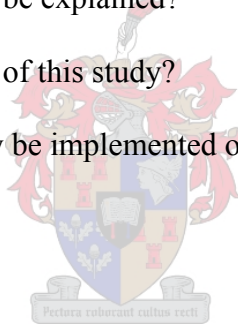
- Wax particles that are spherical in shape
- Particles smaller than 5 μm in diameter
- Narrow size distribution

Micronisation of solids by supercritical fluids has been studied recently, and has shown some significant improvements on particles obtained by conventional processes. A number of techniques exists, which are mostly determined by the solubility of the solid in the supercritical fluid.

The investigation of the proposed micronisation with supercritical fluids will encompass the following:

1. Deciding on the specific supercritical fluid micronisation technique that will be used. This includes:
 - A literature overview of the supercritical fluid micronisation techniques, from which the positive and negative aspects of each will be compared.
 - Deciding on the most suitable solvents, co-solvents or anti-solvents, as applicable, by taking into account the solvent power of each as a function of temperature and pressure.
2. A qualitative overview of the underlying theory, in order to:
 - Identify the process parameters that are most likely to influence the final product.

- Draw conclusions on how these process parameters might influence the final product.
3. Construction of an experimental set-up to investigate the influence of these process parameters on the final product, which will include:
- Deciding on the range of parameters that will be investigated
 - An overview of the type of experimental set-ups used by other researchers
 - The development of an experimental technique to investigate the parameters
4. A qualitative investigation of the results, that will answer the questions:
- What range of parameters leads to a product conforming to the desired specifications?
 - Is the process applicable to a wide variety of waxes?
 - Can the observed trends be explained?
 - What are the limitations of this study?
 - Can the process possibly be implemented on industrial scale?



2 SUPERCRITICAL FLUIDS

2.1 Background

A supercritical fluid is a substance that is at conditions in excess of its critical temperature and pressure. The supercritical region is indicated in Figure 2-1.

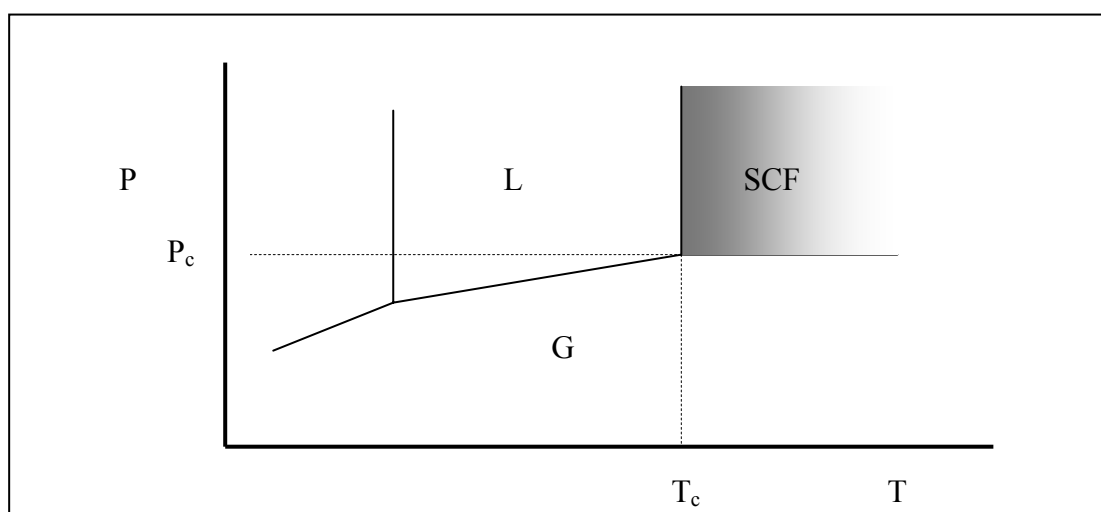


Figure 2-1 The Supercritical Fluid (SCF) Region of a Substance

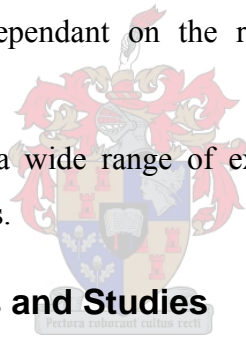
2.1.1 Properties

When a substance is at supercritical conditions, no clear gas or liquid phase can be observed. At these conditions, a substance exhibits a unique combination of properties that makes it of interest in chemical processes. The properties of supercritical fluids are typically between that of a liquid and a gas, as is apparent from the textbook of McHugh and Krukonis (McHugh and Krukonis 1994).

- **Density:** When the pressure on a gas is increased, its character changes and its density approximates that of a liquid. Since the solvent power of a compound is dependent on density, supercritical fluids have a much higher solvent power than when in the gas phase. The solvent power of a supercritical fluid can be tailored by manipulation of the temperature and pressure thereof.

- **Viscosity:** The viscosity of a supercritical fluid is very much gas-like, even at very high pressures. This would suggest improved mass and heat transfer in supercritical fluid extraction compared to that in liquid-liquid extraction. An increase in temperature leads to lower viscosities.
- **Diffusivity:** The diffusivity of substances is generally much larger in supercritical fluids than in liquid solvents. This would mean a much lower resistance to mass transfer into the supercritical solvent than the liquid solvent. (Nieuwoudt 1994)
- **Surface Tension:** The surface tension of supercritical fluids is very low, allowing good penetration into porous and microporous substrates.
- **Mass Transfer:** The characteristics of low viscosity, improved diffusivity and low viscosity would suggest improved mass transfer between a supercritical phase and the solute. As McHugh points out though, the mass transfer rate is still dependant on the rate-limiting step. (McHugh and Krukonis 1994)

These properties have led to a wide range of extraction, fractionation, cleaning, impregnation and other processes.



2.1.2 Early Developments and Studies

Baron Cagniard de la Tour first noticed the existence of the critical point in 1822. He sealed a liquid and ball in cannon barrel, heated the barrel and listened for sound changes while rocking the barrel.

Dr Thomas Andrews studied the phase behaviour of carbon dioxide in the mid 1800's and reported critical temperatures and pressure surprisingly close to those accepted today. (McHugh and Krukonis 1994)

The first major event in the field of supercritical fluids came only by the end of the 1800's when Hannay and Hogarth came to the conclusion that a substance has increased solvent power when it is in the supercritical region. It was in this same piece of research, that first mention was made of the possibility of creating very small particles from supercritical solution: "When the solid is precipitated as by suddenly reducing pressure, it is crystalline, and may be brought down as a 'snow' in the gas or on the glass as a 'frost' ..."(McHugh and Krukonis 1994)

In 1896 Villard continued the work on the solubility properties of supercritical fluids by studying methane, carbon dioxide, ethylene and nitrous oxide as solvents for an array of compounds, including paraffin wax. (McHugh and Krukonis 1994)

In the early to mid 1900's extensive studies were made on the solubility of a wide variety of solids in supercritical fluids. Naphthalene in carbon dioxide proved to be a particular favourite among researchers. Despite all the research, supercritical fluids were slow to gain a place in industry, mainly because there was no need to change existing technologies at the time. (Worthy 1981), (Basta and McQueen 1985)

2.1.3 Industrial Applications

Supercritical fluids have been slow in gaining acceptance in the process industry. Even by 1985 only limited industrial development was evident (Basta and McQueen 1985). The largest drawback is of course the high pressure required in supercritical processes and the associate high capital cost necessary to build and commission a plant capable of these high operating pressures.

But as time passed, supercritical fluids have become an alternative to conventional organic solvents, mainly due to the following:

- **Solubility control:** The solvent power of a supercritical solvent can be manipulated by changing its temperature and pressure. This allows for the separation of fractions with different solubilities by reducing the solvent power in a stepwise fashion. The ROSE process (see below) is a good example where this property is used advantageously.
- **Low operating temperatures:** Since the critical temperature of most substances of low polarity is rather low, supercritical fluids are a useful alternative for processing heat sensitive materials. The mild temperatures required also reduce utility costs, if the solvent to feed ratios can be kept low.
- **Environmental issues:** Supercritical fluids are alternatives to many organic solvents, such as halocarbons and cyclic compounds. Many of these compounds have been banned by legislation due to the toxicity thereof.

- **Product quality:** Many materials, such as certain fragrances and aromas, can only be manufactured to the desired quality by supercritical fluid processing.

Supercritical fluid processing is German in origin, and hence the first supercritical plants were erected here. (Perrut 2000). The food industry is at this stage the largest user of supercritical fluid on industrial scale. Some thirty plants are located worldwide, most of which are in Europe and Asia and a few in the United States. (Chordia and Robey 2000) The following processes are some of the more established supercritical processes in use:

Petroleum Processing

As early as 1936 the enhanced solvent properties of near-critical and supercritical propane was used to deasphalt, dewax and refine heavy oils. The process involved three different steps, each at decreased propane solvent power compared to the previous step. (Wilson et al. 1936)

The ROSE (Residuum Oil Supercritical Extraction) process (Nelson and Roodman 1985) from Kerr-McGee utilises butane or pentane as solvent. It is very similar to the propane deasphalting process. The ROSE process is based on the variation in solvent power of a near- and supercritical fluid with changing temperature and pressure. The ROSE process is shown in Figure 2-2. The residuum oil is mixed with the solvent. Only the undesirable asphaltene is insoluble and is precipitated. By increasing the temperature of the overhead stream (consisting of butane, resins and light oils mixture) to just below to the butane critical point, the resins fraction become insoluble and precipitates in a second separator. The overhead stream from this separator (consisting of butane and light oils) is heated to just above the butane critical point. At this point the butane solvent power decreases several fold, and the light oils precipitates.

When the ROSE process was developed in the 1950's little interest was shown because of the low cost of crude petroleum and energy, but a rise in both costs gave rise to the process being re-assessed in 1972. Three ROSE plants were in operation by 1981 (Worthy 1981) and eight by 1985 (Basta and McQueen 1985).

The Solvahl-Asvahl and DEMEX processes (Nieuwoudt 1994) are other similar processes.

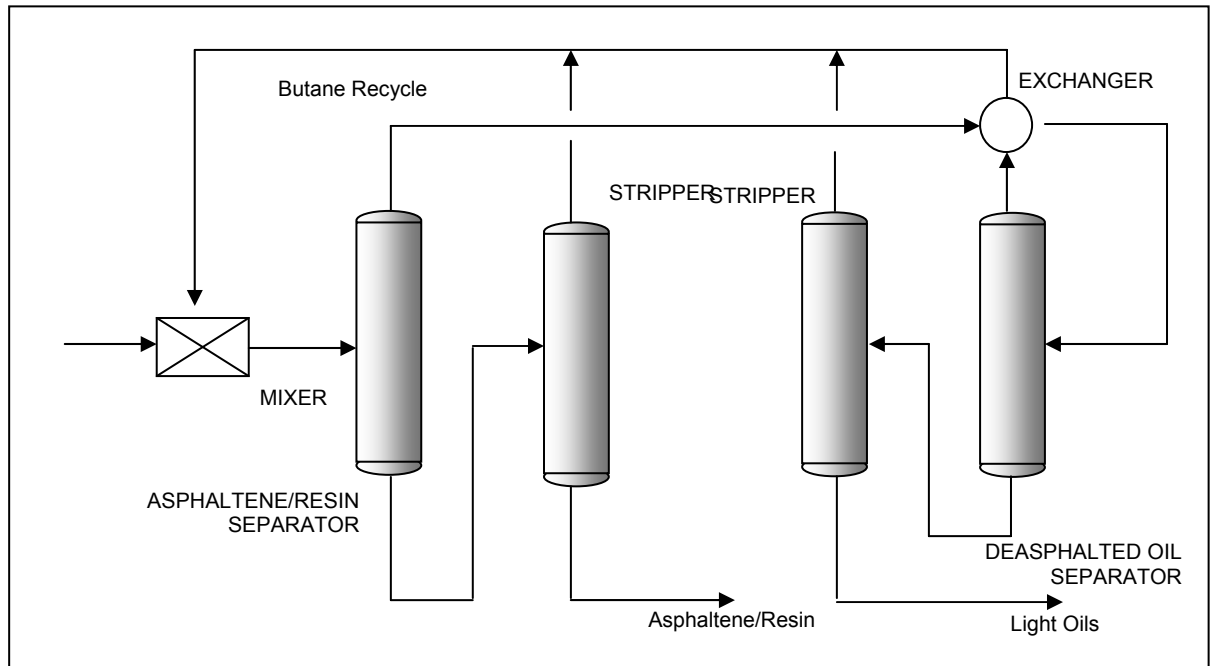


Figure 2-2: The ROSE Process (McHugh and Krukonis 1994)

Food Processing

The Soxhlet process was developed in 1946 by the M.W. Kellogg company. (Dickinson and Meyers 1952), (McHugh and Krukonis 1994) In principle it is not dissimilar to the ROSE process. In this process near-critical propane are used to concentrate polyunsaturated triglycerides from vegetable oils and vitamin A valuables are concentrated from fish oils.

The Zosel process, commercialised in 1978 (Worthy 1981), was developed to remove caffeine from green coffee beans by extraction with supercritical carbon dioxide. The carbon dioxide has a high selectivity for the caffeine above the flavour or aroma components. Conventional solvent extraction leaves traces of harmful chlorinated hydrocarbons – a problem not encountered when using supercritical carbon dioxide. Carbon dioxide extracts the caffeine from the beans in an extractor and separation between CO₂ and caffeine is achieved by adsorption onto activated carbon or absorption into water.

Today, hops extraction and coffee and tea decaffeination is the probably the largest application of supercritical fluids, with large plants in Germany, China and the USA (Perrut 2000). Other commercial scale applications are the extraction of nicotine and oils from various plant materials (McHugh and Krukonis 1994).

Polymer Processing

Polymerisation reactions typically yield a polymer mixture consisting of polymers of different chain length, and degree of branching. The solubility of the polymer in the supercritical fluid is dependent on the chain length and degree of branching. As the pressure of the polymer and supercritical fluid mixture is decreased, the different fractions of polymer become insoluble and are removed from the reaction mixture. To fractionate the reaction mixture, a series of pressure reduction steps yield the desired polymer fractions (McHugh and Krukonis 1994).

It has been proven that supercritical fluids produce superior polymer fractions compared to that obtained from conventional liquid extraction techniques. (Nieuwoudt 1994), (Crause 2001)

2.1.4 Recent Developments

Supercritical fluids are researched on a wide scale worldwide and many companies, such as Separex Co. and Phasex Co., offer toll processing for niche markets. Many of these investigations are unlikely to ever reach industrial scale, but others might develop into viable commercial options as energy costs rise and environmental legislation become more stringent.

Extraction and Fractionation of Natural Products

By moving to supercritical fluids, the properties of the solvent are changed to give much better characteristics for extraction than in the liquid phase. The density is lower, the viscosity is reduced and the diffusion coefficients are higher. The recovery of the solvent is in almost all cases trivial through a reduction in pressure. Many liquid solvents in use have associated health risks, and this is one of the major reasons why supercritical fluid extraction is gaining in popularity, especially where products are for human consumption. The extraction and purification of nutraceuticals, food supplements and active ingredients for pharmaceuticals are areas of specific importance. (Teja and Eckert 2000)

Up to now a large amount of work has been done on the extraction of essential oils from solid matrixes. Essential oils have been extracted from plant material such as cinnamon, ginger, hops, lavender, paprika, pepper and vanilla (Reverchon 1997). These essential oils consist of compounds that give flavour and fragrance associated

with the plant (compounds containing terpene groups), as well as other desirable compounds. Subsequent fractionation of essential oils to remove undesired compounds has been tested. Examples are the removal of the bitter principals from hops essential oils (Reverchon 1997), the removal of fatty acids from fish oil (Riha and Brunner 1999), antioxidants from savoury oil (Esquivel and Ribeiro 1999) and β -carotene from algae (Mendes et al. 2000).

Cleaning

Chlorinated solvents, such as perchloroethylene, are commonly used as cleaning agents. Stringent health and environmental issues have forced a movement toward safer alternatives. Supercritical carbon dioxide has proven to be a favourable alternative solvent in applications such as cleaning of clothes, semi-conductors, mechanical parts and electronics. (Vardag and Bork 1998)

Other examples that can be considered as cleaning processes include the regeneration of activated carbon (McHugh and Krukoniš 1994) and the removal of contaminants from soil (Chordia and Robey 2000).

Dyeing, coating and Impregnation

Because solutes exhibit rather high diffusivity in supercritical fluids, it is possible to obtain a very good distribution of active compounds in various porous matrixes.

Dyeing applications with supercritical carbon dioxide include the dyeing of natural and synthetic fibres (Bork 1998), the dyeing of natural wool fibres (Akgerman and Guzel 1998) and the dyeing of cellulose fibres (Colombo et al. 1998).

Impregnation of organometallic and strengthening agents in paper has improved the longevity of paper (Francais et al. 1998). Of late, there has also been significant interest in the impregnation of polymers with drugs to control the release of the drug when consumed (e.g. (Alessi et al. 1998), (Sze Tu et al. 1998)). Other areas of interest include the controlled release of fertilizers into soil.

Reactions

The use of supercritical fluids as reaction medium has received wide interest. (Perrut 2000). Reactions at supercritical conditions hold several advantages over conventional reaction mechanisms. Diffusion limited reactions in the liquid phase could become

quicker in a supercritical fluid and increased reactant solubility can lead to increased reactant concentrations and thus accelerated reaction rates (Savage et al. 1995).

The range in possible chemical reactions at supercritical conditions includes fields as diverse as biochemical reactions, materials processing, pulp and paper production, fuels processing, catalysis, pollution prevention and environmental control (Teja and Eckert 2000). Several testing units have been constructed to investigate the viability supercritical water oxidation in the destruction of organic material, pollutants and toxic chemicals. (e.g. (Drews et al. 2000), (Cocero et al. 2000)). In recent developments, DuPont has announced plans to conduct research on the viability of supercritical fluid as reaction solvent for fluoropolymer production (Chordia and Robey 2000).

2.1.5 Solvents

Carbon dioxide is the most popular solvent for supercritical processing, due to its favourable properties of low critical temperature, non-toxicity, non-flammability and abundance. On industrial scale, carbon dioxide is still used almost exclusively, but it does have its drawbacks. Many compounds, especially non-polar ones, are sparingly soluble in supercritical carbon dioxide at acceptable process pressures.

Hydrocarbons, such as propane, butane and iso-butane are much better solvents in many cases, leading to lower operating pressures. These solvents have been met with more resistance, mainly because they are highly flammable. Some solvents and their critical constants are given in Table 2-1:

Table 2-1: Critical constants of common gases (Perry and Green 1997)

<i>Solvent</i>	<i>Critical Temperature</i> (°C)	<i>Critical Pressure</i> (bar)
Carbon Dioxide	31.0	73.9
Methane	-82.6	45.9
Ethane	32.2	48.5
Propane	96.7	42.1
Butane	152.1	37.7
i-Butane	135.1	36.2
Pentane	196.6	33.6

2.2 Particles from Supercritical Fluid Processing

When looking to produce very fine particles, the properties of the solid need to be considered before choosing a process. As indicated in chapter one, grinding and spraying processes have been used for wax micronisation, but with limited success. Grinding processes require the product to be reasonably brittle and to withstand high temperatures. Thus the limited success of wax micronisation processes can be understood. Spraying processes have been the most successful, but in order to obtain very small particles complicated nozzles have to be used to atomise the liquid wax into small enough droplets.

In recent times, many workers have studied the micronisation of various substances by utilization of supercritical fluids. There are basically three groups of supercritical fluid based micronisation processes.

- Rapid crystallisation from supercritical solution
- Crystallisation from organic solution by rapidly decreasing its solvent power
- Pulverisation caused by an expanding gas dissolved in a liquid substrate.

A large variety of particles have been processed with supercritical fluids.

- **Explosives and propellants:** Small particles are required to improve the combustion process. The attainment of the highest possible energy release is dependant on particle size.
- **Polymers:** Small polymer particles are of interest as stationary phases in chromatography, adsorbents, catalyst supports and in drug delivery.
- **Pharmaceuticals:** Small particles improve the therapeutic action of many drugs. Transdermal, tracheobronchial and pulmonary drug delivery requires small particles to improve the efficiency of these pharmaceuticals.
- **Other:** Colour strength is enhanced with small dyeing matter particles; catalyst activity is improved with very large surface area of fine powders; superconducting properties are related to the uniformity of the solid solution of its ceramic components.

2.3 Rapid Expansion of Supercritical Solutions (RESS)

2.3.1 Process Description

In the RESS process, the solute is dissolved into a suitable supercritical fluid. The solute is normally packed in an extractor, and the pressurised solvent is allowed to pass over the solute. The amount of solute that dissolves into the solvent is dependant on the temperature and pressure in the extractor. The resulting solution is then rapidly depressurised through an orifice or nozzle to conditions where the solid is no more soluble in the solvent. The residence time within the nozzle is very small (in the region of microseconds). Since the transition from soluble to insoluble occurs in this very short space of time, a sudden increase in supersaturation is obtained leading to a homogeneous outburst of nuclei. The very small residence time also minimises the growth period of the nuclei. Very small particles, with a narrow size distribution, are expected. The solvent leaves the process in the gaseous state, so that the product consists of solvent-free particles.

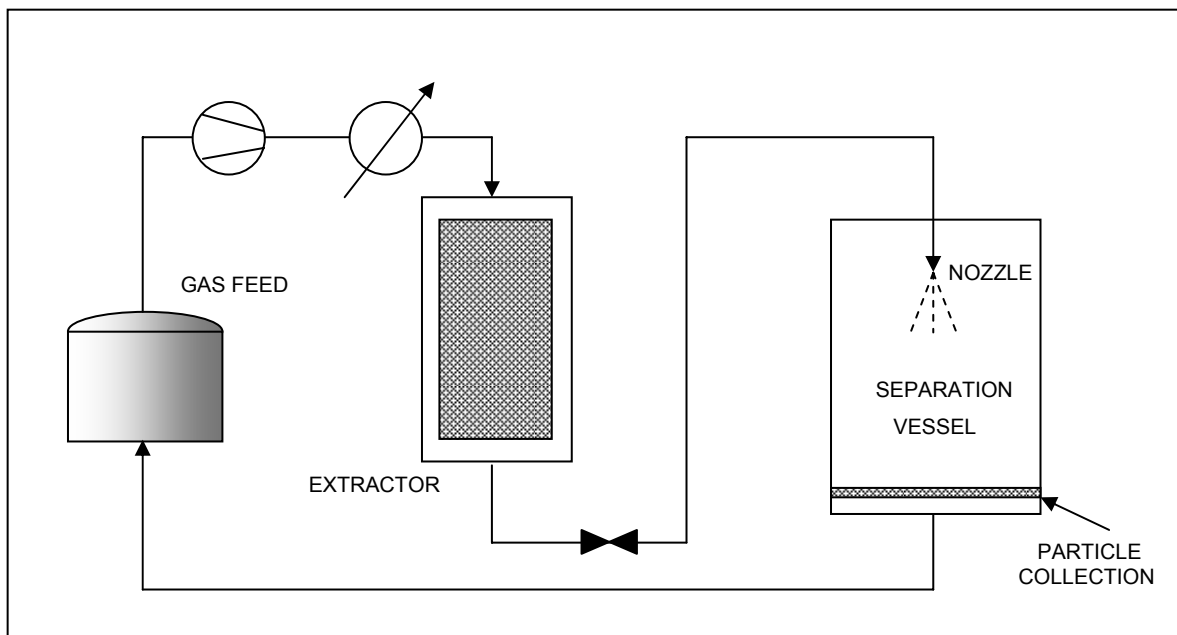


Figure 2-3: Semi-batch RESS process

2.3.2 History

In the 1879 paper of Hannay and Hogarth first mention was made of the possibility of creating very small particles from supercritical solution: “When the solid is precipitated as by suddenly reducing pressure, it is crystalline, and may be brought down as a ‘snow’ in the gas or on the glass as a ‘frost’...”(McHugh and Krukoniš 1994)

In 1981, Krukoniš suggested that this evidence might well be used to “tailor the size and size distribution of difficult to comminute organic materials, or to deposit such materials within a microporous substrate.” (Worthy 1981)

In the early 1980’s Krukoniš laid the foundation for research into the field of rapid nucleation of supercritical solution. The research team at the Batelle institute, led by Matson, Petersen and Smith (Matson et al. 1987) studied the process in much detail and by 1987 they produced a range of exploratory studies on the formation of polymer and inorganic powders by RESS.

In the early 1990’s extensive RESS research on the micronisation of a myriad of substrates were performed, including inorganic salts (e.g. (Hansen et al. 1992)), organic materials (e.g. (Mohamed et al. 1989)) and polymers (e.g. (Tom and

Debenedetti 1991), (Lele and Shine 1992), (Lele and Shine 1994), (Mawson et al. 1995)).

Theoretical studies and modelling of the expansion and nucleation processes were attempted in the mid to late 1990's, although still with several simplifications (e.g. (Debenedetti 1990), (Liang 1994), (Berends 1994), (Türk 2000)).

2.3.3 Applications

Polymers

Lele and Shine precipitated semi-crystalline powders of poly-1-butene, polyethylene succinate and polyhexamethylene sebacate from supercritical CO₂. (Lele and Shine 1992) The particles were obtained from pre-expansion temperatures of 110 and 130 °C and pre-expansion pressures of 90 – 200 bar. The solution was expanded over a stainless steel capillary, 30 and 50 µm in diameter and 0.254 mm long. Conditions of high temperature, high concentration, low pressure and low capillary L/D ratio yielded fibre-like particles, while opposite conditions were more favourable for the formation of spherical particles. The particles obtained varied between 1 and 5 µm in diameter, while the fibres were 2 to 7 µm in diameter.

In later work, Lele and Shine (Lele and Shine 1994) found various morphologies for a range of other polymers. Polycaprolactone and poly (methylmethacrylate) was dissolved in chlorodifluoromethane and expanded over a capillary nozzle to atmospheric conditions. Pre-expansion conditions were varied between 90 and 110 °C and 170 and 310 bar. A stainless steel capillary nozzle with length of 0.254 mm and diameters between 30 and 40 µm were used. Polymer concentrations of between 0.3 and 0.8 weight % were used. Spherical particles were formed for pre-expansion conditions of lower temperature, low polymer concentration, high pressure and high nozzle length/diameter ratios (L/D), which is similar to their earlier work, while fibres formed at high temperatures, high concentration and low pressure. It was postulated that fibres are formed when gas-liquid phase split occurs prior to nozzle entry.

Krukonis performed studies on polypropylene particle fibre formation from supercritical propylene. At pre-expansion conditions of 140 °C and 240 bar fibres of 50 µm in length and 2-3 µm in diameter were found. The nozzle dimensions and nozzle dimensions are unknown. (Berends 1994)

Matson (Matson et al. 1987) investigated the precipitation of polystyrene, polypropylene and cellulose acetate from supercritical pentane. In addition, polyphenyl sulfone and poly (methacrylate) were precipitated from supercritical propane. Pre-expansion temperatures varied between 200 and 400 °C and pre-expansion pressures between 100 and 170 bar. The nozzle consisted of a capillary nozzle, 5 mm in length and 60 µm in diameter. Polystyrene spheres of diameter 20 µm were found at pre-expansion conditions of 170 bar and 350 °C, and fibres at 200 °C and 170 bar. All the other polymer products were fibre-like: 1 µm in diameter and 0.1 to 1 mm in length. Polymer concentration was found to have the largest influence on the morphology of the particles. The concentration was related to the temperature and pressure at which the polymer was dissolved into the supercritical fluid.

Tom and DeBenedetti (Tom and DeBenedetti 1991) precipitated polyhydroxy acids, including poly (L-lactic acid), poly (D,L-lactic acid) and poly (glycolic acid). Pre-expansion conditions varied from 150 to 300 bar and 45 to 65 °C. The polymer concentration that could be obtained from the extraction conditions varied between 0.01 and 0.37 weight %. The nozzle was a stainless steel capillary (25 – 30 µm diameter, L/D = 10). Spherical particles of 4 – 25 µm was found for poly (L-lactic acid) precipitated from CO₂ and a CO₂/acetone mixture. Slightly smaller particles were obtained when chlorotrifluoromethane was used as solvent. Poly (D,L-lactic acid) yielded irregular shaped particles (10 – 20 µm) from CO₂ solvent. Regular shaped particles and needles of poly (glycolic acid) were formed from CO₂ solution.

Blasig (Blasig et al. 2000) studied the effects of concentration and degree of saturation on the product morphology of poly (heptadecafluorodecyl acrylate) precipitated from CO₂. Experiments were conducted with 0.5 and 2 weight % polymer solutions at pre-expansion conditions ranging from 140 to 250 bar at 30, 65 and 100 °C. At the lower concentrations, the results indicated that the degree of saturation has a major influence on the product size. Submicron-sized (0.1 – 0.8 µm) particles formed from unsaturated pre-expansion conditions and micron-sized (1 – 4 µm) particles formed from saturated and supersaturated pre-expansion conditions. At the higher concentration, the particles became elongated, and fibres were observed at solutions expanded from the saturated and supersaturated state.

Mawson (Mawson et al. 1995) studied the same process earlier, finding that the L/D ratio of the capillary nozzle has the largest effect on transition of particle

morphologies from spherical (0.5 – 20 μm) to fibre-like (< 2 μm). They kept the pre-expansion pressure steady at 206 bar and varied the temperature between 45 and 105 $^{\circ}\text{C}$. Two capillary nozzles were used: a 25 μm diameter, 25 mm long fused silica capillary and a 30 μm , 0.25 mm long stainless steel capillary. Two polymer concentrations, 0.5 % and 2 % (wt) were used. The observation regarding concentration was the same as that of Blasig.

Chernyak (Chernyak et al. 2000) 2.8 μm particles of krytoxdiamide of hexamethylene from CO_2 solvent. The experiments were done at pre-expansion conditions of 165.5 bar and 60 $^{\circ}\text{C}$. The 2 wt % solution was sprayed through a capillary with diameter of 152 μm and length of 11 mm. They developed a model that indicated that coagulation might play a large part in particle formation.

Pharmaceuticals and Other Organic Solids

In 1986 Larson and King (Larson and King 1986) compared micronisation of mevinolin by RESS to milling techniques. CO_2 and a 3% methanol were used as solvent mixture. In this mixture the mevinolin solubility was 0.45 % (wt). This solution was expanded through a valve from 380 bar and 105 $^{\circ}\text{C}$ to atmospheric conditions to yield particles 10 – 50 μm in diameter. This was 10 times smaller than those yielded from conventional processes.

Chang and Randolph (Chang and Randolph 1989) studied the micronisation of β -carotene with RESS in a range of solvents as diverse as CO_2 , ethane and ethylene. The carotene was oxidised by the CO_2 , but supercritical ethane ($x < 12 \times 10^{-5}$ mole fraction) and ethylene ($x < 12 \times 10^{-5}$ mole fraction) resulted in platelike particles of 1 – 2 μm in size. When toluene was used as co-solvent to ethylene (0.7 – 2.4 %), solubility increased tenfold. Fine particles of less than 0.5 μm were formed from this solution. Pre-expansion conditions used were 306 – 374 bar and 70 $^{\circ}\text{C}$. The solution was expanded through a metering valve with a 1.6 mm orifice and 8.7 mm length of pass.

Alessi (Alessi et al. 1996) investigated the manufacture of fine particles of progesterone and medroxyprogesterone acetate from supercritical CO_2 . Particle sizes obtained varied between 4 and 9 μm . When post-expansion conditions of temperature and pressure were increased, smaller particles were formed. Post-expansion pressure had a significant effect on the particle morphology, with more spherical particles

evident at lower post expansion pressures. Smaller capillary nozzles seemed to lead to smaller particles. The pre-expansion process conditions used in this work was 100 – 240 bar and 40 – 60 °C. The solubility of progesterone at these conditions were less than 7×10^{-5} (mole fraction) and medroxyprogesterone acetate less than 1.3×10^{-5} (mole fraction). The solution was sprayed through a capillary nozzle (30 – 100 μm) to pressures varying between 1 and 50 bar and temperatures between 40 and 60 °C.

Helfgen (Helfgen et al. 2000) carried out RESS experiments for cholesterol and benzoic acid with CO_2 and trifluoromethane as solvents. Pre-expansion pressure was varied between 130 and 300 bar and temperatures between 40 and 75 °C. The solution was expanded through a capillary nozzle of 45 μm and 350 μm length. Cholesterol particle sizes in the range of 100 – 400 nm and benzoic acid particle sizes in the range of 200 – 1400 nm were found. Typical pre-expansion concentrations were not mentioned. The most marked influence seemed to be that of pre-expansion temperature, which saw an increase in particle size with an increase in temperature.

Reverchon (Reverchon et al. 1995) found griseofulvin particles with two morphologies: long needles (13.4 – 36.4 μm) and quasispherical particles (1.0 – 1.3 μm). The former was attributed to particle formation in the capillary nozzle and the latter to precipitation in the free jet. Trifluoromethane was used as solvent. Pre-expansion pressure ranged from 180 to 220 bar and pressures from 60 to 150 °C. The post expansion pressure was varied between 10 and 25 °C. Very low concentrations ($< 0.25 \times 10^{-3}$ mole fraction) were expanded over a capillary nozzle ($D = 40 \mu\text{m}$, $L = 800 \mu\text{m}$). The major effect was attributed to pre-expansion temperature, with needle length decreasing with increasing temperature.

Türk (Türk 1999) used carbon dioxide as solvent to micronize naphthalene (1.5 – 3 μm), benzoic acid (0.8 – 1.2 μm) and cholesterol ($< 0.35 \mu\text{m}$). Particle sizes show some dependence on the pre-expansion conditions, particularly temperature. Pre-expansion pressure was varied between 130 and 300 bar and temperatures between 40 and 75 °C. The solution was expanded through a capillary nozzle of 45 μm and 350 μm length. Typical pre-expansion concentrations were not mentioned. Cholesterol particles are consisted of aggregates of smaller particles. The range of process conditions seemed to have very little influence on the particle sizes.

Türk (Türk et al. 2002) also processed griseofulvin with the solvent trifluoromethane and β -sitosterol with CO₂. The capillary nozzle had a diameter and length of 50 μm . Pre-expansion conditions were varied between 75 °C and 145 °C and 200 and 300 bar. The concentration was in the region between 7.5×10^{-5} (mole fraction) for griseofulvin and 1.5×10^{-4} (mole fraction) for β -sitosterol. The nozzle was pre-heated to 115 °C. Particles in the 200 nm range were produced. The solvent did not seem to have a marked influence, but lower concentrations resulted in smaller particles.

Liu and Nagahama (Liu 1996) performed RESS experiments on a mixture of phenanthrene and naphthalene to study their separation and crystal properties. For pure naphthalene the following observations were made. Lower concentration (varied: 113×10^{-4} to 167×10^{-4} mole fraction), lower pre-expansion temperature (varied: 87 – 125 °C) and higher nozzle temperatures (varied: 15 – 45 °C) were found to favour the formation of smaller particles. A pre-expansion pressure of 200 bar was used, with capillary nozzle (length: 280 μm) diameters ranging from 35 – 90 μm . Particle sizes ranged between 5 and 25 μm .

Subra (Subra et al. 1998) studied precipitation of anthracene and caffeine in pure and mixed form from CO₂-solution via the RESS process. Parameters were varied around a base of: pre-expansion temperature 96 °C; post-expansion temperature 80 °C; nozzle diameter 150 μm (L = 0.2 cm); concentration 4×10^{-5} (mole fraction) for caffeine and 3.2×10^{-5} (mole fraction) for anthracene. Anthracene particles were tablet-shaped with well-defined edges (5 – 20 μm). An increase in post-expansion temperature to 100 °C yielded larger particles. Caffeine particles were needle-shaped, in the range of 2 – 10 μm . Particle sizes were not strongly influenced by conditions of temperature and pressure.

Domingo (Domingo et al. 1996) found that porous plate (frit) nozzles could produce particles of much smaller diameters than capillary nozzle at similar pre-expansion conditions (45 °C, 160 – 300 bar, CO₂ solvent). The nozzles were preheated to temperatures ranging between 100 and 130 °C. The capillary nozzle had a diameter of 40 μm and length of 200 μm . The frit nozzle pore diameters ranged between 0.5 and 2 μm . Faceted and isometric benzoic acid particles with an average particle size of less than 1 μm were formed with the porous plate nozzle, compared to particles with average sizes of 2 – 6 μm formed in capillary nozzles.

They later also tested the nozzle influence on particles of aspirin, acetyl salicylic acid and phenanthrene (Domingo et al. 1997). The conditions were identical. Similar results to that of benzoic acid was obtained. The concentrations (mole fractions) of the solution was in the order of 2×10^{-3} for benzoic acid and phenanthrene and less than 6×10^{-4} for hydroxy benzoic acid and acetyl salicylic acid.

Peiriço (Peirico et al. 1998) studied RESS of a tropic acid ester and hydrogenated palmitic oil with CO₂ as solvent. Pre-expansion pressures were varied between 110 and 140 bar and pre-expansion temperatures between 70 and 88 °C. The solution concentration was in the order of 8×10^{-5} weight fraction for the ester and more than 100 times lower for the palmitic oil. Aggregates, consisting of 5 µm spherical particles, formed. They verified that below pre-expansion temperatures of 80 °C and pressures of 110 bar no particles formed due to blockage of the nozzle.

Kröber micronised particles of cholesterol in CO₂ by expansion through a converging/diverging nozzle. Two nozzle diameters were investigated: 100 and 150 µm. The pre-expansion conditions varied between 35 and 70 °C and 150 and 200 bar. Concentrations varied between 0.05 and 0.17 weight %. Mean particle sizes of 400 nm were found, with the influence of pre-expansion conditions and nozzle diameter being small. (Kröber et al. 2000)

2.3.4 RESS Process Variables

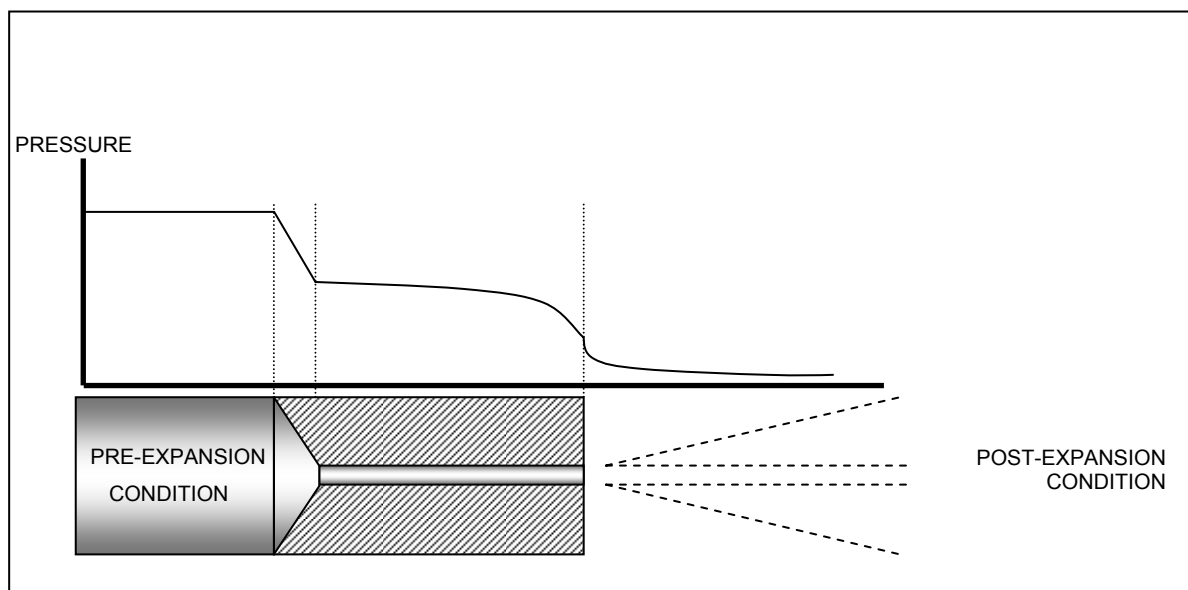


Figure 2-4: A Capillary Nozzle as used in RESS Set-up with Typical Pressure Profile

- **Pre-expansion Temperature and Pressure:** Temperature and pressure determines the solubility of the solute in the supercritical solvent. By increasing pressure prior to expansion, the onset of nucleation and further growth processes is delayed until the solution has moved further down the nozzle, or even in the free jet outside the nozzle. The latter will give rise to a very sudden supersaturation.
- **Pre-expansion Concentration:** At higher concentration, an expanding solution becomes supersaturated at higher pressure. The degree of supersaturation that can be obtained is generally higher for higher concentrations, but occurs further upstream in the expanding solution. A larger amount of small nuclei is obtained but chances of growth processes, such as coagulation and agglomeration are higher due to the higher number concentration of solute particles.
- **Post-expansion Conditions:** An increase in post-expansion pressure decreases the pressure difference over the nozzle. The expansion rate of the solution will be lower and this could lead to longer crystal growth periods.
- **Nozzle Effects:** The shape of the nozzle can influence the temperature and pressure profile of the expanding solution. Capillary nozzles have a larger pressure drop due to streamline contraction at the nozzle inlet. This might lead to supersaturation earlier in the expansion device, or even prior to nozzle entry.

2.4 Anti-solvent Processes (GAS/SAS/ASES/SEDS)

2.4.1 Process Description

In anti-solvent processes, supercritical fluids are used as an anti-solvent to expand a solution of an organic liquid and the substrate to be micronised. The solution is mixed with a supercritical fluid. This supercritical fluid serves as anti-solvent in that it dissolves into the solution and causes expansion of the solvent, lowering its solvent power. The mixture becomes supersaturated and the solute precipitates as small particles. There are four groups of anti-solvent processes.

- The **Gas Anti-solvent (GAS)** process is a batch type process, and is schematically represented in Figure 2-5. The precipitator is partially filled with a solution of the solid and a suitable liquid solvent. A supercritical anti-solvent is pumped into the vessel at the desired temperature and pressure. The expanded solution can be held for a certain length of time to allow growth of the particles to a desired particle size. After the desired growth period has elapsed, a filtration step is performed at the same pressure to separate the solids from the solvent and anti-solvent mixture. The solvent and anti-solvent separation can be achieved by decreasing the system pressure, but the ease of separation is dependant on the solvent/ant-solvent interaction. The solvent and anti-solvent can be recycled if required. This process is sometimes called the liquid batch anti-solvent process.

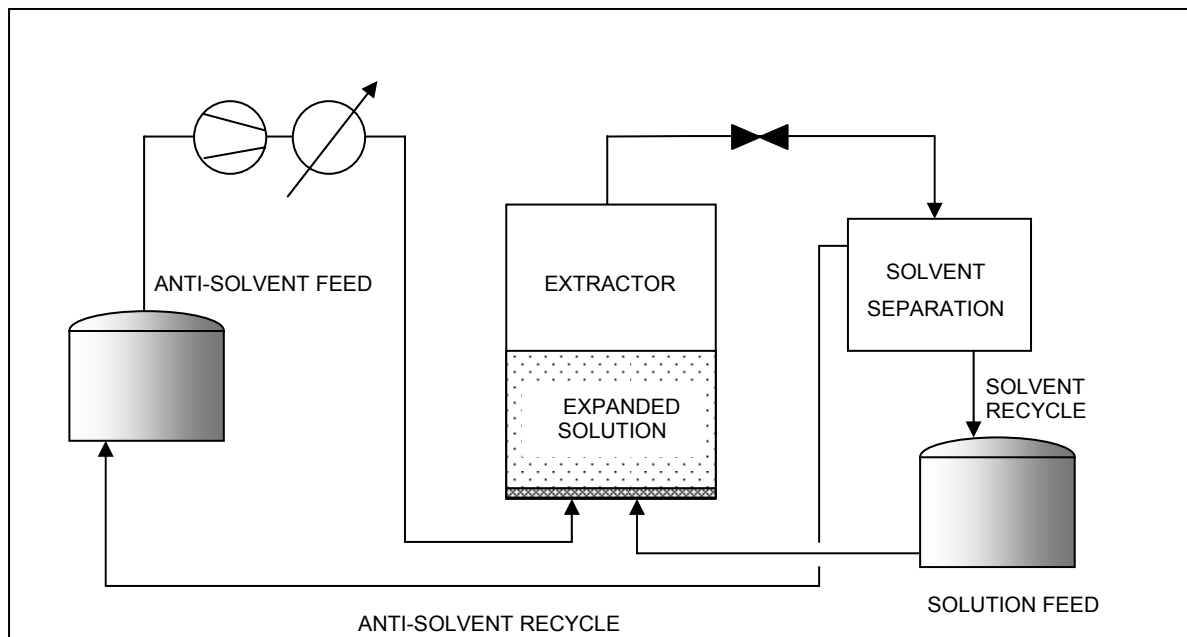


Figure 2-5: Batch GAS process

- The **Particles from a Compressed Anti-solvent (PCA)** process involves the spraying of the liquid solution through a nozzle into a batch of supercritical fluid. The solution forms small liquid droplets upon leaving the nozzle. The solvent is highly soluble in the anti-solvent and dissolves by preference into the anti-solvent. This causes large supersaturation of the solvent, resulting in small solid particles. The solids, solvent and anti solvent is removed similar as in the GAS process. This process is sometimes called the gas batch anti-solvent process.

- The **Aerosol Solvent Extraction System (ASES)** process is the continuous equivalent of the PCA process. It involves the spraying of the solution into a vessel swept by the supercritical anti-solvent. The solvent/anti-solvent mixture flows to a depressurisation tank where the gas-liquid separation is achieved. The solvent and anti-solvent are recycled and the particles collected on a filter at the bottom of the precipitation vessel. The set-up is essentially the same as SEDS (see Figure 2-6), except that the anti-solvent is not fed to the precipitation vessel via the nozzle, but at a different point in the precipitation vessel.

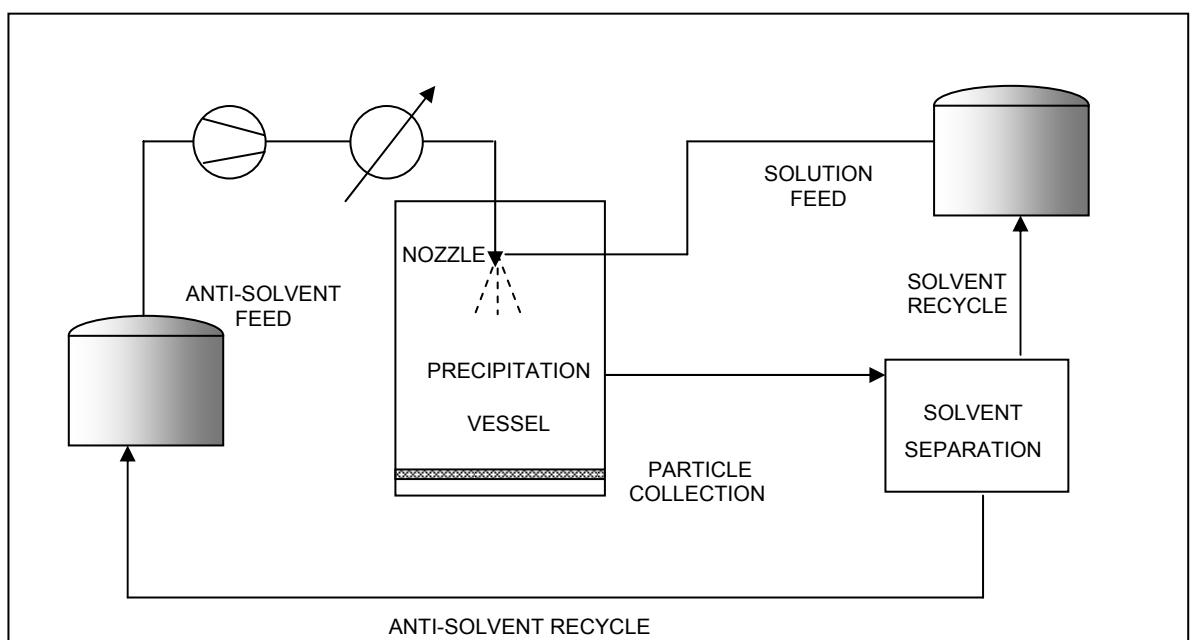


Figure 2-6: The SEDS process

- Solution Enhanced Dispersion of Supercritical fluids (SEDS) involves to simultaneous feeding of the solution and the supercritical anti-solvent into a specially designed co-axial nozzle. This nozzle has the advantage that small droplet size and more intense mixing between solution and anti-solvent is achieved.

The spraying is done into a temperature and pressure controlled spraying vessel. There is a facility at Bradford University where SEDS toll processing is available.

Coaxial spray nozzle configurations were developed and patented (Jung and Perrut 2001). An example of such a nozzle is given in Figure 2-7.

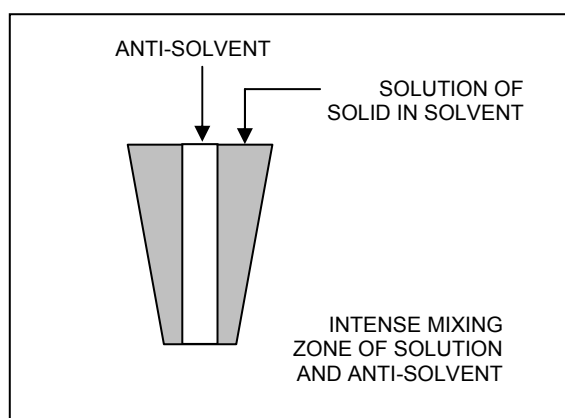


Figure 2-7: Coaxial nozzle set-up for SEDS

The liquid solution passes on the outside of the passage containing the anti-solvent. At the exit of the nozzle there is an intense mixing zone of liquid solution and anti-solvent. The high velocity of the anti-solvent helps break up the solution into very small droplets.

2.4.2 History

The GAS concept can most probably be attributed to the pioneering work of Francis (Francis 1954), who studied the solubility of liquid solvents in supercritical carbon dioxide. He noted: “CO₂ exerts a demixing or precipitating effect.” (Jung and Perrut 2001)

The process was brought up again only by the late 1980’s by Gallagher and co-workers. They micronised heat sensitive explosives, such as RDX, dissolved in acetone or cyclohexanone, with CO₂ as anti-solvent (McHugh and Krukoniš 1994). This process, called Gas Anti-solvent Recrystallization was duly patented in 1991 (Krukoniš et al. 1991).

Schmitt vaguely alluded to the ASES concept in a patent (Schmitt 1988) describing the injection of a solution into a supercritical fluid to produce a wide variety of fine powders.

The SEDS concept was developed extensively at Bradford University in order to achieve smaller droplet size and intense mixing of solution and anti-solvent to increase mass transfer rates.

In the early 1990's the process was extensively used in the formation of fibres and flocculated microspheres of polymers such as N,N-dimethyl formamide and polystyrene (Dixon et al. 1993).

2.4.3 Applications

Explosives

The formation of powder of explosives materials represented some of the earliest work done with the GAS process. Gallagher micronised nitroguanidine, using N,N-dimethyl formamide and N-methyl pyrrolidone as solvents. CO₂ and chlorodifluoromethane were used as anti-solvents. Different morphologies, such as spheres, snowballs and starbursts were reported, depending on the expansion path followed. Smaller and more uniform particles formed with faster anti-solvent addition. A variety of sizes, ranging from 1 – 100 µm were formed (Reverchon 1999).

Gallagher and Krukonis's aim was to separate the cyclonite and homocyclonite to obtain cyclonite particles (free homocyclonite) of more approximately 200 µm in size. A solution, slightly below the saturation point (10 – 12 weight %) was charged to a vessel. CO₂ was added to this solution until visible nucleation could be observed. The CO₂ feed was terminated and the cyclonite particles allowed to grow for 30 to 60 minutes, whereafter the spent solution was fed to a second stage where a rapid expansion was achieved. It was found that γ -butyrolactone is a more suitable solvent to separate the cyclonite and homocyclonite, because of the relatively higher solubility of homocyclonite compared to acetone (19 weight % vs 3 weight % at 25 °C). The trace elements of homocyclonite stayed in solution as the cyclonite crystallised out. The maximum process pressure was less than 70 bar. (Gallagher et al. 1991). The same system was also investigated by other researchers. They found that particles of 65 µm could be formed with acetone as solvent and 90 µm with γ -butyrolactone as solvent. The particle growth period is unknown. (Jung and Perrut 2001)

In recent years, Lim (Lim et al. 1998) studied the GAS-micronisation of 3-nitro-1,2,4-triazole-5-one (NTO) with dimethyl formamide (DMFA), dimethylsulfoxide (DMSO) and methanol as solvents and CO₂ as anti-solvent. The solubility of NTO in DMFA and DMSO was about 40 weight % (10 – 70 °C) and 5 to 7 weight % (10 – 30 °C) in methanol. Various morphologies were observed, including spheres, cubic

particles and spherical aggregates, with the size ranges varying between 0.5 and 20 μm .

Polymers and Biopolymers

In the field of polymers and biopolymers, a lot of work has centred on the formation of poly (L-lactic acid) (PLLA) particles. Bleich found spherical particles 1 – 10 μm in diameter using the ASES process with methylenechloride as solvent. When the solution was injected into a batch of CO_2 anti-solvent (the PCA process), it was observed that agglomerates tend to form whenever the glass transition temperature of the polymer was exceeded (Reverchon 1999).

Randolph also performed PCA and ASES experiments of PLLA with methylene chloride as solvent. The two processes yielded similar results. PLLA solutions of 0.3 to 1 weight % were introduced via a 75 μm fused quartz tubing into a chamber containing CO_2 (31-40 $^\circ\text{C}$, 55-97 bar, spraying time 1 min, holding time 15 min). Concentration had the most significant influence on particle morphology. A solute concentration of less than 1 weight %, spherical particles was formed, but in tests with concentrations of more than 4 weight %, fibres were formed. For all concentrations an increase in temperature and pressure caused the formation of larger particles. Particle sizes ranged from 0.6 – 4.0 μm (Randolph et al. 1993).

Bodmeier also micronised PLLA, along with poly-methylmethacrylate (PMMA), poly-caprolactone (PCL) and ethyl cellulose. PLLA and ethyl cellulose were dissolved in methylene chloride expanded with CO_2 . Spherical particles of less than 5 μm in diameter were formed with higher polymer concentrations yielding fibres (Reverchon 1999). This corresponds to the observations made above.

Rantykyla (Rantykyla et al. 1998) used the SEDS process to investigate PLLA micronisation. They used a coaxial nozzle (Inner tube: ID 0.15 mm, L 5 mm, outer passage 0.35-0.7 mm, L 15 mm) to spray a PLLA-methylene chloride solution (15-30 mg/l, 0.3-0.5 ml/min) and CO_2 (10 g/min) into an extraction chamber (28-60 $^\circ\text{C}$, 85-170 bar). The particles were irregular and of different shape, ranging between 5-100 μm .

PLLA and poly-(lactide-co-glycolide) (PLGA) micronisation from, methylene chloride and acetone respectively, was investigated by Sze Tu. The ASES process was used with a three-passage coaxial nozzle. Microspheres, less than 2 μm in diameter

was formed. The PLGA particles formed agglomerates. An increase in the system pressure yielded larger PLLA particles. (Sze Tu et al. 1998)

Polystyrene, micronised polystyrene from toluene by CO₂, was studied by a number of authors, including Dixon (Dixon et al. 1993) When the solution (1-6 wt %) was injected (100 µm fused silica tubing, 10-15 s) into a batch of CO₂ (PCA-process, 40-230 bar, 0-40°C, linearly depressurised for 50 min). An increase in particle size was observed at higher temperatures. Agglomerated masses of 10-30 µm, consisting of very small spherical primary particles (100 nm) in diameter were found for 1 weight % solutions. Concentrations in excess of 5 weight % resulted in fibres. When they also adding CO₂ to the liquid feed, porous particles were formed.

Johnston found hollow fibres of polyacrylonitrile (PAN) (from toluene and CO₂ anti-solvent) when using the PCA process. The solution (0.05-2.5 wt %) was injected (0.16 to 1.51 ml/min) via a capillary nozzle into a batch of CO₂ (40 °C, 100 bar). Fibre bundles (100-200 µm consisting of 100 nm individual fibres) were found at concentrations less than 0.5 weight %. At higher concentrations, single fibres between 1 and 25 µm in diameter formed. (Johnston et al. 1994)

Benedetti studied the precipitation of ethyl esters of hyaluronic acid (HYAFF) dissolved in dimethylsulfoxide using ASES (85 bar, 40 °C). The solution (0.05 – 1 wt %, 1 ml/min) was sprayed via a 40 µm nozzle into a vessel swept with CO₂ at a rate of 6 or 12 ml/min of solvent. Aggregated structures, in the size range of 5 to 35 µm were formed. (Benedetti et al. 1997) When using GAS (35-60 °C, 100 bar, 0.05-1.5 wt %), they found particle sizes in between 0.3 and 1.0 µm. A strong dependence was found with respect to solute concentration, with the larger concentration resulting in smaller particles. Temperature influence on particle size was minimal.

Other polymers investigated include aromatic polyamides (Yeo et al. 1993). Dimethylsulfoxide and dimethylformamide were used as solvents with polymer concentrations of 0.03-0.12 weight %. Utilising the GAS process with slow expansion rates (0.8-20.6 bar/min up to 103.4 bar at 23-40 °C), polycrystalline spherulites between 1 and 10 µm were formed. The degree of crystallinity was influenced by the turbulence caused of the CO₂ injected into the system. ASES of the same system resulted in microfibrillar structures.

Reverchon and co-workers (Reverchon et al. 2000) have recently also studied the micronisation of biopolymers, including dextran, poly-(L-lactic acid) and poly-(hydroxypropylmethacrylamide) from dimethylsulfoxide solution. The solutions (0.05, 0.5 and 5 wt %) were injected into a batch of CO₂ via a 60 µm nozzle. The conditions in the precipitation were varied between 80 to 150 bar and 30 to 40 °C. Spherical particles were found with sizes ranging between 100 and 200 nm for dextran and 0.8 and 2.3 µm for poly-(L-lactic acid). Poly-(hydroxypropylmethacrylamide) particles were spherical with a mean diameter of 150 nm. The influence of process conditions on particle size and shape was rather weak. It is thought that the large molecular weight and molecular weight distribution is the contributed to this observation, as it influences the rate of growth more than the other process parameters.

Pharmaceutical Compounds

Debenedetti performed studies on hydrophobic enzymes such as insulin, catalase, adrenocorticotrophin hormone and peroxidase from a 90 weight % ethanol mixture with water. ASES was used to produce rectangular and spherical catalase particles of 1 µm diameter. Insulin particles were a mixture of microspheres and thick needles. It was reasoned that particle deposition at different time intervals caused the different morphologies. (Reverchon 1999)

Yeo used dimethylsulfoxide and dimethylformamide as solvents for the formation of insulin particles by the ASES process. Insulin solutions of 5-15 mg/ml solution was sprayed into a cocurrent stream anti-solvent at 25-35 °C and 86.2 bar. The morphology of the formed insulin showed insensitivity toward the temperature and concentration in the ranges used. Amorphous particles formed, 90 % of which smaller than 4 µm. (Yeo et al. 1993)

Salmeterol xinafoate has been precipitated from methanol and acetone by CO₂ in the SEDS process. The precipitation vessel conditions were varied between 90 to 300 bar and 40-90 °C. When conditions were increased above 60 °C and 250 bar, a transition in the morphology of the drug could be detected. Particles smaller than 10 µm were formed. Platelet particles were formed from acetone solvent and needle-like fibres from methanol solvent. The particles sizes were generally less than 10 µm. (Hanna et al. 1998)

Palakodaty performed tests on water-soluble compounds, such as α -lactose monohydrate (0.035 ml/min). Methanol was used as co-solvent (0.665 ml/min) and CO₂ as anti-solvent (14 ml/min). Coaxial nozzles with three passages, one each for solution, anti-solvent and co-solvent were also used. The two path coaxial nozzle delivered the best results, with 5 weight % co-solvent dissolved in the aqueous lactose solution. This led to crystalline, tape-like particles, with a mean particle size of 3 μ m. (Palakodaty et al. 1998)

The micronisation of sodium cromoglicate from methanol by ASES was studied (Reverchon 1999). Amorphous particles were formed, with sizes ranging between 0.1 and 20 μ m. The crystallinity was influenced by the amount of residual solvent in the particles.

Methyl prednisolone was precipitated from tetrahydrofuran with CO₂ and ethane. Dimethyl formamide was used as solvent for hydrocortisone acetate in the same paper and particles of 8-8.5 μ m was found. (110-180 bar, 21-65 °C). Crystal sizes in the 5 μ m were reported. Lower process temperatures (Range: -6 – 63 °C at 100 bar for ethane and 150 bar for CO₂) resulted in smaller particles. (Schmitt et al. 1995)

Reverchon (Reverchon 1999) studied the micronisation of a variety of antibiotics, including tetracycline and amoxicillin. N-methyl pyrrolidone and dimethylsulfoxide was used as solvents and CO₂ as anti-solvent. Dimethylsulfoxide proved futile as solvent and most of the solute was found in the solvent separation vessel, indicating that the solvent/anti-solvent mixture extracted the solute. The particles seemed to consist of parts of smaller particles. The degree of this agglomeration of tetracycline particles was dependant on operating pressure.

Reverchon (Reverchon et al. 2001) also micronised salbutamol particles from dimethylsulfoxide. The anti-solvent/solution flow rate ratio was maintained at a 20:1 ratio (mass based). A variety of morphologies were found with variation in precipitation pressures (100-150 bar). At lower pressure, expanded droplets (balloons) formed, while at higher pressure, rodlike particles (1 – 3 μ m in length) formed. Solution concentration was also varied at the higher pressures, and shorter rods formed at higher concentration. In tests with methanol as solvent, networked particles formed, and an ethanol-water mixture seemed to yield only large particles. The latter two forms were not desired.

Warwick (Warwick et al. 2000) micronised $[\text{Cu}_2\text{-(indomethacin)}_4(\text{DMF})_2]$ from a 90 % saturated dimethylformamide solution using CO_2 as anti-solvent. The effect of the rate of expansion on the produced particle at 25 °C was investigated. Final pressure in the precipitation vessel was always 57-59 bar. Rapid expansion rates resulted in bipyramidal crystalline particles less than 10 μm in size. Slow expansion yielded rhombic crystals with average sizes between 10 and 20 μm .

Chattopadhyay and Gupta (Chattopadhyay and Gupta 2001) micronised tetracycline from tetrahydrofuran solution (5mg/ml) by what they called the SAS-EM process. In this modification of the GAS process, a vibrating surface is used to micronise an incoming jet of solution into microdroplets. Mass transfer is also enhanced by the vibrating surface. Nanoparticles as small as 125 nm were obtained and were 8 times smaller than those obtained by ordinary GAS processes. The conditions in the precipitation vessel were maintained at 96.5 bar and 37 °C. It was found that an increase in the ultrasound power from 0-125 W decreased particle size.

Thiering and coworkers performed micronisation of the proteins lysozyme and insulin from dimethylsulfoxide by the GAS process. Average particle diameters were found to be 0.1 and 1.5 μm respectively. Temperature was maintained between 19 and 50 °C. The expansion rates were varied between 4 kPa/min to virtually instantaneous. This parameter had little effect on the product. Other solvents were studied, including methanol and ethanol, which resulted in submicron particles. The proteins were sparingly soluble in these solvents though, and solvent power was increased with water as co-solvent. Particle size was found to be dependant on the solvent combination used. When solvents with higher protein solubility were used, larger particles resulted. Solute concentrations were varied from 0.03-19 mg/ml. Particle shape was influenced by the concentration of the solution, with porous structures forming at higher protein concentration. (Thiering et al. 2000)

p-Hydroxy-benzoic acid (p-HBA) have been micronised by Thiering by the GAS and ASES processes. The solute was precipitated from methanol with CO_2 as anti-solvent. The experiments were performed for concentrations of 5, 17 and 35 wt % at 70 bar, between 25 and 45 °C. For GAS, the following observations were made. At low solute concentration and moderate rates of anti-solvent addition, small spherical precipitates (1-2 μm) formed. At higher solute concentration, platelets (10-20 μm) formed. The expansion rate (9-750 bar/h) of the liquid solution was also investigated,

with complex needle shapes found at lower rates and amorphous particles at high rates. ASES was also employed at temperatures between 7 and 30 °C, leading to the formation of flat platelet particles (4-5 µm). At higher temperatures, an agglomerated spherical particle mass was found (0.1-1 µm). Other solvents were also tested: acetone and ethyl acetate which yielded fibres of 2 µm width and lengths of 30 and 10 µm respectively. (Thiering et al. 1998)

Cocero found β-Carotene with platelike morphology (2 – 10 µm) from GAS applications while studying the solubility of the solute in an ethyl acetate (solvent) carbon dioxide (anti-solvent) mixture at conditions ranging between 25 and 60 °C and 43 and 82 bar. The CO₂ /ethyl acetate mixture contained 4-7 wt % ethyl acetate. (Cocero et al. 2000)

Other

Other organic and inorganic substances have also been micronised.

Pigments, including Red Lake C, Pigment Yellow 1 and Pigment Yellow 15 have been precipitated from acetone by CO₂. Both GAS and ASES processes were employed. In ASES, it was found that the nozzle dimensions are the most important parameter controlling particle size. Spherical particles as small as 0.6 µm were obtained. (Reverchon 1999)

Superconductor precursors are another application field. Reverchon studied the Ba, Cu, Y, Sm and Nd acetates dissolved in dimethylsulfoxide and precipitated by CO₂ as anti-solvent. The solution (5-150 mg/ml) was fed at 1ml/min and the anti-solvent at rates of 6500 to 12000 ml/min (STD). Operating conditions were varied (60-160 bar, 35-70 °C, solution/anti-solvent ratio 1:20-1:30). Spherical particles as small as 100 nm were formed at high volume expansion of the solvent. The major effect was found to be the expansion rate of the active solution. (Reverchon et al. 1998)

2.4.4 Anti-solvent Process Variables

Reverchon (Reverchon et al. 1998), (Reverchon 1999) gave a systematic summary of the influence of various process parameters on the size and morphology of particles. A brief synopsis of his findings are given below:

- **Particle formation mechanisms:** The different morphologies of particles can be explained when looking at the solvent expansion levels. At low

expansion, the particles are formed from the liquid phase at the bottom of the precipitation vessel. This is due to incomplete dissolution of the liquid phase in the anti-solvent. At intermediate expansion levels, expanded droplets (or balloons) are formed. These can be considered as dried expanded liquid droplets. The precipitation starts at the fluid-liquid interface and propagates inside the liquid, attracting the solute toward the separation surface. At high expansion levels nanoparticles are formed due to disintegration of “balloons”. This is considered as the objective of most micronisation processes.

- **Coalescence:** Physical coalescence is the result of interaction between two particles, during impact. Sonication is considered sufficient to separate such particles. Chemical coalescence involves the interaction of particles with the liquid solvent for instance. This results in the fusion of particles in groups where single particles lose its own identity.
- **Growth:** Growth in the precipitation vessel is a slow mechanism whereby particle size and shape are strongly influenced. The formation of complex morphologies, such as rod-like and butterfly formed particles are often attributed to growth.
- **Solvent/Co-solvent Interaction:** When co-solvents are used, interaction between the co-solvent and solvent might be so strong that the anti-solvent only marginally decreases the solvent power of the solvent/co-solvent mixture. Thus most of the solute ends up in the solvent separator.
- **Liquid Phase Formation:** When a liquid phase forms at the bottom of the precipitator, networked particles, films or large crystals are most often formed at the bottom of the precipitation vessel.
- **Pressure and Temperature:** The rate of pressure increase in the precipitation vessel in GAS processing is the most relevant parameter in controlling particle size and morphology. In ASES and SEDS however, as some authors report a particle size increase and other a size decrease for reduction in precipitation pressure. Reverchon states that at asymptotic expansions (expansion where a small pressure increase results in a large expansion increase), the influence of increasing temperature and pressure is

small. At higher temperatures, growth might be a better explanation for the formation of larger particles.

- **Concentration Effect:** The increase of concentration can significantly influence particle size in as far as nucleation and growth processes are concerned. When a higher solute concentration is expanded, there will be a larger concentration of solute particles formed than at the lower concentration. This will increase the chances of growth by coagulation and agglomeration in the same way as with the RESS process.
- **Solvent Effect:** Different behaviour can be obtained by changing the liquid solvent. Possible interactions between solvent/anti-solvent may cause it to be a very good solvent for the solid. This “new” solvent may dissolve the solid just as it forms.
- **Solute Effect:** If the solute has a complex chemical structure, it can exhibit further growth processes and form secondary particles. Solutes with simple chemical structure only form primary particles.

2.5 Particles from Gas Saturated Solutions (PGSS)

2.5.1 Principle

The solubility of many solutes in supercritical fluids is quite low. The supercritical fluid may however be very soluble in the molten solid. When this “gas saturated solution” is then expanded through an orifice, the dissolved gas becomes insoluble in the solid and pulverizes the solute into small particles.

Another interesting variation of the process has been the micronisation of water-soluble drugs. The drugs are dissolved in water and mixed with a supercritical fluid, especially carbon dioxide. The supercritical carbon dioxide dissolves into the aqueous solution to some extent. The drug/water/CO₂ solution is expanded over a restrictor and the CO₂ undergoes a huge expansion, in the process pulverising the aqueous drug solution into a very fine aerosol. The aerosol is fed to a drying system. The mixing of the drug solution and carbon dioxide is performed in a low dead-volume mixing tee, as indicated in Figure 2-8.

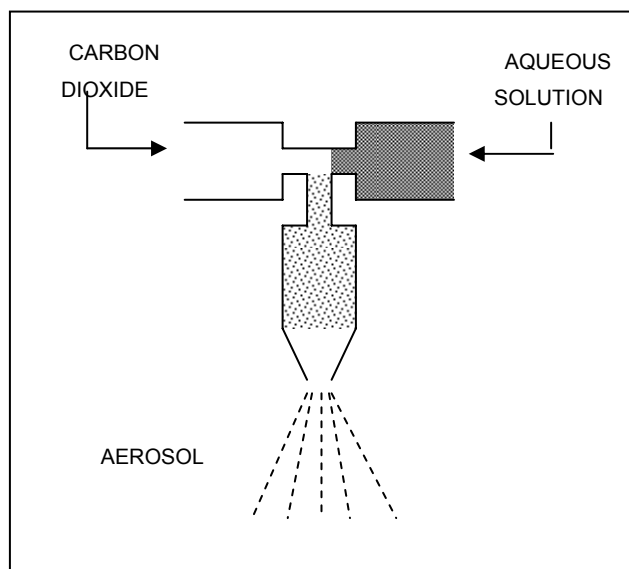


Figure 2-8: Low dead volume mixing tee (Sievers 1999)

The process flow is almost identical to RESS. The only difference is in the extractor, which is replaced by a saturation vessel. (see Figure 2-3) The substance to be precipitated is in the molten state. The gas is fed to the saturation vessel where the molten solid is saturated with the gas. The resulting gas saturated solution is rapidly expanded over a large diameter nozzle (100 – 1000 μm typically), and the particles can be collected in a collection chamber.

2.5.2 History

Graser described the basis of the PGSS process when he patented a process whereby pigments were dispersed in an organic solvent. The pigments were, amongst others, isolated by means of a “spray drying process” by “forcing the conditioning mixture through a valve by means of an inert gas.” (Jung and Perrut 2001)

Weidner patented the process of PGSS in 1994 (Weidner et al. 1994 a) and presented the principles thereof at the third international symposium of supercritical fluids in Strasbourg, France in 1994 (Weidner et al. 1994 b).

2.5.3 Applications

Pharmaceuticals

Sievers (Sievers et al. 2000) mixed an aqueous solution (0.1 M) of drugs, including albuterol sulfate, cromolyn sodium and tobramycin, with CO_2 and subsequently decompressed the mixture through a flow restrictor. Pre-expansion conditions used in these experiments were in the range of 75 to 100 bar and 25 $^\circ\text{C}$. The resulting dense aerosol plume was dried at temperatures ranging from 25 – 95 $^\circ\text{C}$. The CO_2 solubility

was in the order of 2 mole %. The restrictor consisted of a fused silica capillary, 5 cm in length and 50 – 130 μm in diameter. The product consisted of mostly spherical particles with residual moisture of less than 1 %. For some substances, such as sodium chloride, mannitol and tobramycin sulphate, hollow particles can be formed. For others, such as lactose and albuterol sulphate, solid spherical particles with diameters between 0.5 and 5 μm were formed.

Sievers (Sievers et al. 1999) also studied the formation of small droplet aerosols of a number of other water-soluble compounds for use in drug delivery, including alkaline phosphatase, glucose oxidase, glutathione and horseradish peroxidase. The aqueous solutions of the drugs were expanded through the same type nozzle (D: 25 – 170 μm) as described above. Pre-expansion conditions were varied between 75 and 345 bar and 35 and 100 $^{\circ}\text{C}$. CO_2 -solubility are in the region of 1.5 – 2.0 mole %. The system generated spherical drug particles less than 3 μm in size.

Kerč (Kerc et al. 1999) performed the micronisation of the drugs nifedipine, felopidine and fenofibrate. Irregular particles were observed with sizes ranging between 15 and 30 μm for nifedipine and 42 μm for felopidine. Particle sizes seemed to decrease with increasing pre-expansion pressure (100–200 bar) Pre-expansion temperatures used were just higher (~ 5 $^{\circ}\text{C}$) than the melting point of the particular drug. Nozzle diameters of 250 and 400 μm were used. Agglomeration of fenofibrate particles was observed.

Inorganic Salts

Sievers (Sievers et al. 1999) further performed experiments on the formation of mixed iron oxide particles. Mean diameters of approximately 0.4 μm were found. The iron oxide was obtained by aerosolising an iron acetate solution, dehydrating the solution and pyrolysing the formed iron acetate particles. The conditions used were similar to that described above.

Polymers

Weidner (Weidner et al. 1996) micronised polyethylene glycols, saturated with carbon dioxide. They found that nozzle diameter had the largest influence on particle size. The smallest particles (170–370 μm) were obtained by using a 400 μm diameter capillary nozzle. Nozzles of 500 and 1000 μm diameter were also used. Pre-expansion temperature (50–70 $^{\circ}\text{C}$) had a slight influence, with higher temperatures resulting in

larger particles. Pre-expansion pressure (100-200 bar) had no visible influence on particle size. Experimental concentrations varied between 0.2 and 0.7 kg CO₂ per kg of polyethylene glycol. Although a spongy type particle was the norm, spherical particles were found at higher initial temperature and fibres for the higher molar weight polyethylene glycols.

Other

Weidner performed a systematic investigation on the influence of pre- and post-expansion conditions, and solute concentration upon the crystallinity, particle size and particle distribution for the model system glyceride-CO₂. (Knez and Weidner 2001) The glycerides consisted of mainly monoglycerides (50-55 wt %), diglycerides (35-40 wt %), monoglycerides (3-8 wt %) and fatty acids (< 1 wt %). Investigated pre-expansion pressures varied between 80 and 200 bar, with a decrease in particle size at the higher pressures. Higher pre-expansion temperatures, which ranged between 10 and 40 °C above the glyceride melting point, resulted in larger particles for all the pre-expansion pressures investigated. The formed particles seem to be a porous network of glyceride and air, with typical average sizes varying between 12 and 50 µm. Smaller particles were formed when the gas concentration is higher (5 – 20 wt %).

Knez reported on the micronisation of cocoa butter saturated with carbon dioxide. (Knez and Weidner 2001) The pre-expansion pressure was in the range of 60 to 200 bar and pre-expansion temperature in the range of 20 to 80 °C. Micronisation with a 250 µm resulted in fine spongy particles with median particle sizes of about 62 µm.

2.5.4 PGSS Process Variables

The process variables that influence the particle shape and size, can be summarised as follows (Knez & Weidner 2001):

- **Pre-expansion temperature and pressure:** The pre-expansion conditions determine the phase behaviour of the system. The further away from the two-phase region the solution is upon entering the nozzle inlet, the further down the nozzle the gas will start expanding the solution and less likely the chances for coagulation and agglomeration are. A high pre-expansion temperature will cause the substrate to be in the liquid phase when exiting the nozzle, which will enhance chances of spherical particles. If, upon the

phase split, the temperature is below the substrate melting point, the less likely it is to form spherical particles.

- **Gas Concentration:** In order to minimise particle size, a high gas supersaturation will cause a more sudden expansion of gas than that at lower supersaturations. A higher gas concentration will lead to higher supersaturation ratios, a more sudden expansion and ultimately smaller particles.
- **Nozzle Dimension:** The nozzle dimension influences the pressure and temperature profile of the expanding solution. To minimise coagulation and agglomeration effects, the position of the phase split should preferentially be nearer the outlet of the nozzle.
- **Post expansion temperature and pressure:** The temperature and pressure can influence the expansion profile, and thus the point of nucleation. A higher post-expansion temperature can favour the formation of spherical particles, if the solid to be micronised is still molten when it exits the nozzle.

2.6 Comparison of SCF Micronisation Processes

Now that the supercritical micronisation processes have been evaluated, a decision on the most suitable supercritical fluid micronisation process needs to be made. In Table 2-2, some of the major advantages and disadvantages of each of the processes are highlighted.

Table 2-2: Comparison of the Supercritical Fluid Micronisation Processes

<i>Process</i>	<i>Typical Particle Sizes</i> (μm)	<i>Advantages</i>	<i>Disadvantages</i>
Rapid Expansion of Supercritical Solutions	1-10	Very fine particles with a desired size distribution. Solvent free particles are formed.	High solvent/solute ratios due to low solubility. High pressures and temperatures. Separation of sub-micron particles from large volumes of gas.
Gas anti-solvent	1-10	Control over particle size.	Separation of organic solvents and particles. Batch-wise operation. Medium to large volume of equipment.
Particles from Gas Saturated Solutions	1-500	Solvent free particles are formed. Low solvent/solute ratio. Easy separation between particles and gas.	Difficult to produce sub-micron particles. Control of particle size and morphology.

From this table, it is clear that PGSS will probably not be suitable, because the particles sizes required are much smaller than those found by researchers. Although the bubble drying process used by Sievers (Sievers et al. 1999) has yielded small particles, it requires the use of a solution or suspension of the solid and subsequent drying step to remove solvent.

Anti-solvent processes will be avoided due to the problem of residual anti-solvent in the product. Although particle size and morphology can be well controlled by anti-solvent processes, equipment and process control is rather more intricate and requires higher capital cost.

RESS is left as option, but the large restriction lies in the solubility of the wax in a suitable solvent. The aim is thus to find a solvent wherein paraffin wax is adequately soluble at comparatively mild operating conditions.

2.7 RESS of Paraffin Wax

2.7.1 Finding a Suitable Solvent

Since it is a prerequisite of the RESS process that the solid should be suitably soluble in a supercritical fluid, the different solvent options need to be evaluated.

For paraffin wax, the solvent power of a supercritical fluid is greatest just above its critical temperature. (Nieuwoudt 1994), (Du Rand 2000), (Schwarz 2001). In addition, one would need to keep the solution at temperature above the wax congealing point to prevent wax precipitation. The paraffin waxes used in this project have melting in the range of 80 °C to 105 °C. Thus a solvent with critical temperature in this region is most favourable. Inspection of Table 2-1 will show that propane is a good candidate for supercritical solvent of these waxes.

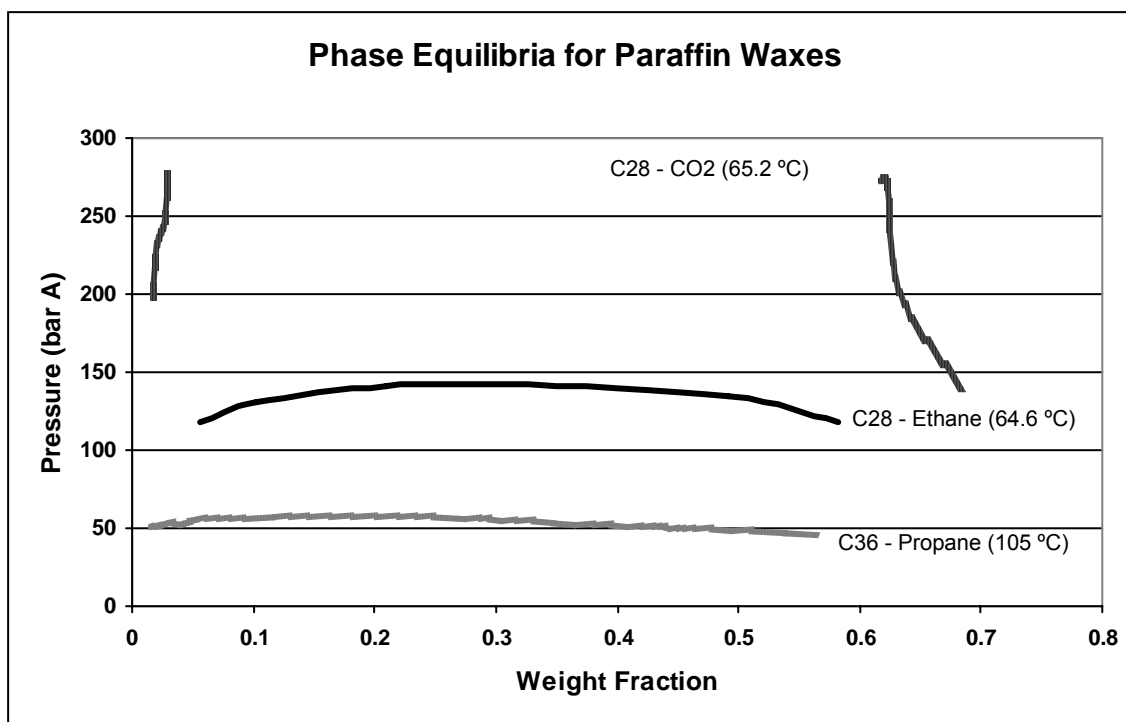


Figure 2-9: Comparison of Solvent strength ((Du Rand 2000), (Schwarz 2001))

In Figure 2-9 the solubilities of two paraffin waxes, n-octacosane (C28) and n-hexatriacontane (C36) given in CO₂, ethane and propane at temperature just slightly above the solvent critical point are compared. At conditions above the curved isotherms the mixture is in one phase, but at conditions below the curves, the wax becomes insoluble and the wax/solvent mixture splits into two phases.

From the graphs, it is evident that supercritical carbon dioxide is a poor solvent for longer chained paraffin wax (Du Rand 2000). It is clear that very high pressure is required to dissolve even small quantities of wax in CO₂. Paraffin wax is however significantly more soluble in supercritical ethane (Du Rand 2000) and even more so in propane [Schwarz, 2001 #10].

Although data for C28 in propane was not measured, it can be seen from the figure that even C36 is much more soluble in propane than C28 in ethane. For higher melting point paraffin wax, as used in this research, higher pressure is required to solubilise a given amount of wax at a certain pressure. From data by Schwarz, it was found that propane could dissolve a substantial amount of C60 wax (15 wt %) at pressures below 150 bar at temperatures as high as 135 °C. The heaviest wax used in this project consists of paraffins of similar chain lengths.

This solubility is similar to that of C28 wax in ethane at much lower temperature. Much higher pressure would be needed to solubilise similar quantities of C60 wax at 135 °C in ethane. It becomes clear that it will not be economic to solubilise substantial quantities of heavier wax fractions in ethane and carbon dioxide due to the large pressure requirements.

From this evidence, it is clear that propane will be a very suitable solvent to use for wax micronisation, as lower pressure is required to dissolve the same fraction of wax at a given temperature. Although iso-butane and n-butane will also be suitable, the higher temperature required will be unfavourable due to higher energy requirements.

2.7.2 Literature Overview of Wax Micronisation by RESS

Up to date two significant publications have dealt with supercritical fluids as wax micronisation tool. Both publications deal with RESS as route in wax micronisation. This gives more confidence that RESS will be the process most likely to produce the best results.

Griscik (Griscik et al. 1995) micronised n-octacosane with supercritical CO₂ as solvent. The pre-expansion temperature was found to have the most significant influence on particle size and shape. The effect of pre-expansion pressure (174 – 222 bar) seemed to be minimal. Larger, fused particles were found when nucleation and growth were thought to occur inside the nozzle ($T_E = 50 - 100$ °C). Smaller particles consisting of distinct faceted subparticles formed when nucleation was thought to occur outside the nozzle in the free jet ($T_E > 140$ °C). They calculated the solubility of the wax in CO₂ with the Patel-Teja equation of state about 2.5×10^{-2} mole % (0.2 mass %).

A patent application held by Xerox Corporation, (Combes et al. 2000) describes the formation of polyethylene and polypropylene wax particles from a solution with a supercritical solvent. A large number of effective solvents are claimed to have yielded successful results, including ethane, propane, n-butane, i-butane, n-pentane, carbon dioxide and chlorodifluoromethane. A very wide range of parameters is mentioned (30 – 400 °C, 40 – 340 bar, 0.001 – 50 g per 100 ml, nozzle diameter 0 – 100 µm) to yield spherical particles with volume average sizes between 0.001 and 4 µm. By the

end of 2002 the patent had not been granted, which does raise some question about the viability of some of the claims made.

2.8 Conclusions

In this chapter a brief overview of supercritical fluids was given. The different technologies to micronise solutes by supercritical fluids were discussed. An overview of the technologies showed that Rapid Expansion of Supercritical Solutions and Anti-solvent processes have yielded particles of the shape and size required. Based on the positive and negative aspects of the processes, RESS seems to be the more favourable process to use.

A large problem of the RESS process is the fact that it requires a suitable solvent to obtain high solubility at reasonably low temperatures. Based on phase equilibria of paraffin waxes with CO₂, ethane and propane, it was seen that propane could dissolve a substantial amount of wax (15 wt %) at pressures below 150 bar at temperatures as high as 135 °C.

It was decided to further investigate this route for achieving the objectives of this report.



3 RESS: A THEORETICAL APPROACH

In the previous chapter it became apparent that the RESS process seems to be the best technique to follow for the production of fine wax particles. Various researchers have attempted to model the RESS process, (Debenedetti 1990), (Ksibi and Subra 1994), (Reverchon and Pallado 1996), (Helfgen et al. 2000), (Weber et al. 2002). The models used by them contain the underlying theory that may be helpful to gain an understanding of what causes the formation of particles with different shapes and sizes in the RESS process.

In this chapter the theory will be approached in four steps, in the order that they follow during a typical expansion:

- The influence of temperature and pressure on the solubility of solute
- The variation of temperature and pressure during an expansion
- The formation of stable particles (nuclei) from solution
- The further growth of particles to their final size

3.1 *Supercritical Propane as a Solvent for Waxes*

A study of phase diagrams are necessary to form an idea as to how a solution will behave at different temperatures and pressures and at which conditions a phase split can be expected. As pointed out in section 2.7 of this thesis, the advantage of propane as wax solvent over other solvents was shown. Let us try and form an idea as to how pressure and temperature will influence the solubility.

Schwarz studied the phase equilibrium between paraffin waxes and supercritical propane. The waxes studied covered the range from n-C₃₂H₆₆ to n-C₆₀H₁₂₂. (Schwarz 2001)

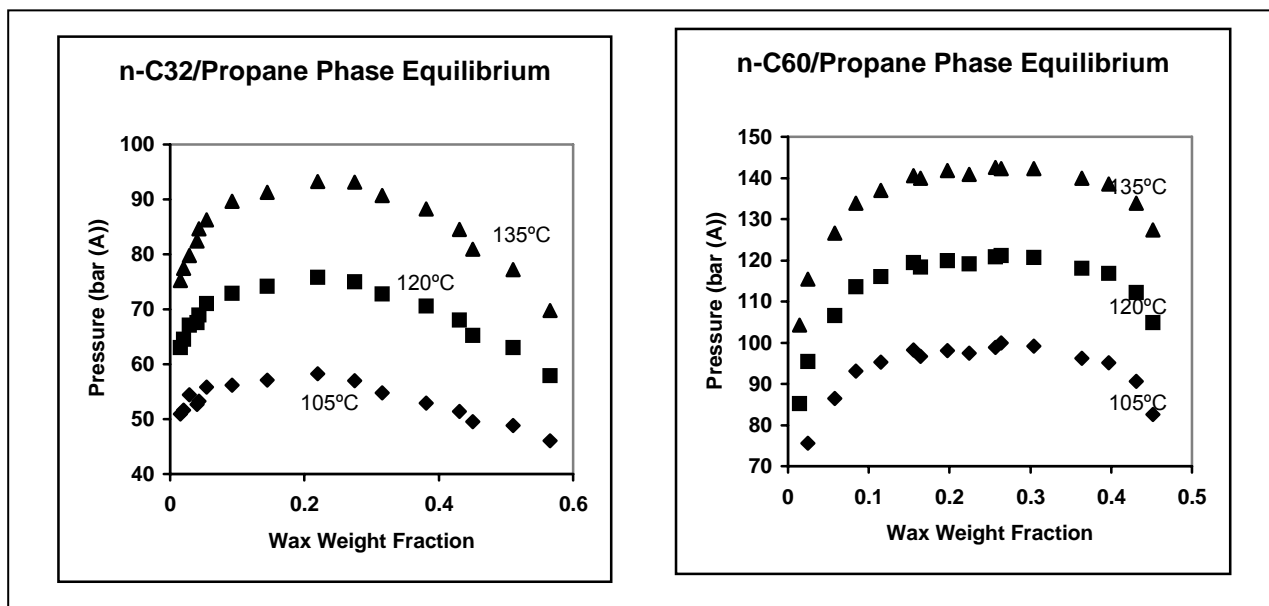
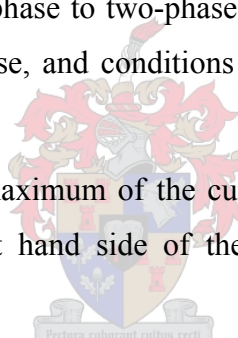


Figure 3-1: Phase Equilibria for Paraffin Waxes and Supercritical Propane (Schwarz 2001)

The curves are isotherms, and indicate the point (at a given composition) whereupon the mixture moves from single phase to two-phase and vice versa. Conditions above the curves indicate a single phase, and conditions below the curves are in the two-phase region.

On the left hand side of the maximum of the curve, the wax is dissolved into the supercritical fluid. On the right hand side of the curve, the supercritical fluid is dissolved into the wax.



It was found that a straight-line relationship exists between the phase equilibrium pressure and the carbon number of the wax at constant temperature and concentration. Thus phase equilibria for waxes other than those measured could be predicted by extrapolation. (Schwarz 2001)

From the phase equilibrium it is clear that the highest solubility is at temperatures just above the solvent's critical point. To dissolve a given amount of wax, lower pressures are required at lower temperatures.

3.2 Nozzles and Pressure Profile

Capillary nozzles, with a variety of lengths and diameters, have been the most extensively used expansion devices. Porous plates and converging/diverging nozzles have also been used at less frequently.

Depending on the dimension of the capillary, the temperature and pressure profile can vary significantly. This temperature and pressure profile is essential, since pressure and temperature influence the phase behaviour of the solution. Let us first consider the different types of nozzles.

3.2.1 Capillary Nozzles

Capillary nozzles are characterised by their length and diameter, both of which plays a major role in the pressure distribution along the nozzle's length. Capillary nozzles have diameters vary between 1 and 200 μm typically have lengths below 15 mm. (Weber et al. 2002)

A particular problem of capillaries is the large pressure drop due to streamline contraction of the fluid just prior to entering the nozzle. In order to prevent premature precipitation of solute, the solution has to be pre-pressurised substantially in order to make up for this pressure loss.

Once the solute has blocked the nozzle opening, the flow has to be stopped, the nozzle removed and the precipitate removed.

Nucleus formation in a capillary is triggered mechanically through pressure reduction, rather than thermally. These mechanical perturbations travel at the speed of sound, and leads to the rapid attainment of uniform conditions in the expanding solution. These uniform conditions are advantageous to yield a narrow size distribution.

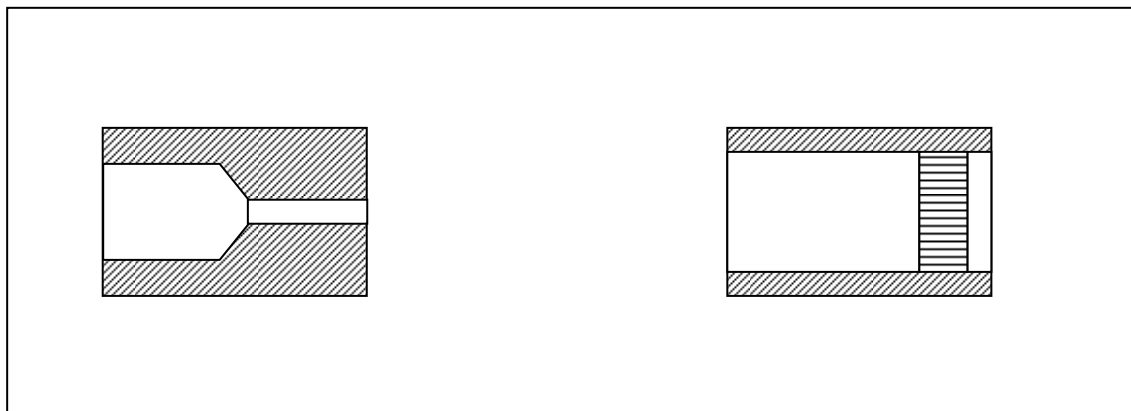


Figure 3-2: The Capillary Nozzle (left) and Porous Plate Nozzle

3.2.2 Frit or Porous Plate Nozzles

In 1994 Nieuwoudt used sintered metal disks in exploratory RESS and PGSS studies to micronise wax. (Nieuwoudt 2002) Berends also proposed the use of porous plates as expansion device (Domingo et al. 1996), (Domingo et al. 1997). The manufacturing of these types of nozzles is relatively simple. Metal particles are sintered to form an intricate network of metal and voids.

The multitude of pathways eliminates streamline contraction, as found when using capillaries. This allows for a lower pressure at the nozzle inlet. The numerous pathways also enable a larger production rate. Porous plate nozzles are much less likely to be blocked, because of the many pathways.

Porous plates are characterised by the average pore size. All pores are naturally not of the same size, but a range of pore sizes are found. The porosity of the plate also plays a part in lowering pressure drop and increasing mass flow rate. The mass flow rate through a porous plate can be altered by manipulation of the area of the plate exposed to the solution.

The disadvantage of porous plates is the fact that there is a pore size distribution. Conditions are likely to be less uniform, which would indicate that a larger particle size distribution could be expected. Porous plates would also be likely to increase chances of agglomerated particles, since the particles exit the sinter metal disk in random directions, increasing chances of collisions between particles.

3.2.3 Subsonic Flow Profile

Until now, RESS modelling has only been attempted for capillary nozzles. An example of this type of nozzle is shown in Figure 3-3. Domingo attempted to model porous plate nozzles by approximating the porous plate as a network of parallel capillaries. (Domingo et al. 1997)

The subsonic part of the expansion includes the capillary, from the inlet to outlet. Modelling of the streamline contraction, just before the nozzle inlet, is normally not attempted, since the progress of this contraction is unknown.

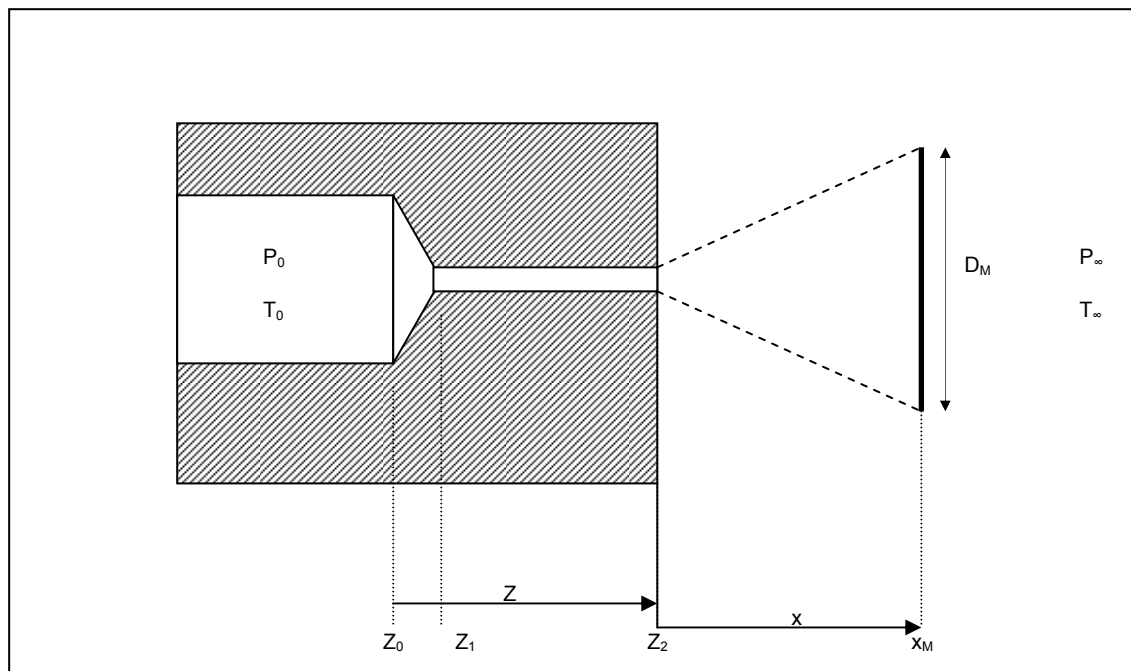


Figure 3-3: Different Sections of a Capillary Nozzle (Helfgen et al. 2002)

A number of assumptions are made in these cases to simplify the flow model for the subsonic part of the nozzle. (Berends 1994)

- Because of the fact that RESS comprises the expansion of solutions with relatively low concentrations, the temperature and pressure profile is modelled with the pure solvent properties.
- Flow in the capillary nozzle is assumed as one-dimensional, steady state and highly turbulent. It is assumed that the walls of the capillary are rough.
- The ratio between the outlet pressure and inlet pressure is significantly high to consider the flow as choked.
- Because of the very short residence time of the expanding solution in the capillary, heat transfer is considered to be minimal. The expansion is thus considered to be adiabatic.
- The changes in potential energy are negligible compared to changes in kinetic energy and enthalpy.

The profile is then obtained by simultaneous solving of the differential equations for conservation of mass, momentum and energy in the flow (z) direction.

Incorporating the necessary assumptions, these equations can be written:

$$\text{Mass} \quad \frac{1}{\rho} \frac{d\rho}{dz} + \frac{1}{w} \frac{dw}{dz} + \frac{1}{A} \frac{dA}{dz} = 0$$

Equation 3-1

$$\text{Momentum} \quad \rho u \frac{du}{dz} + \frac{dP}{dz} = -\frac{2\rho f w^2}{D_{nozzle}}$$

Equation 3-2

$$\text{Energy} \quad w \frac{dw}{dz} + \frac{dh}{dz} = 0$$

Equation 3-3

A fourth relationship is then incorporated in a suitable equation of state for the system to solve the pressure, temperature, velocity and density at a given point.

Solving of these equations relies on knowledge of the capillary length and diameter, the enthalpy as a function of temperature and pressure, the sound velocity as a function of temperature and pressure and Fanning friction factor; f .

Researchers have thus far used the assumption that the capillary is a rough tube containing flows at very high Reynolds number for which a value of 0.05 for $4f$ is assumed. (De Nevers 1991)

The enthalpy and density are functions of the pressure and temperature at a given z . As boundary condition, the flow is choked, so for a given pressure and temperature at the outlet, the sound velocity can be calculated.

Porous plate nozzles are more difficult to model. These nozzles have been modelled as a group of small diameter capillaries parallel to the flow direction. The adiabatic assumption may not be true for porous plates, due to the large amount of heated metal in contact with the expanding solution. This may cause some amount of heat transfer, although the influence thereof is thought to be little. Domingo (Domingo et al. 1997) modelled flow through these nozzles as isothermal. The changed energy balance for isothermal conditions is:

$$w \frac{dw}{dz} + v \frac{dP}{dz} + \frac{2fw^2}{D_{nozzle}} = 0$$

Equation 3-4

3.2.4 Supersonic Flow Profile

Modelling of the flow profile in the supersonic free jet is based on a number of assumptions. The method presented by Ashkenas and Sherman as referenced in Berends will be shown here. (Berends 1994)

The free-jet expansion starts at the nozzle exit where the Mach number equals unity. The Mach number along the centreline of the expanding free jet is calculated by a numerical method based on measurements with a pitot tube.

$$Ma = \alpha \left(\frac{x - x_0}{D} \right)^{\gamma-1} - \frac{1}{2} \frac{\left(\frac{\gamma+1}{\gamma-1} \right)}{\alpha \left(\frac{x - x_0}{D} \right)^{\gamma-1}}$$

Equation 3-5

The fitting factors are α and x_0 .

Pitot tubes were used to measure impact pressure in the centreline of an expanding free jet, and the results was used to fit the equation:

$$\frac{P_i}{P_0} = \left(\frac{\gamma+1}{\gamma-1} \right)^{\gamma/\gamma-1} \left(\frac{\gamma+1}{2\gamma} \right)^{1/\gamma-1} \alpha^{-2/\gamma-1} \left(\frac{x - x_0}{D} \right)^{-2}$$

Equation 3-6

The static pressure is related to the impact pressure by:

$$\frac{P_i}{P_{static}} = \left[\left(\frac{\gamma+1}{2} \right) Ma^2 \right]^{\gamma/\gamma-1} \left[\frac{\gamma+1}{2(Ma)^2 \gamma - (\gamma-1)} \right]^{\gamma/\gamma-1}$$

Equation 3-7

The free-jet temperature is related to the extraction temperature by the ideal isentropic gas law:

$$\frac{T}{T_0} = \left(\frac{P_{static}}{P_0} \right)^{\gamma-1/\gamma}$$

Equation 3-8

The Mach disc is defined as the cross section in the free jet where the flow changes from supersonic to subsonic speeds, and the gas starts to mix up with the surrounding

gases. The static pressure behind the Mach disc is approximately the same as the expansion chamber pressure. (Berends 1994)

$$\frac{x_M}{D} = 0.67 \sqrt{\frac{P_0}{P_\infty}}$$

Equation 3-9

For air ($\gamma = 1.4$) the diameter of the Mach disc was measured and the relationship found to be: $D_M(x_M) = 0.42$ to 0.48 . This ratio depends on the value of γ and is for instance 25 % larger for CO_2 and 25 % smaller for argon. (Berends 1994)

The free jet has a complex flow profile, with flow occurring in three dimensions. Up to date the free jet has been modelled along its centreline. These centreline conditions are only applicable for a very small part of the free jet. The conditions at the perimeter of the free jet are more difficult to obtain.

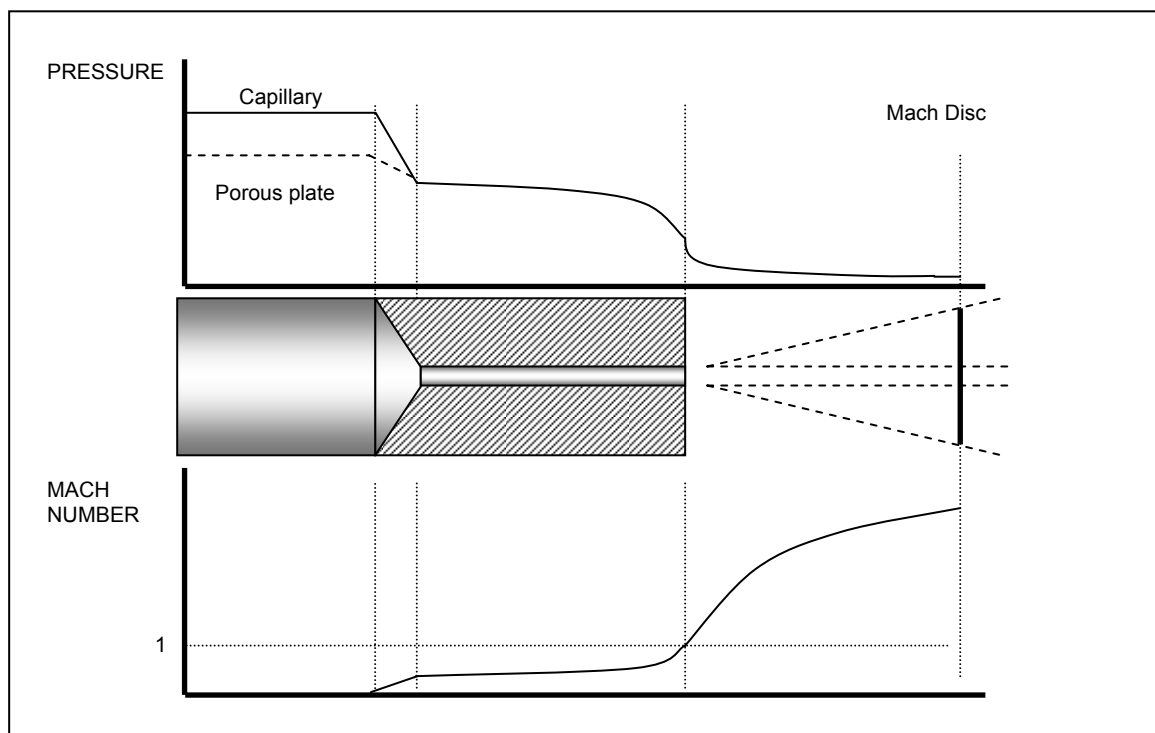


Figure 3-4: Flow profiles for capillary and porous plate nozzles (Adapted from (Berends 1994))

3.3 Homogeneous Nucleation

As the solution expands through the nozzle, the pressure and/or temperature will decrease. At a certain point, the equilibrium line will be transgressed, leading to a phase split and the formation of solute particles. This phase split does not occur as the

phase equilibrium is transgressed, but an amount of “supersaturation” is necessary. In this section it will be shown how this “supersaturation” impacts on the size of the stable particles.

To start of with, consider the formation of a single liquid droplet of solute from solution in an isometric and isothermal system. The molecules in such a system move around in a random way and collide with each other. Due to collisions between vapour molecules, aggregates or embryos containing molecules and groups of molecules form. These embryos are not stable and can easily disintegrate.

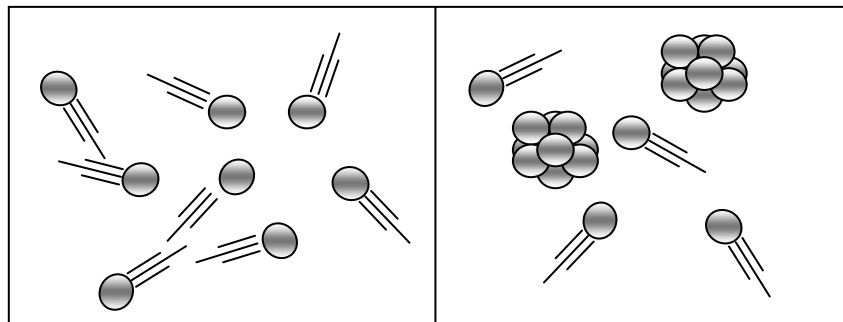


Figure 3-5: Schematical representation of Nucleation

However, if the embryo manages to reach a certain critical size, with radius r^* , it is called a critical nucleus. At this critical point the group of molecules are not stable yet, but the nucleus grows very rapidly through addition of further molecules through condensation until phase equilibrium is achieved. This process whereby critical nuclei form is called homogeneous nucleation, and its occurrence is a prerequisite for the formation of stable particles.

When trying to quantify the effect of homogeneous nucleation, researchers have predominantly used the “classical” nucleation theory. This theory of nucleation is based upon the following assumptions: (Springer 1978)

- The free energy of formation of an embryo is described in terms of the experimentally measured flat-film surface tension.
- Embryos are at rest. This means that they undergo neither translational nor rotational motion.
- The vapour phase is ideal and latent heat released at the liquid/gas interphase is negligible.
- The nucleation process is isothermal.

Consider the thermodynamic behaviour of a single embryo as it increases in size up to the critical size. For a system to reach a stable phase equilibrium, the change in the Gibbs free energy function, caused by the phase transition, must be equal to zero. For the formation of one single embryo, consisting of g solute molecules, the change in Gibbs free energy is given by: (Springer 1978)

$$\Delta G = N_1\mu_V + g\mu_L - n\mu_V + 4\pi r^2\sigma$$

Equation 3-10

n indicates the number of solute molecules in the whole system, g the number of molecules in the solute aggregate (liquid phase) and N_1 the number of solute molecules remaining in the vapour phase, so that $n = N_1 + g$. μ_V and μ_L are the chemical potentials of a single molecule in the vapour and liquid phases respectively, r is the radius of the embryo and σ the flat-film surface tension.

We can conveniently express the amount of molecules in the embryo in terms its volume: $g = 4/3 \pi r^3/v_L$. We can also define the volume of a molecule in the vapour and liquid phases respectively: $v_L = m/\rho_L$ and $v_V = m/\rho_V$. Here m is the mass of a solute molecule and ρ_V and ρ_L the densities of the vapour and liquid phases respectively.

In the case of phase transitions, for stable phase equilibrium the Gibbs free energy is a minimum and for metastable equilibrium it is a maximum. It will be shown that the Gibbs free energy is maximum for supersaturated vapour containing critical nuclei.

At this stage we are looking for that point whereupon further addition of a molecule to the embryo will lead to a decrease in Gibbs free energy and ultimately to stable phase equilibrium.

This equilibrium condition for the single droplet system can be expressed as: (Springer 1978)

$$\left(\frac{\partial \Delta G}{\partial N_1} \right)_{P,T} = 0$$

Equation 3-11

Since the number of solute molecules in the whole system cannot change, n is constant and $n = N_1 + g$, Equation 3-10 can be partially differentiated with respect to N_1 to yield:

$$\mu_V - \mu_L - 4\pi\sigma \frac{dr^2}{dg} = \mu_V - \mu_L - (2\sigma/r)v_L = 0$$

Equation 3-12

By differentiating the above equation at a fixed temperature and using the thermodynamic relationship $d\mu = v dP$, we can obtain:

$$(v_V - v_L)dP = 2\sigma v_L d(1/r)$$

Equation 3-13

Assuming that v_V is much greater than v_L , and applying the ideal gas law, for which $P = kT/v_V$, integration of Equation 3-13 will lead to:

$$\ln S = \frac{2\sigma v_L}{r^* kT}$$

Equation 3-14

k is the Boltzmann constant and is equal to $1.38 \times 10^{-23} \text{ J.K}^{-1}$. It is equivalent to the ideal gas constant and given by R/N_A , where N_A is Avogadro's number. S is the supersaturation ratio as the ratio of the solute mole fraction at a certain temperature and pressure and the equilibrium solute mole fraction:

$$S = \frac{y_s(P, T)}{y_s^*(P, T)} = \frac{P_s}{P_s^*}$$

Equation 3-15

Substitution of Equation 3-12 and Equation 3-14 into Equation 3-10 results in the following form of the Gibbs free energy:

$$\Delta G = -\frac{4\pi r^3}{3} \left(\frac{kT}{v_s} \right) \ln S + 4\pi r^2 \sigma$$

Equation 3-16

The change in Gibbs free energy with the change in embryo size from Equation 3-16 is graphically indicated in Figure 3-4. For supersaturated solutions, the Gibbs free energy increases as more solute molecules condense onto the embryo. This increase

continues until the embryos reach the critical size (r^*). At the maximum point, the embryos are in a metastable equilibrium with the surrounding vapour (ΔG is at a maximum value). Smaller nuclei may disappear while larger ones grow. From the critical point onward, the addition of more solute molecules to the embryo leads to a rapid decrease in the Gibbs free energy. The critical nucleus is thus a threshold size that must be reached before a phase transition can occur.

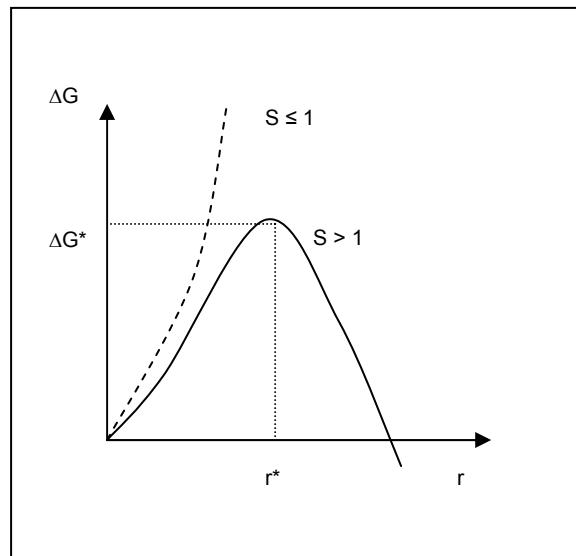


Figure 3-6: : Variation of ΔG with embryo radius.

The critical nucleus size can be determined from rearrangement of Equation 3-14.

$$r^* = \frac{2\sigma v_s}{kT \ln S}$$

Equation 3-17

It is clear that for saturated ($S = 1$) and unsaturated ($S < 1$) solutions, the Gibbs free energy only increases with an increase in embryo size. At these conditions the vapour is in thermal equilibrium and embryos will reach only a fairly small size, before they disintegrate. It is thus clear that stable solute particles can only be reached if $S > 1$.

The rate at which nuclei form can be determined by application of the kinetic gas theory. Some of the principles will be briefly discussed in section 3.4.1. The derivation is however complicated by the fact that embryos are not stable and can disintegrate. Thus the Gibbs free energy must be incorporated into the equation, as well as upper limits for the nucleus size (r^*). The derivation is rather tedious and, if

interested, the reader should consult (Debenedetti 1990) and (Springer 1978) for further detail. The result is:

$$I = 2N_1B \left[\frac{\sigma^{1/2} v_L}{(kT)^{1/2}} \right] \left[\exp \left\{ \left(-\frac{16\sigma v_L^{2/3}}{3kT} \right)^3 \left(\frac{1}{\ln S} \right)^2 \right\} \right]$$

Equation 3-18

Here N_1 represents the total number of solute molecules in the vapour phase. B is the thermal flux of solute molecules, indicating the number of molecules condensing upon arrival at the solute surface. The final exponential term represents the equilibrium concentration of critical nuclei. It is important to note that the free surface energy term, σ , has a very large influence on the value of the nucleation rate. Researchers have often assumed a constant value for this term from other researchers. This is a very dangerous assumption, since the free energy term is temperature and pressure dependant, and even slight deviations in the free surface energy has a large bearing on the value of the nucleation rate.

As mentioned before, the classical nucleation theory assumes that the embryos are at rest. When this is not the case, Equation 3-16 needs to be modified and additional terms added that deals with the translational and rotational movements of a nucleus. For more information, the interested reader is advised to consult the work of Springer. (Springer 1978)

In conclusion, it can be seen that the supersaturation is a prerequisite for the formation of stable solute particles. The degree of supersaturation influences the critical nucleus size. An increase in supersaturation leads to a decrease in the critical Gibbs free energy and critical nucleus size. Thus the formation of many small solute particles is favoured at large supersaturation.

3.4 Condensation and Coagulation

Once a critical nucleus has formed, condensation and coagulation can lead to an increase in solute droplet size. Firstly, consider the definitions of condensation and coagulation:

- **Condensation** is the addition of solute molecules from the vapour phase to the solute droplet. Condensation does not increase the number of solute particles, but increases the mass of solute in the liquid phase.
- **Coagulation** occurs when two solute particles collide to form a new particle. Coagulation results in a decrease of solute droplets, but overall phase mass is unchanged.

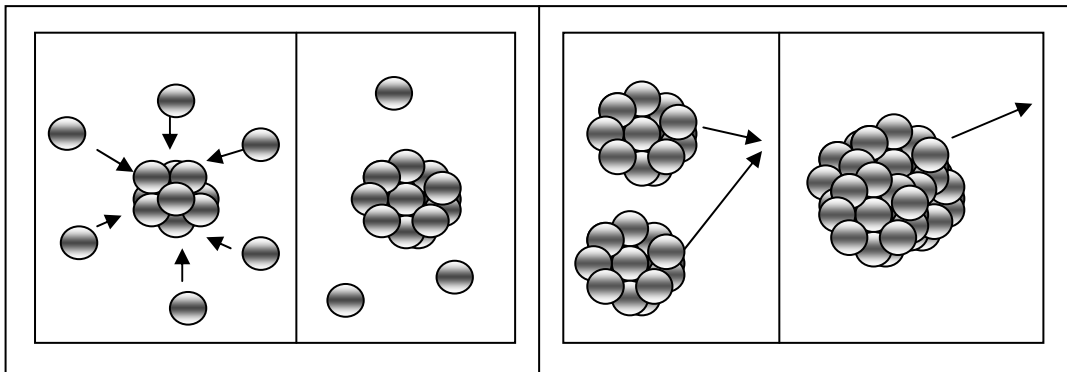


Figure 3-7: The processes of Condensation (left) and Coagulation (Adapted from (Weber and Thies 2000))

In order to investigate the change of particle size due to condensation and growth it is first necessary to consider what is going on in a system containing critical nuclei. At a microscopic level, solute particles move around due to Brownian motion.

For the purposes of this discussion, it will be accepted that two particles (or a particle and molecule) stick together when they collide to form a new particle of larger size. It is logical that the chances of two particles colliding are much greater if the concentration of particles is greater: i.e. there are more molecules in a given volume.

To estimate the growth in supercritical systems, it is necessary to have some sort of idea of the distance between particles or molecules. As explained in chapter 2, a supercritical fluid has transport properties intermediate between that of a gas and a liquid. So let us consider collision frequency in both a liquid and gas to gain some insight of what could be expected in a supercritical fluid.

3.4.1 Collisions in Ideal Gases: Free Molecular

In the free molecular size regime, the particle size is much smaller than the mean free path between particles, as is typical for ideal gas systems. The kinetic gas theory

is used to calculate the frequency of collisions between particles. The following assumptions are made: (Atkins 1994)

- The vapour consists of a swarm of particles (mass = m) in continual random motion
- The particle size is much smaller than the distance travelled between collisions
- Particles undergo completely elastic collisions and have no other interactions

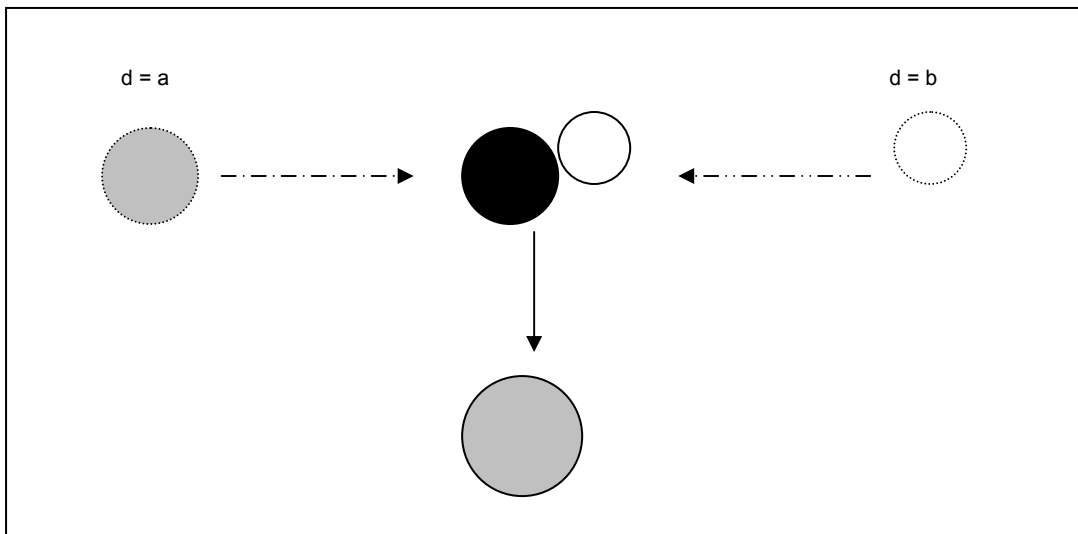


Figure 3-8: The Collision between solute particles

At the kinetic level, the average speed at which a particle of size d travel, is given by: (Atkins 1994)

$$\bar{c} = \sqrt{\frac{8kT}{\pi m}}$$

Equation 3-19

The mean free path is the distance that each particle travel between collisions, and is equal to the average distance travelled in time t divided by the number of collisions that occur in the time: (Atkins 1994)

$$\lambda = \frac{\bar{c}t}{(\pi d^2 \bar{c}t)n_v} = \frac{1}{\pi d^2 n_v}$$

Equation 3-20

Here, d gives the diameter of the particle and n_v is the number of particles per unit volume.

The frequency at which two particles (a and b), of different sizes, collide is obtained by:

$$Z_{ab} = \frac{\bar{c}}{\lambda} = \pi d_{ab}^2 \sqrt{\frac{8kT}{\pi m}} \times n_a n_b$$

Equation 3-21

Here $d_{ab} = \frac{1}{2} (d_a + d_b)$,

$$\text{And } \frac{1}{m} = \frac{1}{m_a} + \frac{1}{m_b}$$

Rearranging Equation 3-21 and converting to the volumes of the colliding particles, we obtain the collision rate between particles of sizes a and b.

$$Z_{ab} = \left(\frac{8kt}{\rho}\right)^{1/2} \left(\frac{3}{4\pi}\right)^{2/3} \left(v_a^{1/3} + v_b^{1/3}\right)^2 \left(\frac{1}{v_a} + \frac{1}{v_b}\right)^{1/2} \times n_a n_b$$

Equation 3-22

Condensation can be considered as the collision between particles and molecules. The condensation rate is derived in exactly the same fashion and the following assumptions can be made (If a denotes the molecule and b the particle). First the molecule volume is negligible in comparison to the particle volume: $v_a \ll v_b$. Then, the number of molecules that can condense on a particle surface is given by $S - 1$. Thus we can write the condensation rate:

$$C = \frac{dv}{dt} = \left(\frac{8kt}{\rho}\right)^{1/2} \left(\frac{3}{4\pi}\right)^{2/3} \left(v_b^{2/3}\right) \left(\frac{1}{v_a}\right)^{1/2} \times (S - 1)n_b$$

Equation 3-23

3.4.2 Collisions in Liquids: Continuum

Molecules in a liquid solution show chaotic movement by what is known as Brownian motion. This is caused by collisions between particles and results in diffusion. The diffusion rates are used to calculate the frequency of collision. The diffusion coefficient is given by the Stokes-Einstein relation: (Atkins 1994)

$$D = \frac{kTC}{3\pi\eta d}$$

Equation 3-24

where D is the diffusion coefficient of a solute particle in the liquid, η is the dynamic viscosity of the liquid and C is the Cunningham correction factor given by:

$$C = 1 + 2.514 \frac{\lambda}{d}$$

Equation 3-25

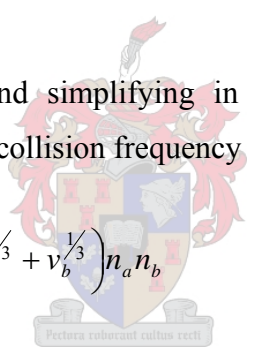
In order to calculate the number of collisions the diffusion coefficient of particle size a to b has to be calculated. By using Fick's law for diffusion and taking into account that both particles are moving due to diffusion, the number of collisions is: (Atkins 1994)

$$Z_{ab} = 2\pi D_{ab} (d_a + d_b) n_a n_b$$

Equation 3-26

Here $D_{ab} = D_a + D_b$

Rearranging Equation 3-26 and simplifying in the same way as for the free molecular regime, we obtain the collision frequency

$$Z_{ab} = \frac{2kT}{3\eta} \left(\frac{C(v_a)}{v_a^{1/3}} + \frac{C(v_b)}{v_b^{1/3}} \right) \left(v_a^{1/3} + v_b^{1/3} \right) n_a n_b$$


Equation 3-27

$$\text{With } C(v_{a,b}) = 1 + 1.257 \lambda \left(\frac{4\pi}{3v_{a,b}} \right)^{1/3}$$

The corresponding condensation rate:

$$C = \frac{dv}{dt} = (48\pi^2)^{1/3} D v_b^{1/3} n_b (S - 1)$$

The interested reader is well advised to consult references such as: (Friedlander 2000), (Pratsinis 1988), (Atkins 1994) and (Berends 1994).

3.4.3 Remarks

An interesting link exists between condensation and coagulation processes. At high nucleation rates, a large number of small nuclei are formed. Because of the high supersaturation and large surface area of embryos, condensation of solute from the

vapour phase is significantly enhanced. As the particle size increase due to condensation, the chances of coagulation between particles increase. Coagulation in turn starts to reduce the number of particles and also the surface area available for solute to condense on. So as coagulation gain in strength, the condensation rate decreases. Since coagulation does not influence the amount of solute molecules in the vapour of liquid phases, the supersaturation will not be decreased. With condensation weakening, an increase in the nucleation rate could be expected. (Weber and Thies 2000) It has been found for instance by Weber that a second burst of nucleation occurs after the original burst of nucleation has occurred. (Weber et al. 2002)

3.5 Concluding Remarks

It is apparent from homogeneous nucleation theory that smaller particles should form at high supersaturation. Ideally, nucleation should be postponed until the solution exits the nozzle, because the pressure drops most rapidly here, and higher supersaturation rates will be achieved. The distance between solute particles will also be largest if precipitation starts in the free jet, since the particles will already be dispersed. This decreases the possibility of coagulation and agglomeration of particles. The aim is to devise a method whereby this can be achieved.

3.5.1 Choice of Temperature and Pressure

The temperature and pressure at the inlet of the nozzle will influence the supersaturation profile of the expanding solution. From the phase equilibrium diagrams of paraffin wax and propane it is clear that a combination of lower temperature and higher pressure will enable the solution to stay in one phase for a longer period of the expansion. Thus nucleation is more likely to occur further down the flow path if these two conditions are met.

The pre-expansion pressure can be increased as desired, but care has to be taken with the choice of a suitable pre-expansion temperature. The temperature must be higher than the wax congealing point to prevent precipitation that could block the nozzle. This is a bare minimum requirement. Furthermore, as the solution expands, the temperature will drop further. The degree of temperature drop depends on the type of nozzle and thus the expansion path. Lower temperatures could be used in an ideal isothermal flow path, as the temperature would remain constant as pressure drop.

At these high speeds it seems totally unrealistic to use isothermal flow - it is approaching the speed of sound and there is no chance that the heat transfer can keep up with the change in momentum. That is why flow is more often considered as adiabatic. For adiabatic flow paths, higher initial temperature is required.

3.5.2 Choice of Nozzle

One of the major aims of this work is to find a wax micronisation process that can be implemented on industrial scale. It is clear that the use of capillary nozzles have their drawbacks in as far as the flow rate is concerned. In addition, the streamline contraction of a stream entering the capillary is significant. Porous plate nozzles negate both of these factors.

Furthermore, since the expansion through capillaries is very rapid, the influence of heat transfer is little and the flow approximates adiabatic conditions. Porous plate nozzles on the other hand offers some degree of heat transfer, although the assumption that an expansion process through these nozzles are isothermal does raise some questions. Since the reduction in temperature and pressure over porous plate nozzles are less severe, and larger flow rates can be achieved, the implementation of these nozzles on an industrial scale does seem to hold some advantage over capillary nozzles.

In addition, the multitude of pathways reduces the chance of blockage. Even if one pathway is to block, there remain a larger number of other clear pathways for the solution to expand through. This would greatly reduce the chances of having to shut the plant down for nozzle cleaning or replacement purposes. The relatively low production cost of a porous plate in comparison with a capillary is another positive aspect of these nozzles.

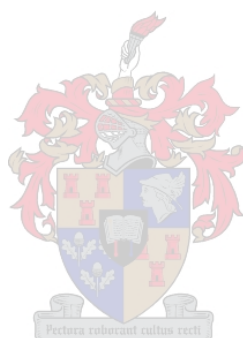
3.5.3 Concentration Effects

Higher wax concentration leads to higher production rates, which is sought after in industrial applications. Furthermore, higher supersaturation is possible at higher wax concentration. Consulting the phase equilibrium diagrams though, it can be seen that higher temperature and pressure is required to keep such a solution in the vapour phase until the nozzle outlet.

Once a solution of higher concentration has precipitated, the higher number concentration of solute particles significantly decreases the distance between particles, increasing effects of agglomeration and coagulation. This can negatively influence the particle shape and size. More rapid particle growth as a result of condensation at higher concentrations is also to be considered.

If this process were to be implemented on industrial scale, capital cost would need to be kept as low as possible. This means that the temperature and pressure should be kept as low as possible and the wax concentration as high as possible. It is evident that porous plate nozzles give a better chance of achieving this, because the pressure drop is lower than in capillaries.

In the following chapters, the details of the experimental work will be discussed to prove the observations made in this chapter. First the construction of a suitable experimental method will be undertaken.



4 EXPERIMENTAL DESIGN AND PROCEDURE

In order to investigate the parameters highlighted in the previous chapter, a design of a proper experimental set-up and procedure is required. For an expansion application, the experimental set-up must cater for the solution to be pressurized and heated to the desired conditions. It must be insured that the solution reaches phase equilibrium. Hereafter the solution is to be expanded over some or other expansion device, in itself a process variable.

In this chapter, the set-ups used by other workers will be reviewed and upon that information, a set-up will be chosen and implemented that will allow for the experimental investigation of the effects of process conditions on the product. Further, the process control, instrumentation, experimental procedures and safety considerations will be discussed.

4.1 *Experimental Set-up: Literature Overview*

A literature survey is done to evaluate the experimental procedures most commonly used in RESS research. Three general steps must be catered for in RESS experiments.

- Preparation of the solution to be expanded
- Expansion of the solution through a suitable restrictor
- Collection of the product

4.1.1 Preparation of Pre-expansion Solution

In order to prepare the solution to be expanded, one of three routes have been followed by researchers:

Batch Process

In a typical batch set-up (Figure 4-1) the solution to be expanded is loaded into an equilibrium cell. Concentration control is trivial since the solute and solvent is added in known quantities.

The cell is placed in a heating bath, or heating fluid is passed through a heating jacket around the cell.

Pressure is generated in the cell by compression of the cell volume. A pressurised gas is applied on top of the piston, which in turn compresses the cell volume. The solvent, pressurised by a displacement pump, can be used for this purpose. (Mawson et al. 1995)

The cell contents are agitated for some time, normally between 1 and 2 hours, to ensure that the cell contents have reached equilibrium prior to expansion of the solution. Stirring magnets placed in the cell volume is the popular choice. The cell can be equipped with a sight glass, through which the cell content can be observed. (e.g. (Blasig et al. 2000), (Charoenchaitrakool et al. 2000)) This has the added advantage that phase equilibrium can be checked prior to expansion.

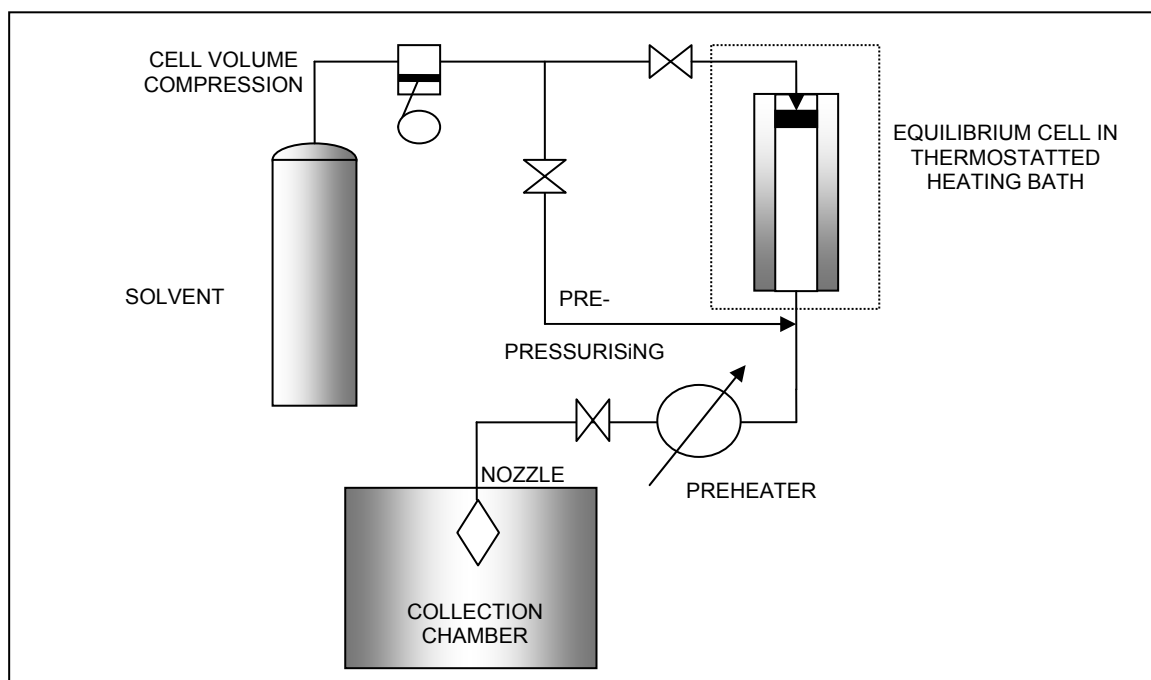


Figure 4-1: The Batch RESS Process

Semi-continuous Process

In the semi-continuous process, solvent is continuously fed through a bed of solute. The solvent is fed from a cylinder, chilled to the liquid phase and pumped to the required pressure in a displacement pump. The solvent is then heated to the extraction pressure in a heat exchanger of some sort. Although the packed bed normally consists of solid only, some workers have used alternating layers of glass and solid. (Griscik et

al. 1995) The solid dissolves into the passing supercritical fluid as the solvent percolates through the bed. From here the solution passes to the expansion device.

The solvent temperature and pressure determines the solubility of the solute. The whole extractor can be placed in a heating bath for temperature control. (Mohamed et al. 1989), (Berends 1994)

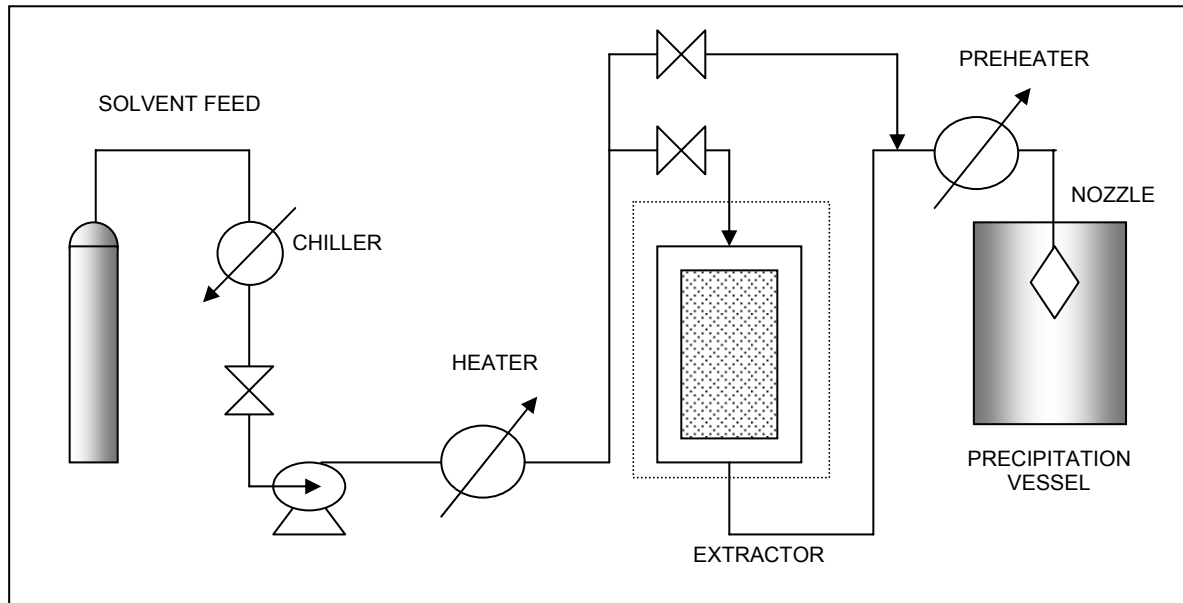


Figure 4-2: The RESS Semi-continuous Process

Continuous Process

If the solute is a liquid at extraction conditions, it is possible to pressurise both solute and solvent stream by displacement pumps. The two streams, pressurised and heated to the desired conditions, can then be mixed, in a static mixer for instance, (Weidner et al. 2002) and fed to the expansion device. This set-up would be similar to that used by Sievers for bubble drying of aqueous solutions. (Sievers et al. 1999), (Sievers et al. 2000) In the set-up, the solvent and an aqueous solution are impinged on each other in a low dead volume tee (see Figure 2-8). This mixing tee apparatus would require a good knowledge of the solubility of the solid in the solvent in order to maintain the desired flow rates of solvent and solute into the tee. For low concentration processes, this set-up might be more difficult as one leg of the tee would have a much higher flow rate than the other.

4.1.2 Expansion of Solution

The equilibrated solution must now be fed to the expansion device. In order to prevent precipitation prior to the nozzle, the line could be heated or pressurised before the solution enters it. Many authors add a pre-heater to just before the nozzle (see Figure 4-1 and Figure 4-2). This could severely influence whether the entering solution is in the single phase or two-phase region. In the case of this particular project, pre-heating is undesirable, since it will move the solution closer to the dew point, causing a phase split to occur further upstream in the expansion, which is undesirable. A proper knowledge of the phase behaviour is known before the amount of preheating (or cooling) is determined.

A bypass solvent line, for cleaning and pre-pressurizing, is found in most experimental set-ups. Just prior to commencement of a spray run, all the necessary tubing can be pressurised by passing pure solvent through all lines between the extractor or equilibrium cell and expanding device. After the desired spraying time has elapsed, the solution is shut off, the by-pass line opened and the expansion device can be cleared of all of the solute that might have precipitated in the restriction.

The expansion device and line between the cell and expansion device may be heat traced. The line can also be coiled and passed through a heating oven, but it is preferential to keep the distance between cell and expansion device as short as possible. (Lele and Shine 1992), (Matson et al. 1987), (Alessi et al. 1996)

An inline filter can be placed in this line to prevent foreign particles from blocking the nozzle.

4.1.3 Precipitation and Particle Harvesting

Expansion of the solution is most conveniently done in a vessel sealed off from the environment. The particles precipitated from solution are gathered in most cases on a filter consisting of a sinter metal (Kröber et al. 2000) or paper filter (Berends 1994). The expanded solvent leaves the chamber via this filter, and if very small particles are formed, may move on to further screens, such as electrofilters.

In experiments where post-expansion conditions were controlled, the whole of the expansion chamber could be kept in a temperature-controlled bath. Pressure control of

the expansion chamber is regulated by the rate of solvent removal from the expansion chamber. (Mohamed et al. 1989), (Berends 1994)

4.1.4 Comparison of RESS Methods

Before deciding on an experimental design, the aspects of batch and continuous solution preparation must be weighed up.

Table 4-1: Comparing Batch and Continuous Processes

<i>Process Type</i>	<i>Semi-Continuous</i>	<i>Batch</i>
Equilibrium	Short contact time between solid and solvent leads to uncertainty about equilibrium	Mixture can be agitated to ensure equilibrium
Control	Extraction vessel pressure controlled by solvent flow rate. Heating bath/jacket controls extractor temperature. Solubility depends on T, P in extractor, which may differ from pre-expansion T,P. Flow rate depends on nozzle type and nozzle inlet conditions.	Pressure control by exertion of pressure on cell volume. Heating bath/jacket controls temperature. Only pre-expansion T, P control required. Concentration controlled by addition to cell volume. Flow rate depends on nozzle type and nozzle inlet conditions.
Equipment	Pumps, extractors and heat exchangers required for solvent feed.	No equipment needed for solvent feed.
Steady State	Larger inventory of material. Steady state conditions can be reached.	Short spraying times. Steady state conditions less likely.
Safety	In case of line/valve failure, materials feed has to be shut off.	Small inventory of Material; Line/Valve failure leads to small and sudden material release.

4.2 Design Considerations

The criteria for deciding on the type of equipment can be summarised as follows:

- **Control over the investigated parameters:** The parameters investigated were pre-expansion temperature and pressure and concentration. These parameters need to be controlled and varied in order to investigate their effect on the product.
- **Sample collection:** The particles have to be gathered so that a representative sample can be analysed. Here it is especially important to ensure that a representative sample of the product is obtained to get.
- **Safety:** Propane is a highly flammable solvent. After the solvent and solute separated in the precipitation vessel, the propane must be removed to a safe environment to prevent possible explosions

Because of the safety concerns due to the propane flammability, it was decided to keep the inventory of solvent as small as possible. This would be best achieved if a batch apparatus were used. Construction of such an apparatus would be cheap, since no mechanical equipment is required. Solvent concentration is a very important process parameter in this work, and it can best be controlled if the exact quantities of solvent and solute are known. The batch apparatus would be better suited to achieve this. In addition to all of the above considerations, the lower consumption of chemicals would result in cost savings.

It was decided that the experimental set-up should cover the following range of parameters.

- **Temperature:** The pre-expanded solution must be heated to at least the solvent critical temperature. Since propane has a critical temperature of 96.6 °C, water will not suffice as heating medium. The temperature range used in these experiments varied from 125 to 160 °C.
- **Pressure:** In order to keep the wax in solution for as far down in the nozzle as possible, the pre-expansion pressure should be kept as high as possible. However, the mechanical strength of the nozzle and valves used in the

system should be considered. For safety, it was decided that pressures no higher than 180 bar would be used in experiments.

It was envisaged that the batch experiments would be used to identify a set of parameters where a satisfactory product would result. The use of a continuous set-up to verify the results found with the batch set-up could be performed at a later stage.

4.3 Experimental Design

The set-up consists primarily of four parts.

- Equilibrium cell chamber
- Counterbalance piston for pressure application
- Expansion part, i.e. the expansion valve and nozzle
- Precipitation vessel, where the product is gathered

4.3.1 Principle

A mixture of the solvent and wax is added into the equilibrium cell in the desired concentration. The cell content is brought up to temperature by heating oil flowing through the jacket of the equilibrium cell.

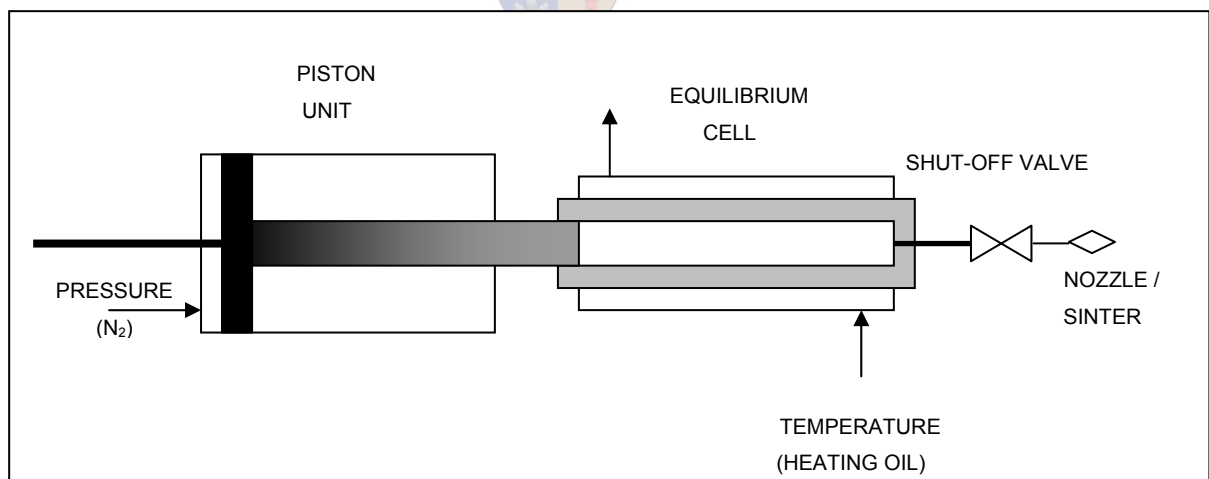


Figure 4-3: Experimental Equipment to be used

Pressure is generated when a counterbalance piston moves into the cell volume, thus decreasing volume. Nitrogen, with regulated to typical pressures of 1-17 bar was readily available for this purpose.

The content is agitated well in order to ensure that equilibrium is reached. When equilibrium is reached, the shut-off valve is opened and the solution expands rapidly over the expansion device, such as a nozzle or sinter plate.

The particles can be collected in a large enclosed volume, such as a drum or bag. The propane is removed to a safe environment and wax particles can be left to precipitate at the bottom of the vessel or collected on a filter. Analysis of the product completes the experimental procedure.

Mechanical drawings of the different parts of the experimental set-up can be found in Appendix F.

4.3.2 Equilibrium Cell

The cell is made from stainless steel. When the counterbalance piston is screwed into the cell, it has a maximum volume of 41 cm³ when the piston is fully retracted and 8 cm³ when fully extended.

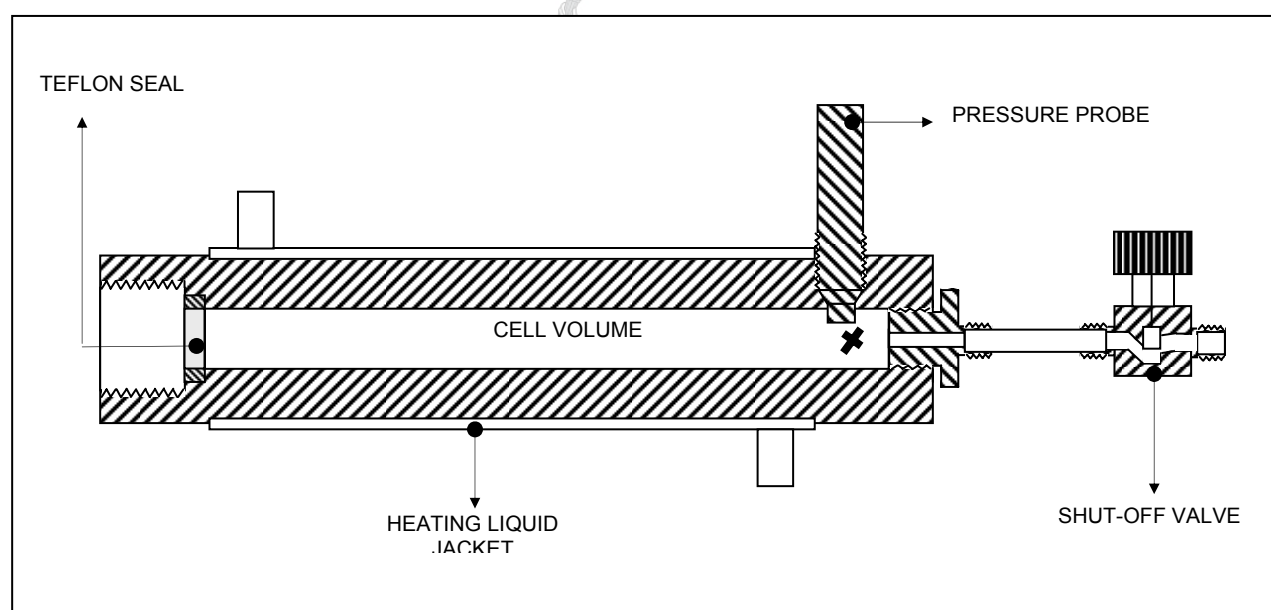


Figure 4-4: The Equilibrium Cell

The concentration was fixed by filling the cell volume with wax and propane in the desired ratio. To prevent changes in the concentration by selective leaking of solvent from the cell, it is important that the content be brought into the one-phase region as quickly as possible. A magnetic stirring bar was added to the contents to hasten the equilibrium process. A Heidolph MR 2002 stirrer heater plate was used. After the cell was loaded, it was placed on this plate, to help heat the cell content and to cause

agitation of the stirring magnet. This heating plate had controls for both temperature and stirring speed.

The equilibrium cell is jacketed so that a heated liquid can supply the required heat to the solution in the cell. Dowtherm heating oil was used as heating liquid. The heating oil temperature was controlled to a maximum temperature of 200 °C in a temperature control unit (Tool-Temp TT-260, acc: 1 °C). The valve body and expansion device was heated by self-regulating heating tape (Thermon TSX) to a temperature of 121 °C.

The cell pressure was measured by a melt pressure gauge (ISI), accurate to within 0.1 bar. The pressure reading was influenced by temperature, and a calibration was done for the whole range of operating temperatures. A dead weight test was used to calibrate the pressure sensor. Results hereof is presented in Appendix C.

At the back end of the cell, the piston unit serves as seal. The shoulder of the piston presses down on a teflon ring so that it is compressed axially. This expands the ring radially so that it forms a seal at the perimeters of the ring. The pressure piston can deliver a 13:1 pressure ratio. A pressure regulator on the nitrogen cylinder is used to control the nitrogen feed pressure up to 17 bar. The nitrogen feed line includes a vent valve to relieve the pressure applied to the piston. A set of three Viton o-rings serve as backup seal to the teflon ring seal in the equilibrium cell.

4.3.3 Shut-off Valve and Spray Device

A soft-seat valve seals off the equilibrium cell from the porous plate nozzle. (Swagelok SSDP14) The valve seat is made from polyether-ether ketone (PEEK). When the cell content has reached equilibrium, the valve is opened as quickly as possible to guide flow to the expansion device. In the experimental runs sinter plates, cut from inline filter cartridges, were used as expansion devices. The filters available had average pore diameters of 15, 25 and 60 µm. The sinter plates are manufactured by isostatic pressing of stainless steel powder, yielding a porous network.

The sinter plate was placed as close as possible to the valve opening to minimise the pressure drop due to the dead space between the valve stem and sinter plate surface.

A standard ¼ inch nut was modified to house the sinter plate. The front-end opening was chamfered away so that less of the expanded solution would hit the metal.

Further, the inner part of the nut, on which the Teflon seal rests, is sold with a slight slope. This slope was machined away to prevent the Teflon seal from being pressed out when tightening the nut onto the valve.

An aluminium washer was placed between the valve body and sinter. The size of the hole in the aluminium washer influences the flow rate that can be achieved through the nozzle. This softer aluminium deforms when the nut is tightened so that the steel valve tube connection bites into the aluminium. A Teflon ring is placed between the sinter plate and the nut. When the nut is tightened, the Teflon deforms and causes a second seal.

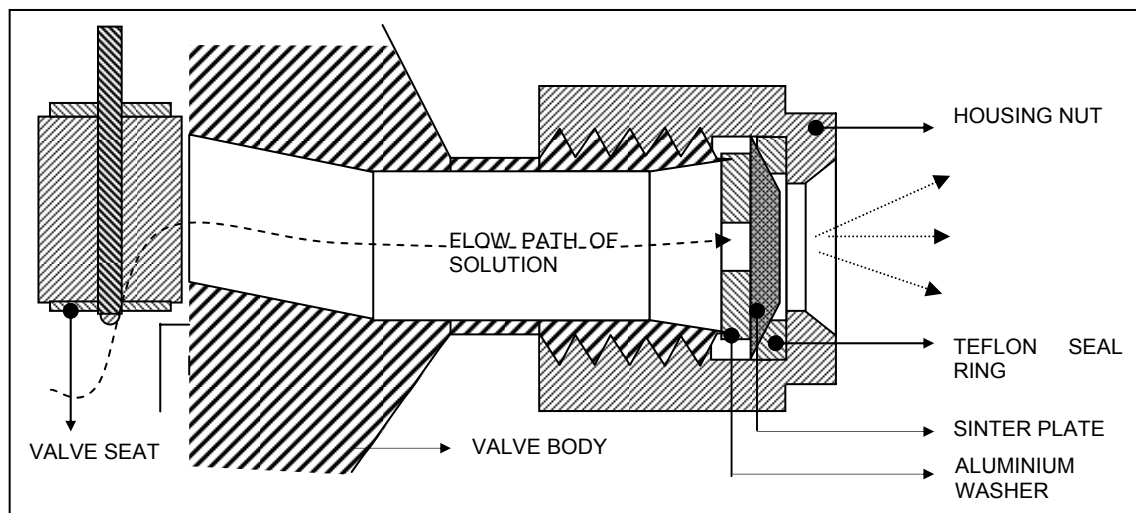


Figure 4-5: Expansion of Supercritical Solution

4.3.4 Expansion Vessel

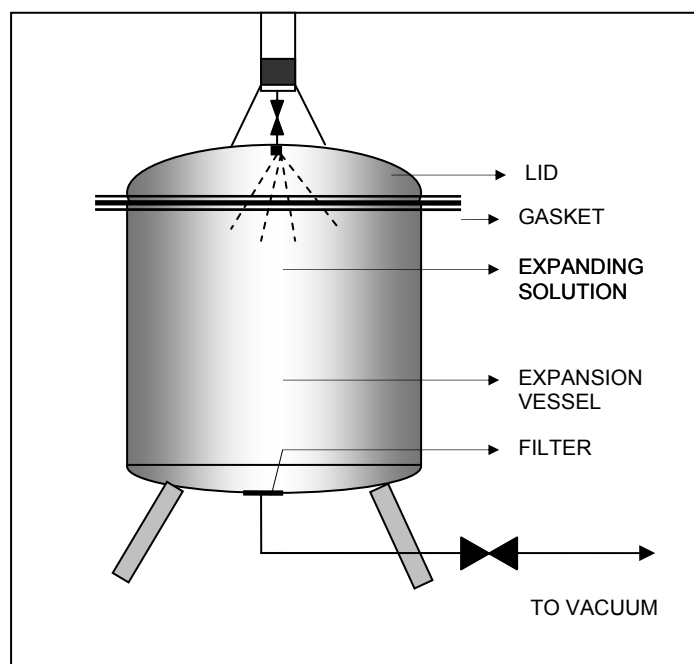


Figure 4-6: Expansion vessel

Since propane is a highly flammable gas, the expanding cell content had to be sprayed into a sealed vessel. A stainless steel vessel, 1 meter in diameter and length was used for this purpose. The vessel was wide enough so that the spray cone would not touch the sides of the vessel.

The experimental set-up was placed in a vertical position just prior to the spraying process, with the sinter plate just inside the vessel.

A vacuum line was attached at the bottom of the vessel to draw the wax particles toward the filter. A piece of vacuum filter bag (Electrolux) was taped over the opening to trap all the wax particles in the form of filter cake. The propane was removed to a safe environment via the filter by applying a pressure difference across the filter.

4.4 Experimental Procedure

The experimental procedure can be summarised in four steps:

- Loading of Equilibrium Cell
- Phase Equilibrium Period
- Spraying
- Unloading and Cleaning of Equilibrium Cell
- Sample Preparation

4.4.1 Loading of Equilibrium Cell

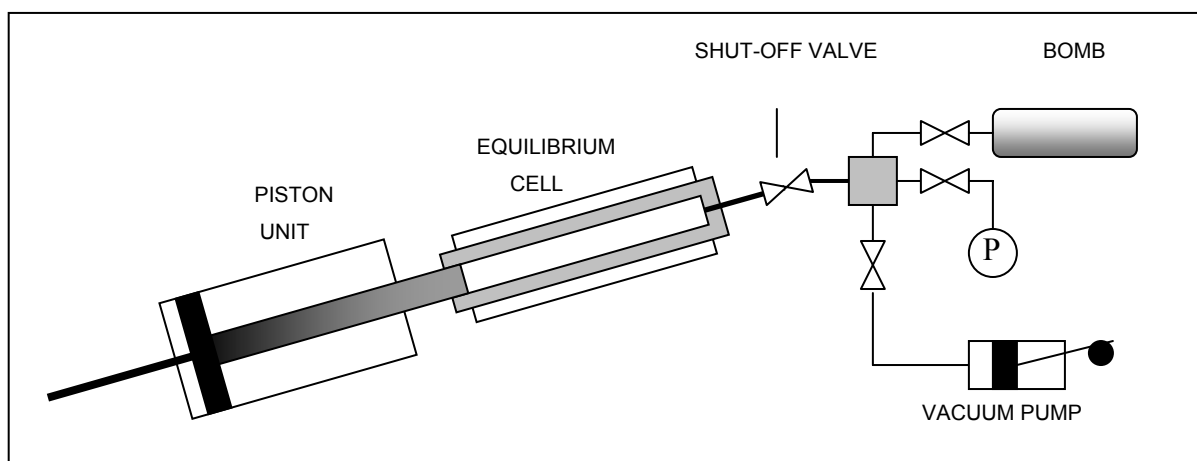


Figure 4-7: Loading of the Equilibrium Cell

The wax is weighed off on a scale balance (Ohaus Precision Plus) accurate to 0.001 g and poured into the equilibrium cell, along with the magnetic stirring bar. The piston unit is screwed onto the equilibrium cell and tightened to ensure thorough sealing of the cell volume.

The solvent (liquid) is transferred from the gas cylinder to a bomb by cooling of the bomb to a temperature below that of the gas cylinder. This causes a pressure difference between the bomb and cylinder, so that the solvent will flow from a higher to lower pressure. The mass of solvent in the bomb is determined by weighing (Precisa 3100 C) the bomb before loading and after loading the solvent (accurate to 0.01 g). The cell is evacuated to a maximum of 100 Pa.

The solvent is fed from the bomb to the equilibrium cell by heating the bomb with a hot air gun to a temperature above that of the cell to drive the solvent from the bomb.

4.4.2 Phase Equilibrium

It is now of utmost importance that the cell contents reach equilibrium prior to the spraying process.

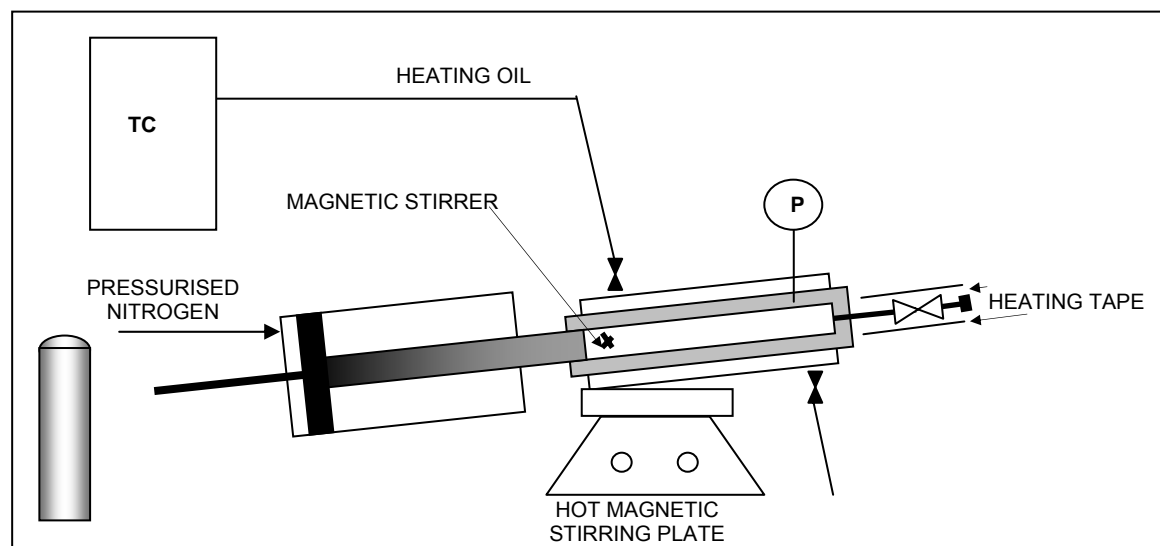


Figure 4-8: Phase Equilibrium Stage

The experimental set-up is placed on the magnetic stirrer / hot plate in a tilted position, as indicated in Figure 4-8. This tilting has a twofold purpose: 1) any molten wax that is trapped in the piece of tubing between the equilibrium cell volume and the shut-off valve will flow back into the cell volume and 2) to ensure that the stirring bar and molten wax will be in a position directly above the stirrer.

The lines from the heating bath were connected to the equilibrium cell. The heating bath was switched on and pre-set to the desired temperature value. Heating was tape bound tightly on either side of the valve body and the nozzle-housing nut. All of the heated areas were covered with a fibreglass-type insulation material.

The nitrogen feed line was attached to the counterbalance piston. The pressure on the cell is increased by regulation of the nitrogen feed pressure to the counterbalance piston.

When the temperature bath reached the desired value, the stirring magnet is switched on to start agitation of the cell content. The set-up was allowed between two to three hours in this position to insure that the cell contents had reached equilibrium.

4.4.3 Spraying

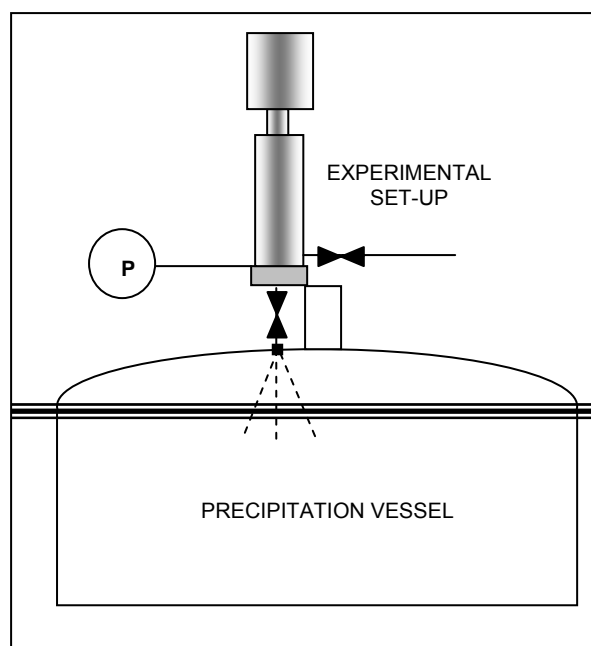


Figure 4-9: Spraying Process

The expansion vessel was prepared by removing all wax from the walls of the vessel, taping a piece of filter bag over the opening at the bottom of the vessel where the vacuum will be applied, and replacing the lid of the vessel

The experimental set-up was carefully removed from the magnetic stirrer and the cell body and placed in a vertical position so that the nozzle exit was just inside of the vessel volume. Prior to expanding the solution, the air inside the expansion vessel should be filled with carbon dioxide in order to inertise the environment and prevent possible ignition of the expanded propane in the vessel.

The temperature and pressure in the equilibrium cell was closely monitored and noted. Spraying is initiated by opening the shut-off valve as quickly and as widely as possible to try and minimise pressure losses over the valve orifice. A temporary decrease in the cell pressure, approximately 30 bar in most cases, was noted as the shut-off valve was opened. The lag due to friction between the piston and the o-ring seals in the pressure piston unit caused this temporary pressure drop, but the pressure recovered to its original value after a short period (2 – 3 s). As soon as the cell volume was close to empty, the expansion valve was closed briskly. The cell volume was judged by the position of the rod on the counterbalance piston.

Typical spraying times varied between the spray nozzles used. Typical spraying times for the 15 and 60 μm porous plate nozzle was in the region of 15 – 20 seconds, while the more porous 25 μm nozzle had a typical spraying time of 4 – 8 seconds.

The expansion vessel was placed under a small vacuum of no less than 85 kPa. The particles were slowly drawn onto the filter paper by the movement of the solvent from of the expansion vessel via the filter paper. After a period of a few (app. 3 h) hours, the sample on the filter could be removed and prepared for analysis.

Details regarding the cleaning of the equilibrium cell and the major safety considerations can be found in Appendix D.

4.4.4 Sample Preparation

The sample collected on the paper filter, was divided into four parts. One of the parts was chosen at random. The particles in the filter cake were carefully mixed, and a random scoop from the mixture was taken and placed on an SEM stub. A droplet of methanol was added to the wax particles, causing everything to gently spread out over the stub and left for 24 hours to allow the methanol to evaporate.

4.5 Product Analysis

Analysis of particle size and morphology is normally executed from scanning electron microscope (SEM) photographs. Other methods of analysis used in work by other researchers, include three-wavelength-extinction-measurement (3-WEM) and optical microscopy. (e.g. (Helfgen et al. 2000), (Türk 1999)) In this project SEM was chosen as analysis method, because equipment and trained personnel was readily available.

The sample was gold sputtered to enhance the quality of photographs. The gold was pulse sputtered for 60 seconds (20 applications of 3 seconds each) onto the sample, to prevent local heating of the sample and possible melting of some of the wax. The product was analysed by Scanning Electron Microscopy (SEM).

The SEM images were taken using a Leo S440 Scanning Electron Microscope. A secondary detector was used to with magnification ranges varied between 5000 and 10 000, working distances of 16-18 mm, and accelerating voltage (EHT) of 10 kV.

5 RESULTS

5.1 Dew Points for Propane/Wax Mixtures

Prior to the commencement of micronisation experiments, the dew points of the C80 wax measured. The C80 wax is polydisperse mixture with a congealing point of 82 °C. (Schümann-Sasol 2002) The dew points were measured in an apparatus used by Schwarz for high pressure phase equilibrium measurements. (Schwarz 2001) This was done to form an idea of the pressure at which the phase split could be expected. The measurement was done at concentrations of approximately 3 % and 5 %, which was in the concentration range used in the micronisation experiments. Details of the procedure of these measurements can be found in Appendix B and the thesis of Schwarz. (Schwarz 2001)

The dew points for propane and C80 wax are given in Table 5-1.

Table 5-1: Dew Points of 3 % and 5.5 % C80 Wax Solution

x_{wax}	<i>Equilibrium Pressure</i>		
	<i>(bar (A))</i>		
<i>Wt %</i>	<i>109.2 °C</i>	<i>126.2 °C</i>	<i>143.7 °C</i>
2.9	62.9	84.9	104.6
<i>Wt %</i>	<i>114.9 °C</i>	<i>133.2 °C</i>	<i>150.8 °C</i>
5.4	68.1	89.8	111.1

It is clear that the dew point pressure is strongly influenced by temperature. The lower the temperature, the lower the pressure required to keep the wax in solution. It is important that the solution was at a high enough pressure at the nozzle inlet to prevent premature phase splits possible blockage of the nozzle.

5.2 Micronisation of C80 Wax

5.2.1 The Influence of Concentration and Porous Plate Nozzles

Particle Sizes

The influence of concentration on the economic viability of the process is very important. If the desired product can be obtained at a higher concentration, then the solvent/solute ratios will be much less and equipment costs will be lower.

For this reason, concentration was the first parameter that was investigated. The results obtained for C80 wax expanded from base conditions of 160 °C and 150 bar are presented in Table 5-2.

Table 5-2: C80 Particle Sizes obtained from Various Nozzles and Concentrations at 150 bar and 160 °C

<i>No</i>	<i>T</i> (°C)	<i>P</i> (bar)	<i>x_{wax}</i> (wt %)	<i>Pore</i> <i>Size</i>	<i>d₁₀</i> (µm)	<i>d₅₀</i> (µm)	<i>d₉₀</i> (µm)	<i>d_{avg}</i> (µm)
1	160	150	1	15	0.97	1.79	4.19	2.27
2	160	150	2	15	0.66	1.31	2.56	1.54
3	160	150	3	15	0.55	0.98	1.67	1.06
6	160	150	1	60	0.83	1.41	2.62	1.63
5	160	150	2	60	0.79	1.27	2.17	1.37
4	160	150	3	60	0.79	1.26	2.02	1.35
19	160	150	5	60	0.67	1.22	2.30	1.42
23	160	150	2	25	0.63	1.10	1.81	1.23
24	160	150	5	25	0.61	0.95	1.57	1.08

In this table, d_{10} refers to particle size under which 10 % of the particles lie, d_{50} the size under which 50 % of the particle lie, etc. This should give an indication of the size distribution. The values were obtained by physically measuring the diameter of a particle and creating a list of the measured diameters. The values are based on the number of particles. In all cases at least 150 particles were measured. Different SEM

images of the sample, taken at different locations on the SEM stub were considered in order to have as representative an indication as possible.

From Table 5-2, the following conclusions are drawn:

- Average particle sizes are in the region of 1.5 μm in all cases, except for the low concentration expanded through the 15 μm nozzle.
- The particle size distributions for the runs in Table 5-2 are given in Figures 5-2 to 5-4. When comparing the concentration effect in each of these Figures, it seems as if a concentration in the region of 3 mass % yields a narrower size distribution than that obtained from other concentrations. In Figure 5-3 it would seem that the particle size distribution is at its narrowest at 3 %, and then the size distribution becomes slightly wider again at 5 %.
- Evaluating the particles obtained from the 15 and 60 μm nozzle, no clear trend can be seen from the difference in pore size. The particles obtained from the 25 μm nozzle are smaller than that from the other nozzles, with a narrower size distribution.

However, this analysis does not address the very important question relating to particle shape. The particles required must conform to two very important criteria, i.e. the size must be smaller than 5 μm and the particle shape must be spherical. The particle shape is evaluated in the following section.

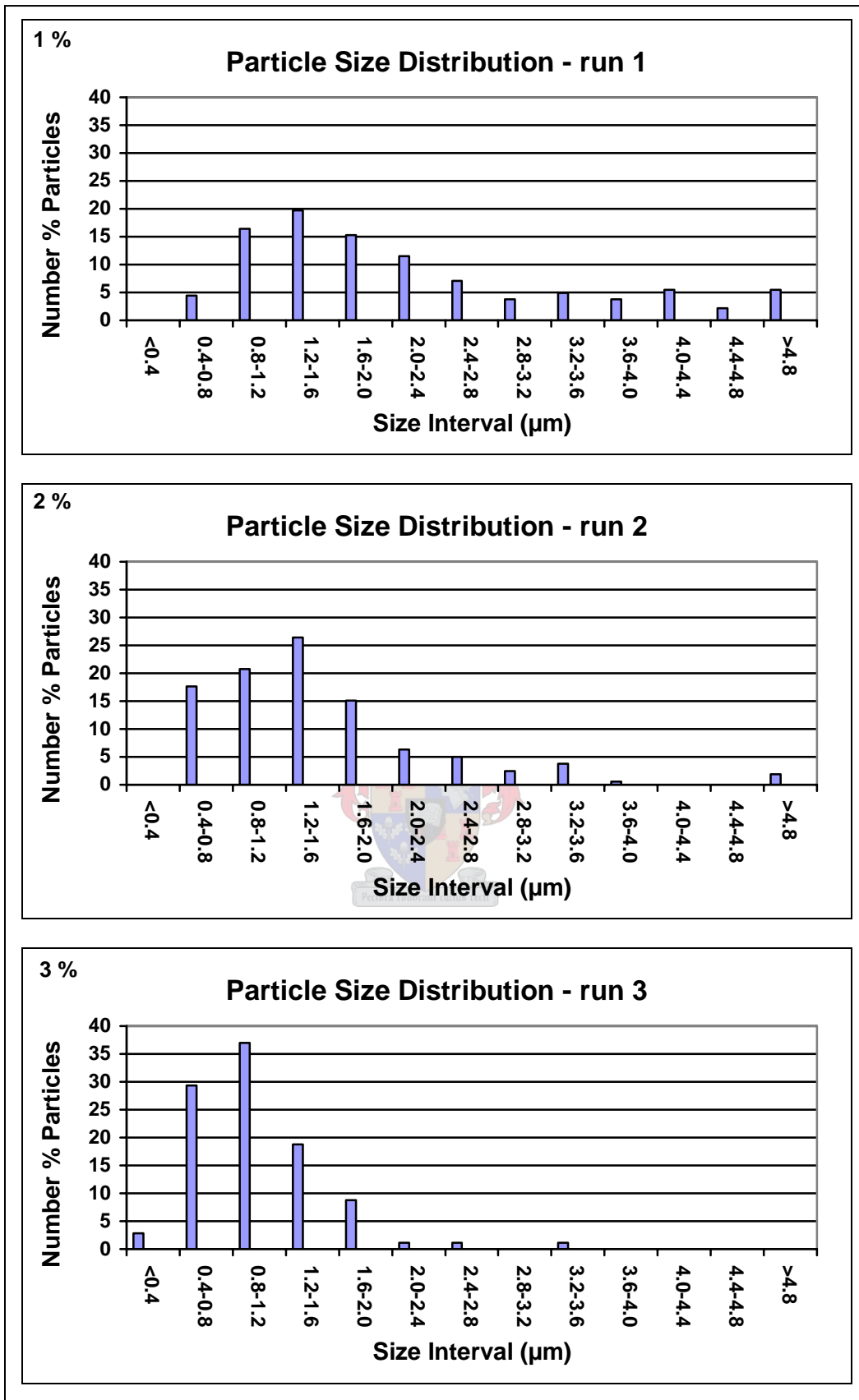


Figure 5-1: Particle Size Distribution at Various Concentrations at Pre-expansion Conditions of T = 160 °C, P = 150 bar, Pore Size = 15 μm .

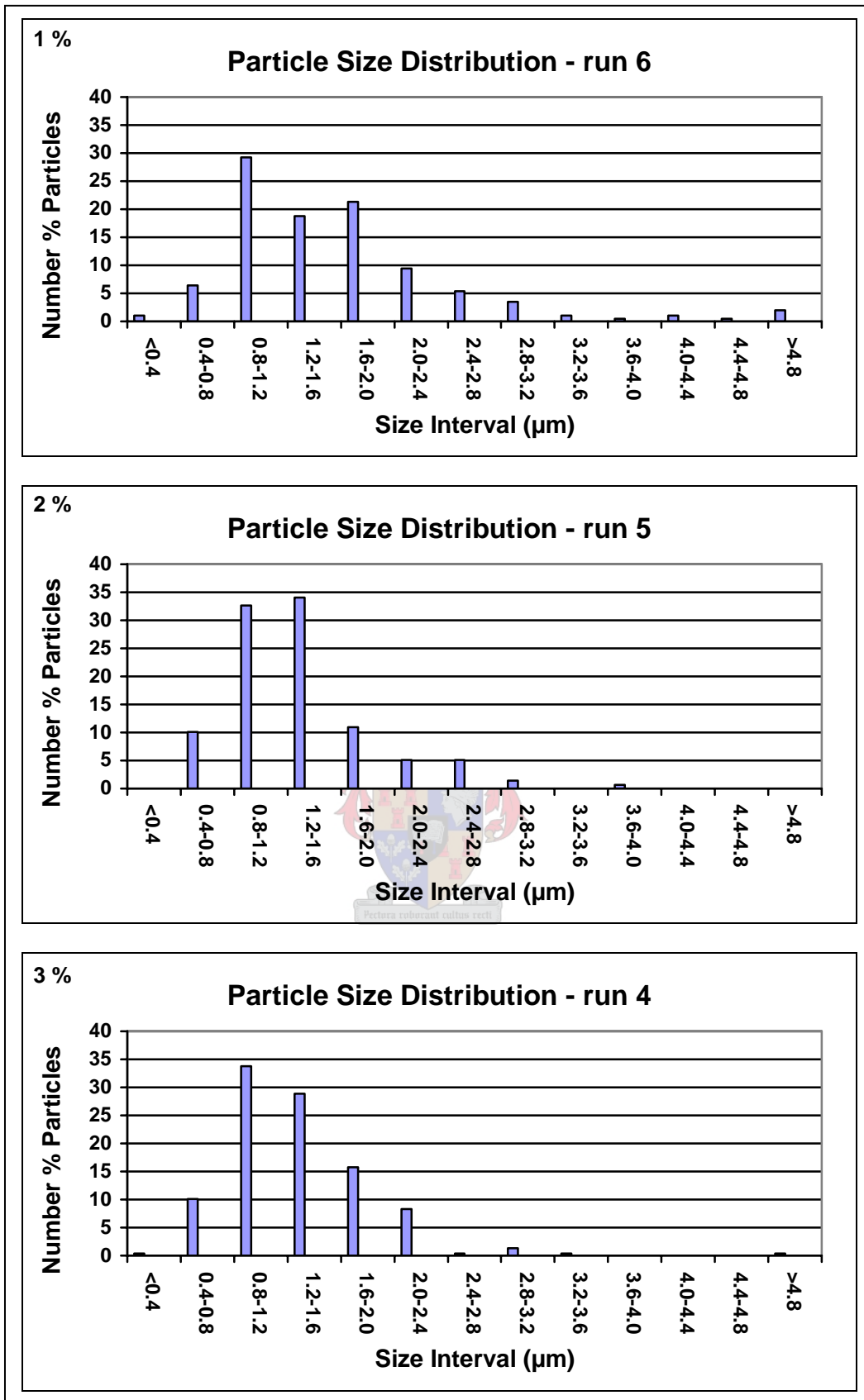


Figure 5-2: C80 Particle Size Distribution at Various Concentrations at Pre-expansion Conditions of T = 160 °C, P = 150 bar, Pore Size = 60 µm.

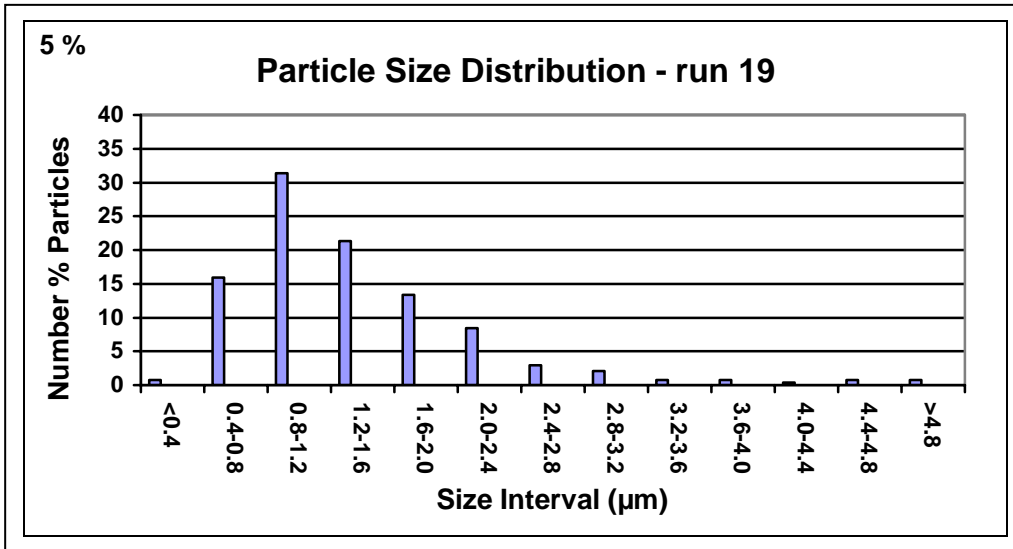


Figure 5-2 (cont): C80 Particle Size Distribution at Various Concentrations at Pre-expansion Conditions of T = 160 °C, P = 150 bar, Pore Size = 60 µm.

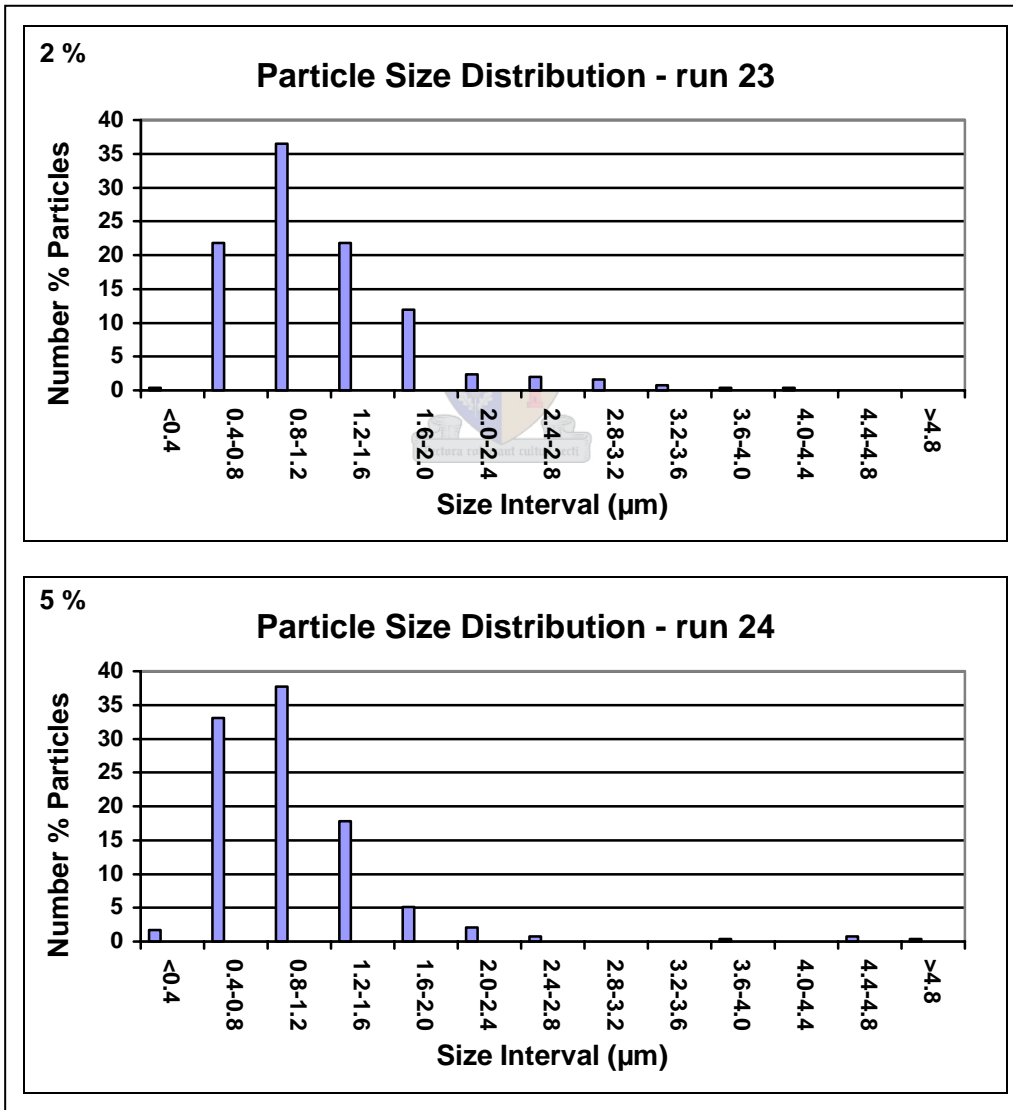


Figure 5-3: C80 Particle Size Distribution at Various Concentrations at Pre-expansion Conditions of T = 160 °C, P = 150 bar, Pore Size = 25 µm.

Particle Shape

The SEM images of the products obtained from the various runs are given in Figure 5-4 to Figure 5-6. From the images it can be seen that the particles obtained are not spherical, but angular. The surface of the particles does not seem to be smooth and has an almost pollen-like texture. Furthermore, the following observations regarding concentration and nozzle size can be made:

The particles obtained with the 25 μm nozzle (Figure 5-6) seems to deliver particles that have a somewhat smoother surface than those from the other nozzles formed at the same concentrations (Figure 5-4 and 5-5). The particles also seem to be of more spherical shape than those obtained from the other nozzles.

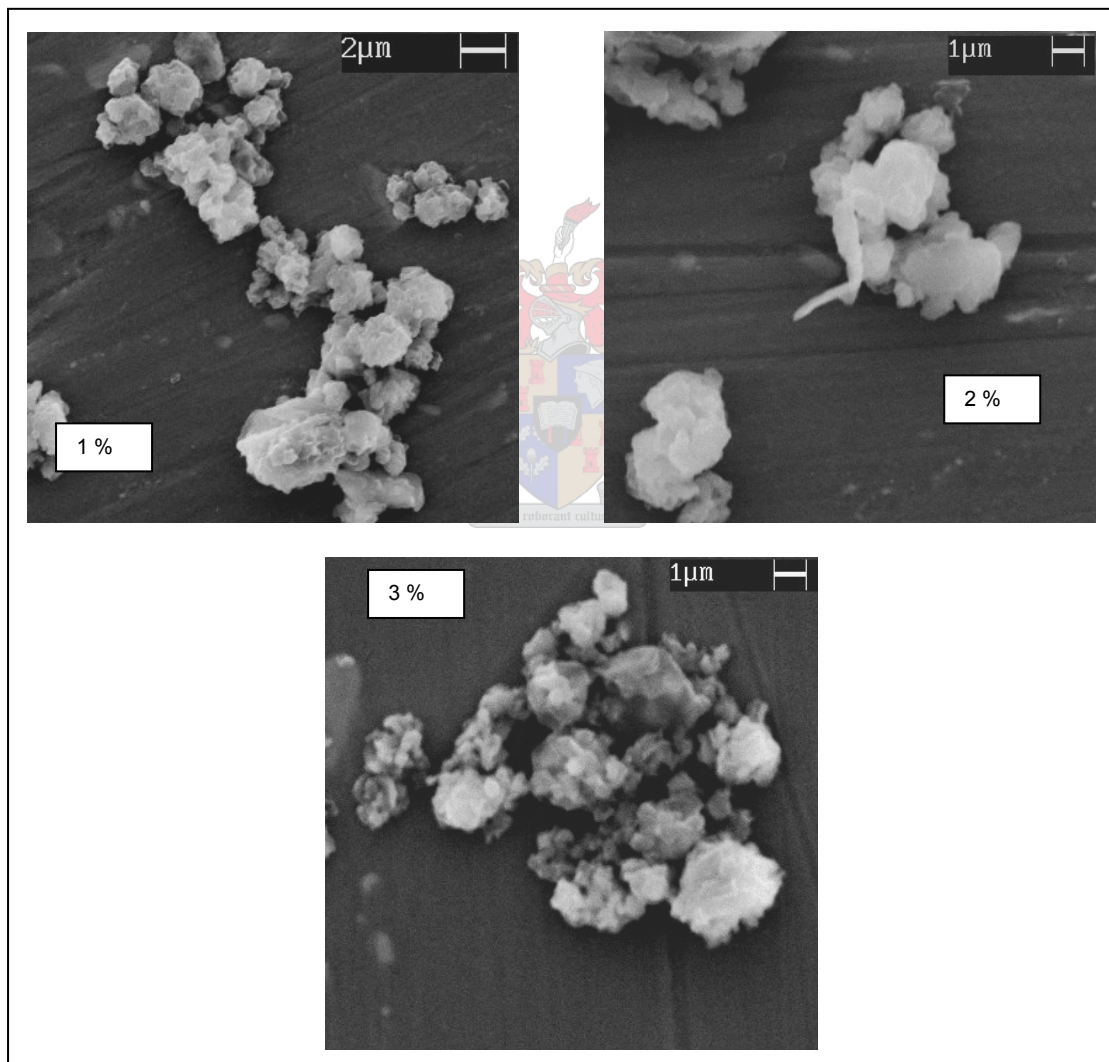


Figure 5-4: Particle Shape Dependence on Concentration at Pre-expansion Conditions of $T = 160\text{ }^{\circ}\text{C}$, $P = 150\text{ bar}$, Pore Size = $15\text{ }\mu\text{m}$.

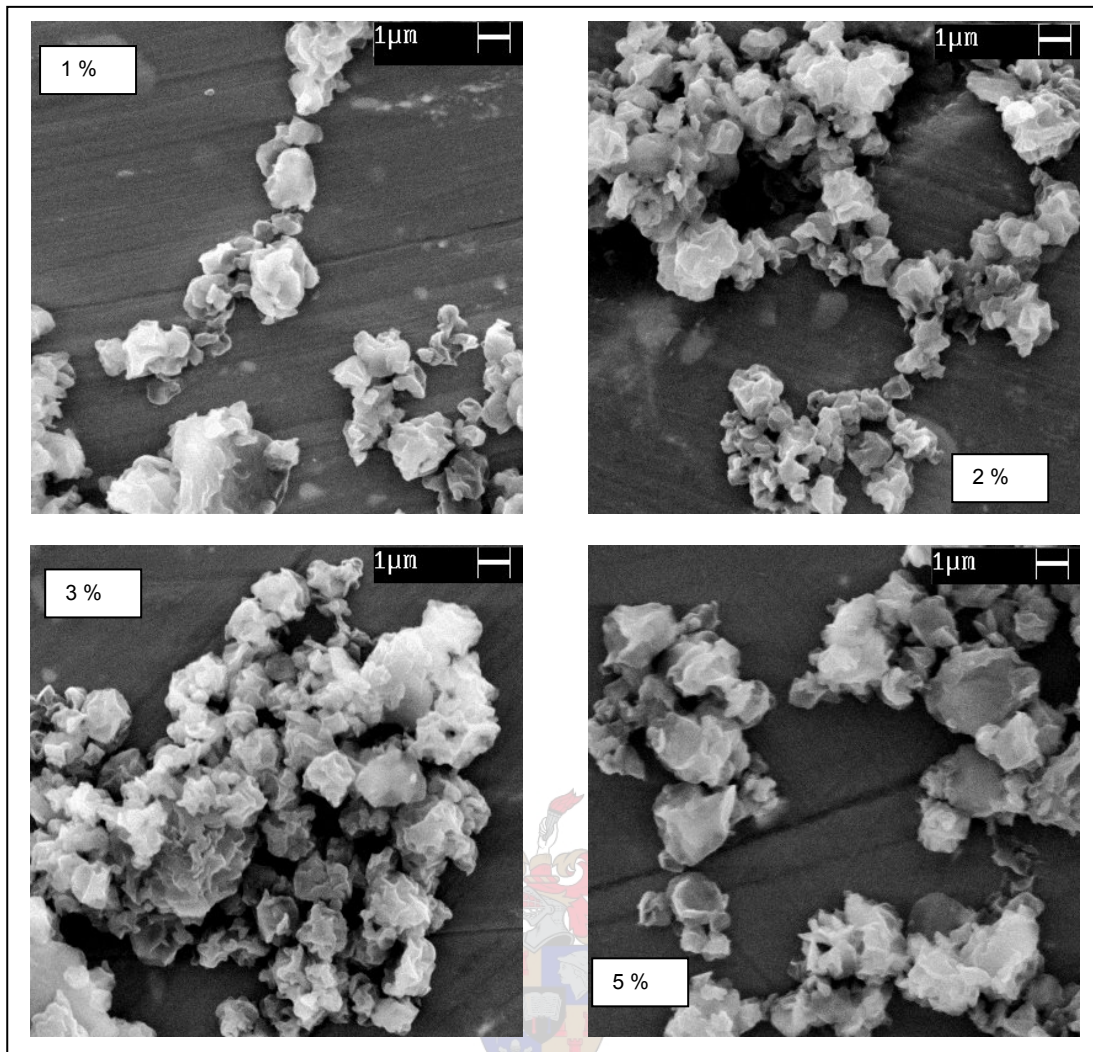


Figure 5-5: Particle Shape Dependence on Concentration at Pre-expansion Conditions of $T = 160\text{ }^{\circ}\text{C}$, $P = 150\text{ bar}$, Pore Size = $60\text{ }\mu\text{m}$.

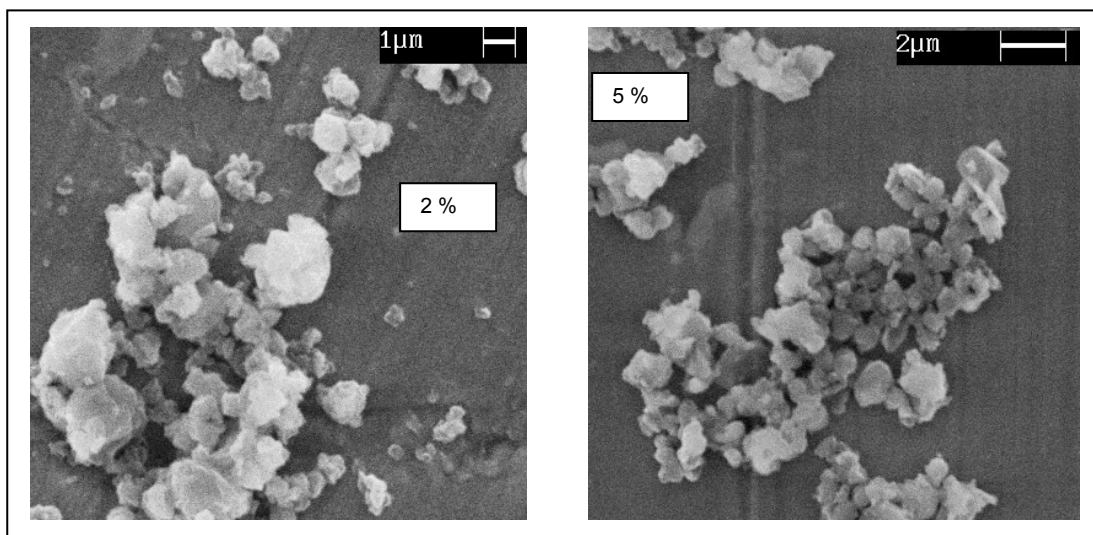


Figure 5-6: Particle Shape Dependence on Concentration at Pre-expansion Conditions of $T = 160\text{ }^{\circ}\text{C}$, $P = 150\text{ bar}$, Pore Size = $25\text{ }\mu\text{m}$.

5.2.2 The Influence of Temperature and Pressure

Particle Size

The pre-expansion conditions were varied in combinations indicated in Table 5-3. The obtained particle sizes and distribution are given there.

Table 5-3: C80 Particle Sizes obtained at Various Process Conditions

<i>No</i>	<i>T</i> (°C)	<i>P</i> (bar)	<i>x_{wax}</i> (wt %)	<i>Pore</i> <i>Size</i>	<i>d₁₀</i> (µm)	<i>d₅₀</i> (µm)	<i>d₉₀</i> (µm)	<i>d_{avg}</i> (µm)
3	160	150	3	15	0.55	0.98	1.67	1.06
7	130	150	3	15	0.50	0.96	2.14	1.18
8	130	175	3	15	0.53	0.92	1.73	1.05
22	130	150	2	60	0.87	1.39	2.44	1.58
21	130	175	2	60	0.56	0.99	2.17	1.21

- Comparison of run 21 with 22 and run 8 with 7 shows a decrease in particle size at higher pressure.
- The particle size distribution, given in Figures 5-7 and 5-8, would seem to indicate that a slightly narrower particle size distribution exists at the combination of 175 bar and 130 °C. In Figure 5-7, both of these temperature/pressure combinations resulted in narrower size distributions than that of the combination of 130 °C/150 bar.

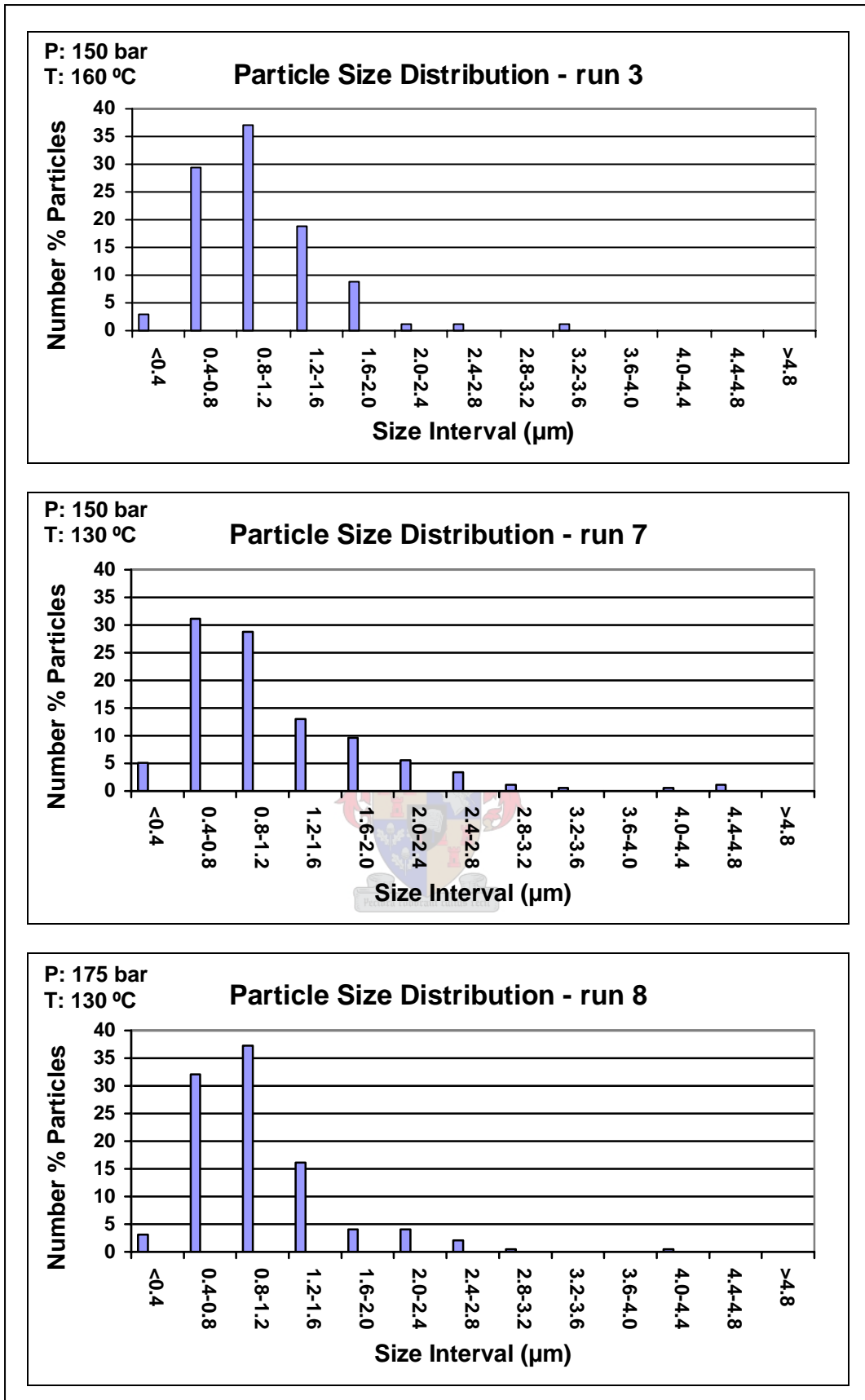


Figure 5-7: C80 Particle Size Distribution at Various Pre-expansion Conditions of a 3 % solution expanded via a 15 µm Nozzle

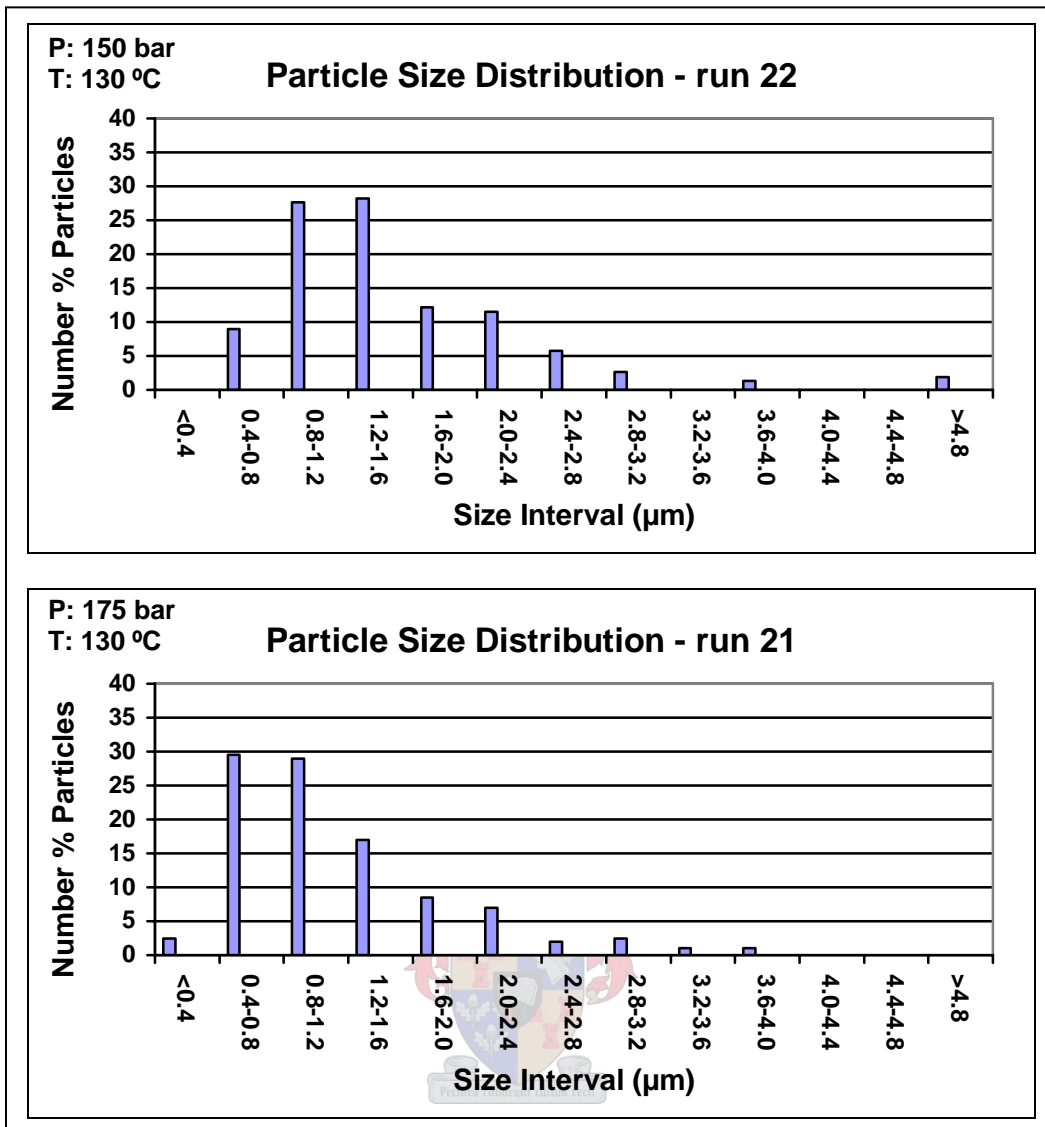


Figure 5-8: C80 Particle Size Distribution at Various Pre-expansion Conditions of a 2 % solution expanded via a 60 μm Nozzle

Particle Shape

Consider Figure 5-9. The combination of low temperature and high pressure does seem to yield particles that are of a more round shape and smoother surface. The particles from run 3 (150 bar, 160 °C) are rougher than those from the other two runs. The particles obtained at 150 bar and 130 °C does not seem to have well defined edges and also seem to be less smooth than the particles from the 175 bar solution.

The combination of high pressure and low temperature also seem to yield rounder and smoother particles when a 2 % solution was expanded through a 60 μm nozzle (Figure 5-10).

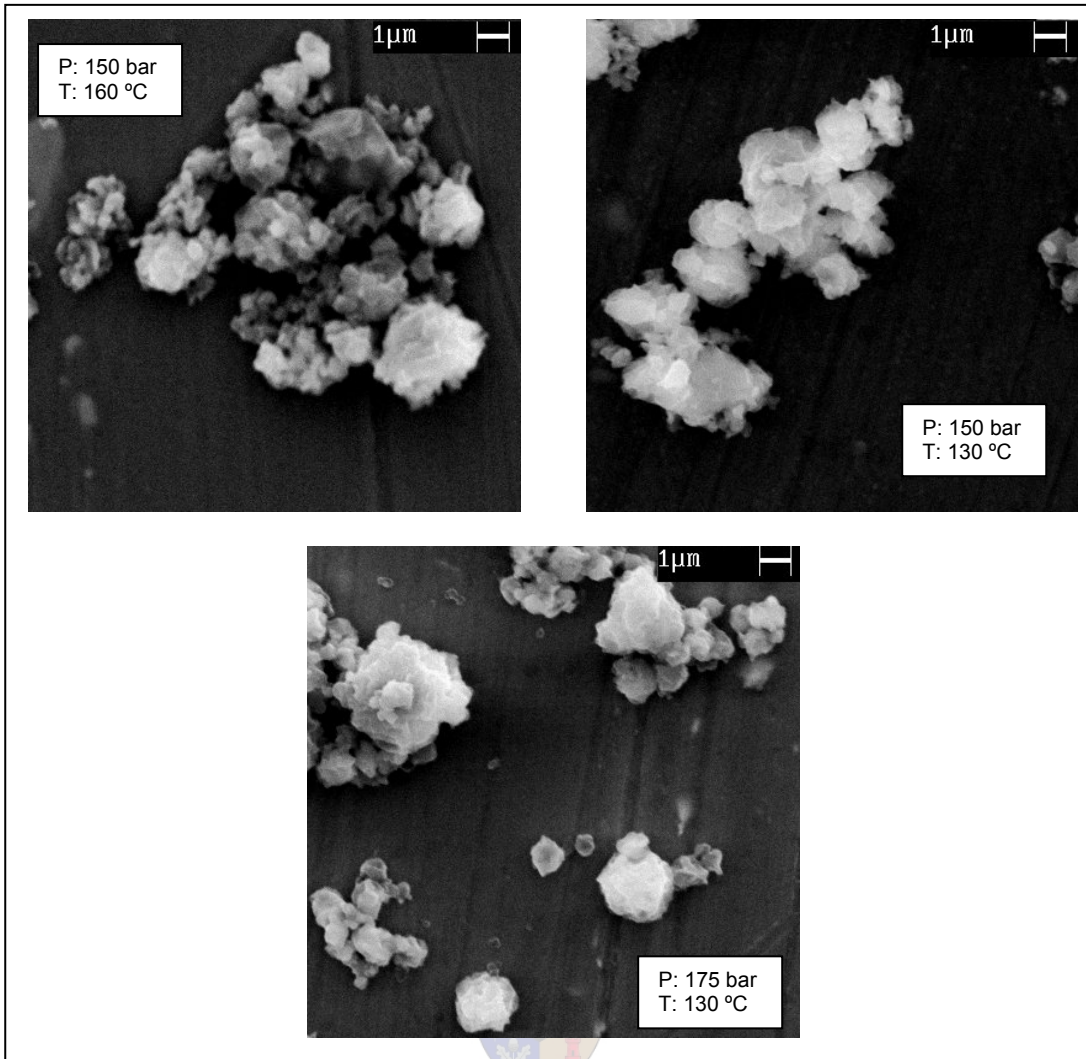


Figure 5-9: Particle Shape Dependence on Pre-expansion Conditions of a 3 % solution expanded via a 15 μm Nozzle

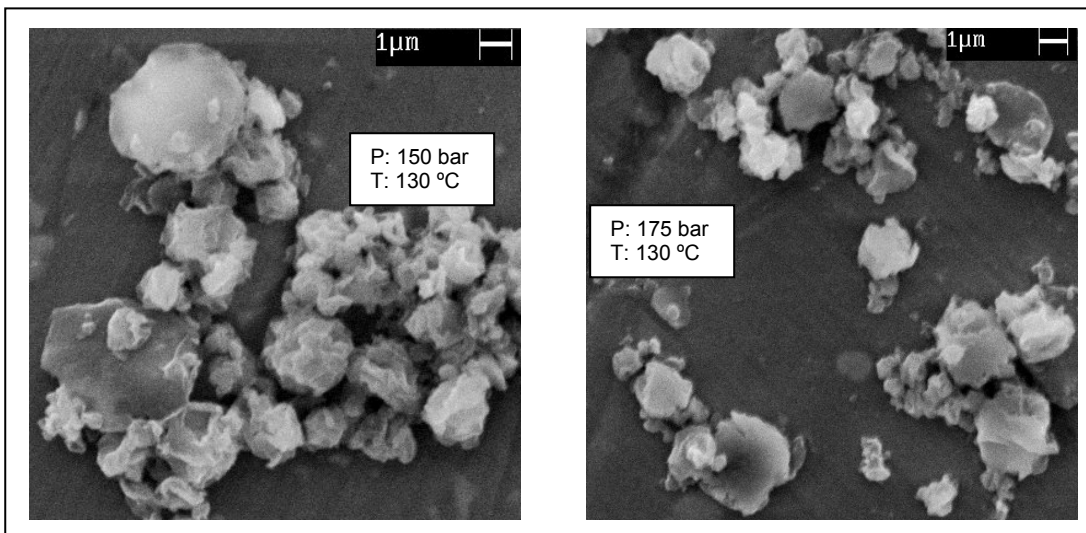


Figure 5-10: Particle Shape Dependence on Pre-expansion Conditions of a 2 % solution expanded via a 60 μm Nozzle

5.3 Micronisation of C105 Wax

5.3.1 The Influence of Concentration and Porous Plate Nozzles

The resultant particle sizes obtained by micronising C105 wax at concentrations of 2 and 5 % through 25 and 60 μm nozzles are presented in Table 5-4. When trying to expand a 2% solution through the 15 μm porous plate nozzle at conditions of 130 $^{\circ}\text{C}$ and 150 bar, the nozzle blocked instantaneously, and it was decided to abort any further runs with this nozzle.

Particle Sizes

Table 5-4: C105 Particle Sizes obtained from Various Nozzles and Concentrations

<i>No</i>	<i>T</i> ($^{\circ}\text{C}$)	<i>P</i> (bar)	<i>x_{wax}</i> (wt %)	<i>Pore</i> <i>Size</i>	<i>d₁₀</i> (μm)	<i>d₅₀</i> (μm)	<i>d₉₀</i> (μm)	<i>d_{avg}</i> (μm)
14	130	175	2	60	0.51	0.90	1.78	1.06
17	130	175	5	60	0.57	0.92	1.47	1.00
16	160	150	2	60	0.50	0.94	2.01	1.13
18	160	150	5	60	0.73	1.42	2.44	1.57
25	160	150	2	25	0.34	0.70	1.41	0.87
26	160	150	5	25	0.38	0.75	1.58	0.90

From Table 5-4, the following conclusions seem to be justified.

- Average particle sizes are in the region of 1.0 μm in all cases, except for run 18, where a 5 % concentration was expanded from 150 bar and 160 $^{\circ}\text{C}$.
- The influence of concentration on the particle size was small.
- A higher particle size was observed when a 5 % solution was sprayed through the 60 μm sinter plate, but the size difference observed for the other nozzles are insignificant.
- The size distribution for concentration of 2 % and 5 % are very similar. The particles obtained from the 25 μm nozzle is smaller than that from the 60 μm nozzle, and the size distribution is narrower compared to the particles

obtained from the 60 μm nozzle. The size distributions are shown in Figures 5-11 to 5-14.

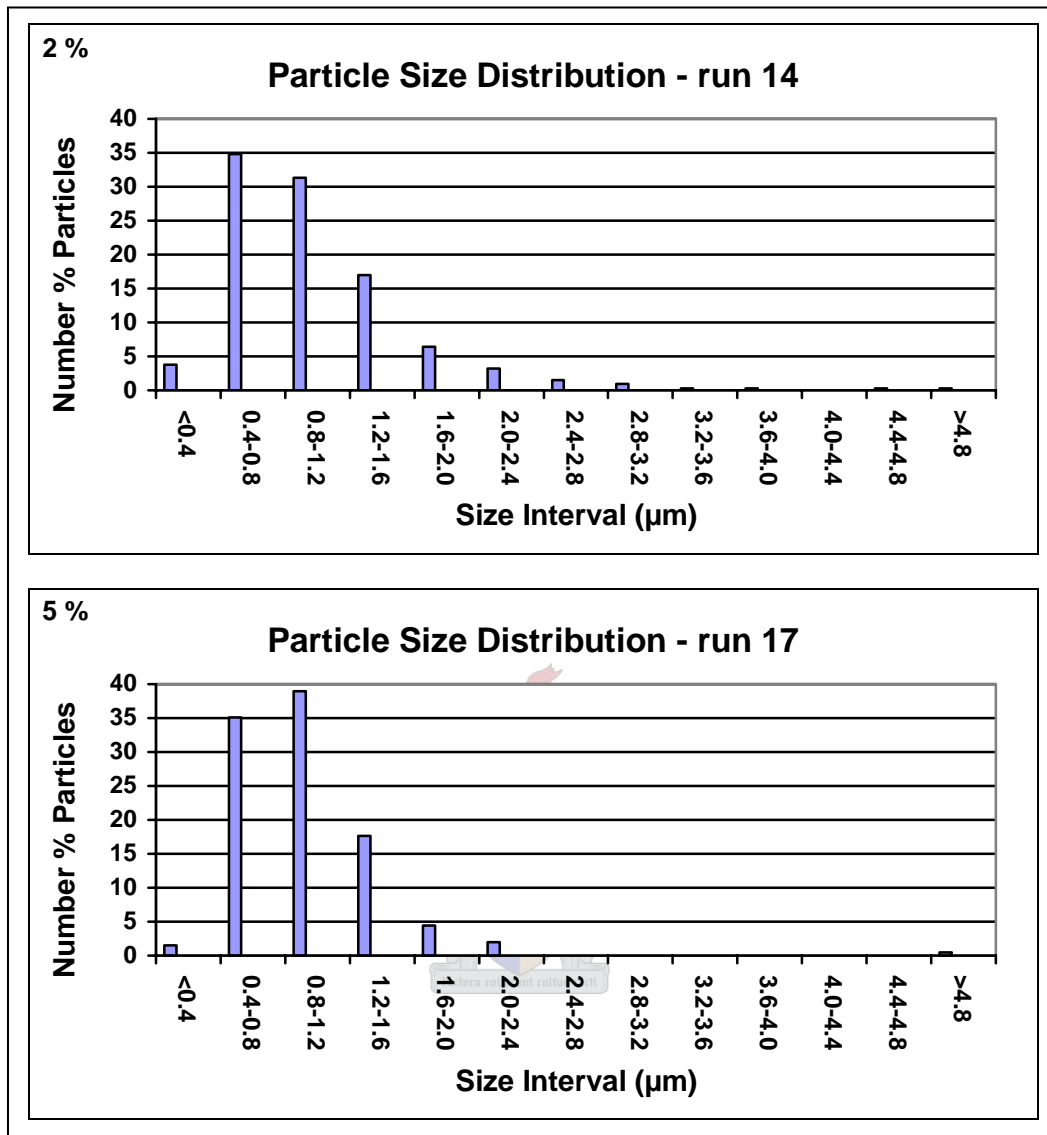


Figure 5-11: C105 Particle Size Distribution at Various Concentrations at Pre-expansion Conditions of $T = 130\text{ }^{\circ}\text{C}$, $P = 175\text{ bar}$, Pore Size = $60\text{ }\mu\text{m}$

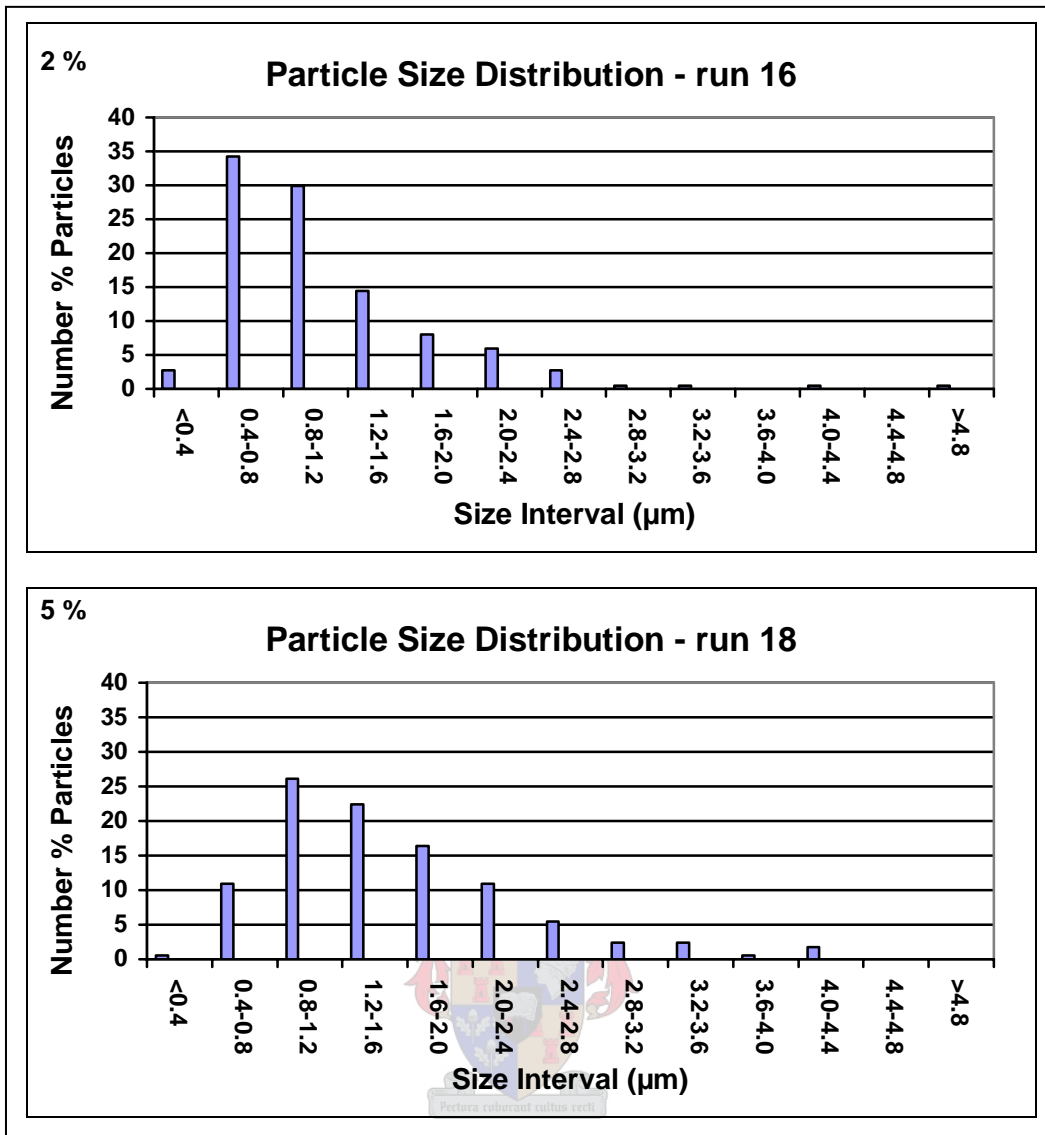


Figure 5-12: C105 Particle Size Distribution at Various Concentrations at Pre-expansion Conditions of T = 160 °C, P = 150 bar, Pore Size = 60 µm

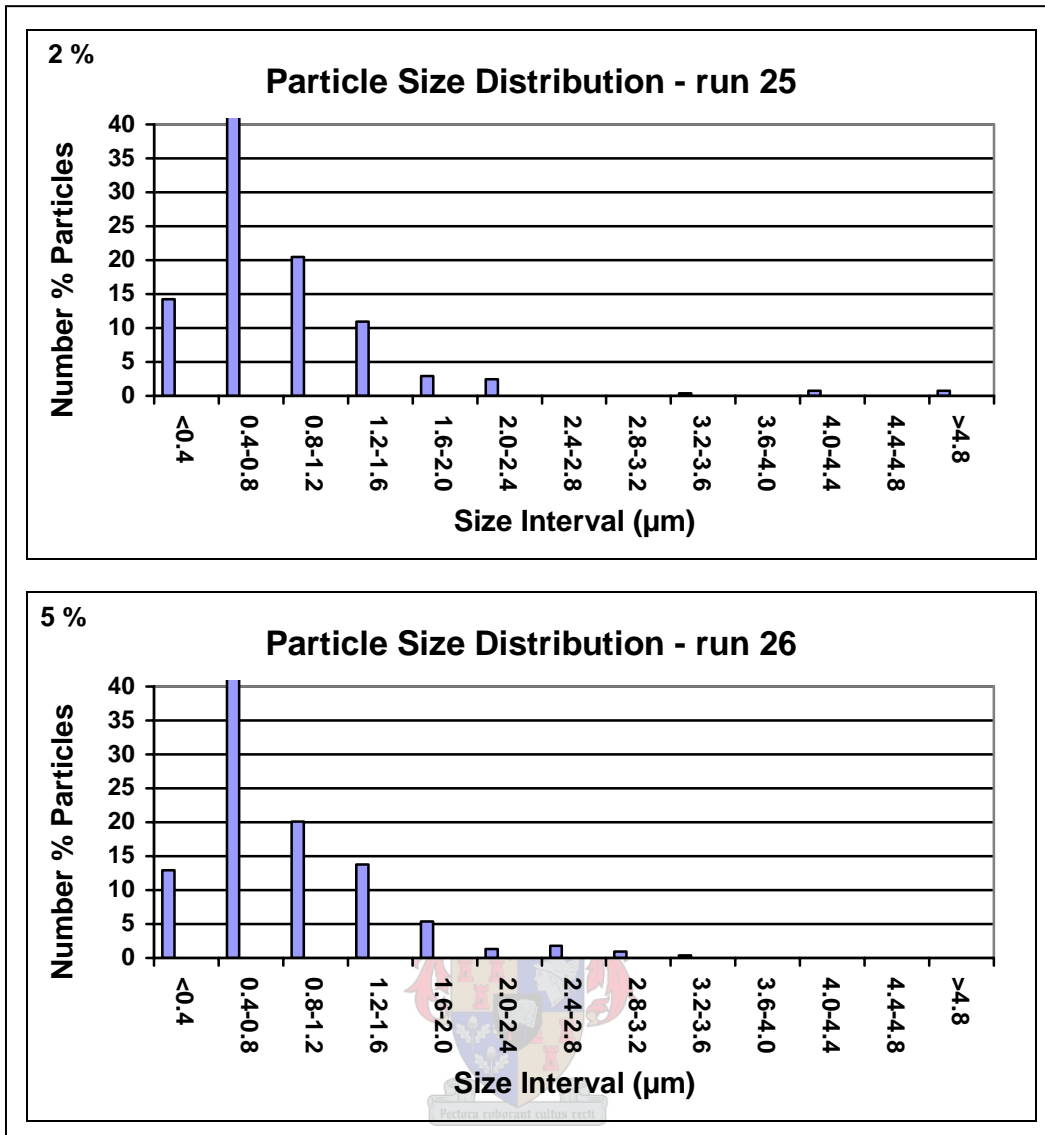


Figure 5-13: C105 Particle Size Distribution at Various Concentrations at Pre-expansion Conditions of T = 160 °C, P = 150 bar, Pore Size = 25 μm

Particle Shape

In Figure 5-14 to Figure 5-16 sections of the SEM images of particular samples are shown.

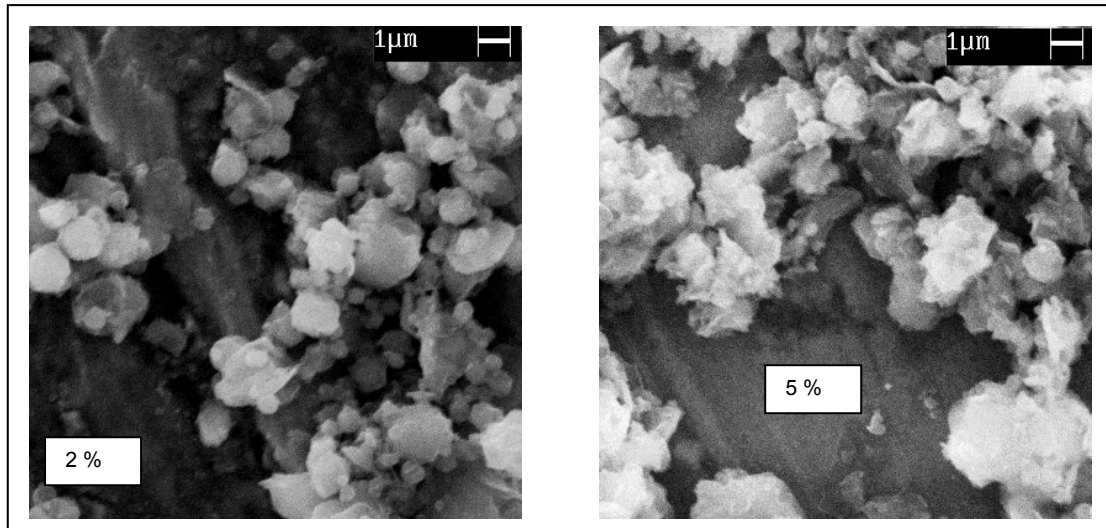


Figure 5-14: C105 Particle Shape Dependence on Concentration at Pre-expansion Conditions of T = 160 °C, P = 150 bar, Pore Size = 60 µm

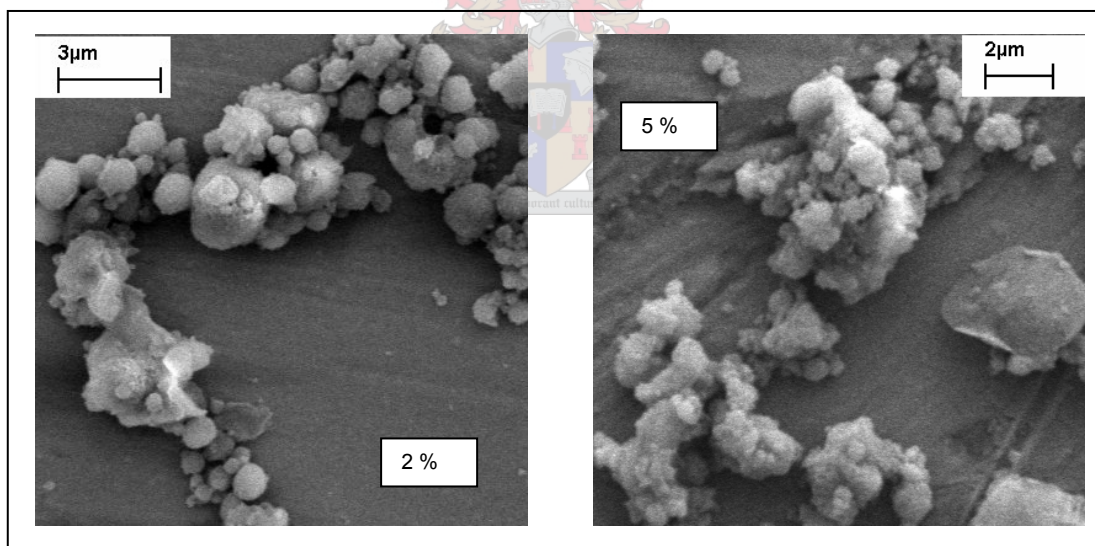


Figure 5-15: C105 Particle Shape Dependence on Concentration at Pre-expansion Conditions of T = 160 °C, P = 150 bar, Pore Size = 25 µm

From Figure 5-14 and Figure 5-15 it was observed that a few larger odd-shaped particles along with a multitude of small particles formed at the higher concentration. The particles formed at the lower concentration are visibly smoother than the particles formed at the higher concentration.

From Figure 5-15, it is evident that much better particles result when expansion occurred through the 25 μm . The particles are more spherical in shape, more discreet and generally the sort of product desired. The particles obtained from the 60 μm nozzle were more angular and pointy, and the particles seem to consist of aggregates of smaller particles.

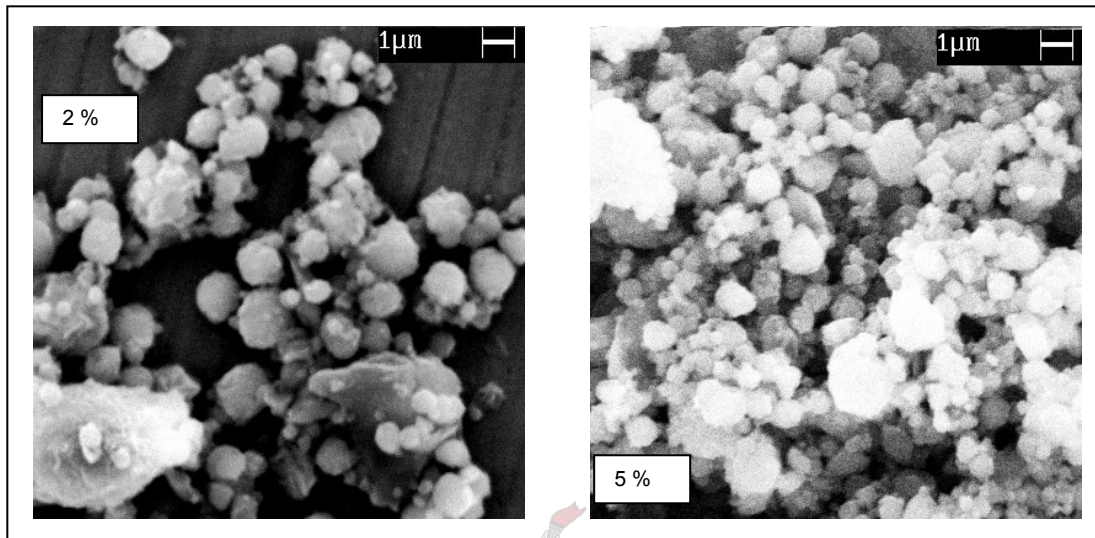


Figure 5-16: Particle Shape Dependence on Concentration at Pre-expansion Conditions of $T = 130\text{ }^{\circ}\text{C}$, $P = 175\text{ bar}$, Pore Size = 60 μm

The particles obtained at the conditions of higher temperature and pressure are of much better shape than those obtained in the other runs so far, with the exception of those from run 14, shown in Figure 5-16 above. The influence of the conditions will be discussed in the following section though. If the shape of the particles obtained from the two different concentrations is compared, there does not seem to be a large difference in the shape. Both batches seemed to mostly contain reasonably spherical particles, with no sub-particles seemingly present.

5.3.2 The Influence of Temperature and Pressure

As was already seen in section 5.3.1, the C105 particles formed at higher pressure was of much more desired shape compared to other particles found thus far. Consider the particles formed from different conditions.

Particle Size

Table 5-5: C105 Particle Sizes obtained at Various Process Conditions

<i>No</i>	<i>T</i> (°C)	<i>P</i> (bar)	<i>x_{wax}</i> (wt %)	<i>Pore</i> <i>Size</i>	<i>d₁₀</i> (μm)	<i>d₅₀</i> (μm)	<i>d₉₀</i> (μm)	<i>d_{avg}</i> (μm)
16	160	150	2	60	0.50	0.94	2.01	1.13
15	130	150	2	60	0.47	0.95	1.85	1.10
14	130	175	2	60	0.51	0.90	1.78	1.06
18	160	150	5	60	0.73	1.42	2.44	1.57
17	130	175	5	60	0.57	0.92	1.47	1.00

- The influence of the temperature and pressure on the average particle size does not seem to be significant at the lower pressure, but at 5 % concentration larger particles were formed when the inlet conditions were closer to the solution's dew point.
- There also seems to be a slightly narrower size distribution at these conditions at conditions of high pressure and low temperature.
- In the runs at higher concentration, the high pressure/low temperature combination quite clearly yields particles with smaller size and narrower size distribution.
- The particle size distributions, showed in Figures 5-17 (runs 14, 15 and 16) for a 2 % solution expanded through a 60 μm nozzle are virtually identical. In Figure 5-18 it is however very clear that a much narrower size distribution was obtained when the solution was expanded from higher pressure.

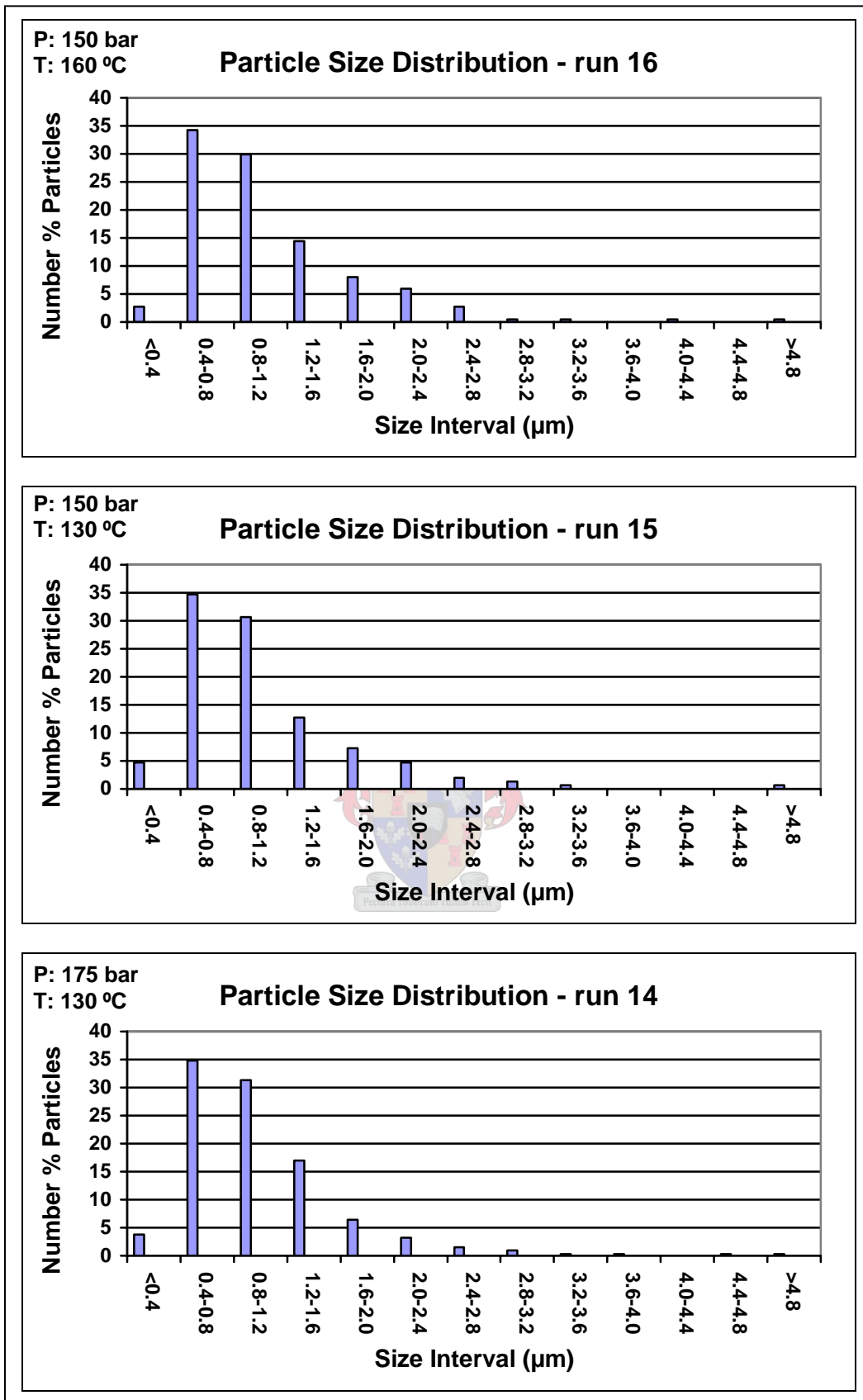


Figure 5-17: C105 Particle Size Distribution for Various Pre-expansion Conditions of a 2 % solution expanded via a 60 µm Nozzle

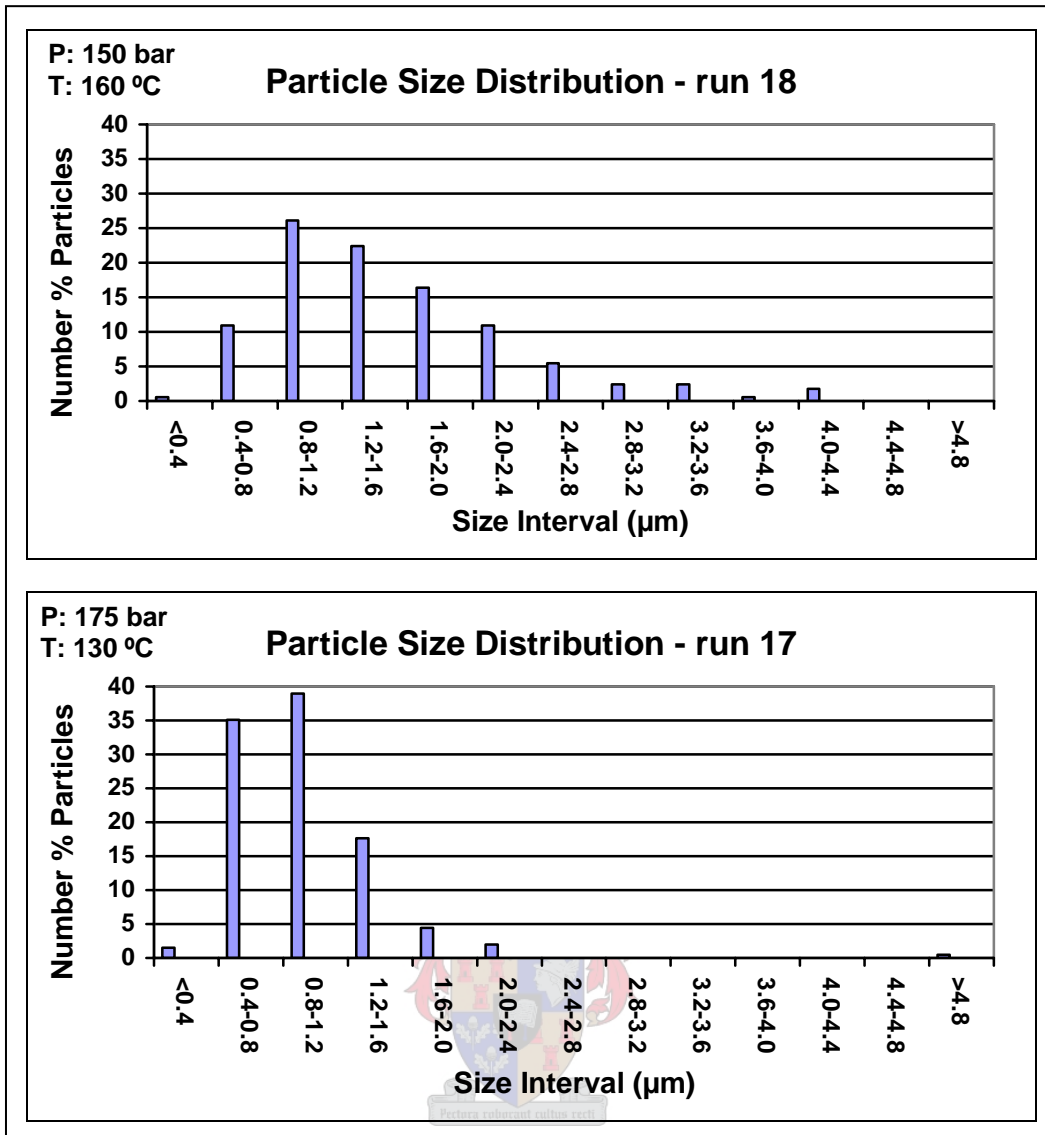


Figure 5-18: C105 Particle Size Distribution for Various on Pre-expansion Conditions of a 5 % solution expanded via a 60 μm Nozzle

Particle Shape

The particle shape of the samples obtained in Table 5-5 can be seen in the SEM images given in Figure 5-19 and Figure 5-20. It is quite clear that pre-expansion conditions of 175 bar and 130 °C lead to the formation of spherical particles with a smooth surface. These particles are discreet with well-defined edges, in comparison with the particles that formed from the other conditions.

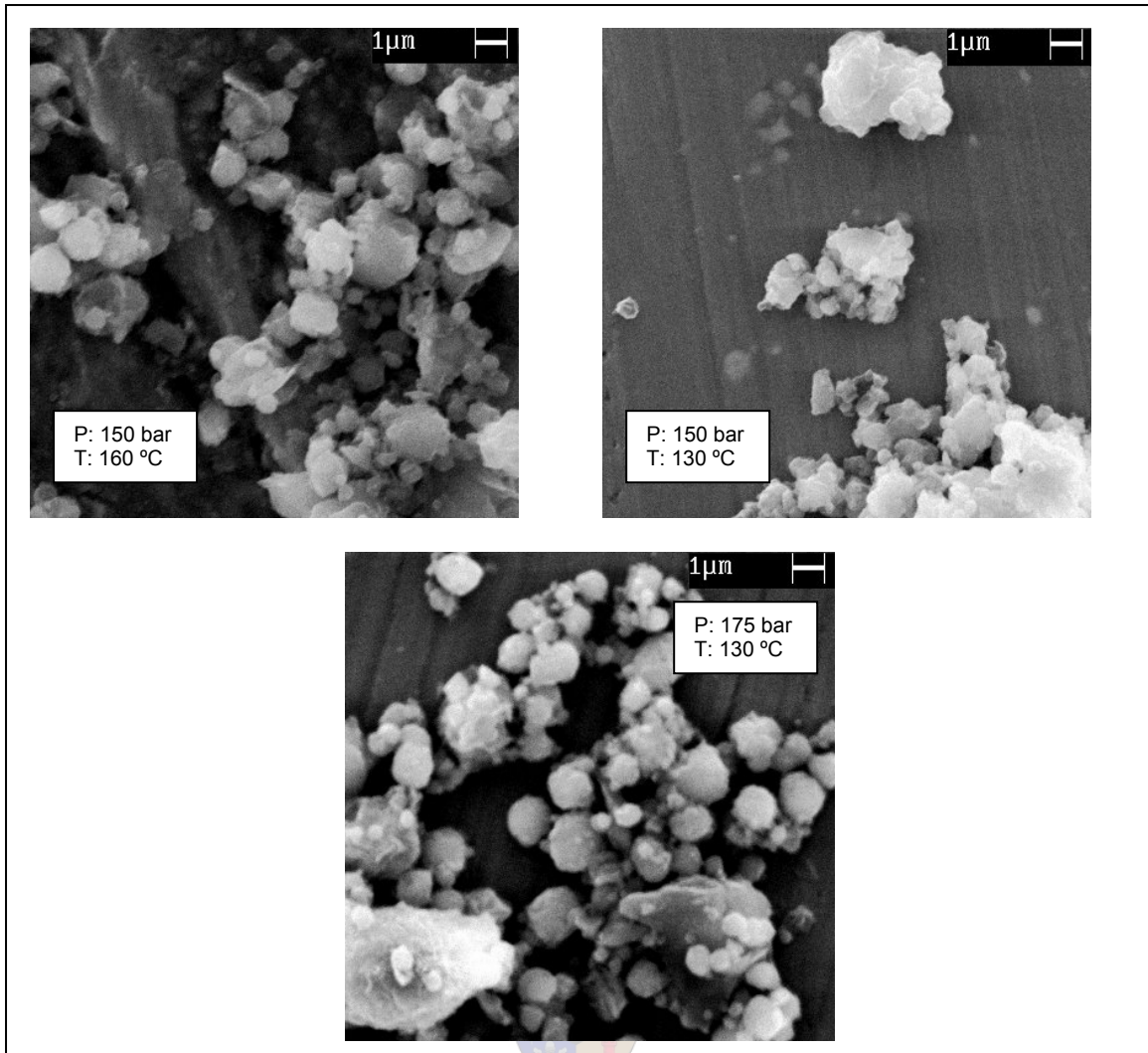


Figure 5-19: C105 Particle Shape Dependence on Pre-expansion Conditions of a 2 % solution expanded via a 60 μm Nozzle

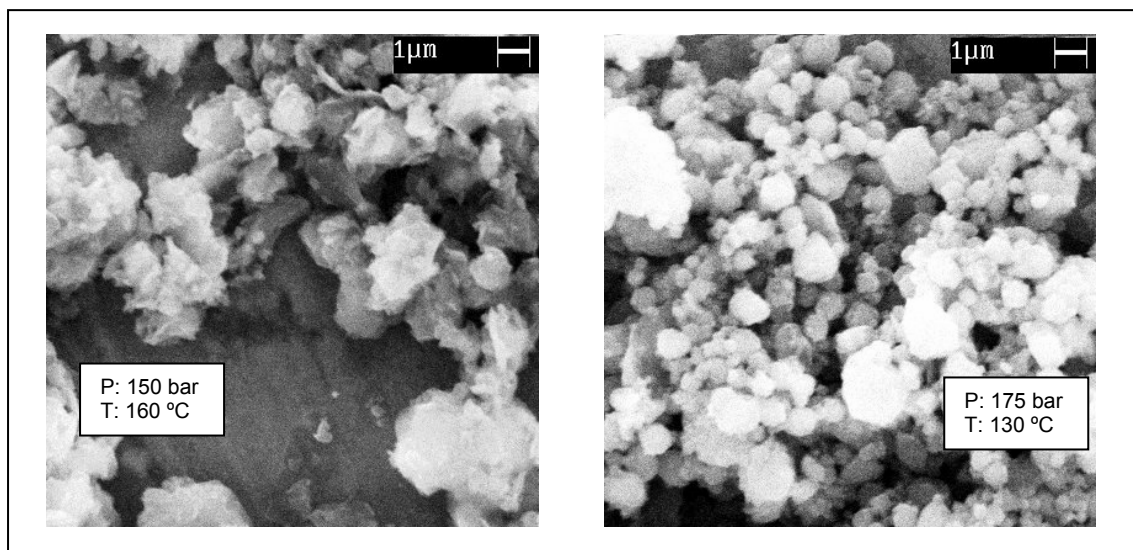


Figure 5-20: C105 Particle Shape Dependence on Pre-expansion Conditions of a 5 % solution expanded via a 60 μm Nozzle

5.3.3 Upper Concentration Limit

Particle Size

The C105 wax particles have been of a more spherical shape than the C80 wax. An effort was made to determine the maximum wax concentration whereby a satisfactory product could still be obtained. It was decided to utilise the combination of high pre-expansion pressure, low pre-expansion temperature and the 25 μm porous plate nozzle that seemed to give the better results. The particle sizes that were obtained are summarised in Table 5-6.

Table 5-6: C105 Particle Sizes obtained from Various Concentrations at 175 bar and 130 °C via Expansion through a 25 μm Nozzle

<i>No</i>	<i>T</i> (°C)	<i>P</i> (bar)	<i>x_{wax}</i> (wt %)	<i>Pore</i> <i>Size</i>	<i>d₁₀</i> (μm)	<i>d₅₀</i> (μm)	<i>d₉₀</i> (μm)	<i>d_{avg}</i> (μm)
27	130	175	3	25	0.57	1.34	2.34	1.43
28	130	175	4	25	0.39	0.77	1.80	0.98
29	130	175	5	25	0.56	1.00	2.18	1.25
30	130	175	6	25	1.22	1.81	3.25	2.02

From Table 5-6 the smallest particles were obtained from the 4 % solution, but the 3 % and 5 % solution also gives satisfactory results as far as particle sizes are concerned. From Figure 5-21 it was also very evident that a much narrower particle size distribution was found at a concentration of 4 %.

But before a conclusion is drawn regarding the upper concentration limit of satisfactory particles, let us first consider images of the particle shape.

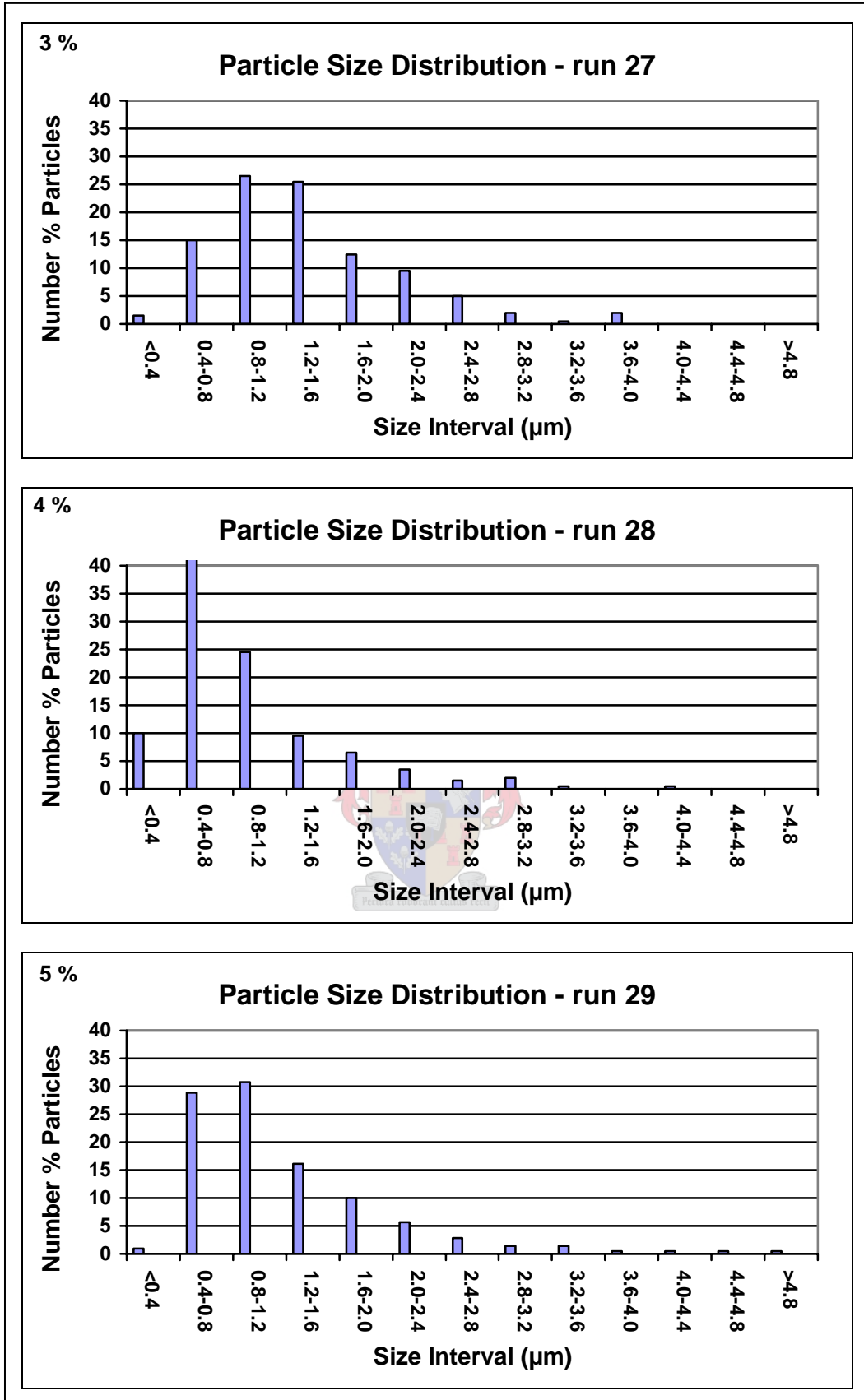


Figure 5-21: Particle Shape Dependence on Concentration at Pre-expansion Conditions of $T = 130\text{ }^{\circ}\text{C}$, $P = 175\text{ bar}$, Pore Size = $25\text{ }\mu\text{m}$

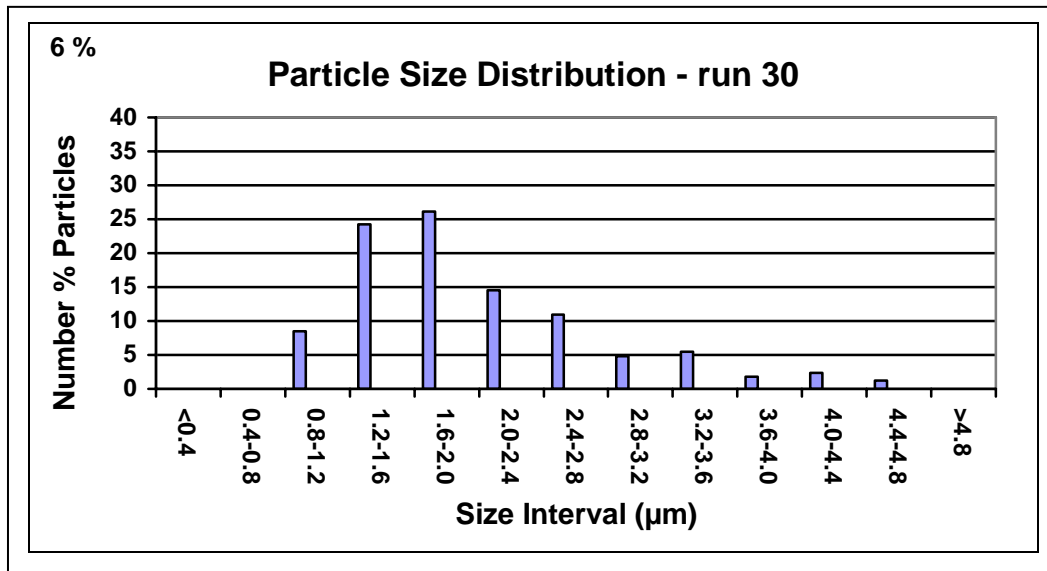


Figure 5-21 (cont): Particle Shape Dependence on Concentration at Pre-expansion Conditions of T = 130 °C, P = 175 bar, Pore Size = 25 µm

Particle Shape

The particle shape of the particles obtained from these four runs can be seen in Figure 5-22. The particles obtained from concentrations of 3-4 % seem to be spherical within requirements of this project. As soon as concentrations as high as 5-6 % were used, an increase in angular non-uniform particles were seen. Although the particles obtained from the 5 % solution still contains some spherical particles, this is much less evident at the 6 % concentration.



From the evidence gathered here, it is recommended that concentration in the region of 4 % be used to obtain the particles required in this project.

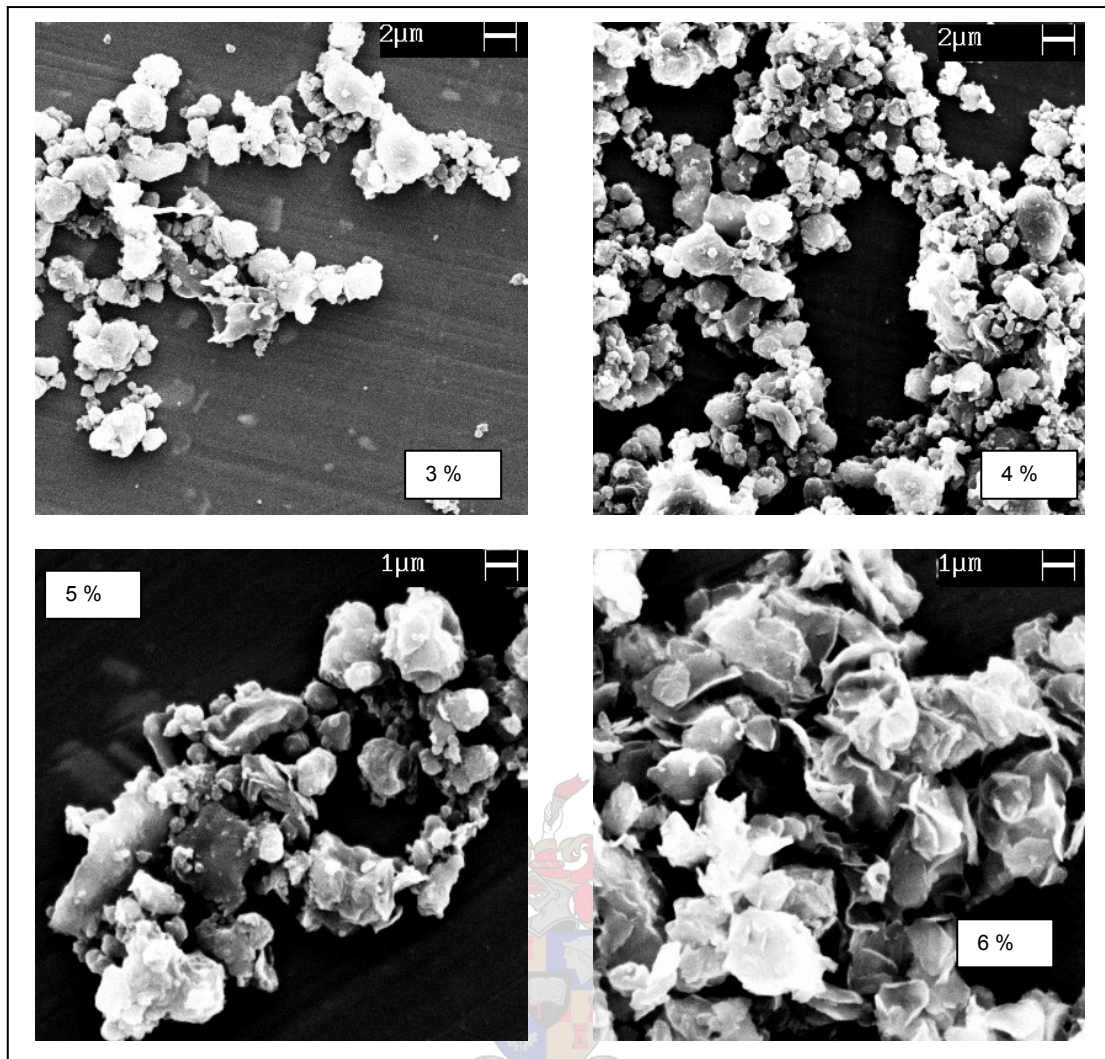


Figure 5-22: Particle Shape Dependence on Concentration at Pre-expansion Conditions of $T = 130\text{ }^{\circ}\text{C}$, $P = 175\text{ bar}$, Pore Size = $25\text{ }\mu\text{m}$

5.4 Repeatability of Experimental Data

In order to have confidence in the experimental results obtained, two further questions needed answering. The first of these pertained to the repeatability of the experiments, and the second to the accuracy of the obtained particle sizes.

5.4.1 Repeatability Experiments

Two experiments were chosen at random, and repeated as closely as possible to the original runs. The chosen experiments were runs 4 and 17.

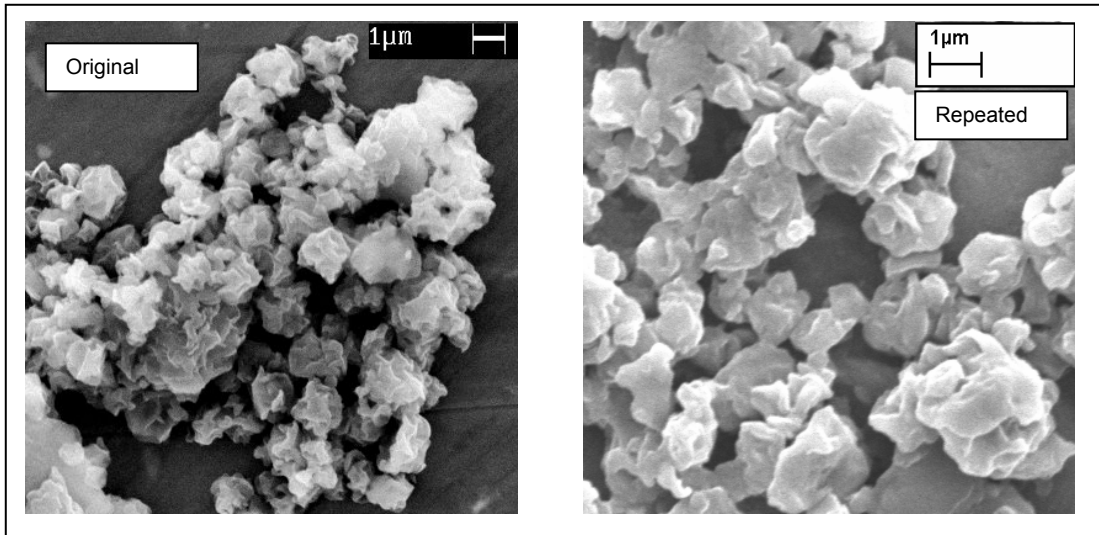


Figure 5-23: Comparison of original run (left) and repeated run for C80 wax at pre-expansion conditions: T = 160 °C, P = 150 bar, x = 3.0 wt %, Pore size = 60 μm

From the SEM images, it seems as if the particles obtained in the two runs are of the same shape. In both cases the particles are seem to be non-spherical and almost pollen-like in appearance.

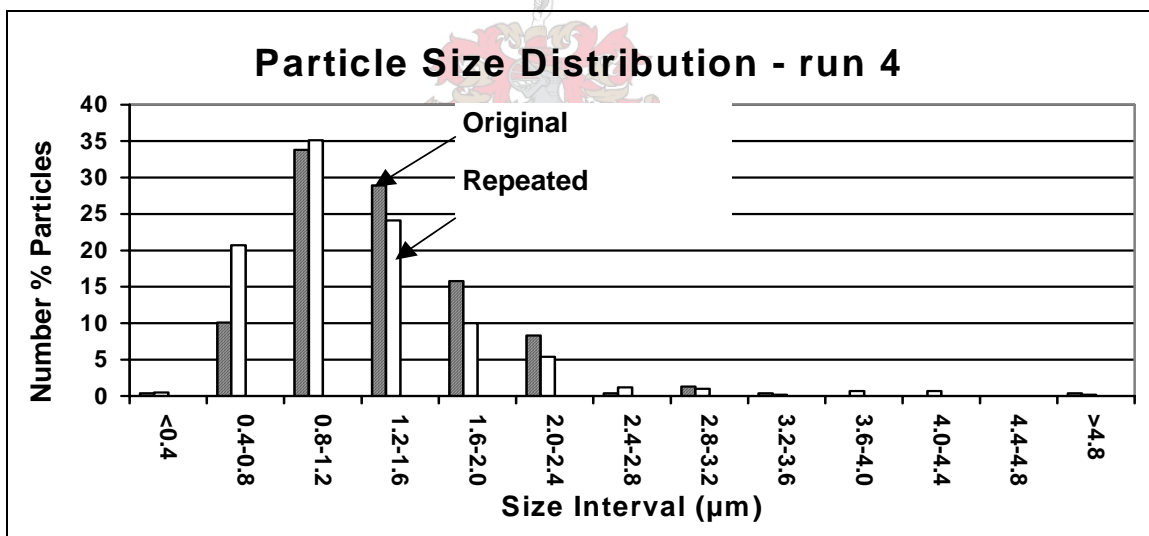


Figure 5-24: Comparison of Particle Size Distribution of Original and Repeated Run

In Figure 5-24 the particle size distribution is shown. The repeated run delivered somewhat smaller particles than the original run. The obtained average particle size for the repeated run was 1.26 μm in comparison to 1.35 μm of the original run.

Since the particle shape and size for the two runs were quite similar, run 4 seems fairly repeatable. In order to make more concrete conclusions on the repeatability of the experiments though, more runs should be repeated and analysed.

5.4.2 Repeatability of Particle Size Analysis

In order to verify the validity of the particle size analysis method, a sample SEM photograph of experimental run 4 was taken, and re-analysed twice after a period of two months after the original analysis. The same image was also analysed by an independent person who used the same technique during experimental work with vesiculated beads. Run 4 was specifically chosen, because the particles are not completely spherical, thus making the particle analysis more susceptible to discrepancies. The analysed SEM image of the analysed sample is shown in Figure 5-25.

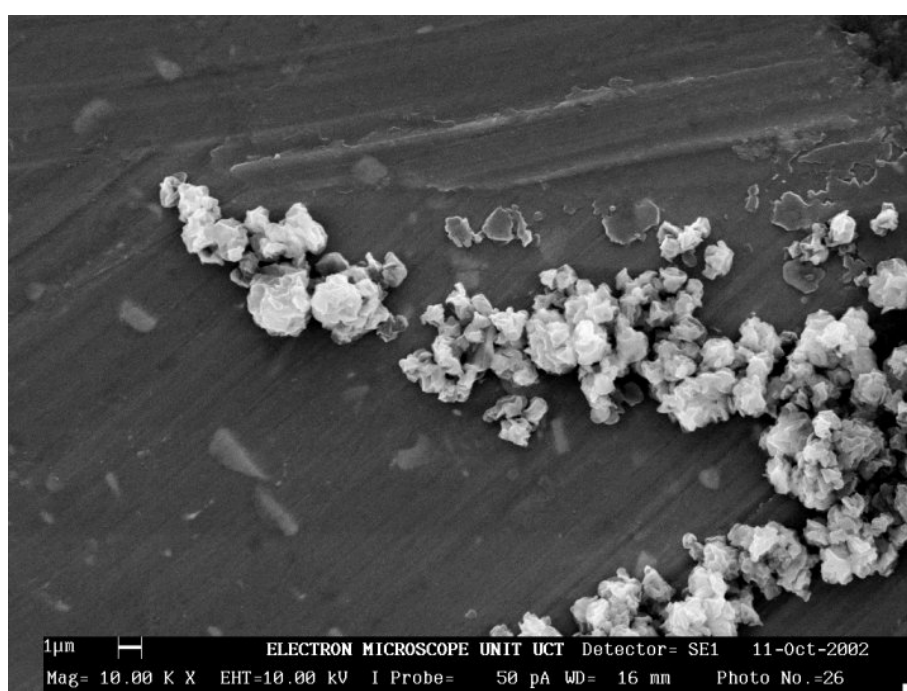


Figure 5-25: Sample on which Particle Size Repeatability Analysis were Performed

In Table 5-7, the repeated particle size is shown. The repeated counts indicates that accuracy within 0.1 μm seems achievable if a single operator performs all the analysis. The particle size obtained by the independent operator was notably smaller.

It would thus seem as if the chosen particle size analysis method could be used to compare particles accurately within 0.1 μm if one operator performs the all analysis. The fact that the independent operator found much smaller particles is indicative of the fact that the operator also influences particle size.

It is advised that the particle sizes shown in this thesis be used as indication of the size of the particle, but not as the precise particle size.

Table 5-7: Results of Repeated Particle Size Determination

	<i>Original</i>	<i>Repeat 1</i>	<i>Repeat 2</i>	<i>Independent</i>
d ₁₀	0.79	0.80	0.86	0.74
d ₅₀	1.26	1.26	1.28	1.05
d ₉₀	2.02	1.91	2.02	1.66
d _{avg} (μm)	1.36	1.35	1.40	1.15

5.5 The Effect of Wax Type

It was seen in the resultant SEM images that the C80 wax particles are of irregular shape and also seem to consist of smaller particles that are fused together. Throughout the results it is evident that the harder C105 wax resulted in particles of a rounder shape.

If the dew points of the waxes are considered (see section 5.1) it would suggest that for the same nozzle entry conditions, C80 wax will fall out of solution further down the nozzle compared to the C105 wax. This should theoretically decrease the period for particle growth. Yet the shape of the C80 wax would suggest strong influences of agglomeration and coagulation in the particle formation. This was less prevalent in C105 waxes formed from the same nozzle entry conditions.

One possible explanation could lie in the composition of the waxes. The C80 wax contains 0.75 % oil compared to the 0.1 % of C105 wax. (www.schumann-sasol.com July 2002)

As the pressure of the expanding solution decreases, the different fractions of wax become insoluble in the supercritical propane and fall out of solution. This is much the same as in a fractionation process. The oil fraction is the lightest of the wax fractions and will be the last to leave the solution. The oils will condense onto the surface of the already formed particles. This oil may well alter (soften) the surface of the particles, that could enhance coagulation or maybe even agglomeration effects. In Figure 5-26 a RESS experiment of pure n-C₃₆H₇₄ (n-C36) versus the C80 wax is shown.

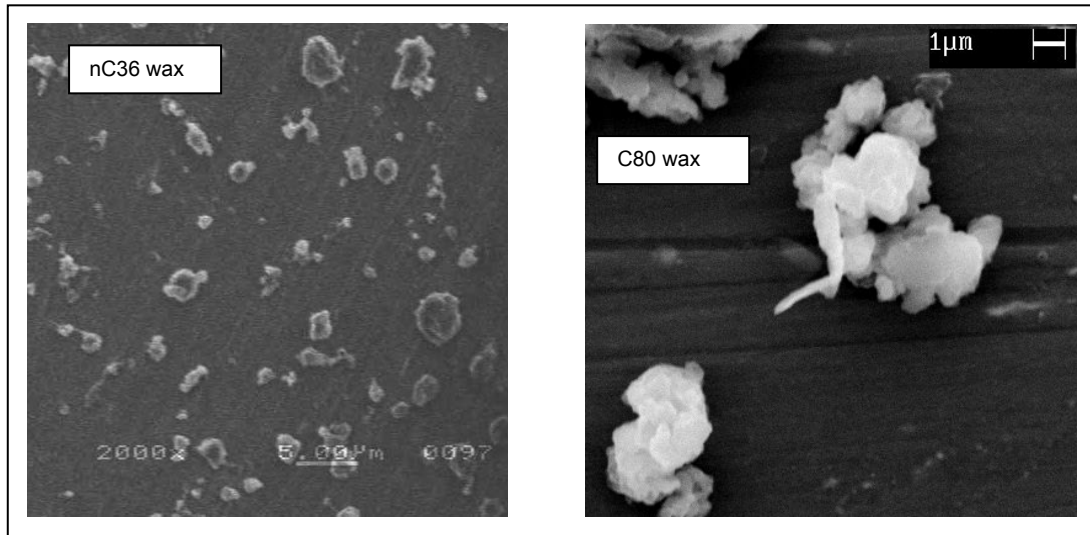


Figure 5-26: Comparison of n-C36 (left) and C80 wax at pre-expansion conditions: $T = 160\text{ }^{\circ}\text{C}$, $P = 150\text{ bar}$, $x = 2.0\text{ wt } \%$, Pore size = $15\text{ }\mu\text{m}$

From the Figure it seems as if the pure alkane particles are more spherical and more discrete than that of the C80 wax. The n-C36 particles does not seem to consist of agglomerated sub-particles.

This could possibly explain the reason for the non-spherical and aggregated C80 particles compared to C105 particles. A lower pre-expansion temperature may be considered for the micronisation of C80 wax. Since the C80 is still a liquid at the propane critical temperature, a supercritical fluid with a slightly lower critical temperature may be considered. Here an ethane/propane mixture might be a possible alternative solvent.

5.6 Discussion

From the results obtained, it seems obvious that the following conditions seem to yield particles that are most sought after:

5.6.1 Pre-expansion Temperature and Pressure

From the results it became evident that better particles could be obtained when the pre-expansion conditions were further away from the dew point. This was especially clear in the obtained C105 particles. This trend is in accord with theoretical expectations, since the phase transition would be postponed until later in the nozzle, or the free jet. The period for particle growth is lower if nucleation takes place further down the nozzle.

The pressure would need to be kept to a minimum to save on energy costs. From the batch experiments it was evident that the optimum pressure for formation of spherical particles was in excess of 175 bar.

At the high pressure, a temperature of 130 °C was sufficient to yield particles with the desired spherical shape. A higher temperature of 160 °C was also used at the lower pressure of 150 bar. At the lower temperature, with C80 wax at 3 % (15 µm sinter) the lower temperature gave larger particles. Virtually no change in size was observed for the C105 wax (2 %, 60 µm sinter) between the two temperatures (Table 5-3 and 5-5). The shape of the particles did not change remarkably with a change in the temperature. (Compare Figure 5-4 and 5-9) Unfortunately, higher temperatures was not used at the higher pressure due to the pressure rating of the shut-off valve. From an industrial viewpoint, the lower temperature would lead to lower energy cost.

5.6.2 Concentration

As explained in chapter 4 of this thesis, a higher wax concentration could lead to higher supersaturation ratios. This in turn will lead to high nucleation rates of small particles. However, the higher number concentration of particles and smaller distances between particles increase the chances of collision and resultant coagulation and agglomeration effects. From the SEM images presented in this thesis it could be seen that more angular particles formed at higher concentration. This shape is typical of particles that have undergone growth processes, including coagulation and agglomeration.

From the experiments done to obtain the upper limit of concentration for the C105 wax, it was seen that concentration could be increased up to about 4 %, above which the particles visibly became less spherical. It does thus seem that at concentrations above 4 %, the large amount of small particles formed form rapid nucleation undergoes interaction to form larger composites of smaller particles.

5.6.3 Expansion Nozzle

From the results it was rather clear that the 25 µm porous plate nozzle yielded particles that were more desired. It is significant that the 15 and 60 µm nozzles were from the same manufacturer (Swagelok), but that the 25 µm porous plate were from a different manufacturer (Hoke).

Although further specifications on the filters were not available, it became clear through experimental observation that the flow rate through the 25 μm nozzle was higher than that through the 15 and 60 μm nozzles. Since all nozzles had the same area exposed to the solution, and were of the same thickness, the only conclusion that could be drawn was that the 25 μm nozzle was more porous than the 15 and 60 μm nozzles. This was confirmed when inspecting images of the inlet flow area of the tree separate porous plate nozzles (Figure 5-27). The flow area (pore) to metal area ratio seems to be quite significantly larger for the 25 μm nozzle. This would indicate that a larger pressure drop could be expected through the nozzles with the smaller porosity, which would lead to precipitation further upstream of the nozzle.

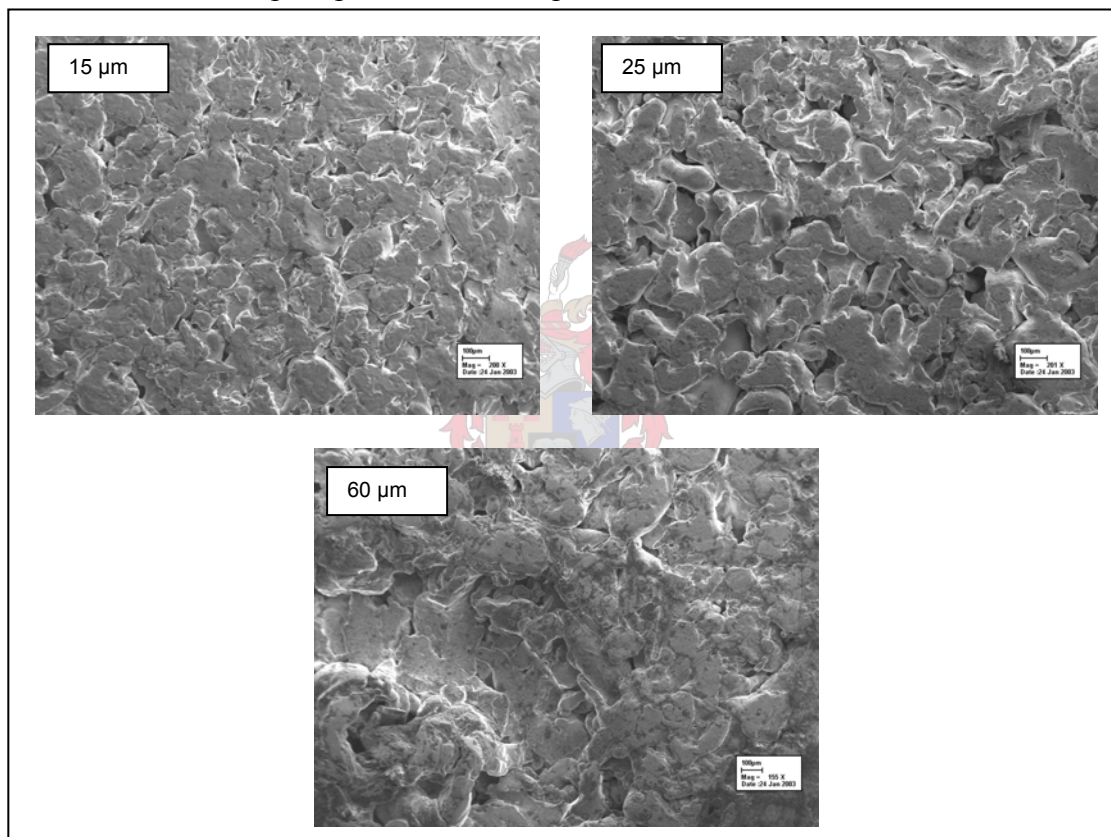


Figure 5-27: SEM Image of Inlet Flow Area of Porous Plate Nozzles

It can be concluded here, that porous plate nozzles should always be characterised on more than just the average pore size, since porosity seems to play a vital role in the expansion process.

5.6.4 Production Rate

When using these 25 μm spraying nozzles, a full cell of solution was emptied in approximately 4-8 seconds. As the cell contained approximately 16 g of solution, and

taking a conservative value of 5 seconds spraying time, this gives a flow rate of 11.5 kg/h. As a cylindrical area of 3 mm was exposed to the solution, an estimation of the flow rate was found to be approximately 160 kg/h/cm². If a 4 % wax solution is used, this leads to a wax powder production tempo of 6.4 kg/h/cm².

5.7 Limitations of Experimental Set-up

When considering the results obtained, it is essential to consider the limitations of the experimental set-up with which the experiments were done. There are two specific points of concern with the experimental set-up used.

5.7.1 Steady State Temperature

Due to the short spraying times observed (less than 20 s), it is unlikely that steady state was obtained. The temperature of the nozzle is bound to change as the solution starts flowing through it. Due to the very high flow rate through the nozzle, coupled with short flowing distance through nozzle, the effect of heat transfer on the temperature of the expanding fluid is probably not as pronounced.

5.7.2 Steady State Pressure

Once the expansion valve has been opened to allow flow of the solution to the nozzle, a pressure drop was observed in the equilibrium cell. The pressure pulse is caused as the pressurised solution leaves the cell and has to fill the dead space between the expansion valve and the nozzle. The second reason for the pressure drop could be attributed to the friction caused by the o-rings in pressure piston. This causes a slight lag time as the piston moves to readjust the pressure to the original value. The pressure drop was typically in the order of 30 bar, which is quite significant at lower pre-expansion pressure.

5.7.3 Further Testing

Based on the above factors, it is recommended that a continuous pilot plant studies be done to verify the results obtained with the batch runs. A similar to that proposed by Weidner (Weidner et al. 2002) is shown in Figure 5-28. The wax and propane will be fed continuously to a low volume tee, where the streams will impinge on another, and thoroughly mixed in a series of static mixers.

All lines will be heat traced from the same heating source to provide uniform heating of all lines. A temperature and pressure gauge will be added just prior to the nozzle inlet. Adjusting the flow rates of the two metering pumps will control the solution composition and pressure at the nozzle inlet.

With this set-up much longer spraying times can be achieved, thus ensuring that steady state is achieved. Important questions will be answered, of which there is not certainty at this stage. Will the nozzle block eventually, and how long does it take to block? What production rates that can be achieved? But the most important factor that will be addressed is that relating to steady state conditions.

It is this important question that needs answering before a final conclusion on the viability of the RESS process for wax micronisation is made.

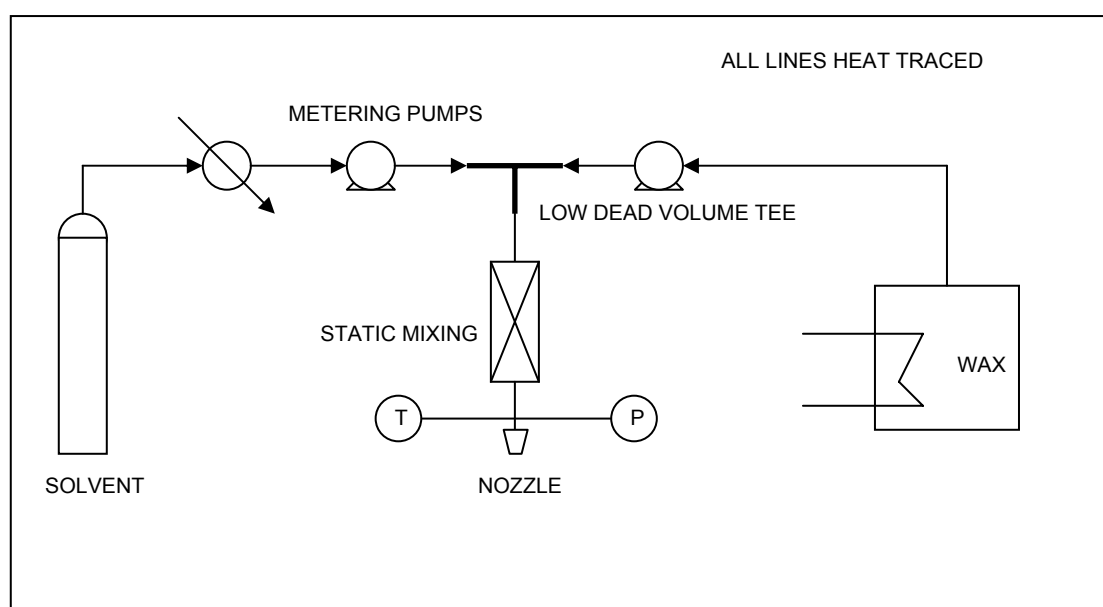


Figure 5-28: Proposed Continuous Pilot Plant

5.8 Other Experimental Work

Along with the results of the work described above, some further experiments were carried out on a trial and error basis to try and quantify the boundaries for which spherical wax particles could be obtained. These trials are summarised below.

Some exploratory experimental work was carried out with $n\text{-C}_{36}\text{H}_{74}$ and propane as solvent. A temperature and pressure combination of 150 bar and 160 °C was used with nozzles of 15 μm and 60 μm . Wax concentrations were varied between 2 and 10 weight %. In Figure 5-29, SEM images of the results for the 15 μm nozzle are shown.

The SEM images of the 60 μm nozzle are of very poor quality and will not be shown here, but the trends observed are similar as that for the 15 μm nozzle.

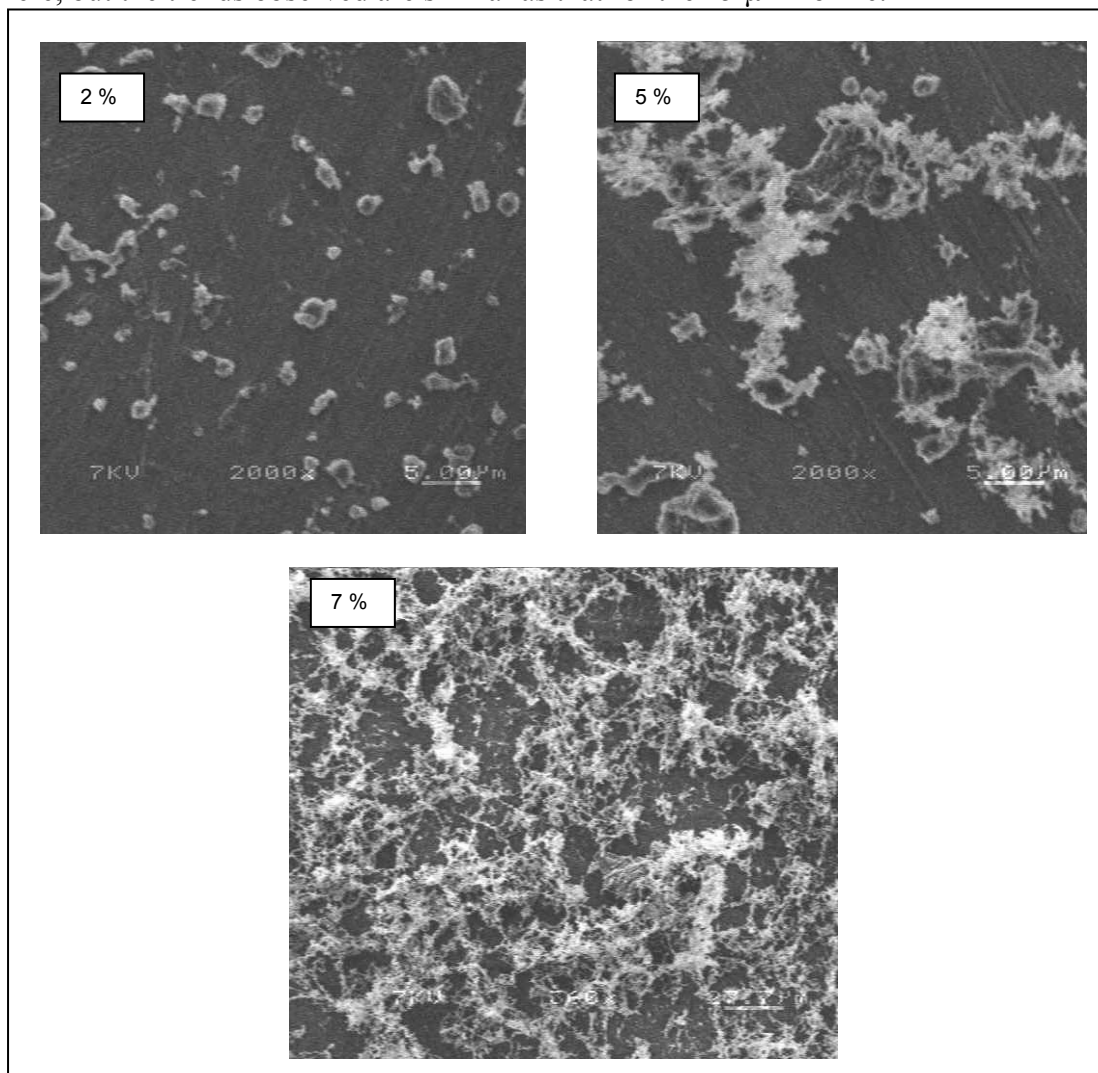


Figure 5-29: Comparison of n-C₃₆H₇₄ Particles obtained from expansion from 150 bar, 160 °C through 15 μm nozzle and different concentrations

From the images it can be seen that single particles form at low concentrations of less than 5 %. At the higher concentrations, a fibrous network of particles could be seen. At the higher concentration, it is probable that particle deformation by coagulation and agglomeration occurred.

In the exploratory stages of this project, a 15 weight % C80 wax solution was also sprayed through a 60 μm porous plate nozzle. The temperature was varied between 130 and 160 °C and the pressure between 150 and 175 bar. The results obtained for all the experiments showed a porous network of particles. An example of is given in Figure 5-30

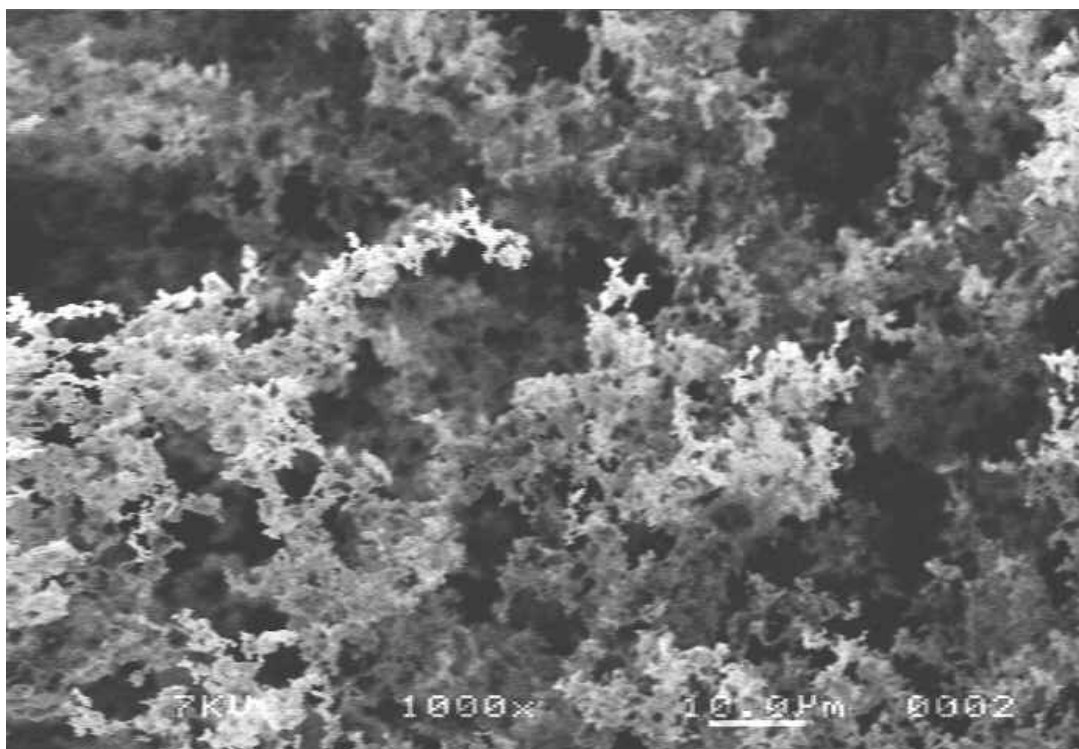


Figure 5-30: Porous Mass of Particles found at 15 % C80 Concentration for a variety of conditions

Trials with a 500 μm capillary tube (length 8 mm), for the same conditions as that in Figure 5-30 resulted in large porous flakes (1-3 mm in diameter). Under SEM microscopy these flakes had a similar structure as that in Figure 5-30.

Some experiments of $n\text{-C}_{24}\text{H}_{50}$ with ethane as solvent, was expanded via the 15 μm nozzle from conditions ranging from 50 – 70 $^{\circ}\text{C}$ and pressures from 150 – 180 bar. A pre-expansion concentration of 4.5 % was used. The SEM images of these particles are of poor quality and will not be shown here. Single “gravel-shaped” particles with an number average particle size in the range 1.0 – 1.1 μm was found, along with some agglomerates of these particles.

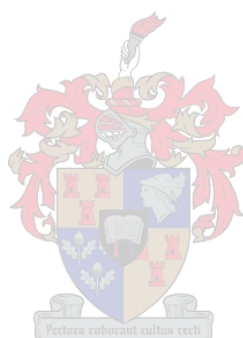
5.9 Concluding Remarks

The most important question regarding the RESS process is in regards to its industrial application. From the last C105 runs, it was concluded that the maximum concentration that seemed to deliver reasonable results are in the region of 4-4.5 weight %. This equates to a solvent to wax ratio of 24:1, which is quite high. The solvent is however completely recyclable, but the higher flow rate required would increase compression cost.

The high observed flow rates through the sinters would certainly be beneficial on industrial scale. For a 4 wt % solution, expanding from 175 bar and 130 °C, a wax production rate of 6.4 kg/h/cm² seems achievable through the 25 µm sinter used.

The RESS process for wax micronisation on industrial scale shows promise as very few particles produced are in excess of the maximum limit of 5 µm, thus reducing recycling of undesired wax particles. If the size distributions presented in this chapter is compared to those found in Figure 1-3 for a commercial wax, it is seen that the RESS process deliver much smaller particles with a narrow size distribution. Virtually no product recycling would be required, which means that the desired size of particles can be obtained with almost no recycling of wax.

However the higher pressure and solvent recycling costs would need to be weighed up against the advantages that the product may hold.



6 CONCLUSIONS AND RECOMMENDATIONS

With the RESS process, it was found that small particles, less than 5 μm in size could readily be produced for the whole range of parameters investigated. Average particle sizes of less than 2 μm were found in virtually all cases.

It was found that only C105 wax could be processed to yield the desired spherical particles. C80 wax particles were in general not as smooth as C105 particles and the shape thereof tended to be more angular.

The results would suggest that high pressure at the nozzle inlet is beneficial to the spherical shape of the product. A pressure of 175 bar was found to give best results. At 150 bar, the particles formed were less spherical, and tended to have a less smooth surface than the results obtained at 175 bar. This makes sense, since the solution is further away from the dew point, causing the solute to fall out of solution further down the nozzle. The influence of particle growth is thus minimised.

Some C80 runs at 125 bar were tried, but were only successful when the 60 μm nozzle was used. The resultant particles were angular with a rough surface. In the other nozzles the pressure drop was too large, causing the phase to split at the nozzle inlet or inside the nozzle.

The influence of temperature in the investigated range was not clear. At 150 bar, the temperature variation between 130 and 160 $^{\circ}\text{C}$ did not have a clear influence on the particle size or shape. Contrasting results were found here for C80 wax compared to C105 wax. It was expected that the solution 130 $^{\circ}\text{C}$, which is further away from the dew point give slightly better results.

The 25 μm porous plate nozzle seemed to yield the best results. This might indicate that the porous plate cannot only be characterised by its pore size, but that its morphology also plays an important role.

Higher wax concentration did seem to give smaller individual particles, but particle shape visibly deteriorated as the concentration increased. From experiments with C105 wax, at conditions of 175 bar and 130 $^{\circ}\text{C}$ and the 25 μm nozzle, it seems as if a maximum concentration between 4 and 5 % is achievable, above which the particle

shape visibly deteriorated. Due to the higher supersaturation that can be achieved with higher concentration, it is expected that nucleation will give smaller nuclei, but that the high number concentration of the particles will increase chances of growth by coagulation or agglomeration, which could explain the rougher, less spherical shape of these particles.

The study was limited to small volumes due to the safety concerns with the propane solvent. The spraying times were small, leading to uncertainty pertaining the steady state and flow rate that can be achieved. Due to the pressure concern of certain parts of the experimental set-up, especially the shut-off valve, a maximum pressure of 175 bar was used. This high pressure was only used at the lower temperature of 130 °C.

It is at this stage strongly recommended that pilot plant studies be done so that longer spraying times, pressure and temperature can be achieved. These studies would also address the factor of continual particle harvesting. The proposed pilot plant involves the mixing of the solute and solvent in a series of static mixers, before the resultant solution is expanded over the nozzle.



7 REFERENCES

Akgerman, A. & Guzel, B. (1998). "Natural fibres mordant dyeing from supercritical fluids". Proceedings of the fifth meeting on supercritical fluids, Tome 1; Perrut, M. & Subra, P. (Eds), Nice: 351 - 356.

Alessi, P., Cortesi, A., Kikic, I., Foster, N. R., MacNaughton, S. J., et al. (1996). "Particle production of steroid drugs using supercritical fluid processing." Ind. Eng. Chem. Res. **35**: 4718 - 4726.

Alessi, P., Cortesi, A. & Kikic, I. (1998). "Effect of operating parameters on the impregnation of polymers with drugs". Proceedings of the fifth meeting on supercritical fluids, Tome 1; Perrut, M. & Subra, P. (Eds), Nice: 373 - 378.

Atkins, P. W. (1994). Physical chemistry. Oxford, Oxford University Press.

Basta, N. & McQueen, S. (1985). "Supercritical fluids: still seeking acceptance." Chem. Eng. February, **4**: 14 - 17.

Benedetti, L., Bertucco, A. & Pallado, P. (1997). "Production of micronic particles of biocompatible polymer using supercritical carbon dioxide." Biotech. Bioeng. **53**: 232 - 237.

Berends, E. M. (1994). Supercritical crystallization: the RESS-process and the GAS-process. Ph.D Thesis, Technische Universiteit Delft.

Blasig, A., Norfolk, C. W., Weber, M. & Thies, M. C. (2000). "Processing polymers by RESS: the effect of concentration on product morphology". Proceedings of the fifth international symposium on supercritical fluids; Bush, D. (Ed), Atlanta.

Bork, M. (1998). "Supercritical fluid dyeing of synthetic fibres." Proceedings of the fifth meeting on supercritical fluids, Tome 1; Perrut, M. & Subra, P. (Eds), Nice: 387 - 392.

BYK-Cera (1996). Micronized waxes for universal application. Technical brochure.

BYK-Cera (1998). Micronized waxes for powder coatings. Technical brochure.

Chang, C. J. & Randolph, A. D. (1989). "Precipitation of microsize organic particles from supercritical fluids." AICHEJ **35**(11): 1876 - 1882.

Charoenchaitrakool, M., Dehghani, F., Foster, N. R. & Chan, H. K. (2000). "Micronization by rapid expansion of supercritical solutions to enhance the dissolution rates of poorly water-soluble pharmaceuticals." Ind. Eng. Chem. Res. **39**: 4794.

Chattopadhyay, P. & Gupta, R. B. (2001). "Production of antibiotic nanoparticles using supercritical CO₂ as antisolvent with enhanced mass transfer." Ind. Eng. Chem. Res. **40**: 3530 - 3539.

Chernyak, Y., Franklin, R. K., Edwards, J. R. & Carbonell, R. G. (2000). "Delivery of perfluoro-polyether coatings from homogeneous solution in CO₂ by rapid expansion of supercritical solution." Proceedings of the fifth international symposium on supercritical fluids; Bush, D. (Ed), Atlanta.

Chordia, L. & Robey, R. (2000). "Industrial applications of supercritical fluids." Proceedings of the fifth international symposium on supercritical fluids; Bush, D. (Ed), Atlanta.

Cocero, M. J., Alonso, E., Torio, R., Vallelado, D., Sanz, T., et al. (2000). "Supercritical water oxidation for polyethylene terephthalate industry effluents." Ind. Eng. Chem. Res. **39**: 4652 - 4657.

Cocero, M. J., Ferrero, S. & Vicente, S. (2000). "GAS crystallisation of beta-carotene from ethyl acetate solutions using CO₂ as antisolvent." Proceedings of the fifth international symposium on supercritical fluids; Bush, D. (Ed), Atlanta.

Colombo, M. L., Mossa, A., Sala, L., Seves, A., Testa, G., et al. (1998). "Treatments of cellulosic material with natural products dissolved in scf-CO₂." Proceedings of the fifth meeting on supercritical fluids, Tome 1; Perrut, M. & Subra, P. (Eds), Nice: 357 - 360.

Combes, J. R., Kumar, S., Smith, L. S., Mahabadi, H. K. & Odell, P. G. (2000). "Supercritical fluid processes." US H1839. US Patent Application, Xerox Corporation.

Crause, J. C. (2001). Supercritical fluid extraction of paraffin wax. Ph.D. Thesis, University of Stellenbosch.

De Nevers, N. (1991). Fluid mechanics for chemical engineers. New York, McGraw-Hill, Inc.

Debenedetti, P. G. (1990). "Homogeneous nucleation in supercritical fluids." AIChEJ **36**(9): 1289 - 1298.

Debenedetti, P. G. (1993). "Supercritical fluids as particle formation media." Proceedings of the NATO Advanced Study Institute on supercritical fluids - fundamentals for application; Kiran, E. & Levelt Sengers, J.M.H. (Eds), Antalya: 719 - 729.

Dickinson, N. L. & Meyers, J. M. (1952). "Solexol fractionation of menhadin oil." J. Am. Chem. Soc. **29**(6): 235 - 239.

Dixon, D. J., Johnson, K. P. & Bodmeier, R. A. (1993). "Polymeric materials formed by precipitation with a compressed antisolvent." AIChEJ **39**(1): 127 - 139.

Domingo, C., Berends, E. M. & Van Rosmalen, G. M. (1996). "Precipitation of ultrafine benzoic acid by expansion of a supercritical carbon dioxide solution through a porous plate nozzle." J. Crystal Growth **166**: 989 - 995.

Domingo, C., Berends, E. M. & Van Rosmalen, G. M. (1997). "Precipitation of ultrafine organic crystals from the rapid expansion of supercritical fluids over a capillary and frit nozzle." J. Supercrit. Fluids **10**: 39 - 55.

Drews, M. J., Barr, M. & Williams, M. (2000). "A Kinetic Study of the SCWO of a Sulfonated Lignin Waste Stream." Ind. Eng. Chem. Res. **39**: 4784 - 4793.

Du Rand, M. (2000). High pressure fluid phase equilibria. M.Sc.Eng Thesis, University of Stellenbosch.

Esquivel, M. M. & Ribeiro, M. A. (1999). "Supercritical extraction of savory oil: study of antioxidant activity and extract characterisation." J. Supercrit. Fluids **14**: 129 - 138.

Francais, E., Majewski, W. & Perrut, M. (1998). "Deacidification and strengthening of paper by supercritical fluid processing." Proceedings of the fifth meeting on supercritical fluids, Tome 1; Perrut, M. & Subra, P. (Eds), Nice: 367 - 372.

Francis, A. W. (1954). "Ternary systems of liquid carbon dioxide." J. Phys. Chem. **58**: 1099 - 1114.

Friedlander, S. K. (2000). Smoke, dust and haze: fundamentals of aerosol dynamics. New York, Oxford University Press.

Gallagher, P. M., Krukonis, V. J. & VandeKieft, L. J. (1991). "Gas anti-solvent recrystallisation: application to the separation and subsequent processing of RDX and HMX." Proceedings of the second international symposium on supercritical fluids; McHugh, M.A. (Ed), Boston: 45 - 48.

Griscik, G. J., Rousseau, R. W. & Teja, A. S. (1995). "Crystallization of n-octacosane by the rapid expansion of supercritical solutions." J. Crystal Growth **155**: 112 - 119.

Hanna, M., York, P. & Shekunov, B. Y. (1998). "Control of the polymorphic forms of a drug substance by solution enhanced dispersion by supercritical fluids." Proceedings of the fifth meeting on supercritical fluids, Tome 1; Perrut, M. & Subra, P. (Eds), Nice: 325 - 330.

Hansen, B. M., Hybertson, R. M. & Sievers, R. E. (1992). "Supercritical fluid transport - chemical deposition of films." Chem. Mat. **4**: 749 - 752.

Helfgen, B., Hils, P., Holzknicht, C., Türk, M. & Schaber, K. (2002). "Simulation of particle formation during the rapid expansion of supercritical solutions." J. Aerosol Science **32**: 295 - 319.

Helfgen, B., Türk, M. & Schaber, K. (2000). "Theoretical and experimental investigations of the micronization of organic solids by rapid expansion of supercritical solutions." Powder Tech. **110**: 22 - 28.

Johnston, K. P., Luna-Barcenas, G., Dixon, D. & Mawson, S. (1994). "Polymeric materials by precipitation with a compressed fluid antisolvent." Proceedings of the third international symposium on supercritical fluids, Tome 3; Brunner, G. & Perrut M. (Eds), Strasbourg: 359 - 364.

Jung, J. & Perrut, M. (2001). "Particle design using supercritical fluids: Literature and patent survey." J. Supercrit. Fluids **20**: 179-219.

Kaminsky W. (2000). "Metallocenes." Ullmann's encyclopedia of industrial chemistry, Online Volume. Weinheim, VCH Verlagsgesellschaft mbH. **Online volume** (www.mrw.interscience.wiley.com, November 2002).

Kerc, J., Srcic, S., Knez, Z. & Sencar-Bozic, P. (1999). "Micronization of drugs using supercritical carbon dioxide." Intl. J. Pharm. **182**: 33 - 39.

Knez, Z. & Weidner, E. (2001). "Precipitation of solids with dense gases." High pressure process technology: Fundamentals and applications, Bertucco, A. & Vetter, G. (Eds), Amsterdam, Elsevier Science B.V.

Kröber, H., Teipel, U. & Krause, H. (2000). "Manufacture of Submicron Particles via Expansion of Supercritical Fluids." Chem. Eng. Tech. **23**: 763 - 765.

Krukonis, V. J., Gallagher, P. M. & Coffey, M. P. (1991). "Gas anti-solvent recrystallisation process." US5360478. US Patent, Phasex Corp.

Ksibi, H. & Subra, P. (1994). "Hydrodynamic and thermodynamic profiles of a supercritical fluid expansion applied to the RESS process." Proceedings of the third international symposium on supercritical fluids, Tome 3; Brunner, G. & Perrut M. (Eds), Strasbourg: 331 - 336.

Kuehnle, A. (1989). "Process for the production of micronized waxes" US4846887. US Patent, Huels Aktiengesellschaft.

Larson, K. A. & King, M. L. (1986). "Evaluation of supercritical fluid extraction in the pharmaceutical industry." Biotech. Prog. **2**(2): 73 - 82.

Lele, A. K. & Shine, A. D. (1992). "Morphology of Polymers Precipitated from a Supercritical Solvent." AIChEJ **38**(5): 743 - 752.

Lele, A. K. & Shine, A. D. (1994). "Effects of RESS dynamics on polymer morphology." Ind. Eng. Chem. Res. **33**: 1476 - 1485.

Letcher, C. S. (1992). "Waxes." Kirk-Othmer encyclopedia of chemical technology; M. Grayson and Eckroth, D. (Eds), New York, John Wiley and sons. **24**: 466 - 481.

Liang, M.-T. (1994). "The application of nucleation theories to the particles formation in expansion of supercritical solutions." Proceedings of the third international symposium on supercritical fluids, Tome 3; Brunner, G. & Perrut M. (Eds), Strasbourg: 247 - 252.

Lim, G.-B., Lee, S.-Y., Koo, K.-K., Park, B.-S. & Kim, H.-S. (1998). "Gas antisolvent recrystallisation of molecular explosives under subcritical to supercritical

conditions." Proceedings of the fifth meeting on supercritical fluids, Tome 1; Perrut, M. & Subra, P. (Eds), Nice: 271 - 272.

Liu, G.-T. (1996). "Application of rapid expansion of supercritical solutions in the crystallization separation." Ind. Eng. Chem. Res. **35**: 4626 - 4634.

Matson, D. W., Fulton, J. L., Petersen, R. C. & Smith, R. D. (1987). "Rapid expansion of supercritical fluid solutions: solute formation of powders, thin films, and fibers." Ind. Eng. Chem. Res. **26**: 2298-2306.

Mawson, S., Johnston, K. P., Combes, J. R. & DeSimone, J. M. (1995). "Formation of poly(1,1,2,2-tetrahydroperfluorodecyl acrylate) submicron fibres and particles from supercritical carbon dioxide solutions." Macromolecules **28**: 3128 - 3191.

McHugh, M. A. & Krukonis, V. (1994). Supercritical fluid extraction: principles and practice. Stoneham, Butterworth-Heinemann: 1 - 282.

McMurry, J. (1996). Organic chemistry. Pacific Grove, John Wiley and sons.

Mendes, R. L., Nobre, B. P. & Palavra, A. F. (2000). "Supercritical CO₂ extraction of beta-carotene from *dunaliella salina*." Proceedings of the fifth international symposium on supercritical fluids; Bush, D. (Ed), Atlanta.

Mohamed, R. S., Debenedetti, P. G. & Prud'homme, R. K. (1989). "Effects of process conditions on crystals obtained from supercritical mixtures." AIChEJ **35**(2): 325 - 329.

Nelson, S. R. & Roodman, R. G. (1985). "ROSE: the energy efficient bottom of the barrel alternative." Chem. Eng. Prog. **81**: 63 - 68.

Nieuwoudt, I. (1994). The fractionation of high molecular weight alkane mixtures with supercritical fluids. Ph.D. Thesis, University of Stellenbosch.

Nieuwoudt, I. (2002). Wax micronisation with sinter metal plates. Personal communication, Stellenbosch.

Palakodaty, S., York, P., Hanna, M. & Pritchard, J. (1998). "Crystallization of lactose using solution enhanced dispersion by supercritical fluids technique." Proceedings of the fifth meeting on supercritical fluids, Tome 1; Perrut, M. & Subra, P. (Eds), Nice: 275 - 280.

Peirico, N. M., Matos, H. A., Gomes de Azevedo, E. & Nunes da Ponte, M. (1998). "Production of drug-compatible polymer microsize composites by RESS with supercritical CO₂." Proceedings of the fifth meeting on supercritical fluids, Tome 1; Perrut, M. & Subra, P. (Eds), Nice: 313 - 318.

Perrut, M. (2000). "Supercritical fluid applications: industrial developments and economic issues." Ind. Eng. Chem. Res. **39**: 4531 - 4535.

Pratsinis, S. E. (1988). "Simultaneous nucleation, condensation, and coagulation in aerosol reactors." J. Colloid and Interf. Sci. **124**(2): 417 - 427.

Randolph, T. W., Randolph, A. D., Mebes, M. & Yeung, S. (1993). "Sub-micrometer-sized biodegradable particles of poly (L-lactic acid) via the gas antisolvent spray precipitation process." Biotechnol. Prog. **9**: 429.

Rantkyyla, M., Jantti, M., Jaarmo, S. & Aaltonen, O. (1998). "Modeling droplet-gas interaction and particle formation in gas anti-solvent-system." Proceedings of the fifth meeting on supercritical fluids, Tome 1; Perrut, M. & Subra, P. (Eds), Nice: 333 - 338.

Reverchon, E. (1997). "Supercritical fluid extraction and fractionation of essential oils and related products." J. Supercrit. Fluids **10**: 1 - 37.

Reverchon, E. (1999). "Supercritical antisolvent precipitation of micro- and nano-particles." J. Supercrit. Fluids **15**: 1 - 21.

Reverchon, E., Della Porta, G., De Rosa, I., Subra, P. & Letourneur, D. (2000). "Supercritical antisolvent micronisation of some biopolymers." J. Supercrit. Fluids **18**: 239 - 245.

Reverchon, E., Della Porta, G., Pace, S. & Di Trolio, A. (1998). "Supercritical antisolvent precipitation of submicronic particles of superconductor precursors." Ind. Eng. Chem. Res. **37**: 952.

Reverchon, E., Della Porta, G. & Pallado, P. (2001). "Supercritical antisolvent precipitation of salbutamol particles." Powder Tech. **114**: 17 - 22.

Reverchon, E., Della Porta, G., Taddeo, R., Pallado, P. & Stassi, A. (1995). "Solubility and micronization of griseofulvin in supercritical CHF₃." Ind. Eng. Chem. Res. **34**: 4087 - 4091.

Reverchon, E. & Pallado, P. (1996). "Hydrodynamic modelling of the RESS process." J. Supercrit. Fluids **9**: 216 - 221.

Riha, V. & Brunner, G. (1999). "Separation of fish oil ethyl esters with supercritical carbon dioxide." J. Supercrit. Fluids **15**: 33 - 50.

Savage, P. E., Gopalan, S., Mizan, T. I., Martino, C. J. & Brock, E. E. (1995). "Reactions at supercritical conditions: applications and fundamentals." AIChEJ **41**: 1723 - 1778.

Schmitt, W. J. (1988). "Finely divided solid crystalline powders via precipitation into an anti-solvent" US5707634. US Patent, Upjohn Co.

Schmitt, W. J., Salada, M. C., Shook, G. G. & Speaker, S. M. (1995). "Finely divided powders by carrier solution injection into a near or supercritical fluid." AIChEJ **41**: 2476.

Schwarz, C. E. (2001). Equilibrium of alkanes and supercritical fluids. M.Sc.Eng. Thesis, University of Stellenbosch.

Sievers, R. E., Karst, U., Milewski, P. D., Sellers, S. P., Miles, B. A., et al. (1999). "Formation of aqueous small droplet aerosols assisted by supercritical carbon dioxide." Aerosol Sci. Tech. **30**: 3 - 15.

Sievers, R. E., Milewski, P. D., Sellers, S. P., Miles, B. A., Korte, B. J., et al. (2000). "Supercritical and near-critical carbon dioxide assisted low-temperature bubble drying." Ind. Eng. Chem. Res. **39**: 4831 - 4836.

Springer, G. S. (1978). "Homogeneous Nucleation." Adv. Heat Transf. **14**: 281 - 346.

Subra, P., Boissinot, P. & Benzaghrou, S. (1998). "Precipitation of pure and mixed caffeine and anthracene by rapid expansion of supercritical solutions." Proceedings of the fifth meeting on supercritical fluids, Tome 1; Perrut, M. & Subra, P. (Eds), Nice: 307 - 312.

Sze Tu, L., Dehghani, F., Dillow, A. K. & Foster, N. R. (1998). "Applications of dense gases in pharmaceutical processing." Proceedings of the fifth meeting on supercritical fluids, Tome 1; Perrut, M. & Subra, P. (Eds), Nice: 263 - 270.

Teja, A. S. & Eckert, C. A. (2000). "Commentary on supercritical fluids: research and applications." Ind. Eng. Chem. Res. **39**: 4442 - 4444.

Thiering, R., Charoenchaitrakool, M., Sze Tu, L., Dehghani, F., Dillow, A. K., et al. (1998). "Crystallization of para-hydroxybenzoic acid by solvent expansion with dense carbondioxide." Proceedings of the fifth meeting on supercritical fluids, Tome 1; Perrut, M. & Subra, P. (Eds), Nice: 291 - 296.

Thiering, R., Dehghani, F. & Foster, N. R. (2000). "Micronization of model proteins using compressed carbon dioxide." Proceedings of the fifth international symposium on supercritical fluids; Bush, D. (Ed), Atlanta.

Tom, J. W. & Debenedetti, P. G. (1991). "Formation of bioerodable polymeric microspheres and microparticles by rapid expansion of supercritical solutions." Biotechnol. Prog. **7**: 403 - 411.

Türk, M. (1999). "Formation of small organic particles by RESS: experimental and theoretical investigations." J. Supercrit. Fluids **15**: 79 - 89.

Türk, M. (2000). "Influence of thermodynamic behavior and solute properties of homogeneous nucleation in supercritical solutions." J. Supercrit. Fluids **18**: 169 - 184.

Türk, M., Hils, P., Helfgen, B., Schaber, K., Martin, H.-J., et al. (2002). "Micronization of pharmaceutical substances by the rapid expansion of supercritical solutions (RESS): a promising method to improve the bioavailability of poorly soluble pharmaceutical agents." J. Supercrit. Fluids **22**: 75 - 84.

Vardag, T. & Bork, M. (1998). "Cleaning with supercritical gases: an overview." Proceedings of the fifth meeting on supercritical fluids, Tome 1; Perrut, M. & Subra, P. (Eds), Nice: 167 - 170.

Warwick, B., Dehghani, F., Foster, N. R., Biffin, J. R. & Regtop, H. L. (2000). "Synthesis, purification and micronization of pharmaceuticals using the gas anti-solvent technique." Ind. Eng. Chem. Res. **39**: 4571 - 4579.

Weber, M., Russell, L. M. & Debenedetti, P. G. (2002). "Mathematical modeling of nucleation and growth of particles formed by the rapid expansion of a supercritical solution under subsonic conditions." J. Supercrit. Fluids **23**: 65 - 80.

Weber, M. & Thies, M. C. (2000). Improving prediction of particle sizes in RESS. Proceedings of the fifth international symposium on supercritical fluids; Bush, D. (Ed), Atlanta.

Weidner, E., Knez, Z. & Novak, Z. (1994a). "Process for the production of particles or powders." US6056791, US Patent.

Weidner, E., Knez, Z. & Novak, Z. (1994b). "PGSS (Particles from Gas Saturated Solutions) - a new process for powder generation." Proceedings of the third international symposium on supercritical fluids, Tome 3; Brunner, G. & Perrut M. (Eds), Strasbourg: 229 - 234.

Weidner, E., Petermann, M., Kilzer, A., Pross, A. & Reichert, P. "Manufacture of particles from high viscous melts using supercritical fluids." Proceedings of the fourth international symposium on high pressure technology and chemical engineering, CD-rom volume; Bertuccio, A. (Ed), Venice.

Weidner, E., Steiner, R. & Knez, Z. (1996). "Powder generation from polyethylene glycols with compressible fluids." High Pressure Chemical Engineering; Von Rohr, P.R. & Trepp, C. (Eds) Amsterdam, Elsevier Science B. V.: 223 - 228.

Wilson, R. E., Keith, P. C. & Haylett, R. C. (1936). "Liquid propane: use in dewaxing, deasphalting and refining heavy oils." Ind. Eng. Chem. **28**: 1065 - 1078.

Wolfmeier, U., Schmidt, H., Heinrichs, F.-L., Michalczyk, G., Payer, W., et al. (1996). "Waxes." Ullmann's encyclopedia of industrial chemistry. B. Elvers and Hawkins, S. (Eds), Weinheim, VCH Verlagsgesellschaft mbH. **A28**: 103 - 163.

Worthy, W. (1981). "Supercritical fluids offer improved separations." Chem. Eng. News **August, 3**: 16 - 17.

www.cheresources.com (November 2002). Website of Chemical Resources

www.marcusoil.com (July 2002). Website of Marcus Oil & Chemical Company.

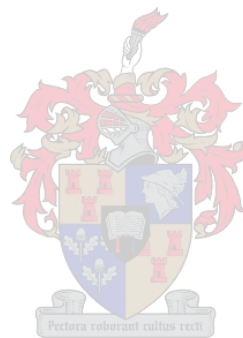
www.mooremunger.com (July 2002). Website of Moore & Munger Inc.

www.schuemann-sasol.com (July 2002). Website of Schümann-Sasol Inc.

www.wax.org (July 2002). Website of The European Wax Federation.

Yeo, S.-D., Debenedetti, P. G. & Bernstein, H. (1993). "Formation of microparticulate protein powders using a supercritical fluid antisolvent." Biotech. Bioeng. **41**: 341 - 346.

Yeo, S.-D., Debenedetti, P. G., Radosz, M. & Schmidt, H.-W. (1993). "Supercritical antisolvent process for substituted para-linked aromatic polyamides: phase equilibrium and morphology study." Macromolecules **26**: 6207 - 6210.

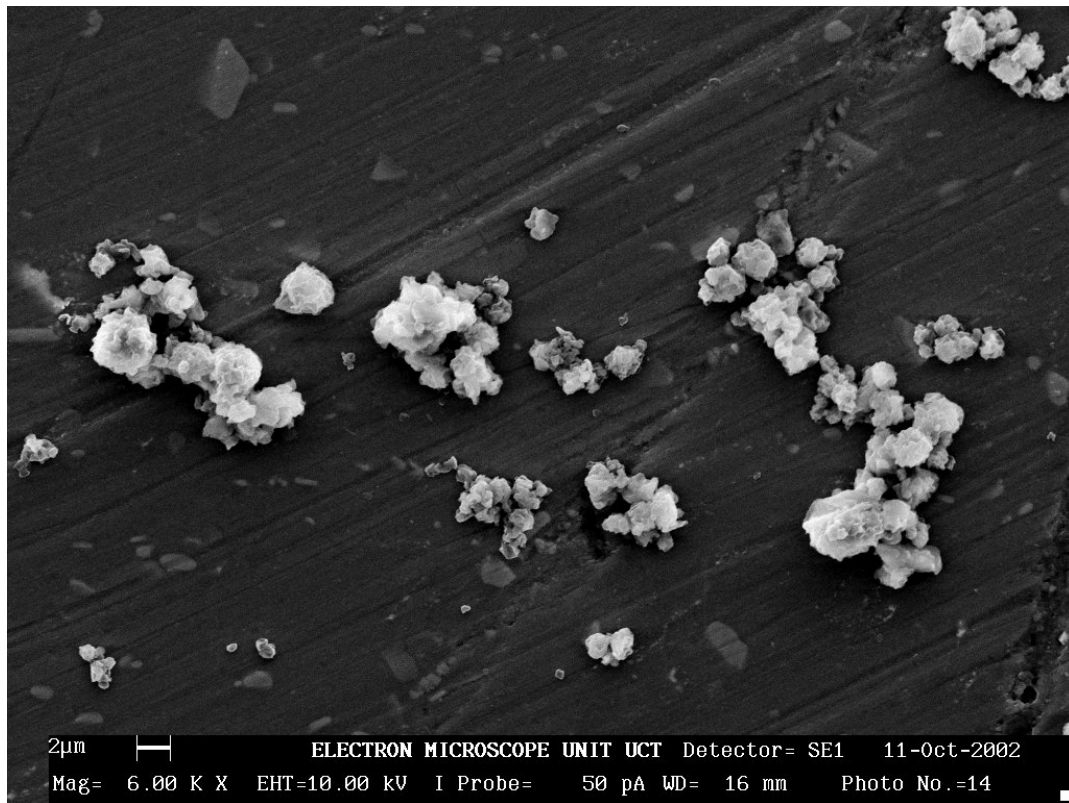


A EXPERIMENTAL DATA

Table A-1: Summary of Experimental Conditions for C80 and C105 Experimental Runs

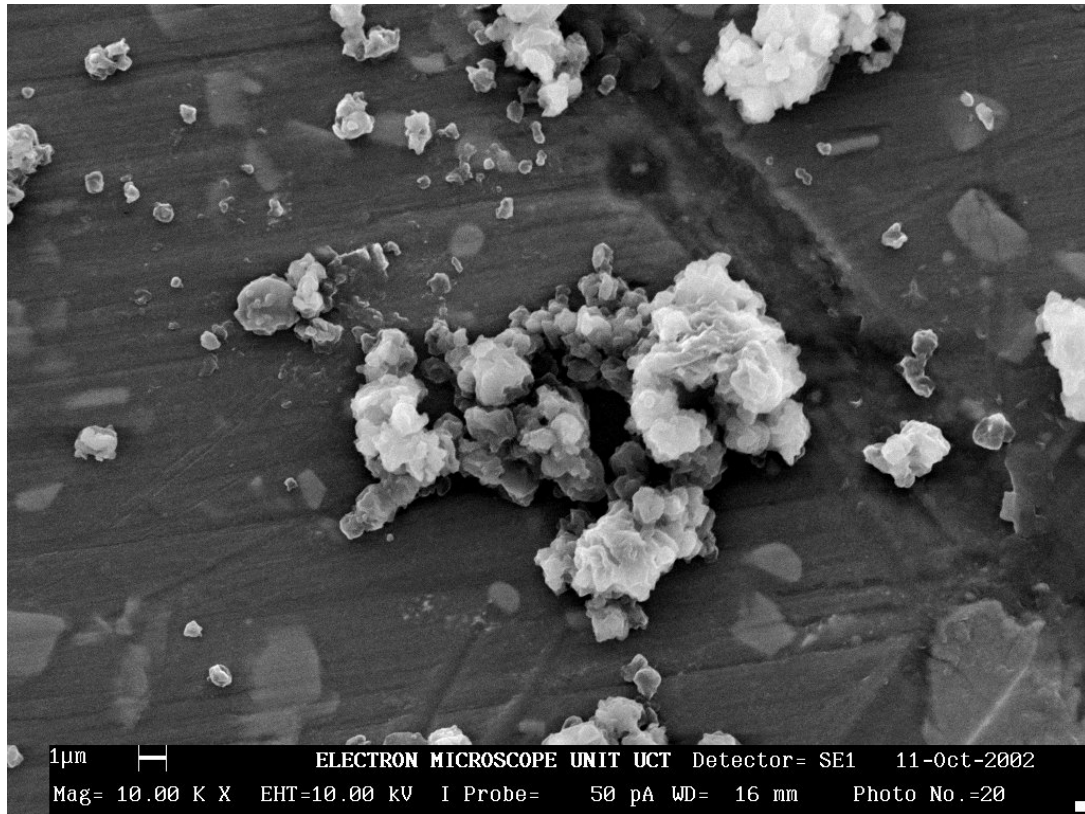
<i>Sample</i>	<i>Wax</i>	<i>Sinter pores</i>	<i>x</i>	<i>T</i>	<i>P</i>
Number		μm	weight %	$^{\circ}\text{C}$	bar (A)
1	C80	15	1	160	150
2	C80	15	2	160	150
3	C80	15	3	160	150
4	C80	60	1	160	150
5	C80	60	2	160	150
6	C80	60	3	160	150
7	C80	15	3	130	150
8	C80	15	3	130	175
9	C80	15	3	130	125
10	C80	15	3	130	125
11	C80	15	3	160	125
12	-	-	-	-	-
13	C105	15	2	160	150
14	C105	60	2	130	175
15	C105	60	2	130	150
16	C105	60	2	160	150
17	C105	60	5	130	175
18	C105	60	5	160	150
19	C80	60	5	160	150
20	C80	60	3	160	125
21	C80	60	2	130	175
22	C80	60	2	130	150
23	C80	25	2	160	150
24	C80	25	5	160	150
25	C105	25	2	160	150
26	C105	25	5	160	150
27	C105	25	3	130	175
28	C105	25	4	130	175
29	C105	25	5	130	175
30	C105	25	6	130	175

Run	Wax	Pore Size	m_{wax}	$m_{loaded\ bomb}$	$m_{emptied\ bomb}$	$m_{propane}$	x_{wax}	T_0	P_0
No.	Type	μm	g	g	g	g	mass %	$^{\circ}C$	bar (A)
1	C80	15	0.16	1019.6	1003.8	15.8	1.0	157	147



Size Interval (μm)	No % Particles in Range	Size Interval (μm)	No % Particles in Range	Particle Size (μm)	
<0.4	0.0	2.8-3.2	3.8	Min	0.41
0.4-0.8	4.4	3.2-3.6	4.9	D10	0.97
0.8-1.2	16.4	3.6-4.0	3.8	D50	1.79
1.2-1.6	19.7	4.0-4.4	5.5	D90	4.19
1.6-2.0	15.3	4.4-4.8	2.2	Max	7.43
2.0-2.4	11.5	>4.8	5.5	Avg	2.27
2.4-2.8	7.1			Skew	1.31

Run	Wax	Pore Size	m_{wax}	m_{loaded} bomb	$m_{emptied}$ bomb	$m_{propane}$	x_{wax}	T_0	P_0
No.	Type	μm	g	g	g	g	mass %	$^{\circ}\text{C}$	bar (A)
2	C80	15	0.32	1019.6	1004.2	15.4	2.0	157	153

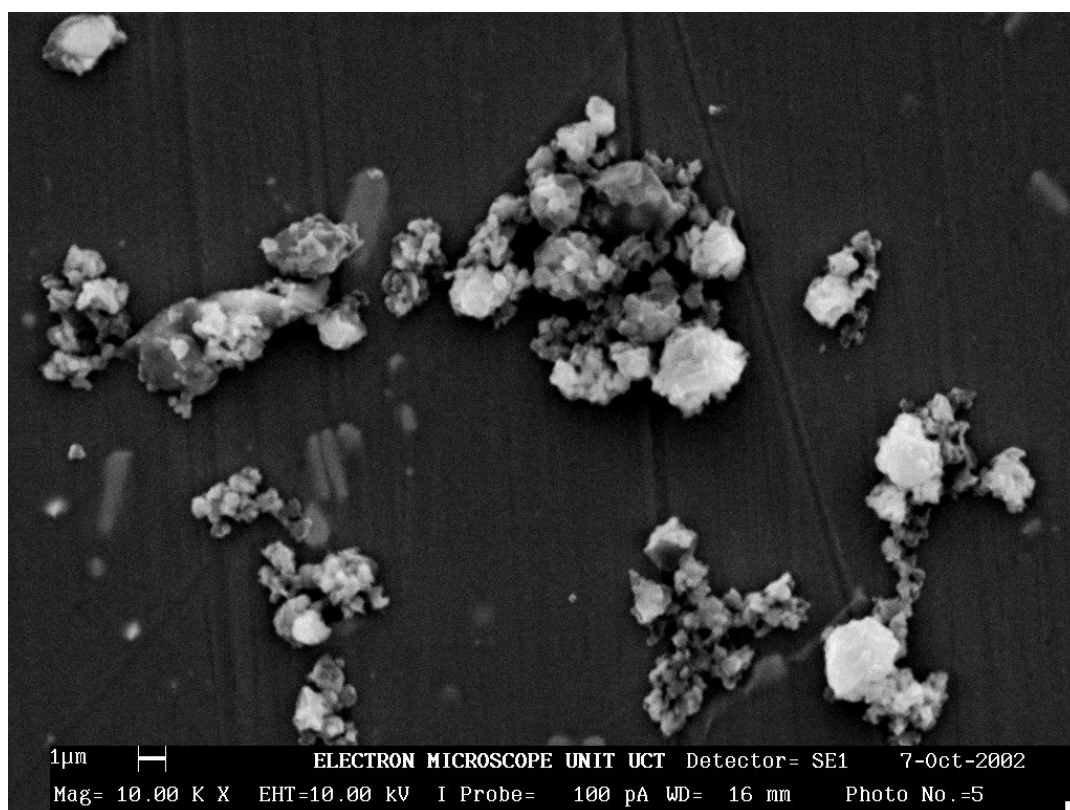


Size Interval (μm)	No % Particles in Range
<0.4	0.0
0.4-0.8	17.6
0.8-1.2	20.8
1.2-1.6	26.4
1.6-2.0	15.1
2.0-2.4	6.3
2.4-2.8	5.0

Size Interval (μm)	No % Particles in Range
2.8-3.2	2.5
3.2-3.6	3.8
3.6-4.0	0.6
4.0-4.4	0.0
4.4-4.8	0.0
>4.8	1.9

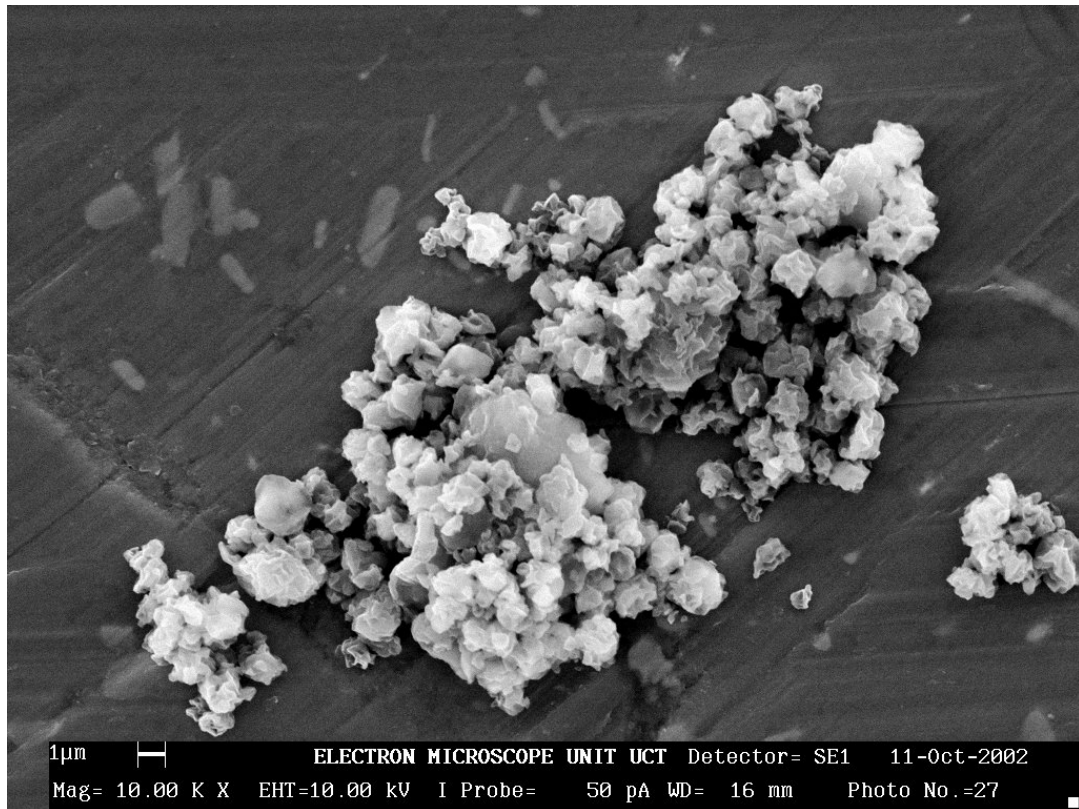
Particle Size (μm)	
Min	0.4
D10	0.66
D50	1.31
D90	2.56
Max	5.53
Avg	1.54
Skew	1.84

Run	Wax	Pore Size	m_{wax}	$m_{loaded\ bomb}$	$m_{emptied\ bomb}$	$m_{propane}$	x_{wax}	T_0	P_0
No.	Type	μm	g	g	g	g	mass %	$^{\circ}C$	bar (A)
3	C80	15	0.48	1019.3	1004.2	15.1	3.1	157	148



Size Interval (μm)	No % Particles in Range	Size Interval (μm)	No % Particles in Range	Particle Size (μm)	
<0.4	2.8	2.8-3.2	0.0	Min	0.23
0.4-0.8	29.3	3.2-3.6	1.1	D10	0.55
0.8-1.2	37.0	3.6-4.0	0.0	D50	0.98
1.2-1.6	18.8	4.0-4.4	0.0	D90	1.67
1.6-2.0	8.8	4.4-4.8	0.0	Max	3.52
2.0-2.4	1.1	>4.8	0.0	Avg	1.06
2.4-2.8	1.1			Skew	1.63

Run	Wax	Pore Size	m_{wax}	$m_{loaded\ bomb}$	$m_{emptied\ bomb}$	$m_{propane}$	x_{wax}	T_0	P_0
No.	Type	μm	g	g	g	g	mass %	$^{\circ}C$	bar (A)
4	C80	60	0.48	1019.4	1004.0	15.4	3.0	157	155

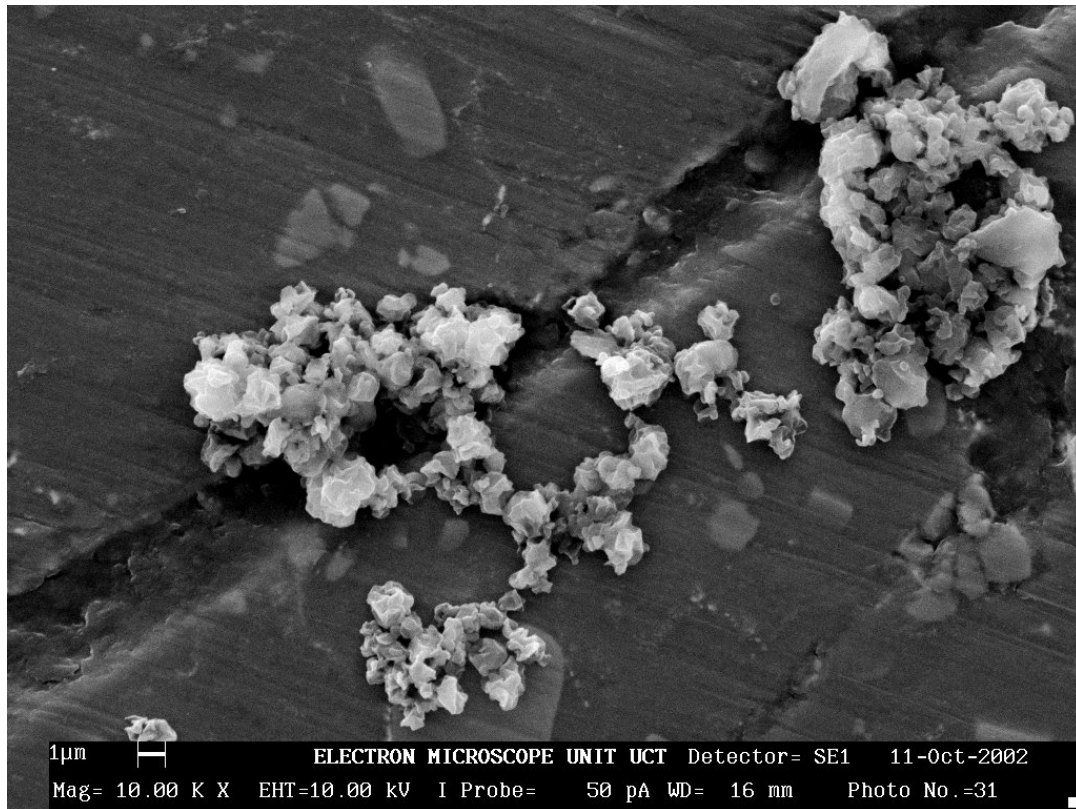


Size Interval (μm)	No % Particles in Range
<0.4	0.4
0.4-0.8	10.1
0.8-1.2	33.8
1.2-1.6	28.9
1.6-2.0	15.8
2.0-2.4	8.3
2.4-2.8	0.4

Size Interval (μm)	No % Particles in Range
2.8-3.2	1.3
3.2-3.6	0.4
3.6-4.0	0.0
4.0-4.4	0.0
4.4-4.8	0.0
>4.8	0.4

Particle Size (μm)	
Min	0.31
D10	0.79
D50	1.26
D90	2.02
Max	5.42
Avg	1.35
Skew	2.18

Run	Wax	Pore Size	m_{wax}	$m_{loaded\ bomb}$	$m_{emptied\ bomb}$	$m_{propane}$	x_{wax}	T_0	P_0
No.	Type	μm	g	g	g	g	mass %	$^{\circ}C$	bar (A)
5	C80	60	0.32	1019.4	1003.9	15.5	2.0	157	154

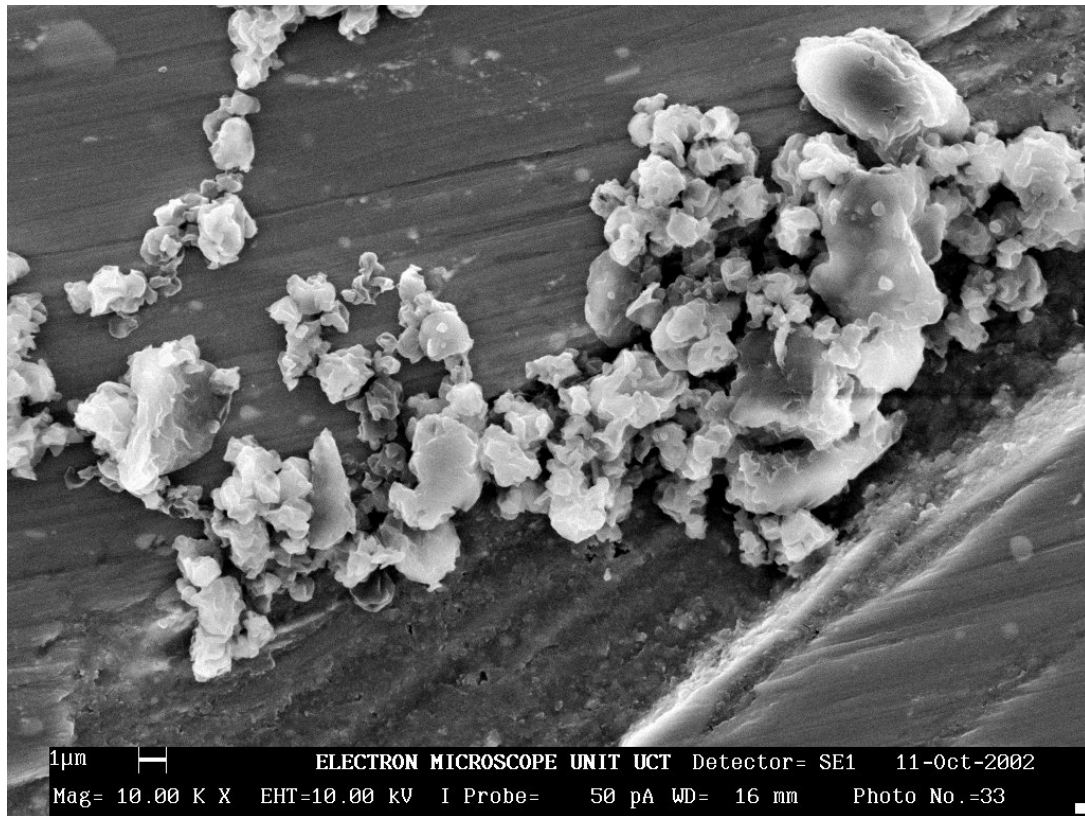


Size Interval (μm)	No % Particles in Range
<0.4	0.0
0.4-0.8	10.1
0.8-1.2	32.6
1.2-1.6	34.1
1.6-2.0	10.9
2.0-2.4	5.1
2.4-2.8	5.1

Size Interval (μm)	No % Particles in Range
2.8-3.2	1.4
3.2-3.6	0.0
3.6-4.0	0.7
4.0-4.4	0.0
4.4-4.8	0.0
>4.8	0.0

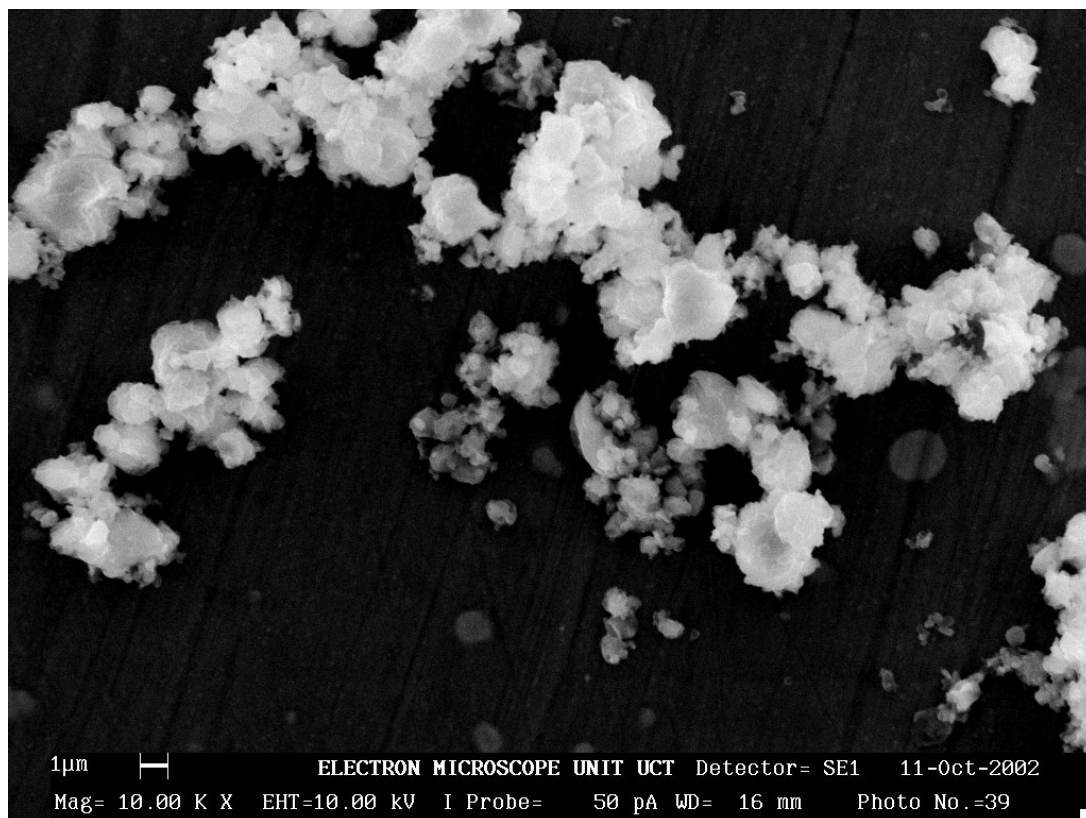
Particle Size (μm)	
Min	0.48
D10	0.79
D50	1.27
D90	2.17
Max	3.63
Avg	1.37
Skew	1.25

Run	Wax	Pore Size	m_{wax}	$m_{loaded\ bomb}$	$m_{emptied\ bomb}$	$m_{propane}$	x_{wax}	T_0	P_0
No.	Type	μm	g	g	g	g	mass %	$^{\circ}C$	bar (A)
6	C80	60	0.16	1019.7	1004.0	15.7	1.0	157	154



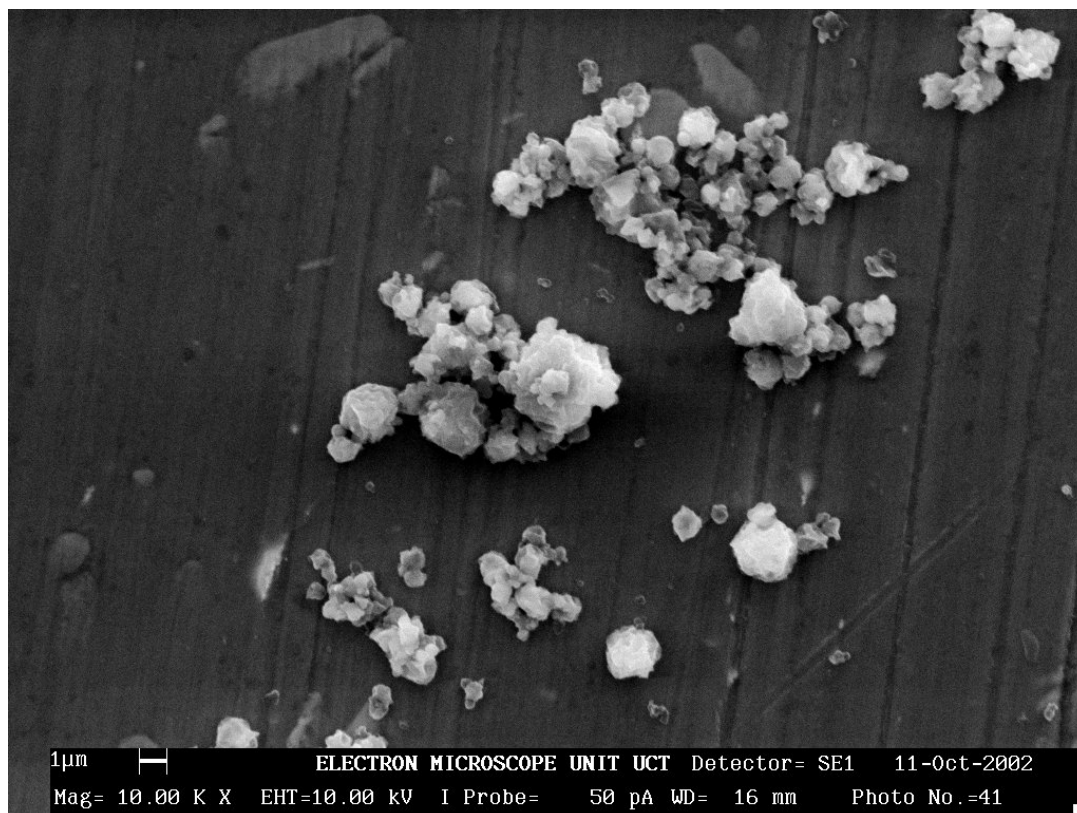
Size Interval (μm)	No % Particles in Range	Size Interval (μm)	No % Particles in Range	Particle Size (μm)	
<0.4	1.0	2.8-3.2	3.5	Min	0.28
0.4-0.8	6.4	3.2-3.6	1.0	D10	0.83
0.8-1.2	29.2	3.6-4.0	0.5	D50	1.41
1.2-1.6	18.8	4.0-4.4	1.0	D90	2.62
1.6-2.0	21.3	4.4-4.8	0.5	Max	5.45
2.0-2.4	9.4	>4.8	2.0	Avg	1.63
2.4-2.8	5.4			Skew	1.77

Run	Wax	Pore Size	m_{wax}	$m_{loaded\ bomb}$	$m_{emptied\ bomb}$	$m_{propane}$	x_{wax}	T_0	P_0
No.	Type	μm	g	g	g	g	mass %	$^{\circ}C$	bar (A)
7	C80	15	0.48	1019.5	1003.7	15.8	2.9	129	153



Size Interval (μm)	No % Particles in Range	Size Interval (μm)	No % Particles in Range	Particle Size (μm)	
<0.4	5.1	2.8-3.2	1.1	Min	0.28
0.4-0.8	31.1	3.2-3.6	0.6	D10	0.50
0.8-1.2	28.8	3.6-4.0	0.0	D50	0.96
1.2-1.6	13.0	4.0-4.4	0.6	D90	2.14
1.6-2.0	9.6	4.4-4.8	1.1	Max	4.55
2.0-2.4	5.6	>4.8	0.0	Avg	1.18
2.4-2.8	3.4			Skew	1.84

Run	Wax	Pore Size	m_{wax}	$m_{loaded\ bomb}$	$m_{emptied\ bomb}$	$m_{propane}$	x_{wax}	T_0	P_0
No.	Type	μm	g	g	g	g	mass %	$^{\circ}C$	bar (A)
8	C80	15	0.48	1019.5	1003.5	16.0	2.9	126	176



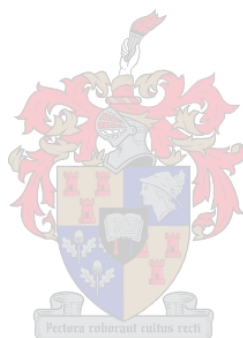
Size Interval (μm)	No % Particles in Range
<0.4	3.1
0.4-0.8	32.1
0.8-1.2	37.3
1.2-1.6	16.1
1.6-2.0	4.1
2.0-2.4	4.1
2.4-2.8	2.1

Size Interval (μm)	No % Particles in Range
2.8-3.2	0.5
3.2-3.6	0.0
3.6-4.0	0.0
4.0-4.4	0.5
4.4-4.8	0.0
>4.8	0.0

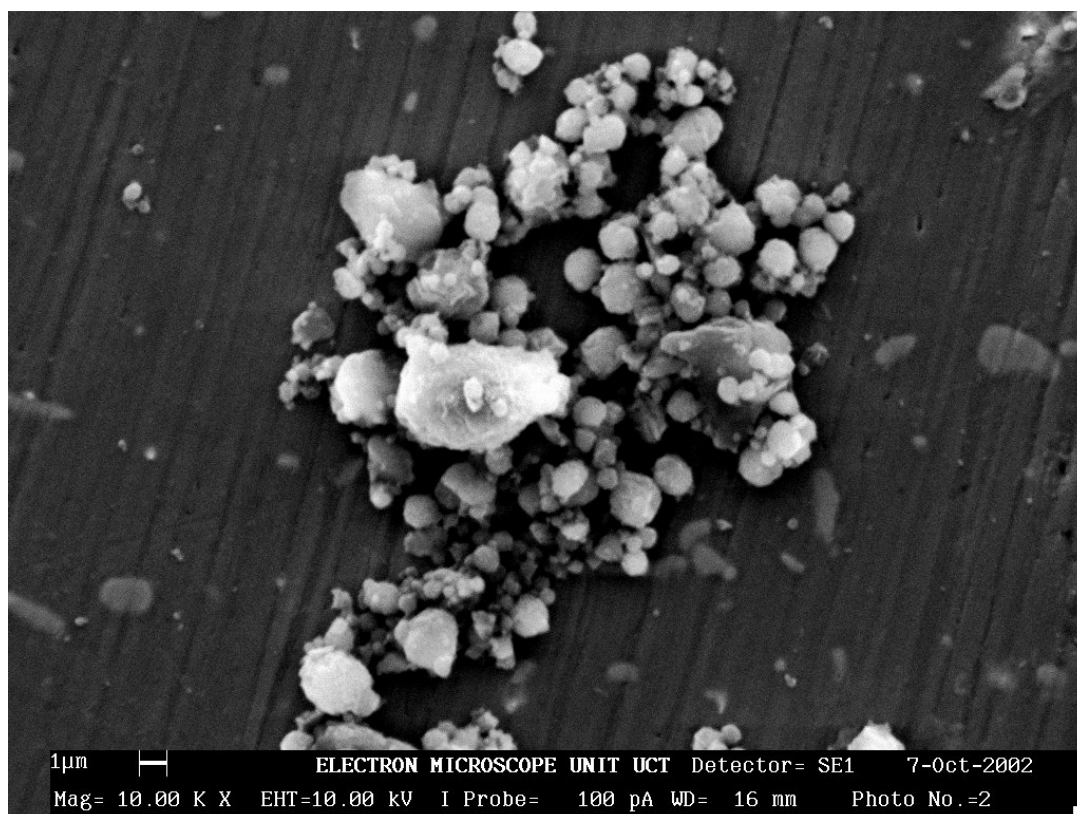
Particle Size (μm)	
Min	0.28
D10	0.53
D50	0.92
D90	1.73
Max	4.03
Avg	1.05
Skew	1.96

Run	Wax	Pore Size	m_{wax}	$m_{loaded\ bomb}$	$m_{emptied\ bomb}$	$m_{propane}$	x_{wax}	T_0	P_0
No.	Type	μm	g	g	g	g	mass %	$^{\circ}C$	bar (A)
9*	C80	15	0.48	1019.4	1003.6	15.8	2.9	129	129
10*	C80	15	0.48	1019.3	1003.2	16.1	2.9	128	125
11*	C80	15	0.48	1019.6	1003.6	16.0	2.9	129	125
12	-	-	-	-	-	-	-	-	-
13*	C105	15	0.31	1019.2	1003.6	15.6	1.9	127	151

* These runs yielded no particles, as the porous plate blocked during the spray run.

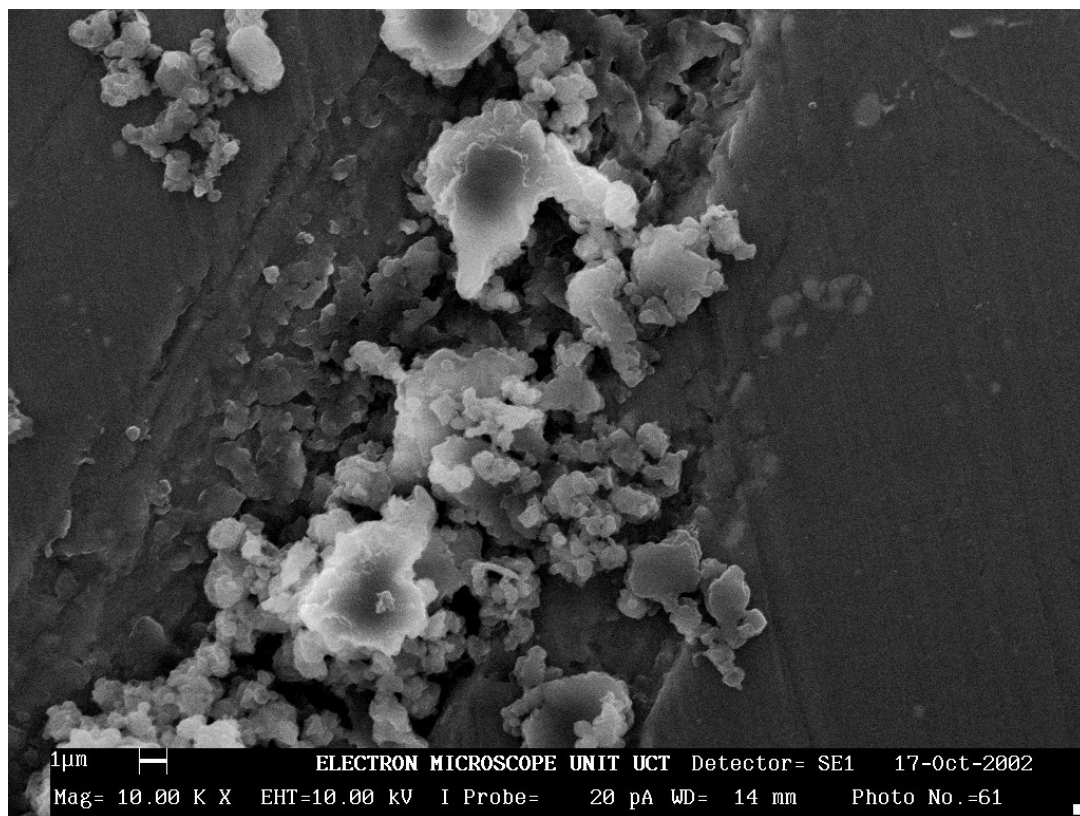


Run	Wax	Pore Size	m_{wax}	$m_{loaded\ bomb}$	$m_{emptied\ bomb}$	$m_{propane}$	x_{wax}	T_0	P_0
No.	Type	μm	g	g	g	g	mass %	$^{\circ}C$	bar (A)
14	C105	60	0.31	1019.3	1004.0	15.3	2.0	127	178



Size Interval (μm)	No % Particles in Range	Size Interval (μm)	No % Particles in Range	Particle Size (μm)	
<0.4	3.8	2.8-3.2	0.9	Min	0.28
0.4-0.8	34.8	3.2-3.6	0.3	D10	0.51
0.8-1.2	31.3	3.6-4.0	0.3	D50	0.90
1.2-1.6	17.0	4.0-4.4	0.0	D90	1.78
1.6-2.0	6.4	4.4-4.8	0.3	Max	5.73
2.0-2.4	3.2	>4.8	0.3	Avg	1.06
2.4-2.8	1.5			Skew	2.76

Run	Wax	Pore Size	m_{wax}	$m_{loaded\ bomb}$	$m_{emptied\ bomb}$	$m_{propane}$	x_{wax}	T_0	P_0
No.	Type	μm	g	g	g	g	mass %	$^{\circ}C$	bar (A)
15	C105	60	0.31	1019.0	1003.7	15.3	2.0	127	155

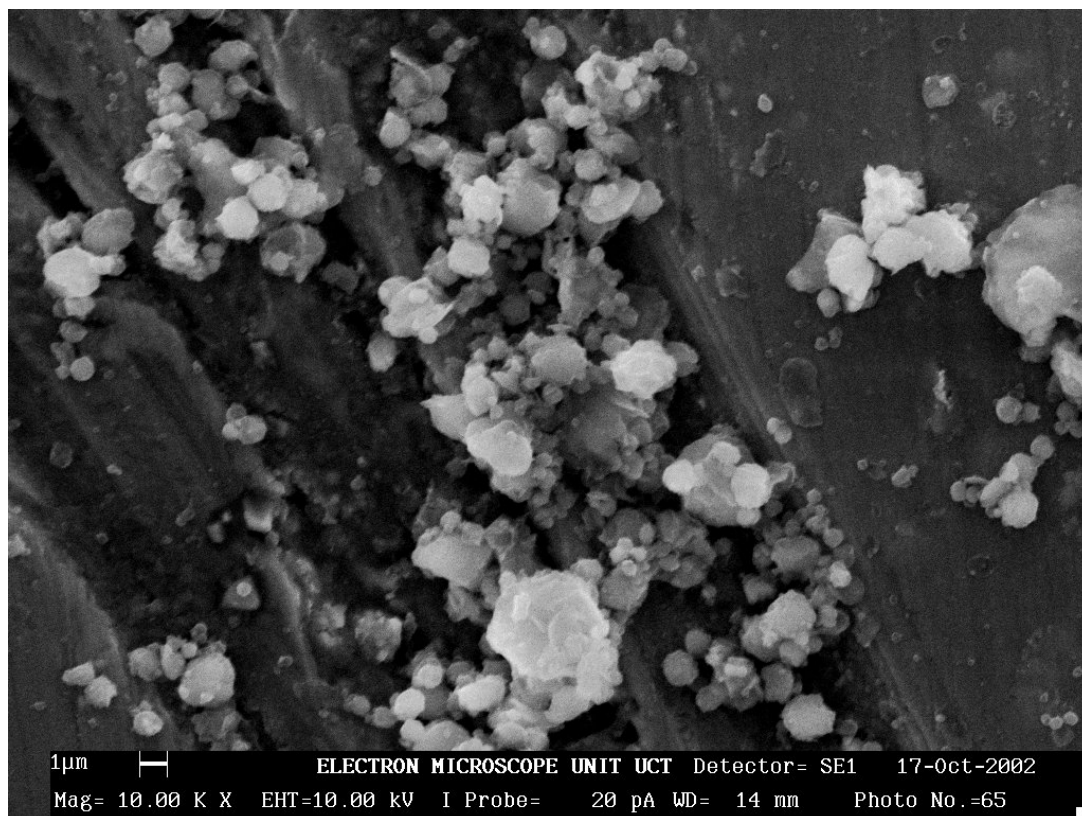


Size Interval (μm)	No % Particles in Range
<0.4	4.7
0.4-0.8	34.7
0.8-1.2	30.7
1.2-1.6	12.7
1.6-2.0	7.3
2.0-2.4	4.7
2.4-2.8	2.0

Size Interval (μm)	No % Particles in Range
2.8-3.2	1.3
3.2-3.6	0.7
3.6-4.0	0.0
4.0-4.4	0.0
4.4-4.8	0.0
>4.8	0.7

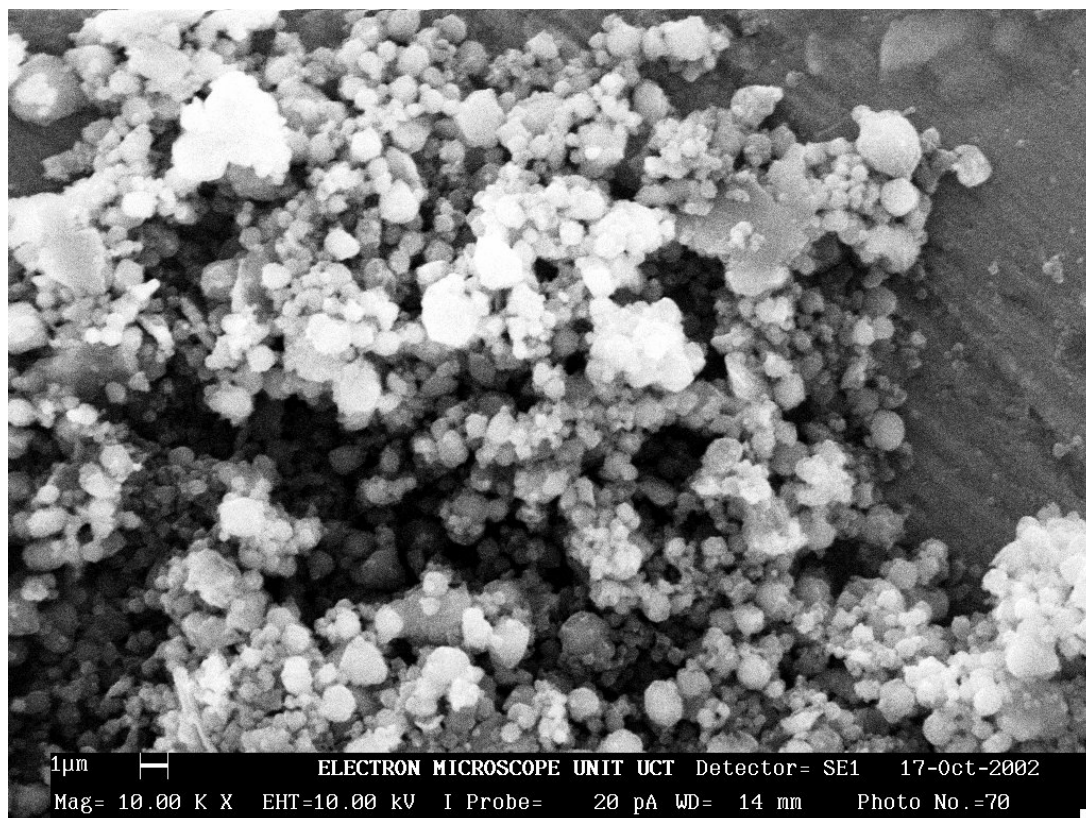
Particle Size (μm)	
Min	0.24
D10	0.47
D50	0.95
D90	1.85
Max	4.81
Avg	1.10
Skew	2.39

Run	Wax	Pore Size	m_{wax}	$m_{loaded\ bomb}$	$m_{emptied\ bomb}$	$m_{propane}$	x_{wax}	T_0	P_0
No.	Type	μm	g	g	g	g	mass %	$^{\circ}C$	bar (A)
16	C105	60	0.79	1019.3	1003.2	16.1	4.7	157	154



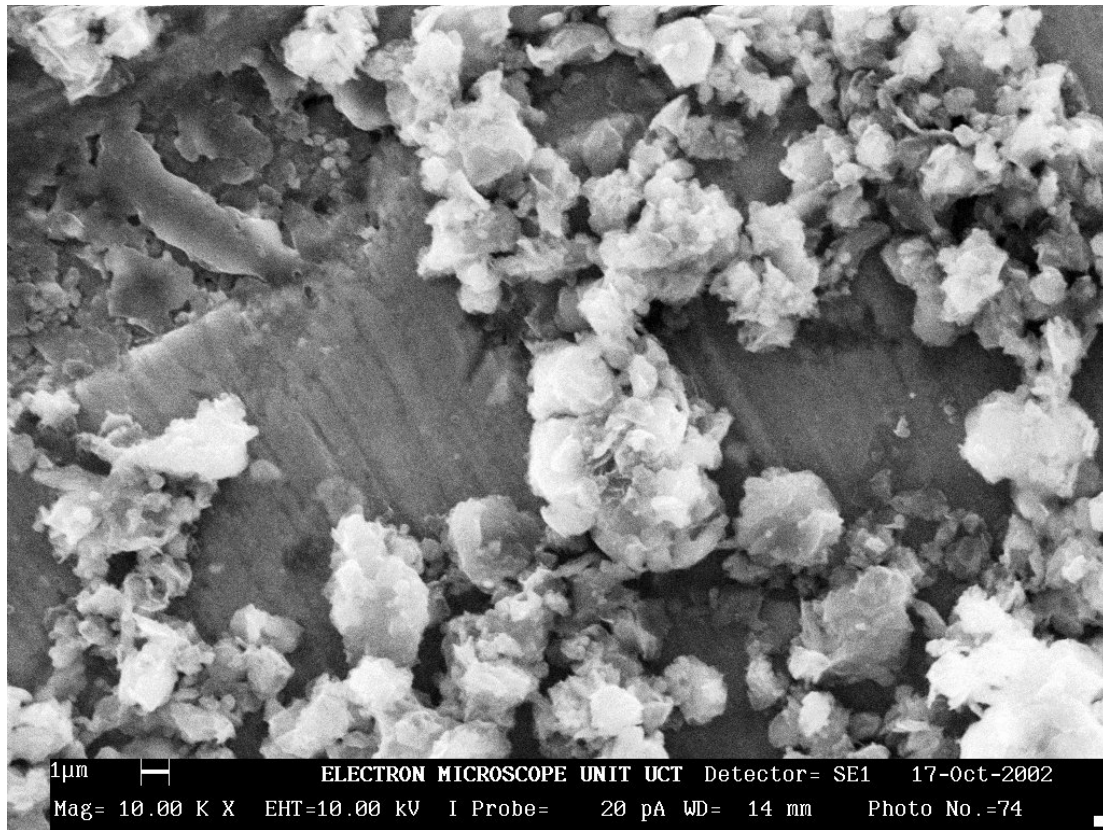
Size Interval (μm)	No % Particles in Range	Size Interval (μm)	No % Particles in Range	Particle Size (μm)	
<0.4	2.7	2.8-3.2	0.5	Min	0.28
0.4-0.8	34.2	3.2-3.6	0.5	D10	0.50
0.8-1.2	29.9	3.6-4.0	0.0	D50	0.94
1.2-1.6	14.4	4.0-4.4	0.5	D90	2.01
1.6-2.0	8.0	4.4-4.8	0.0	Max	5.02
2.0-2.4	5.9	>4.8	0.5	Avg	1.13
2.4-2.8	2.7			Skew	2.08

Run	Wax	Pore Size	m_{wax}	$m_{loaded\ bomb}$	$m_{emptied\ bomb}$	$m_{propane}$	x_{wax}	T_0	P_0
No.	Type	μm	g	g	g	g	mass %	$^{\circ}C$	bar (A)
17	C105	60	0.79	1019.5	1003.6	15.9	4.7	127	179



Size Interval (μm)	No % Particles in Range	Size Interval (μm)	No % Particles in Range	Particle Size (μm)	
<0.4	1.5	2.8-3.2	0.0	Min	0.28
0.4-0.8	35.1	3.2-3.6	0.0	D10	0.57
0.8-1.2	39.0	3.6-4.0	0.0	D50	0.92
1.2-1.6	17.6	4.0-4.4	0.0	D90	1.47
1.6-2.0	4.4	4.4-4.8	0.0	Max	5.22
2.0-2.4	2.0	>4.8	0.5	Avg	1.00
2.4-2.8	0.0			Skew	3.89

Run	Wax	Pore Size	m_{wax}	$m_{loaded\ bomb}$	$m_{emptied\ bomb}$	$m_{propane}$	x_{wax}	T_0	P_0
No.	Type	μm	g	g	g	g	mass %	$^{\circ}C$	bar (A)
18	C105	60	0.79	1019.3	1003.4	15.9	4.7	157	151

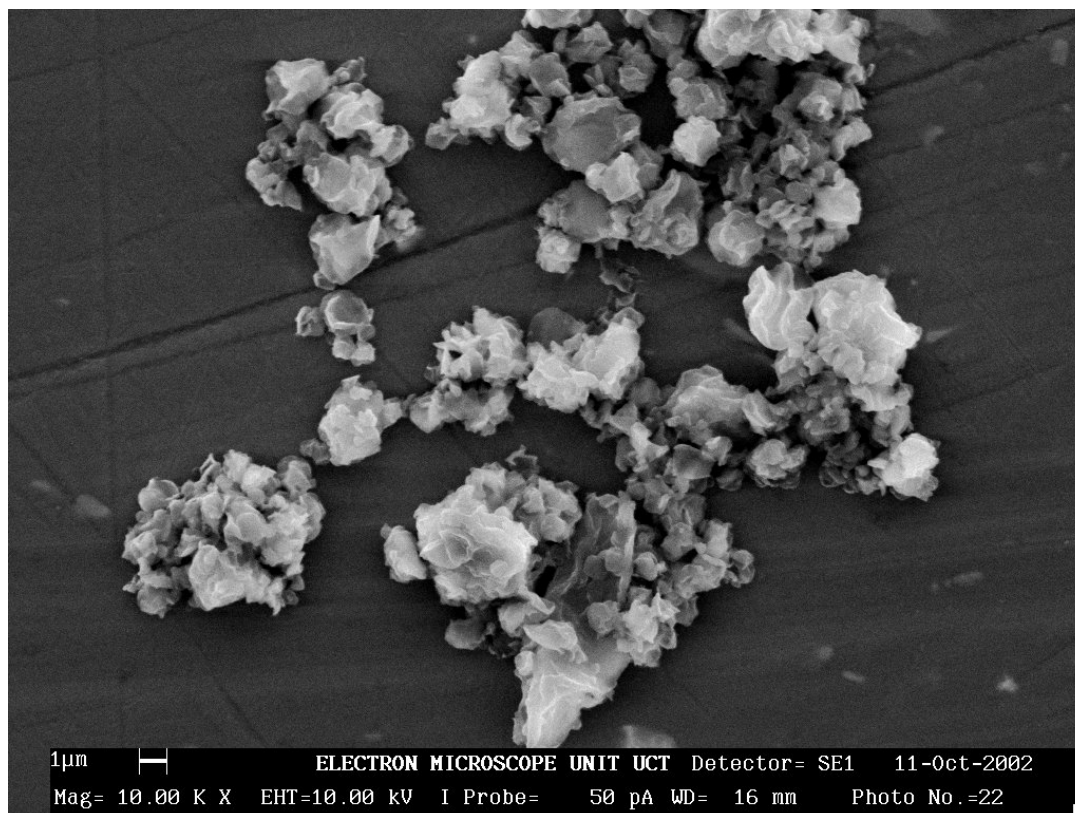


Size Interval (μm)	No % Particles in Range
<0.4	0.6
0.4-0.8	10.9
0.8-1.2	26.1
1.2-1.6	22.4
1.6-2.0	16.4
2.0-2.4	10.9
2.4-2.8	5.5

Size Interval (μm)	No % Particles in Range
2.8-3.2	2.4
3.2-3.6	2.4
3.6-4.0	0.6
4.0-4.4	1.8
4.4-4.8	0.0
>4.8	0.0

Particle Size (μm)	
Min	0.37
D10	0.73
D50	1.42
D90	2.44
Max	4.21
Avg	1.57
Skew	1.21

Run	Wax	Pore Size	m_{wax}	$m_{loaded\ bomb}$	$m_{emptied\ bomb}$	$m_{propane}$	x_{wax}	T_0	P_0
No.	Type	μm	g	g	g	g	mass %	$^{\circ}C$	bar (A)
19	C80	60	0.79	1019.3	1003.5	15.8	4.8	157	154

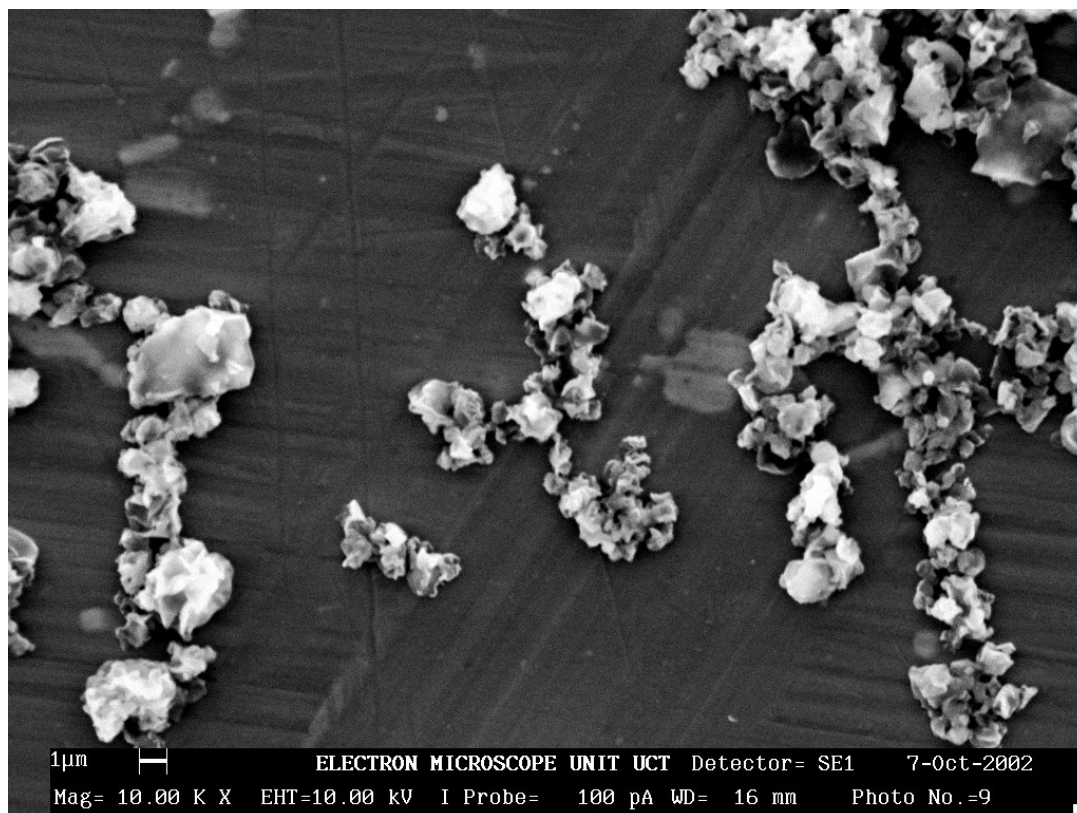


Size Interval (μm)	No % Particles in Range
<0.4	0.8
0.4-0.8	15.9
0.8-1.2	31.4
1.2-1.6	21.3
1.6-2.0	13.4
2.0-2.4	8.4
2.4-2.8	2.9

Size Interval (μm)	No % Particles in Range
2.8-3.2	2.1
3.2-3.6	0.8
3.6-4.0	0.8
4.0-4.4	0.4
4.4-4.8	0.8
>4.8	0.8

Particle Size (μm)	
Min	0.3
D10	0.67
D50	1.22
D90	2.30
Max	5.64
Avg	1.42
Skew	2.12

Run	Wax	Pore Size	m_{wax}	$m_{loaded\ bomb}$	$m_{emptied\ bomb}$	$m_{propane}$	x_{wax}	T_0	P_0
No.	Type	μm	g	g	g	g	mass %	$^{\circ}C$	bar (A)
20	C80	60	0.48	1019.2	1003.3	15.9	2.9	157	125

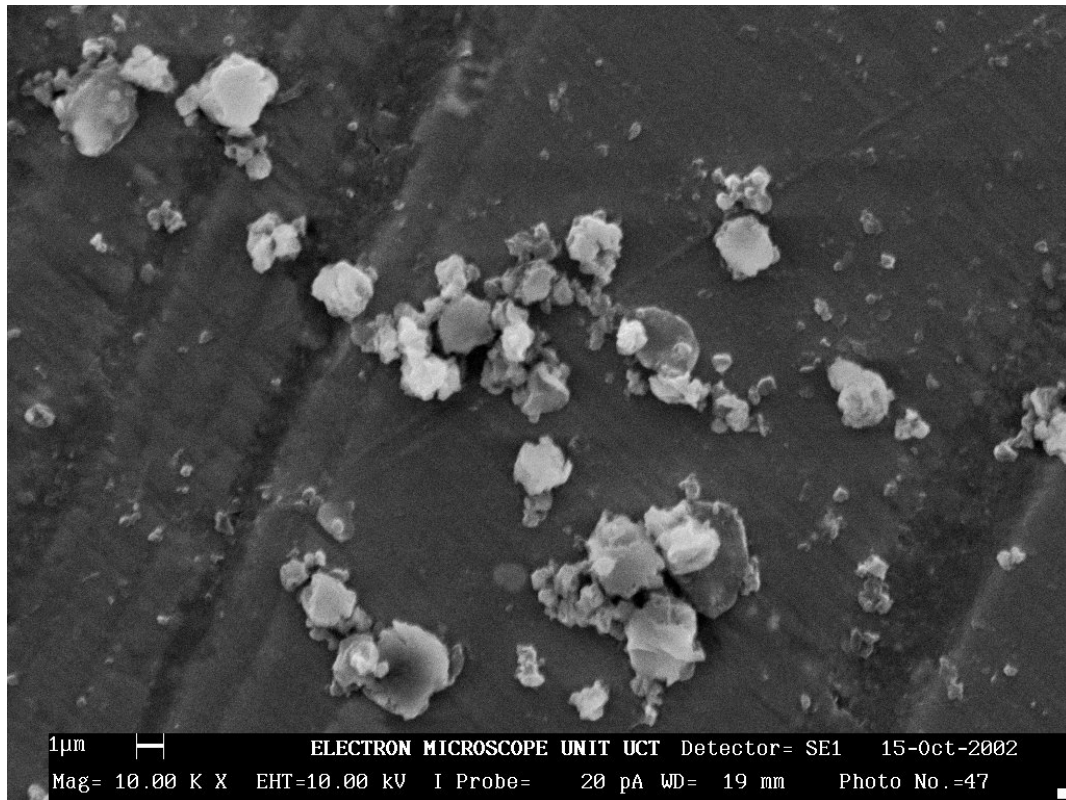


Size Interval (μm)	No % Particles in Range
<0.4	0.6
0.4-0.8	18.9
0.8-1.2	41.7
1.2-1.6	23.4
1.6-2.0	8.0
2.0-2.4	2.9
2.4-2.8	0.6

Size Interval (μm)	No % Particles in Range
2.8-3.2	1.1
3.2-3.6	0.6
3.6-4.0	0.6
4.0-4.4	0.0
4.4-4.8	0.6
>4.8	1.1

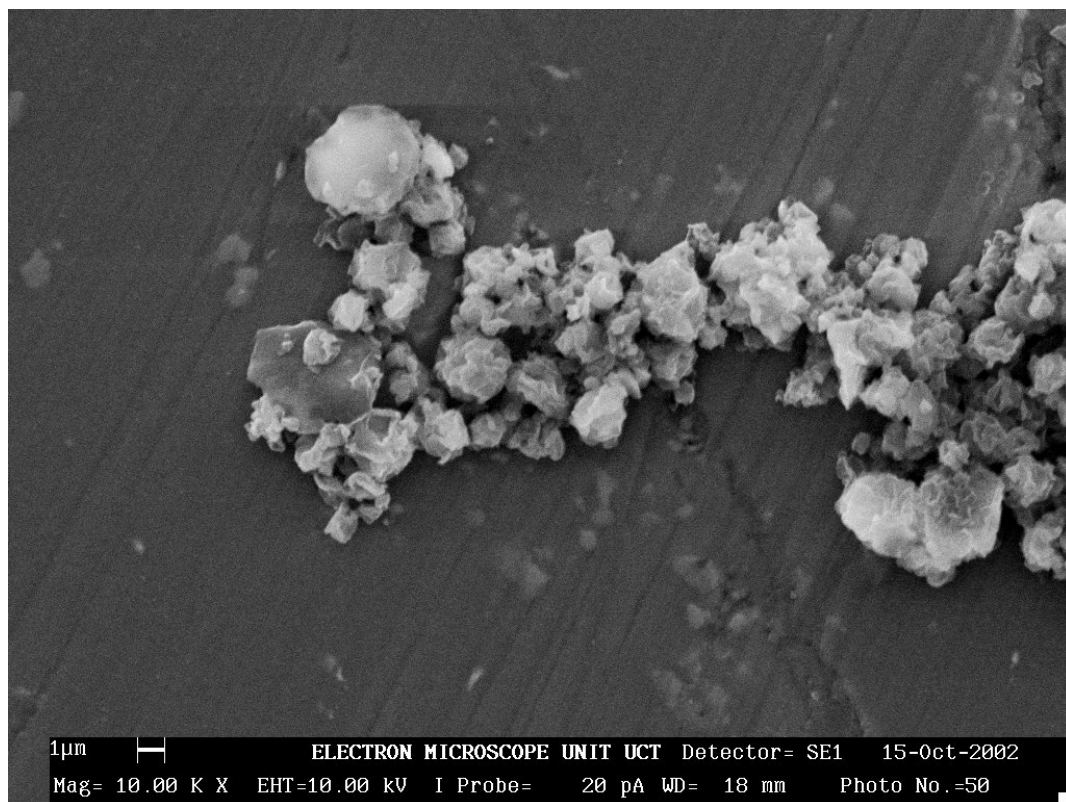
Particle Size (μm)	
Min	0.36
D10	0.63
D50	1.07
D90	1.90
Max	6.17
Avg	1.24
Skew	3.50

Run	Wax	Pore Size	m_{wax}	$m_{loaded\ bomb}$	$m_{emptied\ bomb}$	$m_{propane}$	x_{wax}	T_0	P_0
No.	Type	μm	g	g	g	g	mass %	$^{\circ}C$	bar (A)
21	C80	60	0.32	1019.4	1003.4	16.0	2.0	127	174



Size Interval (μm)	No % Particles in Range	Size Interval (μm)	No % Particles in Range	Particle Size (μm)	
<0.4	2.5	2.8-3.2	2.5	Min	0.32
0.4-0.8	29.5	3.2-3.6	1.0	D10	0.56
0.8-1.2	29.0	3.6-4.0	1.0	D50	0.99
1.2-1.6	17.0	4.0-4.4	0.0	D90	2.17
1.6-2.0	8.5	4.4-4.8	0.0	Max	3.63
2.0-2.4	7.0	>4.8	0.0	Avg	1.21
2.4-2.8	2.0			Skew	1.45

Run	Wax	Pore Size	m_{wax}	$m_{loaded\ bomb}$	$m_{emptied\ bomb}$	$m_{propane}$	x_{wax}	T_0	P_0
No.	Type	μm	g	g	g	g	mass %	$^{\circ}C$	bar (A)
22	C80	60	0.32	1019.4	1003.8	15.6	2.0	127	156

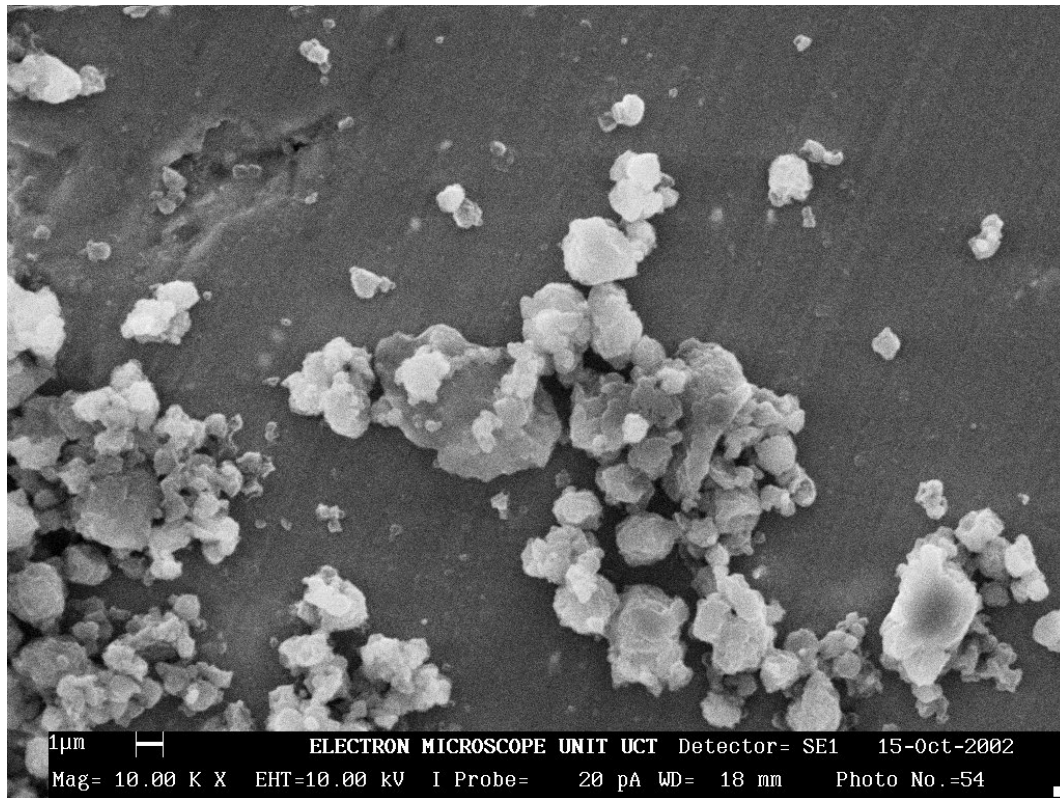


Size Interval (μm)	No % Particles in Range
<0.4	0.0
0.4-0.8	9.0
0.8-1.2	27.6
1.2-1.6	28.2
1.6-2.0	12.2
2.0-2.4	11.5
2.4-2.8	5.8

Size Interval (μm)	No % Particles in Range
2.8-3.2	2.6
3.2-3.6	0.0
3.6-4.0	1.3
4.0-4.4	0.0
4.4-4.8	0.0
>4.8	1.9

Particle Size (μm)	
Min	0.44
D10	0.87
D50	1.39
D90	2.44
Max	8.27
Avg	1.58
Skew	3.35

Run	Wax	Pore Size	m_{wax}	$m_{loaded\ bomb}$	$m_{emptied\ bomb}$	$m_{propane}$	x_{wax}	T_0	P_0
No.	Type	μm	g	g	g	g	mass %	$^{\circ}C$	bar (A)
23	C80	25	0.32	1019.2	1003.7	15.5	2.0	157	153

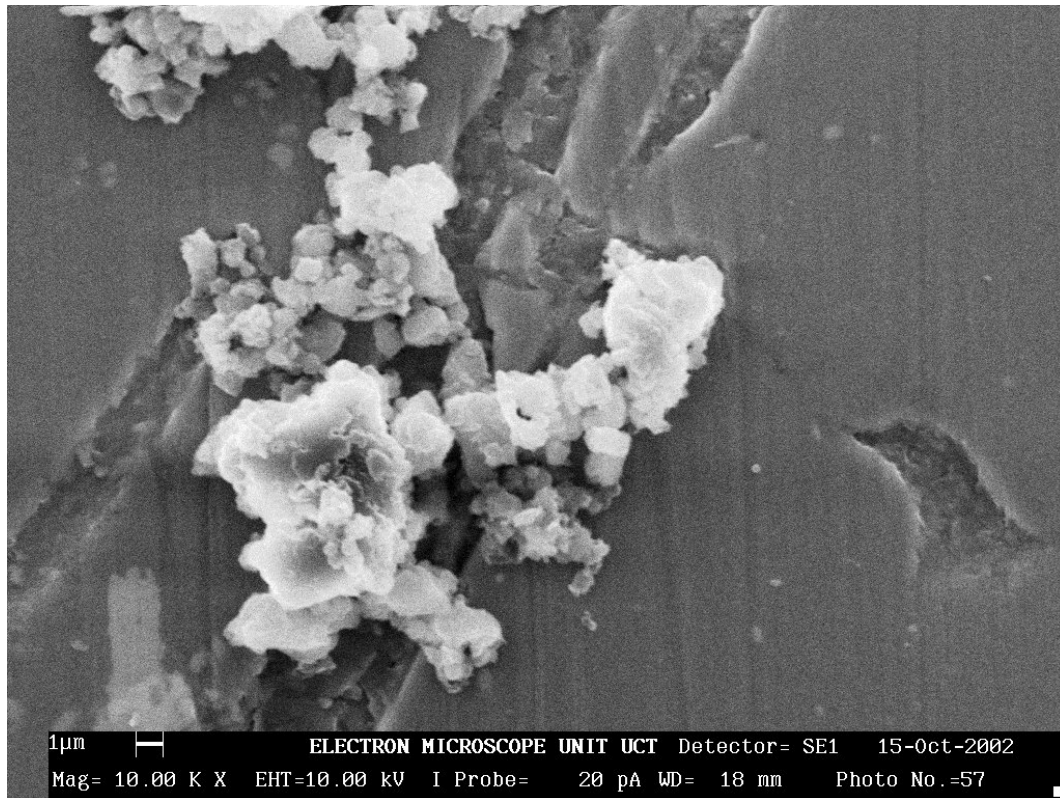


Size Interval (μm)	No % Particles in Range
<0.4	0.4
0.4-0.8	21.8
0.8-1.2	36.5
1.2-1.6	21.8
1.6-2.0	11.9
2.0-2.4	2.4
2.4-2.8	2.0

Size Interval (μm)	No % Particles in Range
2.8-3.2	1.6
3.2-3.6	0.8
3.6-4.0	0.4
4.0-4.4	0.4
4.4-4.8	0.0
>4.8	0.0

Particle Size (μm)	
Min	0.33
D10	0.63
D50	1.10
D90	1.81
Max	4.12
Avg	1.23
Skew	1.88

Run	Wax	Pore Size	m_{wax}	$m_{loaded\ bomb}$	$m_{emptied\ bomb}$	$m_{propane}$	x_{wax}	T_0	P_0
No.	Type	μm	g	g	g	g	mass %	$^{\circ}C$	bar (A)
24	C80	25	0.8	1019.2	1003.4	15.8	4.8	157	150

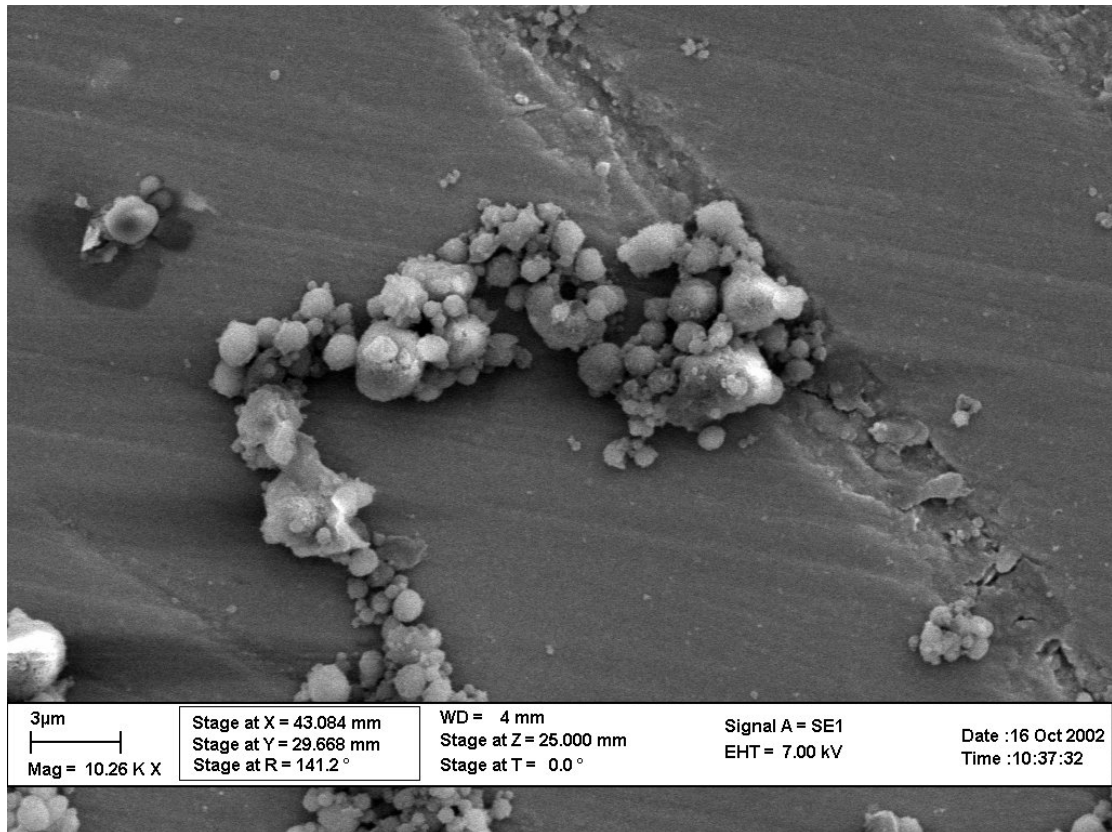


Size Interval (μm)	No % Particles in Range
<0.4	1.7
0.4-0.8	33.1
0.8-1.2	37.7
1.2-1.6	17.8
1.6-2.0	5.1
2.0-2.4	2.1
2.4-2.8	0.8

Size Interval (μm)	No % Particles in Range
2.8-3.2	0.0
3.2-3.6	0.0
3.6-4.0	0.4
4.0-4.4	0.0
4.4-4.8	0.8
>4.8	0.4

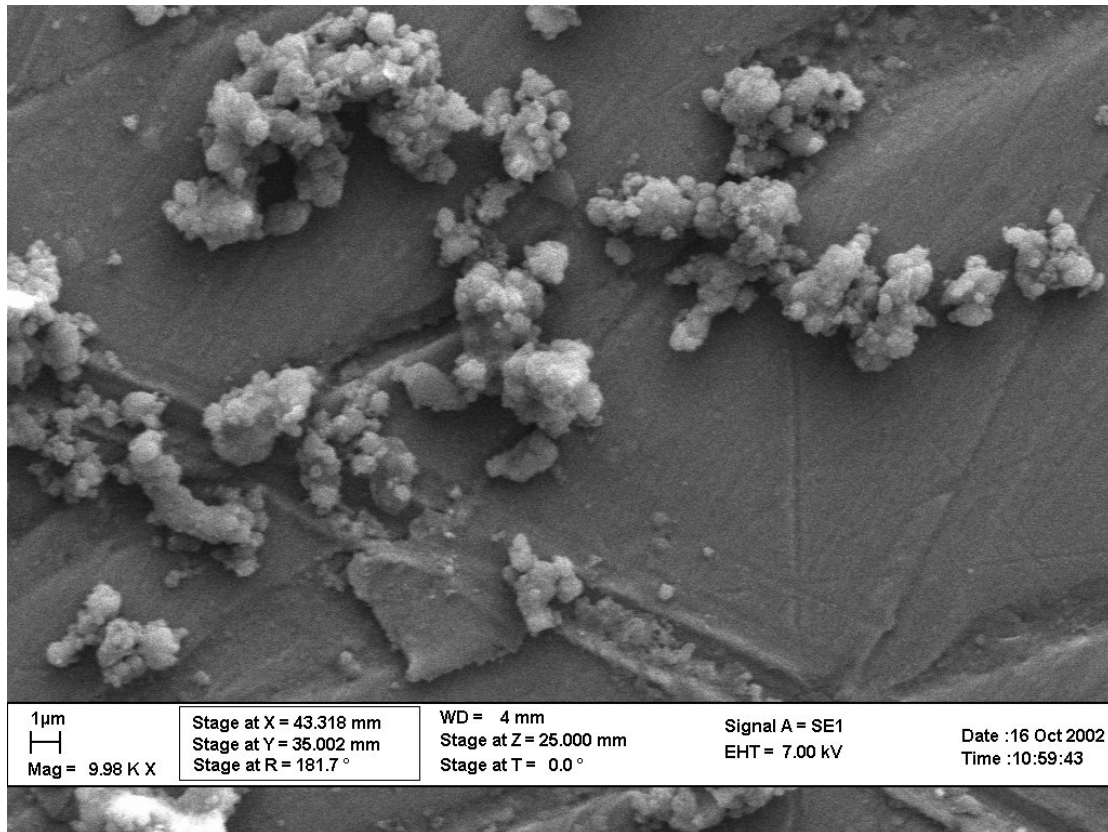
Particle Size (μm)	
Min	0.28
D10	0.61
D50	0.95
D90	1.57
Max	7.78
Avg	1.08
Skew	5.21

Run	Wax	Pore Size	m_{wax}	$m_{loaded\ bomb}$	$m_{emptied\ bomb}$	$m_{propane}$	x_{wax}	T_0	P_0
No.	Type	μm	g	g	g	g	mass %	$^{\circ}C$	bar (A)
25	C105	25	0.32	1019.5	1003.6	15.9	2.0	156	149



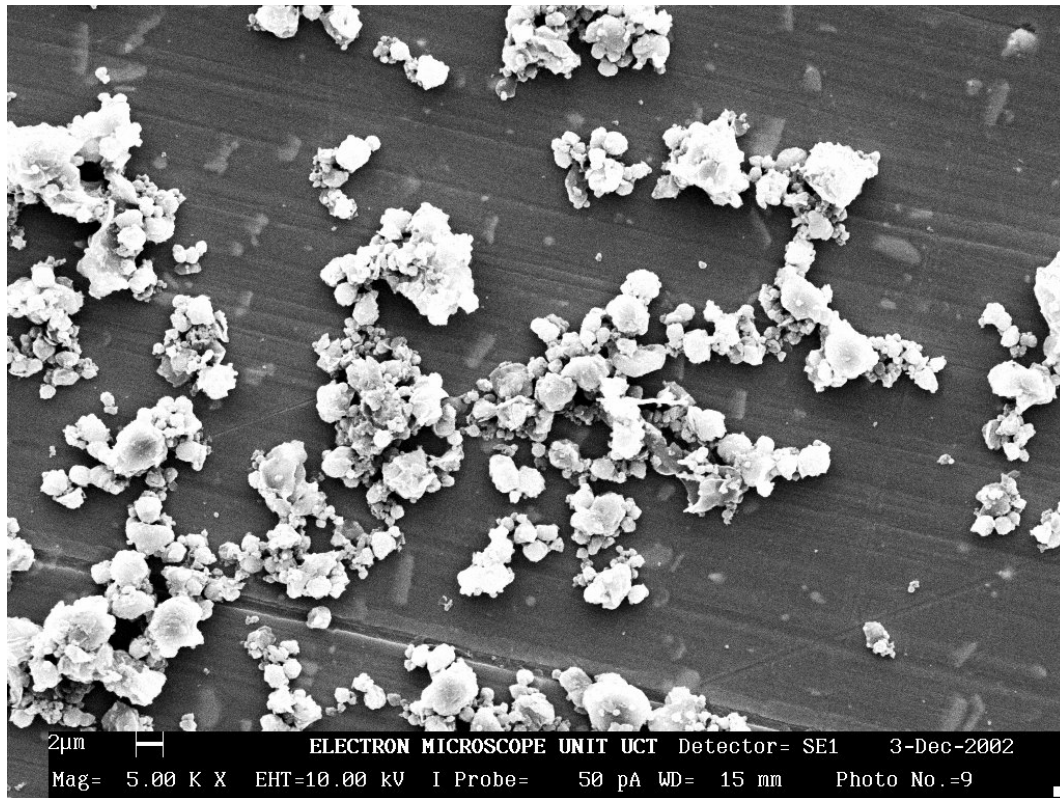
Size Interval (μm)	No % Particles in Range	Size Interval (μm)	No % Particles in Range	Particle Size (μm)	
<0.4	14.2	2.8-3.2	0.0	Min	0.21
0.4-0.8	46.9	3.2-3.6	0.4	D10	0.34
0.8-1.2	20.5	3.6-4.0	0.0	D50	0.70
1.2-1.6	10.9	4.0-4.4	0.8	D90	1.41
1.6-2.0	2.9	4.4-4.8	0.0	Max	5.57
2.0-2.4	2.5	>4.8	0.8	Avg	0.87
2.4-2.8	0.0			Skew	3.84

Run	Wax	Pore Size	m_{wax}	$m_{loaded\ bomb}$	$m_{emptied\ bomb}$	$m_{propane}$	x_{wax}	T_0	P_0
No.	Type	μm	g	g	g	g	mass %	$^{\circ}C$	bar (A)
26	C105	25	0.79	1019.5	1004.1	15.4	4.9	156	150



Size Interval (μm)	No % Particles in Range	Size Interval (μm)	No % Particles in Range	Particle Size (μm)	
<0.4	12.9	2.8-3.2	0.9	Min	0.15
0.4-0.8	43.3	3.2-3.6	0.4	D10	0.38
0.8-1.2	20.1	3.6-4.0	0.0	D50	0.75
1.2-1.6	13.8	4.0-4.4	0.0	D90	1.58
1.6-2.0	5.4	4.4-4.8	0.0	Max	3.56
2.0-2.4	1.3	>4.8	0.0	Avg	0.90
2.4-2.8	1.8			Skew	1.71

Run	Wax	Pore Size	m_{wax}	$m_{loaded\ bomb}$	$m_{emptied\ bomb}$	$m_{propane}$	x_{wax}	T_0	P_0
No.	Type	μm	g	g	g	g	mass %	$^{\circ}C$	bar (A)
27	C105	25	0.48	1019.2	1003.6	15.6	3.0	129	177

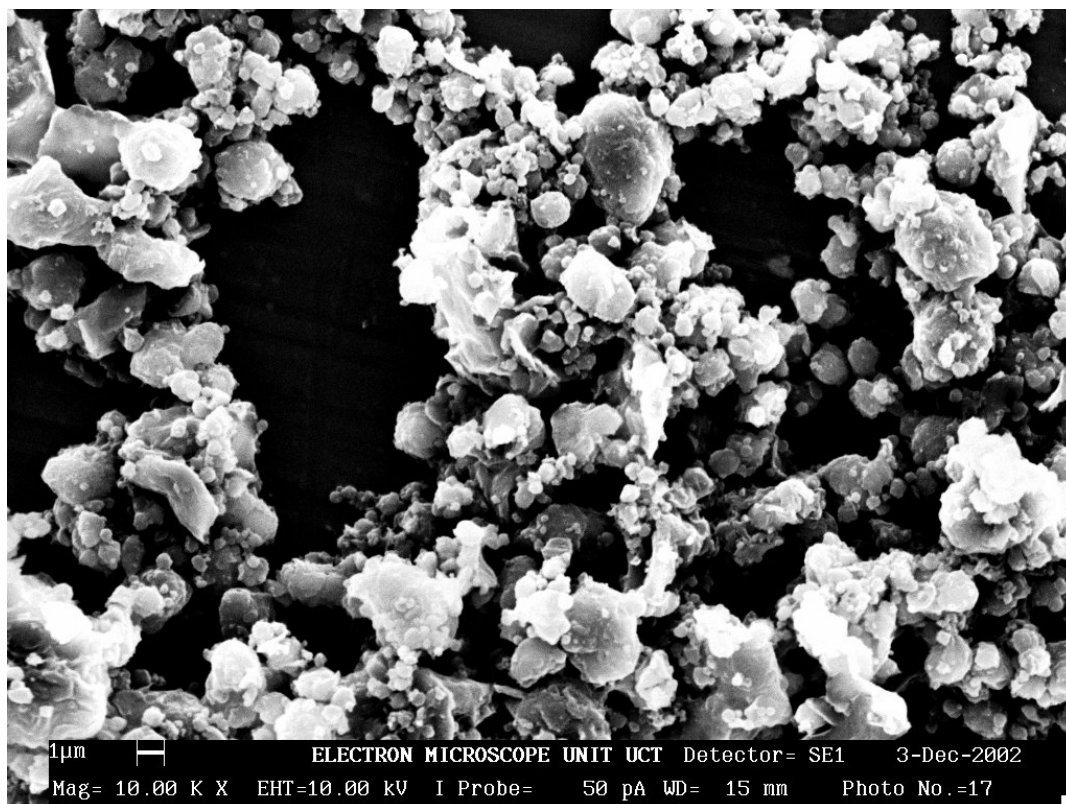


Size Interval (μm)	No % Particles in Range
<0.4	1.5
0.4-0.8	15.0
0.8-1.2	26.5
1.2-1.6	25.5
1.6-2.0	12.5
2.0-2.4	9.5
2.4-2.8	5.0

Size Interval (μm)	No % Particles in Range
2.8-3.2	2.0
3.2-3.6	0.5
3.6-4.0	2.0
4.0-4.4	0.0
4.4-4.8	0.0
>4.8	0.0

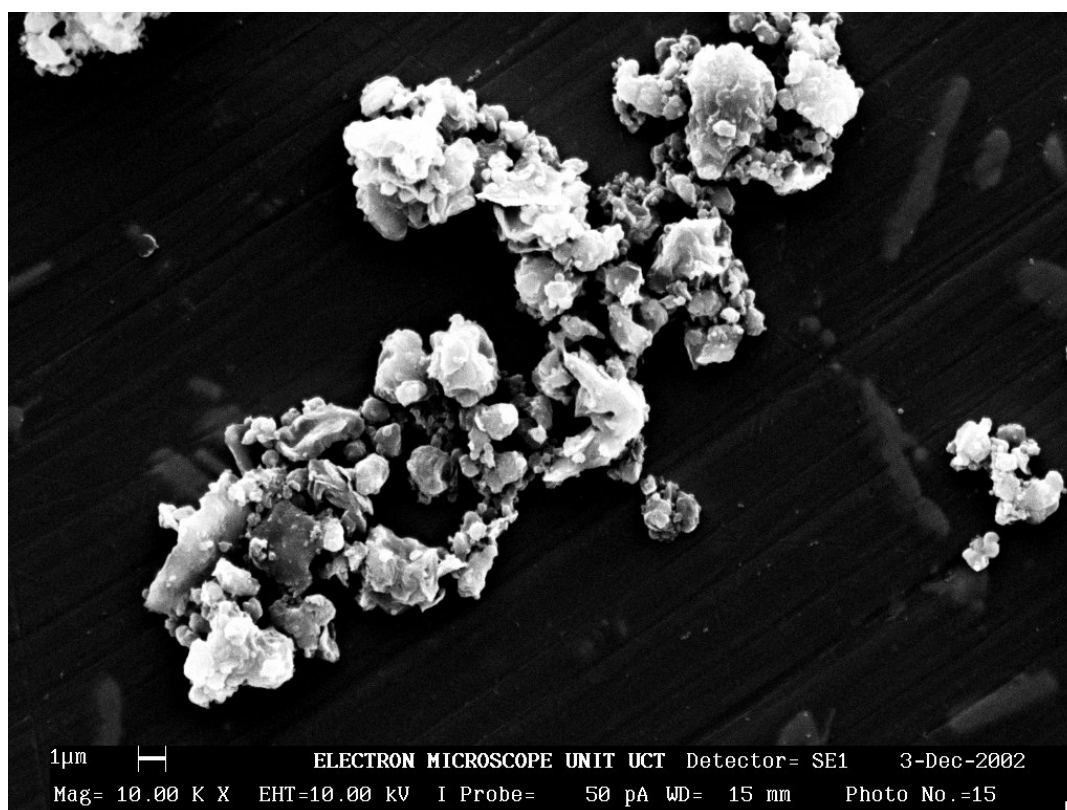
Particle Size (μm)	
Min	0.32
D10	0.57
D50	1.34
D90	2.34
Max	3.96
Avg	1.43
Skew	1.10

Run	Wax	Pore Size	m_{wax}	$m_{loaded\ bomb}$	$m_{emptied\ bomb}$	$m_{propane}$	x_{wax}	T_0	P_0
No.	Type	μm	g	g	g	g	mass %	$^{\circ}C$	bar (A)
28	C105	25	0.63	1019.5	1003.9	15.6	3.9	127	176



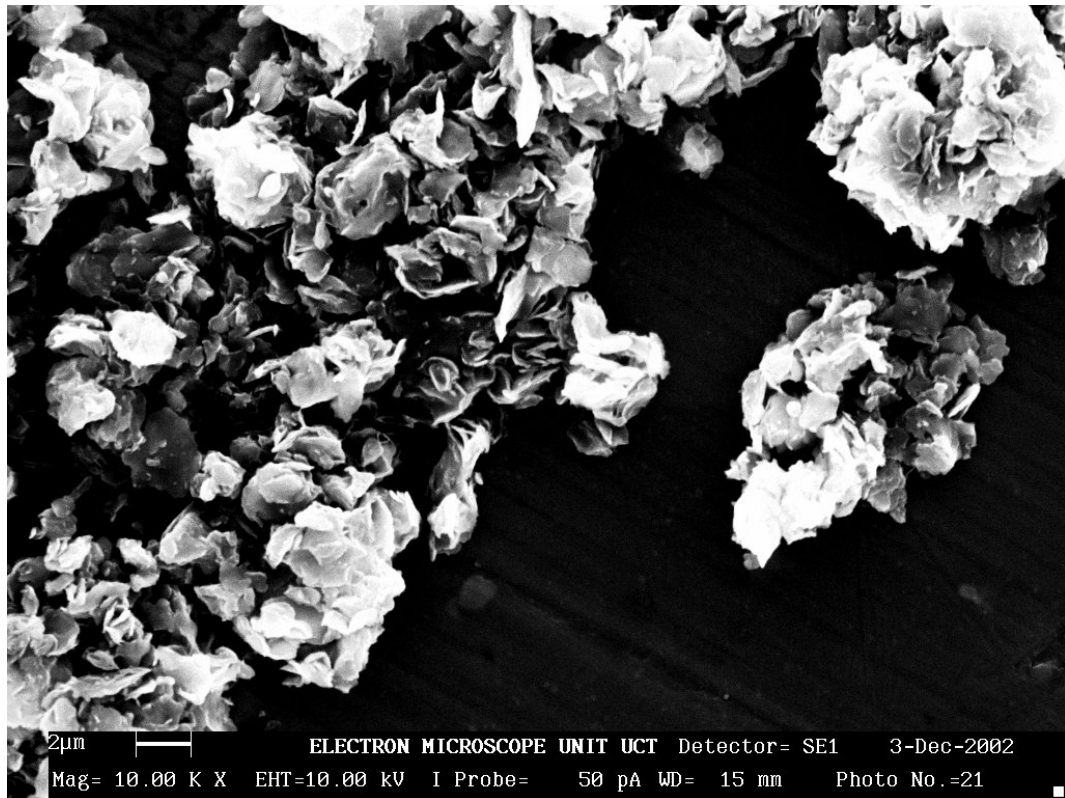
Size Interval (μm)	No % Particles in Range	Size Interval (μm)	No % Particles in Range	Particle Size (μm)	
<0.4	10.0	2.8-3.2	2.0	Min	0.20
0.4-0.8	41.5	3.2-3.6	0.5	D10	0.39
0.8-1.2	24.5	3.6-4.0	0.0	D50	0.77
1.2-1.6	9.5	4.0-4.4	0.5	D90	1.80
1.6-2.0	6.5	4.4-4.8	0.0	Max	4.11
2.0-2.4	3.5	>4.8	0.0	Avg	0.98
2.4-2.8	1.5			Skew	1.79

Run	Wax	Pore Size	m_{wax}	$m_{loaded\ bomb}$	$m_{emptied\ bomb}$	$m_{propane}$	x_{wax}	T_0	P_0
No.	Type	μm	g	g	g	g	mass %	$^{\circ}C$	bar (A)
29	C105	25	0.78	1019.5	1004.1	15.4	4.8	129	178



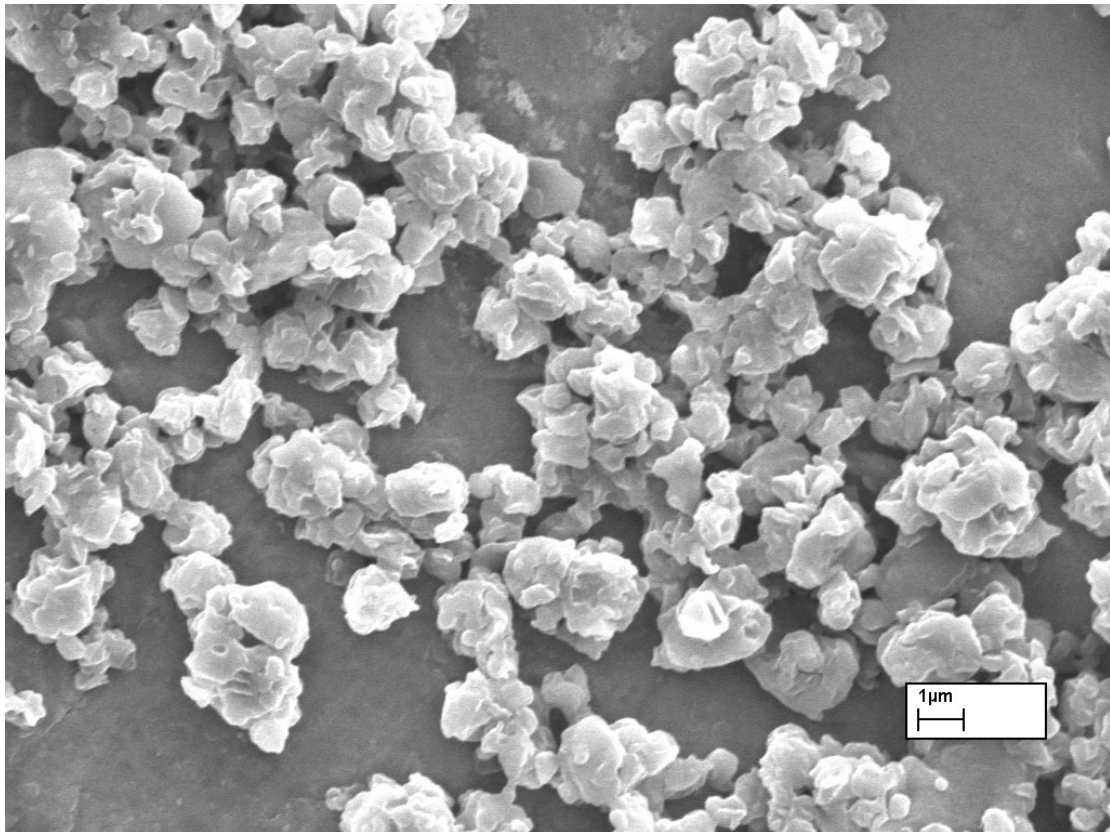
Size Interval (μm)	No % Particles in Range	Size Interval (μm)	No % Particles in Range	Particle Size (μm)	
<0.4	0.9	2.8-3.2	1.4	Min	0.28
0.4-0.8	28.9	3.2-3.6	1.4	D10	0.56
0.8-1.2	30.8	3.6-4.0	0.5	D50	1.00
1.2-1.6	16.1	4.0-4.4	0.5	D90	2.18
1.6-2.0	10.0	4.4-4.8	0.5	Max	6.23
2.0-2.4	5.7	>4.8	0.5	Avg	1.25
2.4-2.8	2.8			Skew	2.38

Run	Wax	Pore Size	m_{wax}	$m_{loaded\ bomb}$	$m_{emptied\ bomb}$	$m_{propane}$	x_{wax}	T_0	P_0
No.	Type	μm	g	g	g	g	mass %	$^{\circ}C$	bar (A)
30	C105	25	0.95	1018.8	1004.0	14.8	6.0	129	176



Size Interval (μm)	No % Particles in Range	Size Interval (μm)	No % Particles in Range	Particle Size (μm)	
<0.4	0.0	2.8-3.2	4.8	Min	0.81
0.4-0.8	0.0	3.2-3.6	5.5	D10	1.22
0.8-1.2	8.5	3.6-4.0	1.8	D50	1.81
1.2-1.6	24.2	4.0-4.4	2.4	D90	3.25
1.6-2.0	26.1	4.4-4.8	1.2	Max	4.56
2.0-2.4	14.5	>4.8	0.0	Avg	2.02
2.4-2.8	10.9			Skew	1.09

Run	Wax	Pore Size	m_{wax}	$m_{loaded\ bomb}$	$m_{emptied\ bomb}$	$m_{propane}$	x_{wax}	T_0	P_0
No.	Type	μm	g	g	g	g	mass %	$^{\circ}C$	bar (A)
R 4	C80	60	0.48	1019.1	1004.3	14.8	3.1	157	149



Size Interval (μm)	No % Particles in Range
<0.4	0.5
0.4-0.8	20.7
0.8-1.2	35.1
1.2-1.6	24.1
1.6-2.0	10.0
2.0-2.4	5.4
2.4-2.8	1.2

Size Interval (μm)	No % Particles in Range
2.8-3.2	1.0
3.2-3.6	0.2
3.6-4.0	0.7
4.0-4.4	0.7
4.4-4.8	0.0
>4.8	0.2

Particle Size (μm)	
Min	0.26
D10	0.72
D50	1.13
D90	1.77
Max	5.83
Avg	1.26
Skew	2.36

B DEW POINTS OF PARAFFIN WAX

The dew points of C80 wax were measured in the phase equilibrium cell used by Schwarz. The cell has maximum volume of 38.6 cm³ and can withstand pressures of 300 bar. The cell is similar to the equilibrium cell used in the RESS experiments. The cell volume was heated by circulation of Dowtherm heating liquid in the cell jacketing. A piston unit was used to pressurise the cell content. The area ratio of the piston unit was much larger than that used in this project, thus enabling application of much larger pressure to the cell content.

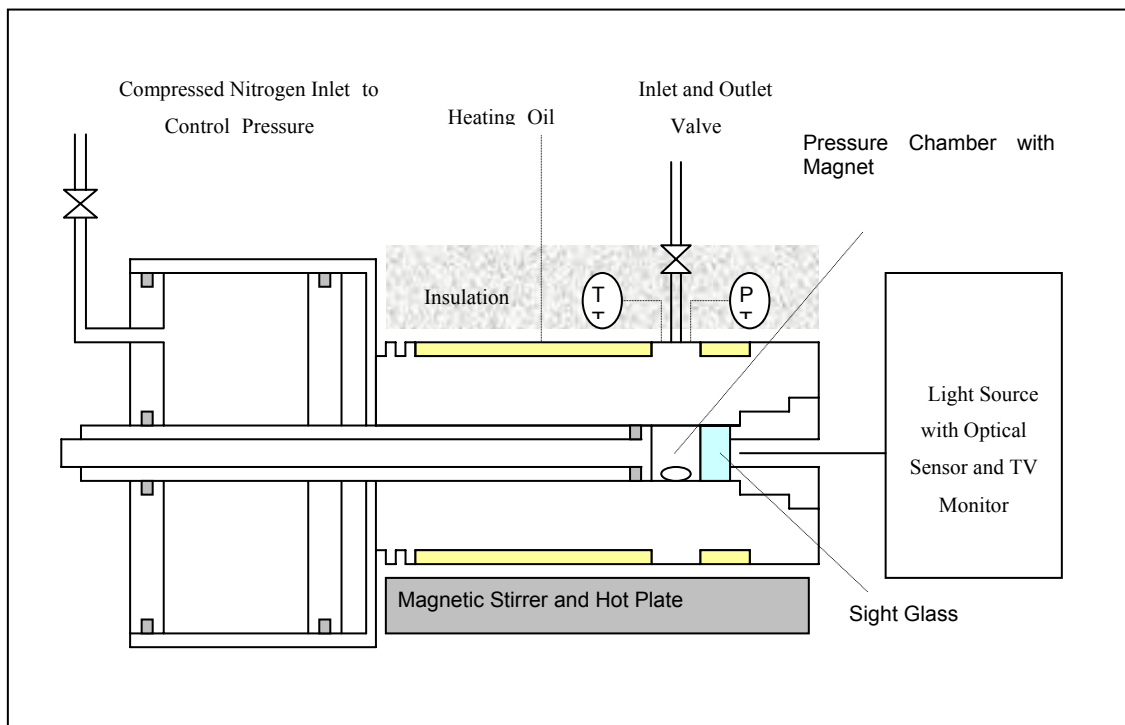
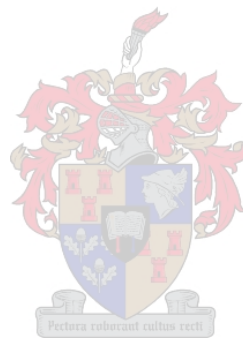


Figure B-0-1: Equilibrium Cell used for C80 Dew Point Measurements (Schwarz 2001)

The cell was loaded to the desired cell concentration, similar to the way in which it was done in these experiments. The contents, at a determined temperature, was pressurised until in one phase. The pressure would then be slowly lowered until the content was in two clear phases. Pressure would be reapplied until the solution was in one phase again. The range of phase transition was now known, and small incremental pressure changes could be made until the phase transition point was determined. The cell was agitated via a magnetic stirring.

The cell is equipped with a sight glass so that phase transition can be observed. A light source is introduced via the sight glass. This light is reflected off the back of the cell chamber and illuminates the cell content. The cell content was viewed via optical sensor and a television monitor. Phase transition was defined as the point the cell content became cloudy during depressurising of the cell content.



C CALIBRATION DATA

Prior to the installation of the pressure probe in the experimental set-up, it was calibrated with a dead weight tester. The influence of temperature on the gauge readings was also investigated. After calibration the following readings was obtained for the pressure range of interest:

Table C-1: Pressure Calibration Data

<i>Applied Pressure</i>	<i>Gauge Reading at Temperature</i>		
	22 °C	127 °C	157 °C
bar (A)			
96	96.3	98.2	98.7
111	111.3	113.1	113.6
126	126.2	128.1	128.5
141	141.1	143.0	143.5
156	156.0	157.9	158.3
171	170.8	172.7	173.2
186	185.8	187.6	188.1

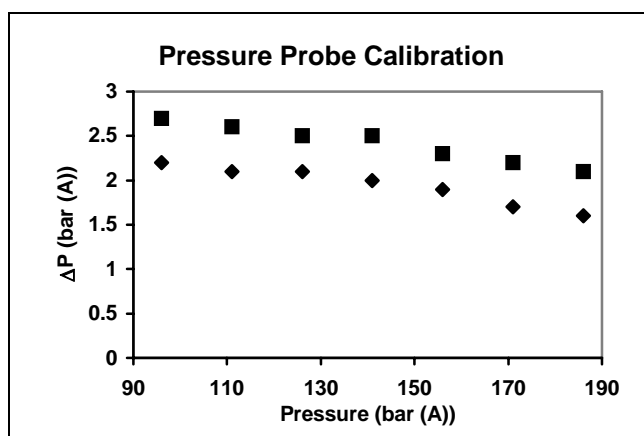
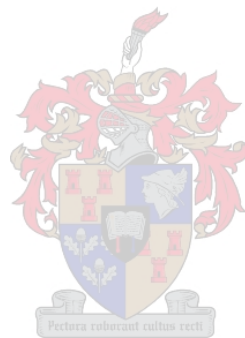


Figure C-1: Pressure Fluctuations with Temperature

The experimental runs used in these experiments were done at pressures from between 125 to 175 bar. As can be seen, at the temperature of approximately 130 °C, a positive pressure difference of about 2 bar was found. At the higher temperature, the positive pressure difference was in the region of 2.5 bar. The difference in pressure due to the temperature effect can be attributed to the expansion of the liquid in the pressure probe.



D ADDITIONAL EXPERIMENTAL PROCEDURES

Unloading and Cleaning of Equilibrium Cell

Most of the cell content will have been removed during spraying, but approximately one sixth of the volume will still have remained.

The nitrogen feed to the counterbalance piston is shut-off and the remaining nitrogen in the nitrogen feed line is bled off. The counterbalance piston should return fully retract.

The heating and nitrogen feed lines were disconnected from the equilibrium cell and the heating oil in the equilibrium cell jacket was carefully drained.

The set-up can now be carefully removed from the expansion vessel, the sinter plate removed and the remaining cell content depressurised by opening the expansion valve in a well-ventilated area.

The counterbalance piston is screwed from the equilibrium cell.

The cell volume and piston were flushed several times with industrial xylene, heated to a temperature where the wax is totally miscible with the xylene solvent. Once the wax was removed, the cell volume was flushed once with methanol to remove residual xylene and the cell volume dried with compressed air.

The sinter was placed in xylene, which was then heated to boiling point. To ensure that the pore holes were clean, pressurised carbon dioxide was sprayed through the sinter to check the flow path.

Safety Considerations

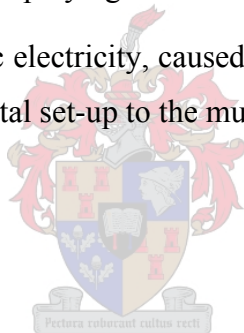
The experimental work requires high temperatures and pressures, requiring the necessary care.

Propane is a highly flammable compound and must be handled with care to prevent explosions and fire. The experimental procedure and set-up had a number of factors incorporated to prevent explosions or fire.

No experimental runs were done whenever any hot work was scheduled in the laboratory.

The expanding solution was sprayed into an extraction vessel so that propane would not form of a low-lying propane cloud in the environment. The extraction vessel should be filled with CO₂ prior to spraying to inertise the chamber volume.

Any possible discharge of static electricity, caused during the experiments was dealt with by grounding the experimental set-up to the municipal water supply.



E PROPERTIES OF CHEMICALS USED

Two waxes were used to determine its influence on the particle size – one of lesser average chain length and melting point than the other. The waxes are synthetic Fischer-Tropsch waxes, as produced by SASOL (Pty) Ltd. The characteristics of the waxes are summarised in Table E-1.

Table E-1: Properties of Wax used in Experimental Investigations (www.mooremunger.com July 2002)

	<i>C80</i>	<i>C105</i>
Congealing Point (°C)	82	108
Needle Penetration (mm) at 25 °C	0.5	0.1
Needle Penetration (mm) at 66 °C	7.0	0.6
Viscosity (cP) at 121 °C	8.0	21.0
Maximum Oil Content (%)	0.75	0.1

The solvent used in this project was propane. The propane was purchased from Afrox (Pty) Ltd. The composition of the propane used is given in Table E-2.

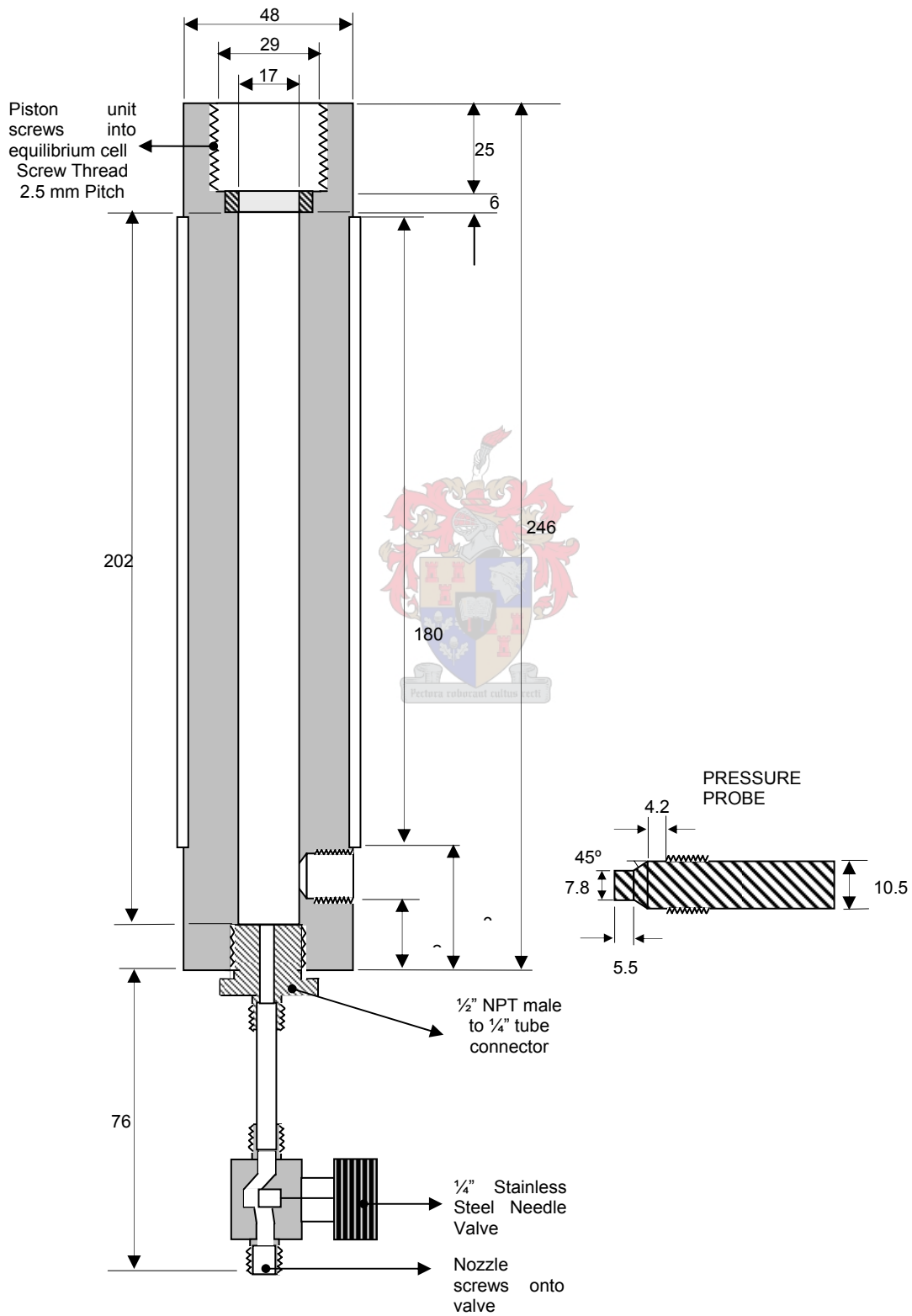
Table E-2: Composition of Propane Solvent used in Experimental Runs (www.afrox.co.za July 2002)

<i>Propane</i>	<i>Other Hydrocarbons</i>	<i>Unsaturated Hydrocarbons</i>	<i>Sulphur Components</i>	<i>1,3 Butadiene</i>
>97% (volume)	50 vpm ¹	3% (volume)	0.1% (volume)	1400 vpm

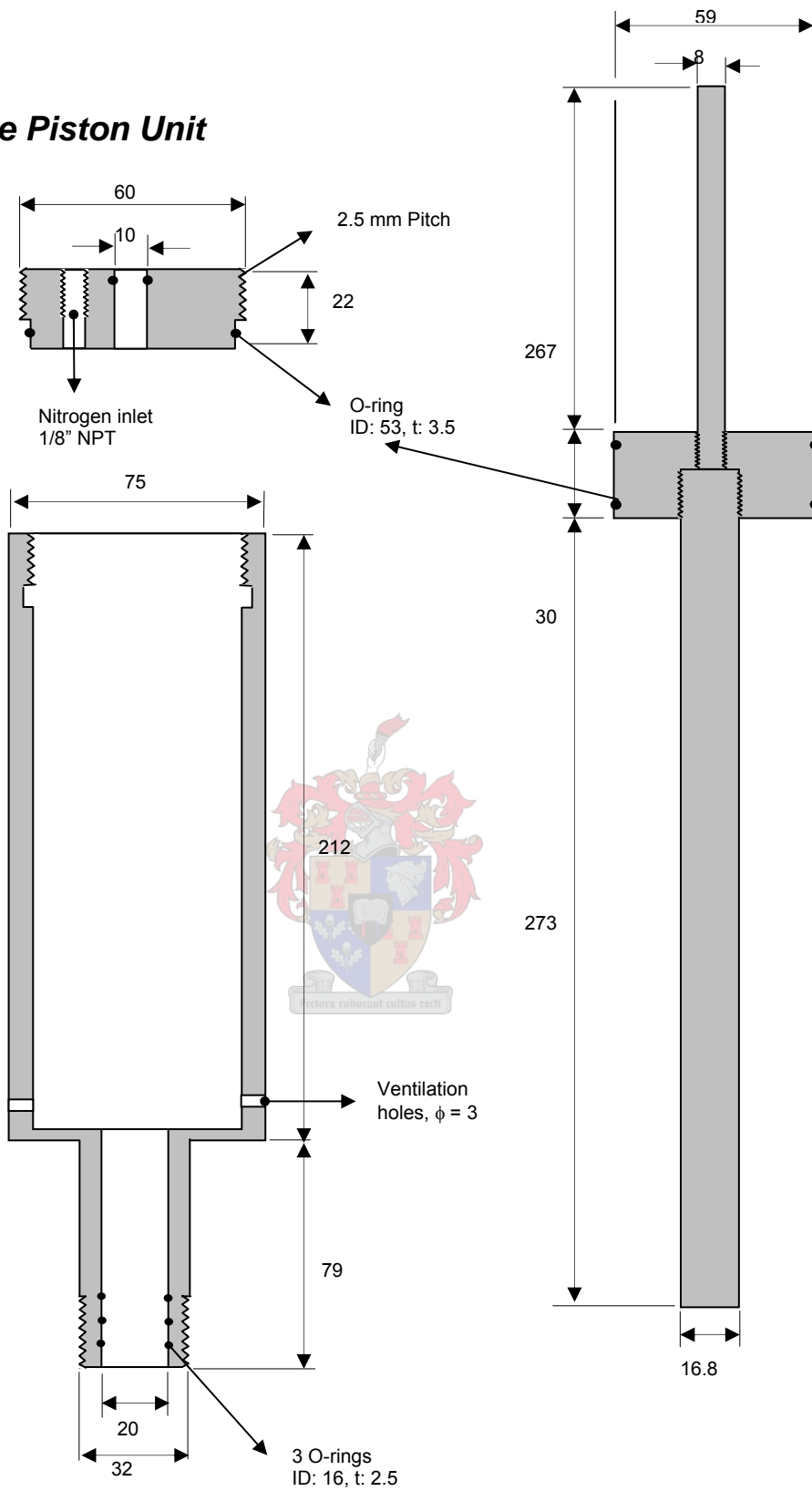
¹ Vapour parts per million

F MECHANICAL DRAWINGS

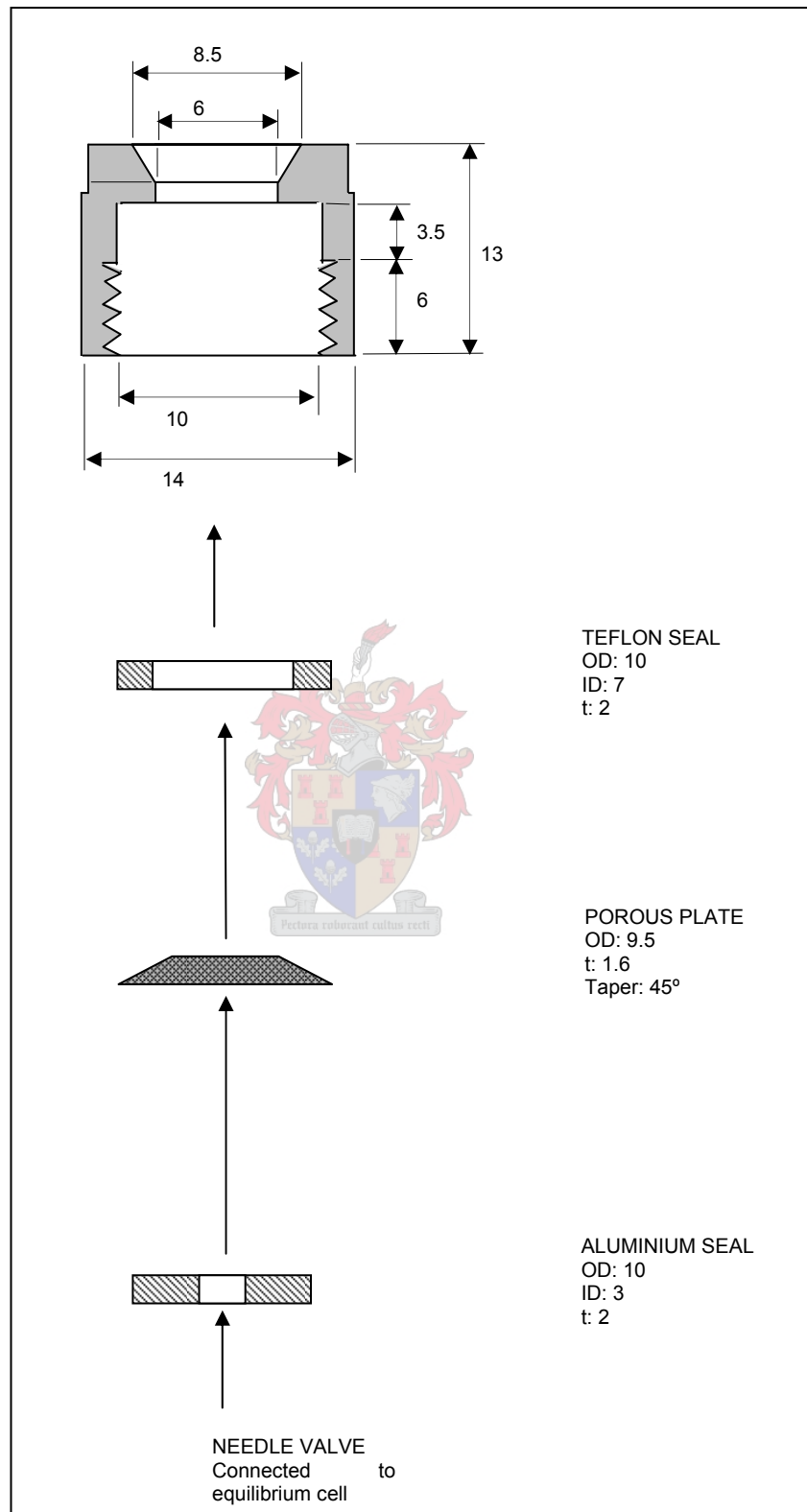
Equilibrium Cell



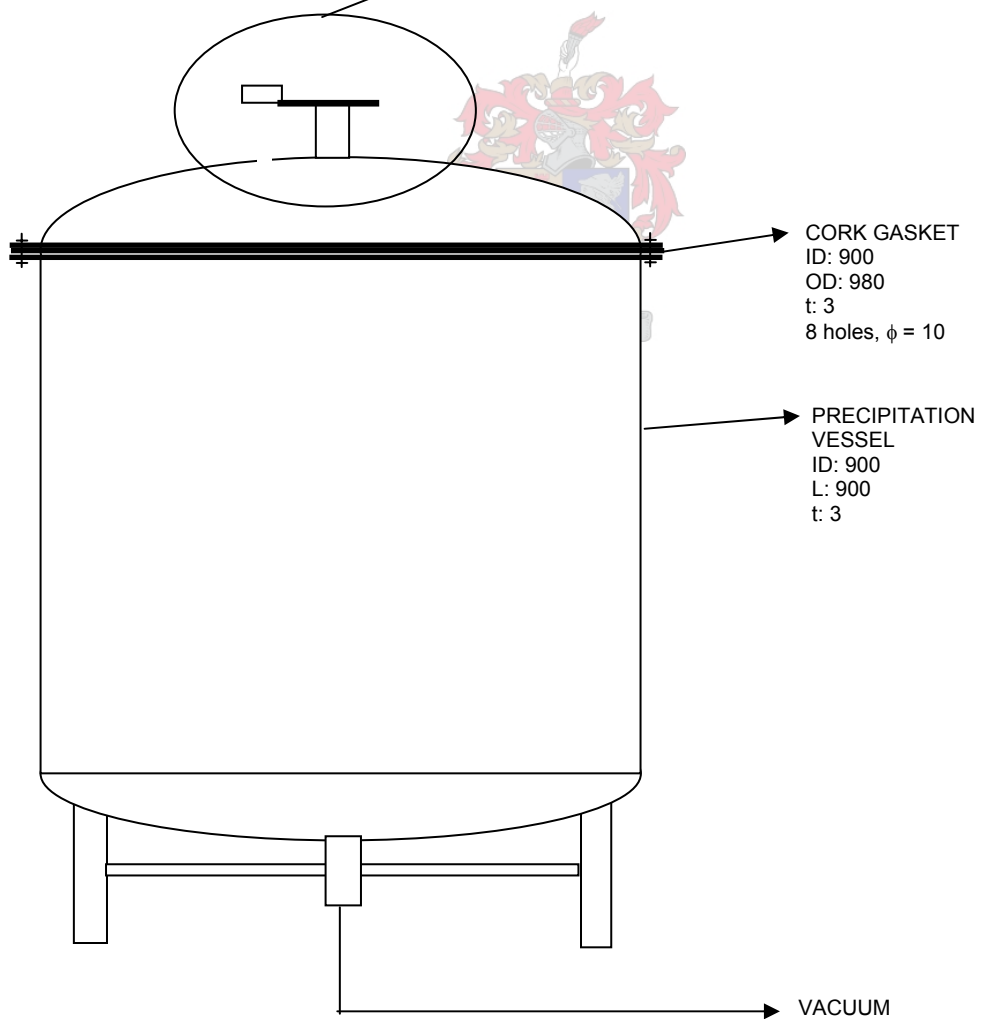
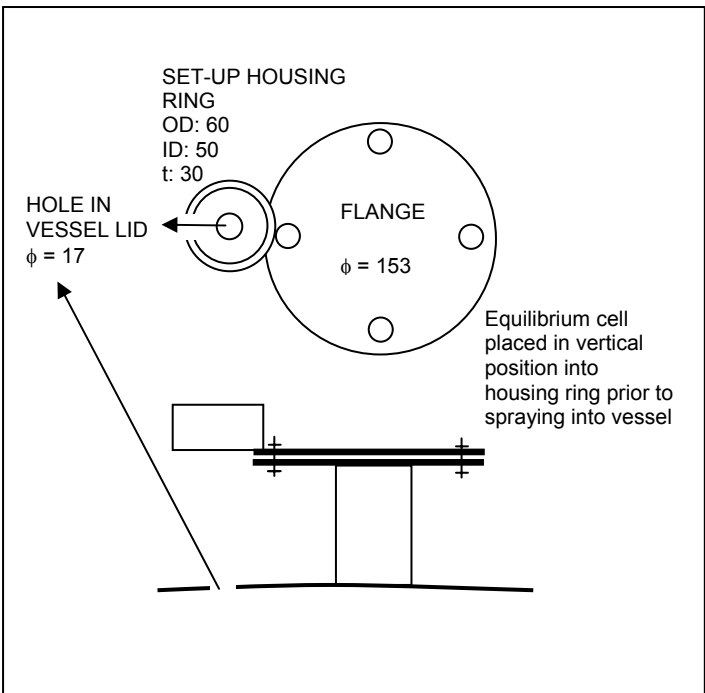
Pressure Piston Unit



Porous Plate Nozzle



Precipitation Vessel



G NOMENCLATURE

Symbols

<i>Symbol</i>	<i>Description</i>	<i>Units</i>
A	Area	m^2
B	Thermal flux	$m^{-2}.s^{-1}$
C	Condensation rate	$m^{-3}s^{-1}$
$C(v)$	Cunningham correction factor	-
D, d	Diameter	m
D	Diffusion coefficient	$m^2.s^{-1}$
f	Fanning friction factor	-
G	Gibbs free energy	$J.kg^{-1}$
h	Enthalpy	$J.kg^{-1}$
I	Nucleation rate	$m^{-3}s^{-1}$
k	Boltzmann constant	$J.K^{-1}$
m	Mass of a molecule	kg
Ma	Mach number	-
N_1	Total number of solute molecules in vapour phase	m^{-3}
n	Particle density	m^{-3}
n_g	Density of particles consisting of g molecules	m^{-3}
P	Pressure	Pa
P_0	Solution pre-expansion pressure	Pa
P_S	Partial pressure of solute	Pa
P_∞	Precipitation vessel pressure	Pa
r	Radius of a spherical embryo or nucleus	m
S	Supersaturation ratio	-
T	Temperature	K
t	Time	s
v	Particle volume	m^3
v_S	Volume of a solute molecule in the liquid phase	m^3
v_L	Volume of a solute molecule in the vapour phase	m^3
w	Velocity	$m.s^{-1}$

x	Distance from the nozzle exit	m
x_0	Fitting factor	-
y_s	Solute mole fraction	-
z	Distance along nozzle	m
Z_{ab}	Collision frequency between particles a and b	$\text{m}^{-3} \cdot \text{s}^{-1}$

Greek Symbols

<i>Symbol</i>	<i>Description</i>	<i>Units</i>
γ	Ideal isentropic factor	-
η	Viscosity	Pa.s
λ	Mean free path length	m
μ	Chemical potential	$\text{J} \cdot \text{kg}^{-1}$
ρ	Density	$\text{kg} \cdot \text{m}^{-3}$
σ	Flat-film surface tension	$\text{N} \cdot \text{m}^{-2}$

Subscripts

<i>Symbol</i>	<i>Description</i>
avg	Average (number average)
M	Mach Disk
S	Solute
V	Vapour
0	At pre-expansion (equilibrium cell) conditions
∞	At the post-expansion (precipitation vessel) conditions



Superscripts

<i>Symbol</i>	<i>Description</i>
*	Equilibrium condition